Journal of Control Science and Engineering

Using Communication Networks in Control Systems: The Theoretical and Practical Challenges

Lead Guest Editor: Yun-Bo Zhao
Guest Editors: Zhihong Man, Jongrae Kim, and Cui-Qin Ma

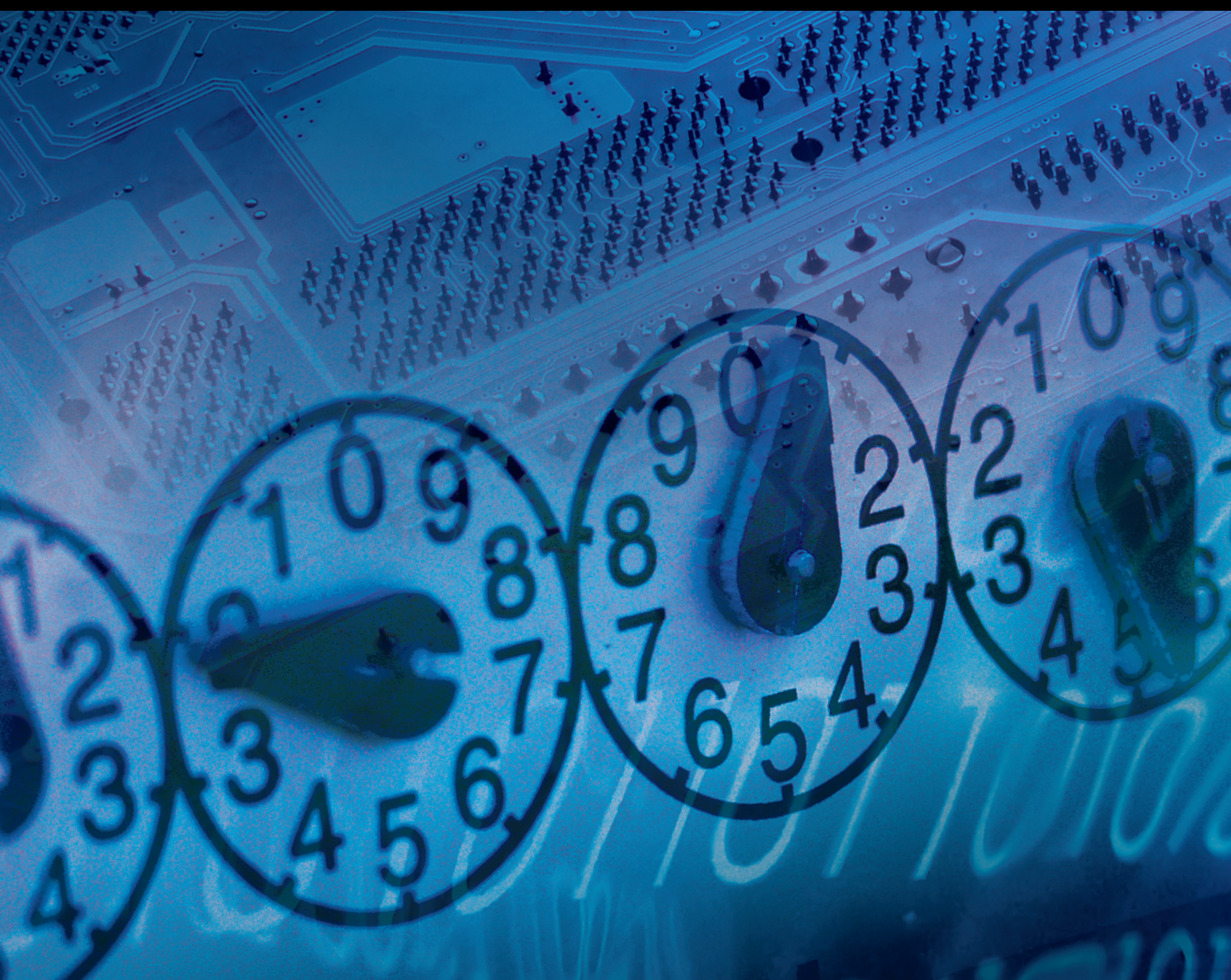

Using Communication Networks in Control Systems: The Theoretical and Practical Challenges

Journal of Control Science and Engineering

Using Communication Networks in Control Systems: The Theoretical and Practical Challenges

Lead Guest Editor: Yun-Bo Zhao
Guest Editors: Zhihong Man, Jongrae Kim, and Cui-Qin Ma

Editorial Board

Contents

Hindawi
Journal of Control Science and Engineering
Volume 2018, Article ID 6714317, 2 pages
https://doi.org/10.1155/2018/6714317

Editorial

Using Communication Networks in Control Systems: The Theoretical and Practical Challenges

Yun-Bo Zhao,[1] **Zhihong Man**,[2] **Jongrae Kim**,[3] **and Cui-Qin Ma**[4]

[1]*College of Information Engineering, Zhejiang University of Technology, Hangzhou 310023, China*
[2]*Faculty of Science, Engineering and Technology, Swinburne University of Technology, Hawthorn, Victoria 3122, Australia*
[3]*School of Mechanical Engineering, University of Leeds, Leeds LS2 9JT, UK*
[4]*School of Mathematical Sciences, Qufu Normal University, 57 Jingxuan West Road, Qufu, China*

Correspondence should be addressed to Yun-Bo Zhao; ybzhao@ieee.org

Received 18 November 2018; Accepted 18 November 2018; Published 2 December 2018

From the perspective of information exchange, three stages can be identified for the evolvement of control systems. Conventional control systems with simple system structure can be implemented in a way that all system components, including the controller, the plant, the sensors, and the actuators, are connected point-to-point via communication cables, meaning that the information exchange within such systems is almost perfect, without any information loss or delay. Later, with the development of complex applications of control systems in industry, the system scale becomes larger and larger, which makes the point-to-point connections too expensive and impractical. In order to facilitate the communication among system components, the bus structure is then proposed, where many control components can share the same bus communication channel. In recent years, communication networks have been more and more popular, and naturally, the information exchange in control systems has taken advantage of these existing communication networks to develop the concept of networked control systems, as well as a few new branches in control field such as cyberphysical systems, Internet of Things, and almost all large intelligent systems including smart home, intelligent transportation, and smart city [1–3].

Using communication networks in control systems is the foundation of many modern intelligent systems. However, such a technical integration has resulted in many challenges in both theories and applications. For instance, the information exchange in modern industrial systems is also carried out via the shared communication channel whose communication characteristics are usually unknown and unpredictable. This then breaks the real-time requirement of information exchange by control systems (the same as in control systems with bus communication channel) and also introduces unpredictable, stochastic nature of information exchange (a brand-new feature for these systems). New methodologies and approaches are therefore needed for making such systems reliably useful in future [4].

This special issue has collected a number of research articles which may shed light on the-state-of-the-art of control systems using communication networks. We briefly outline the key points of these research articles in what follows, and for the detailed works please refer to the articles in this special issue.

The article entitled "Dynamic Output Feedback Control of Discrete Markov Jump Systems based on Event-Triggered Mechanism" by Z. Zhao et. al. investigates the random time delay caused by the communication network and models it as a Markov process. Then, the authors propose an event-triggered mechanism for information transmission and a codesign strategy involving both the event-triggered scheme and a dynamic output feedback controller. The stability of the closed-loop system is finally addressed using the Lyapunov-Krasovskii functional and linear matrix inequality (LMI).

The article entitled "Event-Based Nonfragile H_∞ Filter Design for Networked Control Systems with Interval Time-Varying Delay" by Z. Lu et. al. considers interval time-varying

delay in nonlinear control systems. Similarly, the authors propose an event-triggered scheme to schedule the sampled data transmission through the communication network, and then model the filtering error system as a system with interval time-varying delay. The authors then take advantage of a new Lyapunov-Krasovskii functional and the Wirtinger inequality to derive the sufficient stability conditions, and also propose the LMI based design of the nonfragile filter parameters.

The article entitled "Event-Triggered H_∞ Filtering for Multiagent Systems with Markovian Switching Topologies" by J. Li et. al. considers network-induced delay in the context of multiagent systems with Markovian switching topologies. Again, an event-triggered mechanism is proposed for information transmission, but it is for the directed network topology representing the communication links.

The article entitled "Networked Closed-Loop Model for Smart On-Site Maintenance of Substation Equipment Using Mobile Networks" by Z. Feng et. al. is concerned with mobile networks in the context of smart on-site maintenance of substation equipment. The authors propose a model for such systems, which allows bidirectional communication among the people and the equipment. This article can be regarded as a successful practical application of control systems using communication networks.

The article entitled "Neural Network Predictive Control for Autonomous Underwater Vehicle with Input Delay" by J. Zhao considers input delay for an autonomous underwater vehicle (AUV). The authors propose a predictive control algorithm to compensate for the negative effects of time delay in path tracking, with the use of neural networks to estimate the nonlinear uncertainties of AUV. The authors finally give the stability conditions using the Lyapunov theorem.

In summary, we believe that this special issue has contained sufficiently useful materials on control systems using communication networks and hope that this special issue will provide the reader with a useful reference for their future research.

Conflicts of Interest

The authors declare that there are no conflicts of interest regarding the publication of this article.

Yun-Bo Zhao
Zhihong Man
Jongrae Kim
Cui-Qin Ma

References

[1] R. A. Gupta and M. Y. Chow, "Networked control system: overview and research trends," *IEEE Transactions on Industrial Electronics*, vol. 57, no. 7, pp. 2527–2535, 2010.

[2] A. J. Stankovic, "Research directions for the internet of things," *IEEE Internet of Things Journal*, vol. 1, no. 1, pp. 3–9, 2014.

[3] A. W. Colombo, T. Bangemann, S. Karnouskos et al., *Industrial Cloud-Based Cyber-Physical Systems*, Springer Science & Business Media, 2014.

[4] Y. Zhao, G. Liu, Y. Kang, and L. Yu, "A Brief Tutorial of Networked Control Systems," in *Packet-Based Control for Networked Control Systems*, pp. 1–11, Springer, Singapore, 2018.

Hindawi
Journal of Control Science and Engineering
Volume 2018, Article ID 2738362, 9 pages
https://doi.org/10.1155/2018/2738362

Research Article

Wide-Area Damping Controller Design Based on the Frequency Domain Self-Excitation Method

Lei Gao,[1,2] Yanchao Ma,[3] Yonghui Nie,[2] Shiyun Xu,[1] Xiaojie Chu,[1] and Long Peng[1]

[1]*China Electric Power Research Institute, Beijing 100192, China*
[2]*Northeast Electric Power University, Jilin 132012, Jilin Province, China*
[3]*State Grid Liaoning Power Co., Ltd., Yingkou Power Supply Company, Yingkou 115000, China*

Correspondence should be addressed to Shiyun Xu; xushiyun@epri.sgcc.com.cn

Received 9 May 2018; Accepted 16 August 2018; Published 13 September 2018

Academic Editor: Cui-Qin Ma

In this paper, a wide-area DC damping controller design method is proposed to damp the weak interarea oscillation modes. First, the low-order power system control model identification method is proposed based on the frequency domain self-excitation method to obtain the dominant modes and other related information. In what follows, the identified model is transformed into a low-order state space equation. By comparing the geometric metrics of different schemes, the various input signals and installation locations of the controller are selected. Furthermore, the damping controller parameter calculation is realized based on the self-excitation frequency domain identification method, which does not depend on the detailed model of the system. The design process is simple and it is easy to apply in the practical engineering of large-scale complex power grids. The applicability and effectiveness of the proposed controller design method are demonstrated through simulations of a two-area four-generator power system.

1. Introduction

The AC/DC interconnected power grid can transmit large capacity of power from the remote power basis to the load centers through communication networks. It plays an extremely important role in the energy allocation in China. Since the AC and DC transmission systems are generally coupled with each other, however, disturbances that occur in both the AC and the DC sides may trigger weakly damped low frequency oscillations. If the oscillations are of the interarea type, a large number of generators will participate in and the interconnected power grid will confront severe operational risk [1, 2].

However, due to the deficiency in observability, traditional power system stabilizers (PSS) which use local signals as inputs may fail to damp out the interarea oscillation and maintain system stability. To overcome the shortcoming of traditional PSS, wide-area damping controllers with remote signals obtained from wide-area measurement system (WAMS) have become a better choice in suppressing low frequency oscillation [3–5]. Since DC systems have fast response characteristics, it can effectively improve the stability of the system once faults have occurred in the AC system, and the DC damping control [6–9] that can suppress the interarea low frequency oscillation of AC/DC hybrid system has attracted the attention of researchers.

During the wide-area damping controller design, it is important to choose feedback control signal and installation location. The residue method [10, 11] is widely used for feedback signal selection, but it can only compare the same type of signals. For different types of signals, such as generator speed, line transmission power, and bus voltage, the amplitude of the above-mentioned residual value will not be accurate due to the ratio problem. In [12], a relative gain array (RGA) method is proposed. Although this method reduces the mutual influence among multiple controllers, it has the same disadvantages as the residual method. Other methods, such as the Hankel singular value (HSV) [13], the singular value decomposition (SVD) [14], and the minimum singular values (MSV) [15], have also been proposed to calculate the corresponding observability and controllability indices, but it becomes much more complicated to calculate for practical large-scale power systems. On the other hand, most of the existing damping control design methods require the precise

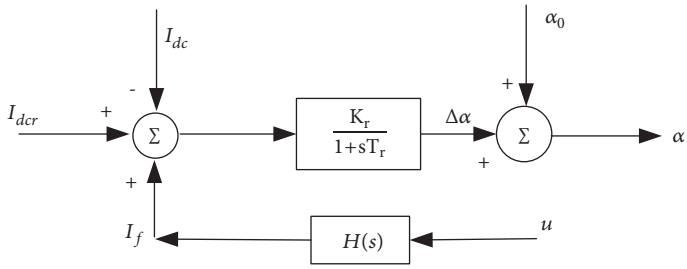

Figure 1: Rectifier current regulator.

system model through linearizing it around an equilibrium point. This may lead to the modeling error due to information incompleteness.

In this paper, the low frequency oscillation of an AC/DC hybrid system is damped by installing a wide-area damping controller in the DC system. Based on the above considerations, the improved geometric lateral index [11, 16] based on the frequency domain excitation identification theory is proposed to solve the wide-area DC supplementary damping control signal selection in AC/DC hybrid systems. This method can effectively solve the problem that different types of input signals have different amplitude ratios and can avoid solving the huge state matrix as well. Moreover, the method based on the self-excitation frequency domain identification is further utilized to configure the DC damping controller, which does not depend on the detailed model of the system. The design process is simple, and it is easy to use in the practical engineering of the complex large power grid. At the end of this study, the AC/DC hybrid system is taken as an example to demonstrate the effectiveness of the proposed controller design method.

2. Problem Formulation

2.1. DC Damping Controller. The DC damping control is a kind of small signal modulation, and the basic principle is to add a supplementary damping controller in the DC main control loop. The controller is usually installed at the rectifier side. In this regard, the power of the DC transmission line is adjusted by tuning the extinction angle α to damp the system oscillation.

The control block diagram is shown in Figure 1. By adding the DC additional control output I_f and the reference current input I_{dcr} to the current control of the inverter can improve the damping of the system. The dynamic equation of the linearized regulator is given as

$$\begin{aligned} \dot{\alpha} &= \frac{K_r}{T_r}\left(I_{dcr} - I_{dc} + I_f\right) - \frac{\alpha}{T_r} \\ \dot{I}_{dc} &= \frac{1}{T_{dc}}\left(-I_{dc} + I_{dcr} + I_f\right) \end{aligned} \tag{1}$$

The supplementary wide-area damping controller transfer function is in the following form:

$$H(s) = \frac{K}{1+sT_1} \cdot \frac{sT_W}{1+sT_W} \cdot \left[\frac{1+sT_2}{1+sT_3}\right]^m \tag{2}$$

where T_{dc}, T_r, T_1, T_2, T_3, T_W are the time constants, K_r and K are the controller proportional coefficient, I_{dc} is the DC current, and u is the feedback signal, which can be chosen as the generator speed deviation, the bus phase difference or any bus voltage, power, and so on.

In this study, the selected feedback signal is processed by the damping controller to the input of the current regulator in the DC main control system, based on the principle of DC damping control. The extinction angle α is maintained within the normal range ($\alpha_{\min} < \alpha < \alpha_{\max}$). In order to select the best alternative signal, the indicators defined by the improved geometric index can be calculated. In this regard, the designed damping controller can damp system oscillation.

2.2. System Model Analysis. By linearizing around the stable equilibrium point, the AC/DC hybrid power system equation can be given as

$$\begin{aligned} \Delta\dot{x} &= A\Delta x + B\Delta u \\ \Delta y &= C\Delta x \end{aligned} \tag{3}$$

where A is an $n \times n$ state matrix, B is an $n \times p$ input matrix, and C is a $q \times n$ output matrix.

For power system with n generators, only part of the oscillation mode of the generator rotor is concerned, and the number of oscillating modes in which any one generator is significantly involved is generally 2~3. Based on this consideration, the state equation of the ith generator can be set as

$$\begin{bmatrix} \Delta\dot{\delta} \\ \Delta\dot{\omega} \end{bmatrix} = \begin{bmatrix} 0 & I \\ -M^{-1}K(s) & -M^{-1}D(s) \end{bmatrix} \cdot \begin{bmatrix} \Delta\delta \\ \Delta\omega \end{bmatrix} \tag{4}$$

where $K(s)$ is the synchronization torque coefficient, $D(s)$ is the damping torque coefficient, and M is the diagonal matrix composed by the corresponding elements of the generator.

It can be seen from Figure 2 that if there is no external disturbance T_x, the differential equation of the corresponding equivalent system can be derived as

$$M(s)\Delta\ddot{\delta} + D(s)\Delta\dot{\delta} + K(s)\Delta\delta = 0 \tag{5}$$

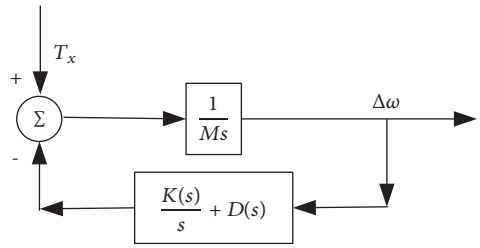

Figure 2: Equivalent system.

Assume that the eigenvalue of (5) is $\lambda_i = \sigma_i \pm j\omega_i$, then

$$\left(M\Delta\ddot{\delta} + D(s)\Delta\dot{\delta} + K(s)\Delta\delta\right)\Big|_{\lambda_i} \stackrel{\text{def}}{=} T_x \longrightarrow 0 \tag{6}$$

In order to calculate the electromechanical mode associated with system oscillation, the self-excited method [17] is utilized by deriving the eigenvalue of (6) through the Newton iteration method. However, the application of the traditional self-excited method is not only sensitive to the initial value but also easily leads to the loss of roots. In this regard, this paper proposes a frequency domain self-excited identification method, which is applied to choose controller inputs. This method avoids the problems of traditional self-excited method, which is described in detail in the following section.

3. Wide-Area DC Damping Controller Design

Generally speaking, the steps in designing a wide-area controller include wide-area signal selection, system reduction, controller design, and validation of the design by numerical simulations. Each of the above steps is briefly described in the following subsections.

3.1. Observable and Controllable Quantitative Index. In order to choose the feedback signal and the installation location of the wide-area damping controller, it is necessary to establish a unified index for the calculation of different types of signals or control points. The quantization index of the observability and controllability of the system based on the improving geometric lateral index can solve the defects of the different types of signals, which is described as follows.

For system (3), by denoting a new state variable $\Delta x = Wz$, the oscillation characteristics of the system can be decoupled and the system with a diagonal state matrix can be derived as

$$\begin{aligned} \dot{z} &= \Lambda z + B'\Delta u \\ \Delta y &= C'z + D\Delta u, \end{aligned} \tag{7}$$

where W is the modal matrix of A, $\Lambda = \text{diag}\{\lambda_i\}$, $B' = W^{-1}B = N^T B$, $C' = CW$, W_i is the right eigenvector corresponding to λ_i, and N_i is the left eigenvector corresponding to λ_i.

The observability index of the ith modal of the system is given as

$$g_{oj}(i) = \cos\left(\alpha\left(W_i, c_j\right)\right) = \frac{\left|c_j W_i\right|}{\left\|W_i\right\| \left\|c_j\right\|} \tag{8}$$

while the controllability index is defined by

$$g_{ck}(i) = \cos\left(\theta\left(N_i, b_k\right)\right) = \frac{\left|b_k^T N_i\right|}{\left\|N_i\right\| \left\|b_k\right\|} \tag{9}$$

where $|\cdot|$ and $\|\cdot\|$, respectively, represent the modulo and Euclidean norm, c_j is the jth line of the matrix C, b_k is the kth column of the matrix B, $\alpha(W_i, c_j)$ is the angle between the output phasor c_j and the right eigenvector W_i, and $\theta(N_i, b_k)$ is the angle between the output phasor b_k and the left eigenvector N_i.

Thus, the comprehensive index corresponding to the ith modal is given by

$$\begin{aligned} g_{coi}(k, j) &= g_{oj}(i)\, g_{ck}(i) \\ &= \cos\left(\alpha\left(W_i, c_j\right)\right)\cos\left(\theta\left(N_i, b_k\right)\right) \end{aligned} \tag{10}$$

Quantitative analysis and comparison of the observability and controllability of different types of alternative signals can be realized by the calculation of the above-mentioned indices. However, in the practical power system, it is difficult to obtain the accurate full-order system model. Based on this consideration, this study carries out power system model identification according to the frequency domain self-excited method, and then the low-order system can be utilized to approximate the original system, which greatly reduces the calculation complicatedness and improves the calculation effectiveness.

3.2. Control Loop Selection. The feedback signals and installation locations selection are the basis for controller design of wide-area damping controller. In this subsection, a new method to select the feedback signal of wide-area damping controller is proposed by combining the basic principle of self-excitation and the method of frequency domain identification.

Based on the basic principle of the self-excited method, it can be derived from (6) that

$$T_x + \frac{dT_x}{ds}\left(\Delta\lambda_i\right) = 0 \tag{11}$$

By analyzing (11), the following necessary conditions are obtained:

$$\begin{aligned} T_x &\longrightarrow 0 \\ \frac{dT_x}{ds} &\longrightarrow 0 \end{aligned} \tag{12}$$

However, since the traditional self-excitation method iteratively solves the eigenvalue of (6) by Newton's method, it may lead to the incompleteness of electromechanical modes.

Therefore, the method proposed in this paper utilizes the frequency domain method to identify the transfer function of the system and then solve the relevant mode information to avoid the above-mentioned problems.

By carrying out the Laplace transform of (6) and (12), the system transfer function can be derived as

$$G(s) = \frac{\Delta\delta(s)}{\Delta T_x(s)} = \frac{s}{M(s)s^2 + D(s)s + K(s)} \tag{13}$$

If a more accurate model of the generator is considered, such as taking the excitation system model into account, (9) still holds, but the order will increase. In this case, $G(s)$ can be expressed as follows:

$$\begin{aligned} G(s) &= \frac{\Delta\delta_i(s)}{\Delta T_{xi}(s)} = K\frac{(s-z_{j1})(s-z_{j2})\cdots(s-z_{ji})}{(s-p_1)(s-p_2)\cdots(s-p_k)} \\ &= \frac{R_{j1}}{s-p_1} + \frac{R_{j2}}{s-p_2} + \cdots \frac{R_{jk}}{s-p_k} \end{aligned} \tag{14}$$

It can be analyzed from (6) and (12) that if the frequency of T_x is equal to the oscillation frequency of the system, only the torque with the amplitude close to zero can stimulate the large response of the oscillation frequency. Assume that T_x can increase the oscillation frequency to $\lambda\omega$, if different generators are selected as the "excitation point", then $G(\lambda_i\omega)$ can be expressed as

$$\begin{aligned} G(\lambda_i\omega) &= \frac{\Delta\delta_i(\lambda_i\omega)}{\Delta T_{xi}(\lambda_i\omega)} \\ &= \frac{R_{j1}}{\lambda_i\omega - p_1} + \frac{R_{j2}}{\lambda_i\omega - p_2} + \cdots \frac{R_{jk}}{\lambda_i\omega - p_k} \end{aligned} \tag{15}$$

Although the "excitation point" varies, the system inter-area oscillation mode keeps the same, where a pair of conjugate poles represents an oscillation mode. Let $\lambda_i = \sigma_i \pm j\omega_i$, then it can be used to calculate the system oscillation frequency and damping ratio.

Once the oscillation mode is determined, the index calculation of the candidate signal should be carried out, when it is necessary to transform the system into the state space form and $G(s)$ can be written as

$$G(s) = \frac{Y(s)}{U(s)} = \frac{b_m s^m + b_{m-1}s^{m-1} + \cdots + b_0}{s^n + a_{n-1}s^{n-1} + \cdots + a_0} \tag{16}$$

In this regard, the state space expression of the system can be derived as

$$\begin{aligned} \Delta\dot{x} &= E\Delta x + F\Delta u \\ \Delta y &= G\Delta x + H\Delta u \end{aligned} \tag{17}$$

where $E = \begin{bmatrix} 0 & I_{n-1} \\ A_0 & A_{n-1} \end{bmatrix}$ is the equivalent matrix of matrix A in (3), which contains the main mode of the original system. $F = [0 \ \cdots \ 1]^T$ and I are the corresponding control matrix and substantial matrix, respectively. $G = B_n - A_n b_n$, $H = b_n$. Equation (17) is the state space model derived by the frequency domain self-exited method.

The state space equation identified by the frequency domain excitation method preserves the main mode of operation of the system. Therefore, (17) can be used to substitute the original system to calculate the quantization index of the observability and controllability of the system.

The new method of selecting feedback signal of wide-area damping controller based on the self-excited frequency domain identification method proposed in this paper can be used in engineering application of large-scale power system without obtaining the full-state model of the system, and the calculation and operation are convenient, which is suitable for the engineering application of large power system.

3.3. Wide-Area Coordinated Controller Design. Once the state space equation is identified by the self-excited frequency domain identification, by carrying out the Laplace transform on (13), the transfer function between the input variable $\Delta\boldsymbol{U}_1$ and the output variable $\Delta\boldsymbol{Y}_1$ can be obtained as

$$G(s) = \frac{\Delta U_1(s)}{\Delta Y_1(s)} = G(sI - E)^{-1}F + H \tag{18}$$

Suppose dominant oscillation modes for (18) are $\lambda_{1,2} = \delta \pm j\omega$, and the desired damping ratio after adding damping controller is ξ. Substituting $s = j\omega_d = j\sqrt{1-\xi^2}\omega$ into (18) derives

$$G(j\omega_d) = \left.\frac{\Delta U_1(s)}{\Delta Y_1(s)}\right|_{s=j\omega_d} = G\angle\phi \tag{19}$$

where G and ϕ are the amplitude and phase of $G(s)$ at $s = j\omega_d$, respectively.

The lead lag link parameters of the wide-area DC damping controller (2) can be calculated by

$$\begin{aligned} \phi_x &= 180 - \phi \\ \alpha &= \frac{1+\sin\phi_x}{1-\sin\phi_x} \\ T_1 &= \frac{\sqrt{\alpha}}{\omega} \\ T_2 &= \frac{T_1}{\alpha} \end{aligned} \tag{20}$$

In order to prevent the damping controller from outputting a constant deviation voltage, the design principle is that, in the frequency range where damping controllers provide damping, no obvious phase displacement should be introduced in the isolating links. The typical value is chosen as 1~10s, and in this study, it is set to be 5s.

The advantage of the above wide-area DC damping controller parameter design based on the self-excited method is that it does not rely on the detailed model of the system, the design process is simple, the derived parameters are stable, and it is applicable to utilize in the practical complex large-scale power grid.

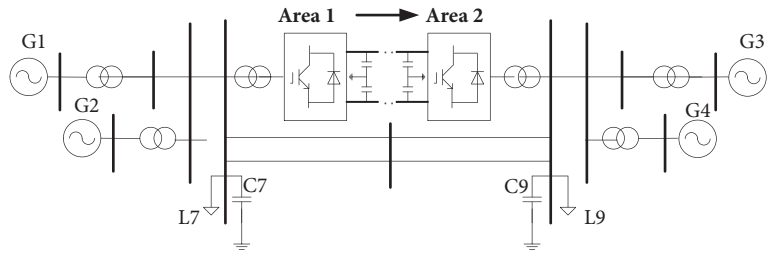

Figure 3: Two-area four-generator AC/DC hybrid system.

Table 1: Interarea oscillation frequency and damping ratio without control.

Operation mode	eigenvalue	frequency	Damping ratio
P=150MW	-0.1462+3.2683i	0.5202	0.0447
P=200MW	-0.1301+3.8321i	0.6099	0.0339
P=300MW	-0.2942+3.5092i	0.5585	0.0835

3.4. Wide-Area Damping Control Design Process. The basic steps of the selection of the feedback signal and the installation location of the wide-area damping controller based on the self-excited frequency domain identification method are as follows:

Step 1. Identify the low-order system based on the frequency domain self-excited method, and calculate the corresponding interarea oscillation modes $\lambda_{1,2} = \delta \pm j\omega$ and the oscillation frequency ω.

Step 2. Select different feedback signals and installation locations of the n groups of controllers, and then the system is able to be operated under the steady state with the open loop operation of the controller. The disturbance test for group i ($0<i<n$) is carried out, and for the disturbance $u_i(t)$ that does not destroy the stability of the original system, record the output response data $y_i(t)$.

Step 3. Extract the variation data $\Delta u_i(t)$ and $\Delta y_i(t)$ of $u_i(t)$ and $y_i(t)$ in the common cycle. Carry out the discrete Fourier transform, respectively, and obtain the varying phasors $\Delta u_i(j\omega)$ and $\Delta y_i(j\omega)$ corresponding to different frequency values, where $i = 1, 2, \ldots, n$, $0 \le j\omega \le 2\pi$.

Step 4. The self-excited method is applied to identify the phasor data $\Delta u_i(j\omega)$ and $\Delta y_i(j\omega)$, and the corresponding transfer function $G_i(s)$ is fitted. Transform the transfer function into the state space form and obtain the corresponding system matrices A_i, B_i, C_i, D_i.

Step 5. Apply the geometric measure index method to calculate each index, which is used as the reference for the input signal of the comparison controller. Based on the above method, that best feedback signal and installation location are determined.

Step 6. Based on the state space equation and the dominant modes, identify the information such as the phase Φ and the oscillation mode ω that are required by controller design. Calculate the controller time constants T_i, $i = 1, 2, \ldots, 4$ by (20).

Step 7. Adjust the controller gain K_i to verify the damping effect, and the operation parameters of the wide-area DC damping controller are finally determined.

4. Case Study

Taking the two-area four-generator AC/DC hybrid system shown in Figure 3 as an example, the detailed model is built with MATLAB and verified by simulation. The specific parameters are taken from literature [18]. The wide-area damping controller is installed in the rectifier of the DC part. The optional input signals of the wide-area damping controller are the rotor speed difference of generator 1 (G1) and generator 3 (G3), the active power of the AC tie-line, the AC line voltage, AC line current amplitude, and difference of voltage phase between two sides of an AC contact line. By modifying the model parameters, the powers of transmission line between two regions are chosen as P = 150MW, P = 200MW, and P = 300MW, and thus three kinds of operation modes are derived (the positive direction of power flow is defined as from Area 1 to Area 2).

According to the procedure described in the previous section, the interarea oscillation modes are analyzed for the transmission power P = 150MW, P = 200MW, and P = 300MW, respectively, which are shown in Table 1.

By carrying out the wide-area damping controller design steps proposed in Section 3.4, the frequency domain self-excited method and the improved geometric lateral index are used to calculate the comprehensive and residue indices for different schemes. The results are shown in Tables 2–4.

As shown in Tables 2–4, the best candidate signals among the three operating modes are the rotor speed difference between G1 and G3 by comparing the comprehensive and residue indices.

In order to verify the validity of the analysis results, the wide-area damping control effect of different feedback signals

Table 2: System indices for P=150MW.

Alternative input signal	Residue index	geometric laterality index	frequency	Damping ratio	Compensation phase
the rotor speed difference of G1 and G3	0.2711	0.9409	0.5536	0.0870	93.7
the active power of the AC line	2.0689e-06	0.7241	0.5700	0.0533	147.4
AC line current amplitude	0.1376	0.8042	0.556	0.0773	16.5
difference of voltage phase between two sides of AC line	1.6235e-06	0.7171	0.567	0.0395	54.6

Table 3: System indices for P=200MW.

Alternative input signal	Residue index	geometric laterality index	frequency	Damping ratio	Compensation phase
the rotor speed difference of G1 and G3	0.3568	0.8951	0.6587	0.0473	97.2
the active power of the AC line	1.2302e-06i	0.7501	0.6331	0.0035	115.5
AC line current amplitude	0.0117	0.7276	0.6245	0.0172	31.4
difference of voltage phase between two sides of AC line	1.4371e-08	0.7330	0.5891	0.0063	29.8

Table 4: System indices for P=300MW.

Alternative input signal	Residue index	geometric laterality index	frequency	Damping ratio	Compensation phase
the rotor speed difference of G1 and G3	0.2967	0.9554	0.5572	0.0566	92.6
the active power of the AC line	6.3309e-06	0.8236	0.5401	0.0670	115.6
AC line current amplitude	0.1087	0.7183	0.5431	0.0070	55.1
difference of voltage phase between two sides of AC line	6.0653e-08	0.7496	0.5587	0.0636	165.8

is simulated by choosing the speed difference between G1 and G3 as the wide-area damping controller feedback signal, which is installed in the DC side of the main control loop. A three-phase short circuit occurred on the AC transmission line at t=10.4s, which is cleared at 10.9s. By carrying out the phase compensation method, parameters of the wide-area controller (2) can be calculated as

$$\begin{aligned} m &= 3, \\ K &= 30, \\ T_1 &= 0.02, \\ T_W &= 10, \\ \alpha &= 0.3218, \\ T_2 &= 0.5035, \\ T_3 &= 0.1620 \end{aligned} \tag{21}$$

where the operating mode corresponding to P=300MW is selected as the compensation phase of the controller parameter calculation, and let $\theta = 92.6^{\circ}$.

From Figures 4–6, it is observed that there are obvious differences in the control effect under the location of installation being selected. Considering the residue method, for the rotational speed differences of G1 and G3 as well as the

Table 5: Interarea oscillation frequency and damping ratio for system under control.

Operation mode	eigenvalue	frequency	Damping ratio
P=150MW	-0.6208+3.5014i	0.5573	0.1746
P=200MW	-0.4446+3.9169i	0.6234	0.1128
P=300MW	-0.4082+3.6602i	0.5825	0.1108

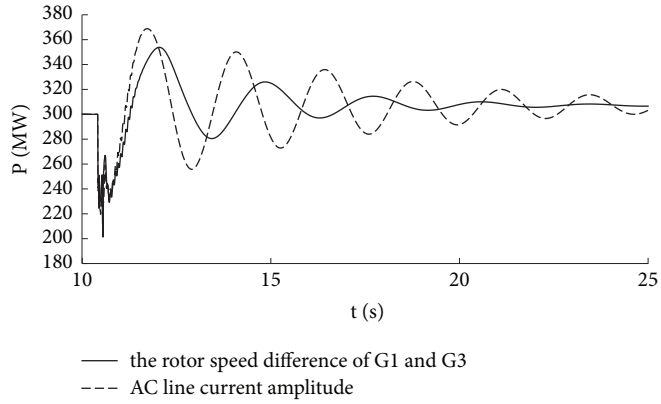

Figure 4: Comparison of power oscillation.

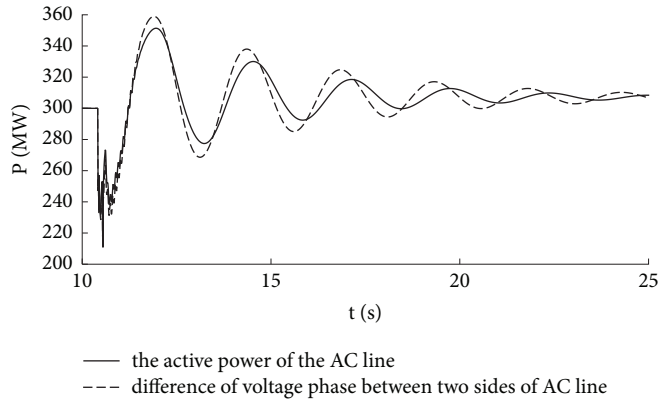

Figure 5: Comparison of power oscillation.

amplitude of the AC link current (Figure 4), the AC tie-line power P and the voltage phase difference of the tie-line (Figure 5), these two types of signals with different amplitudes are displayed as the larger the number of indicators, the better the control effect. However, since the magnitudes of the two types of signal indicators are significantly different, it is impossible to compare them at the same time. In this case, the improving geometric lateral index has a greater advantage, as it can compare different types of signals under the same order of magnitude. As shown in Figure 6, as the analysis results in Tables 2–4, the larger the index value the better the control effect, which verifies the effectiveness of the method in this paper.

For the system under wide-area damping control, the operating modes of the interarea oscillation frequency and damping ratio are calculated based on the frequency domain self-excited method as shown in Table 5.

It can be seen from Table 5 that, for system under control, the damping for each operating mode has been significantly increased, indicating that the system damping is improved under the designed controller. Simulation results of the AC tie-line transmission power with and without the designed damping controller are depicted in Figure 7. The above simulation results have verified the effectiveness and applicability of the proposed wide-area damping controller.

5. Conclusion

In this study, a wide-area damping controller design method for AC/DC hybrid power system is proposed. The input signal of the wide-area damping controller is selected by the improved geometric laterality index, which can be chosen as different types of signals to increase the range of the optional signal to improve the controller design effect. The system model can be identified through the frequency domain self-excitation method, based on which the phase compensation method is further utilized to design the DC

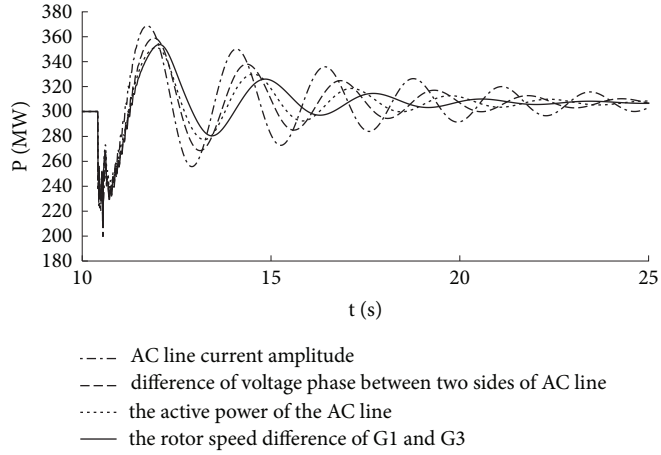

Figure 6: Active power oscillation of the tie-line.

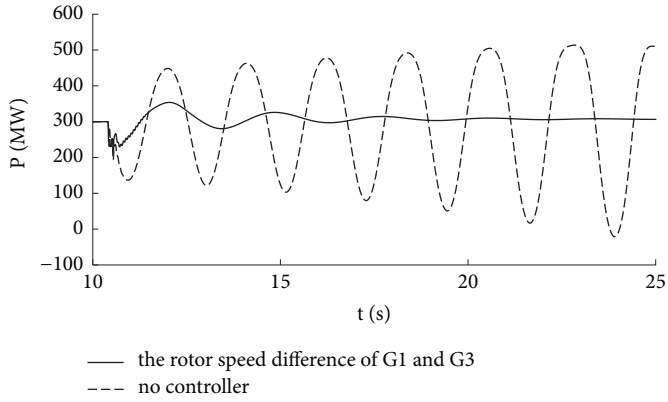

Figure 7: Transmission power comparison of the AC tie-line.

damping controller parameters. The proposed damping controller avoids the complex eigenvalue calculation in large-scale power systems and is not affected by the increase of system order. Moreover, the detailed system modeling is avoided, which may lead to inaccuracy and errors. The design process is simple, which is suitable for practical engineering applications.

Data Availability

The data used to support the findings of this study are available from the corresponding author upon request.

Conflicts of Interest

The authors declare that they have no conflicts of interest.

Acknowledgments

This research has been supported by the Young Elite Scientists Sponsorship Program by CAST (YESS20160157) and CSEE (JLB-2017-305), State Grid Corporation of China, Fundamental and Forecast Projects (XT71-18-014), and the National Natural Science Foundation of China (U1766202, 51777195) as well as the Key Project of Smart Grid Technology and Equipment of National Key Research and Development Plan of China (2016YFB0900600).

References

[1] O. F. Ruiz, I. A. DIaz DIaz, and I. Cervantes, "On the implementation of advanced hybrid controllers of AC/DC converters," *IEEE Latin America Transactions*, vol. 15, no. 9, pp. 1677–1683, 2017.

[2] A. A. Eajal, M. A. Abdelwahed, E. F. El-Saadany, and K. Ponnambalam, "A unified approach to the power flow analysis of AC/DC hybrid microgrids," *IEEE Transactions on Sustainable Energy*, vol. 7, no. 3, pp. 1145–1158, 2016.

[3] R. Jalayer and B.-T. Ooi, "Co-Ordinated PSS tuning of large power systems by combining transfer function-eigenfunction analysis (TFEA), optimization, and eigenvalue sensitivity," *IEEE Transactions on Power Systems*, vol. 29, no. 6, pp. 2672–2680, 2014.

[4] N. Rashidirad, M. Hamzeh, K. Sheshyekani, and E. Afjei, "An effective method for low-frequency oscillations damping in multiBus DC microgrids," *IEEE Journal on Emerging and Selected Topics in Circuits and Systems*, vol. 7, no. 3, pp. 403–412, 2017.

[5] S. Debnath, J. Qin, and M. Saeedifard, "Control and stability analysis of modular multilevel converter under low-frequency operation," *IEEE Transactions on Industrial Electronics*, vol. 62, no. 9, pp. 5329–5339, 2015.

[6] R. Eriksson, "A new control structure for multiterminal DC grids to damp interarea oscillations," *IEEE Transactions on Power Delivery*, vol. 31, no. 3, pp. 990–998, 2016.

[7] Y. Liu, A. Raza, K. Rouzbehi, B. Li, D. Xu, and B. W. Williams, "Dynamic resonance analysis and oscillation damping of multiterminal DC grids," *IEEE Access*, vol. 5, pp. 16974–16984, 2017.

[8] L. Meng, T. Dragicevic, J. C. Vasquez, and J. M. Guerrero, "Tertiary and secondary control levels for efficiency optimization and system damping in droop controlled DC-DC converters," *IEEE Transactions on Smart Grid*, vol. 6, no. 6, pp. 2615–2626, 2015.

[9] A. Fuchs, M. Imhof, T. Demiray, and M. Morari, "Stabilization of large power systems using vsc-hvdc and model predictive control," *IEEE Transactions on Power Delivery*, vol. 29, no. 1, pp. 480–488, 2014.

[10] J. Zhang, C. Y. Chung, C. Lu, K. Men, and L. Tu, "A novel adaptive wide area PSS based on output-only modal analysis," *IEEE Transactions on Power Systems*, vol. 30, no. 5, pp. 2633–2642, 2015.

[11] W. Yao, L. Jiang, J. Wen, Q. H. Wu, and S. Cheng, "Wide-area damping controller of Facts devices for inter-area oscillations considering communication time delays," *IEEE Transactions on Power Systems*, vol. 29, no. 1, pp. 318–329, 2014.

[12] H. N. Villegas Pico, D. C. Aliprantis, J. D. McCalley, N. Elia, and N. J. Castrillon, "Analysis of hydro-coupled power plants and design of robust control to damp oscillatory modes," *IEEE Transactions on Power Systems*, vol. 30, no. 2, pp. 632–643, 2015.

[13] R. Shah, N. Mithulananthan, K. Y. Lee, and R. C. Bansal, "Wide-area measurement signal-based stabiliser for large-scale photovoltaic plants with high variability and uncertainty," *IET Renewable Power Generation*, vol. 7, no. 6, pp. 614–622, 2013.

[14] J. M. Lim and C. L. DeMarco, "SVD-based voltage stability assessment from phasor measurement unit data," *IEEE Transactions on Power Systems*, vol. 31, no. 4, pp. 2557–2565, 2016.

[15] E. T. González and J. G. C. Guizar, "The effect of induction motor modeling in thecontext of voltage sensitivity: Combined loads and reactive power generation, on electric networks steady state analysis," *IEEE Latin America Transactions*, vol. 10, no. 4, pp. 1924–1930, 2012.

[16] D. H. A. Lee, "Voltage stability assessment using equivalent nodal analysis," *IEEE Transactions on Power Systems*, vol. 31, no. 1, pp. 454–463, 2016.

[17] A. Thangali, H. Prasad, S. Kethamakka, D. Demirdjian, and N. Checka, "AESOP: Adaptive Event detection SOftware using Programming by example," in *Proceedings of the IEEE International Symposium on Technologies for Homeland Security, HST 2015*, Waltham, Mass, USA, April 2015.

[18] P. Kundur, *Power System Stability And Control [M.S. thesis]*, McGraw-Hill Education, 1994.

Hindawi
Journal of Control Science and Engineering
Volume 2018, Article ID 8198603, 17 pages
https://doi.org/10.1155/2018/8198603

Research Article

Nonfragile H_∞ Filter Design for Nonlinear Continuous-Time System with Interval Time-Varying Delay

Zhongda Lu,[1,2] **Guoliang Zhang**,[1] **Yi Sun**,[3] **Jie Sun**,[3] **Fangming Jin**,[3] **and Fengxia Xu**[1]

[1]*College of Mechatronic Engineering, Qiqihar University, Qiqihar 161006, China*
[2]*College of Computer Science and Technology, Harbin University of Science and Technology, Harbin 150080, China*
[3]*State Grid Heilongjiang Electric Power Company Qiqihar Power Supply Company, Qiqihar 161006, China*

Correspondence should be addressed to Zhongda Lu; luzhongda@163.com

Received 9 May 2018; Revised 18 July 2018; Accepted 2 August 2018; Published 5 September 2018

Academic Editor: Jongrae Kim

This paper investigates nonfragile H_∞ filter design for a class of continuous-time delayed Takagi-Sugeno (T-S) fuzzy systems with interval time-varying delays. Filter parameters occur multiplicative gain variations according to the filter's implementation, to handle this variations, a nonfragile H_∞ filter is presented and a novel filtering error system is established. The nonfragile H_∞ filter guarantees the filtering error system to be asymptotically stable and satisfies given H_∞ performance index. By constructing a novel Lyapunov-Krasovskii function and using the linear matrix inequality (LMI), delay-dependent conditions are exploited to derive sufficient conditions for nonfragile designing H_∞ filter. Using new matrix decoupling method to reduce the computational complexity, the filter parameters can be obtained by solving a set of linear matrix inequalities (LMIs). Finally, numerical examples are given to show the effectiveness of the proposed method.

1. Introduction

As we all known, in practical control systems, nonlinearity and time delay phenomena are often encountered in various industry and control system, such as networked control system and mechanical drive control system. The control of nonlinear systems has been explored and studied by many scholars in related fields. T-S fuzzy model is a powerful tool to deal with nonlinearity; much effort has been devoted on the networked control system for T-S fuzzy system or time-delayed (see [1–4]). The actuator and sensor faults estimation based on T-S fuzzy model with unmeasurable premise variables were investigated in [5]. The problem of exponential stabilization for sampled-data T-S fuzzy control systems with packet dropouts was investigated in [6]; a switched system approach is proposed to model the data-missing phenomenon. There always exist many kinds of noise interference in the process of transmission among real industrial control system's signal, causing the error between the obtained signals and the desired signals; in order to obtain the accurate data information about the control signal and eliminate the influence of disturbances on the system, it is essential to be filtering. At present, there are the Kalman filtering, fault detection filter, L_2 filtering, H_∞ filtering, and so on. Compared with other filtering methods, H_∞ filtering does not need the exactly known statistics of the external disturbance [7, 8] and H_∞ filtering has excellent robustness against unmodeled dynamics. In recent years, H_∞ filtering system based on the Takagi-Sugeno (T-S) model has attracted much attention from the control community [9, 10], many studies have addressed H_∞ filtering for T-S fuzzy systems with time-varying delay, and the proposed H_∞ filtering technology has been applied to many actual communications system. Authors in literature [11–13] investigated the problem of H_∞ filter design for continuous-time via Takagi-Sugeno fuzzy model approach. In literature [14, 15], the problem of H_∞ filtering for a class of discrete fuzzy system has been reported. Based on discrete inequality technique and the Lyapunov-Krasovskii functional approach, sufficient conditions for the existence of admissible filters are established in terms of linear matrix inequalities. In literature [16], the event-triggered H_∞ filtering for networked

control systems with quantization and network-induced delays was investigated; it improved the usage of network resource.

However, in practical system, it is difficult for an exactly implemented filter to meet the actual requirements because inaccuracies or uncertainties, which include collection error and component aging, may occur during filter implementation. It often degrades the performance of the control system and even instability; the filter has a higher sensitivity to the parameter uncertainty [17]. Thus, we need to design nonfragile H_∞ filter considering the parameter variation and uncertainty. Some achievements have been reported in journal about nonfragile H_∞ filtering for T-S fuzzy systems with time-varying delay. In literature [18], design an H_∞ filter with the gain variations such that the filtering error system was quadratically D stable and guarantees a prescribed H_∞ performance level. Literature [19] is concerned with the problem of nonfragile H_∞ filtering for discrete-time nonlinear systems and considered additive interval uncertainty. In literature [20], the designed nonfragile H_∞ filter was in standard form and the filter was designed, which have two types of multiplicative gain variations; these models were in standard form. In literature [21], the problem of nonfragile H_∞ filter design for linear continuous-time systems was studied; it proposed a notion of structured vertex separator. In literature [22], this paper studied the nonfragile H_∞ filtering problem for a class of discrete-time T-S fuzzy systems with both randomly occurring gain variations and channel fading. In literature [23], the problem of nonfragile H_∞ filter design for linear continuous-time systems has been studied. The filter has been designed; it included additive gain variations. In literature [24], it studied the nonfragile filtering design for a kind of fuzzy stochastic system with time-varying delay and parameter uncertainties. Sufficient conditions for stochastic input-to-state stability (SISS) of the fuzzy stochastic systems were obtained. Papers proposed the filter design methods with occurring additive gain variations according to the filter's implementation.

Motivated by the aforementioned discussion, in this paper, a nonfragile H_∞ filter design method is proposed to enhance the nonfragility of the filter. By considering the multiplicative gain variations and interval time-varying delays according to the filter implementation, a novel filtering error system is established. Different from some existing works, Jensen's inequality is used to tackle the integral items of the derivative of Lyapunov-Krasovskii; a more relaxed H_∞ performance stability criterion is derived. By constructing a novel Lyapunov-Krasovskii function and using the linear matrix inequality (LMI), delay-dependent conditions are exploited to derive sufficient conditions for nonfragile designing H_∞ filter. Our objective is to design nonfragile H_∞ filter which guarantees the filtering error system to be asymptotically stable and satisfies given H_∞ performance index. The filter parameters can be obtained by solving a set of linear matrix inequalities (LMIs).

The rest of this paper is organized as follows. The problem formulation is stated in Section 2; nonfragile filter scheme and filtering error system are employed to enhance system's stabilization. Stability analysis and fuzzy filter design are obtained in Section 3; by constructing a Lyapunov-Krasovskii functional, a new stability criterion is proposed to prove being less conservative than the existing ones. An applicable H_∞ filter is designed in Section 4, which guarantees stability and a desire performance of the filtering error system. In order to show the effectiveness of the proposed method, simulation results are presented in Section 5.

2. Problem Formulation

Consider a nonlinear system with time-varying delay which could be approximated by a class of T-S fuzzy systems with time-varying delays. The T-S fuzzy model with plant rules can be described by the following.

Plant Rule i. If $\theta_1(t)$ is M_{i1}... and $\theta_r(t)$ is M_{ip}, then

$$\begin{aligned} \dot{x}(t) &= A_i x(t) + A_{\tau i} x(t - \tau(t)) + B_i \omega(t) \\ y(t) &= C_i x(t) + C_{\tau i} x(t - \tau(t)) + D_i \omega(t) \\ z(t) &= E_i x(t) \end{aligned} \tag{1}$$

$x(t) = \varphi(t)$, where $\varphi(t)$ is the continuous initial vector function defined on $[-\tau_2, 0]$, M_{ij} are the fuzzy sets, $i = 1, 2, 3, \ldots, r$, and $j = 1, 2, 3, \ldots, p$ is the number of IF-THEN rules. $\theta_1(t), \theta_2(t) \ldots \theta_r(t)$ are the premise variables, $x(t) \in R^n$ is the state vector, $y(t) \in R^m$ is the measured output, $z(t) \in R^p$ is the signal vector to be estimated, $\omega(t) \in R^q$ is the disturbance signal vector which belongs to $\omega(t) \in l_2[0, \infty)$, and A_i, $A_{\tau i}$, B_i, $B_{\tau i}$, C_i, $C_{\tau i}$, D_i, $D_{\tau i}$, E_i are known constant matrices with appropriate dimensions. $\tau(t)$ is interval time-varying delay that satisfies the following inequality: $\tau_1 \le \tau(t) < \tau_2$, $\dot{\tau}(t) \le d$ where τ_1, τ_2, and d are constant scalars.

By employing the commonly used center-average defuzzifier, product interference, and singleton fuzzifier, the overall fuzzy model is inferred as follows:

$$\begin{aligned} &\dot{x}(t) \\ &\quad = \sum_{i=1}^{r} h_i(\theta(t)) \left[A_i x(t) + A_{\tau i} x(t - \tau(t)) + B_i \omega(t) \right] \\ &y(t) \\ &\quad = \sum_{i=1}^{r} h_i(\theta(t)) \left[C_i x(t) + C_{\tau i} x(t - \tau(t)) + D_i \omega(t) \right] \\ &z(t) = \sum_{i=1}^{r} h_i(\theta(t)) \left[E_i x(t) \right] \end{aligned} \tag{2}$$

where $\theta = [\theta_1, \ldots, \theta_r]^T$, $h_i(\theta(t)) = h_i(\theta(t)) / \sum_i^r h_i(\theta(t))$, $h_i(\theta(t)) = \prod_{j=1}^{p} M_{ij}(\theta_j(t))$, $M_{ij}(\bullet)$ represents the grade of membership for $\theta_j(t)$ in M_{ij}, $0 \le h_i(\theta(t)) \le 1$ (i = 1, 2, ..., r), and $\sum_{i=1}^{r} h_i(\theta(t)) > 0$. It can be seen that $h_i(\theta(t)) \ge 0$ (i = $1, 2, \ldots, r$), $\sum_{i=1}^{r} h_i(\theta(t)) = 1$.

Consider the nonfragile fuzzy filter with multiplicative gain uncertainties; we design the following fuzzy H_∞ filter:

$$\begin{aligned}\dot{x}_{fi}(\mathrm{t}) &= \left(A_{fi} + \Delta A_{fi}(\mathrm{t})\right) x_f(\mathrm{t}) \\ &\quad + \left(B_{fi} + \Delta B_{fi}(\mathrm{t})\right) y(\mathrm{t}) \\ z_{fi}(\mathrm{t}) &= \left(C_{fi} + \Delta C_{fi}(\mathrm{t})\right) x_f(\mathrm{t})\end{aligned} \tag{3}$$

Consider the following H_∞ filter form which is analogous to the fuzzy control form through parallel distributed compensation.

Plant Rule i. If $\theta_1(t)$ is M_{i1}... and $\theta_p(t)$ is M_{ip}, then

$$\begin{aligned}\dot{x}_f(t) &= \sum_{i=1}^{r} h_i(\theta(\mathrm{t})) \\ &\quad \cdot \left[\left(A_{fi} + \Delta A_{fi}(\mathrm{t})\right) x_f(\mathrm{t}) + \left(B_{fi} + \Delta B_{fi}(\mathrm{t})\right) y(\mathrm{t})\right] \\ z_f(t) &= \sum_{i=1}^{r} h_i(\theta(\mathrm{t}))\left(C_{fi} + \Delta C_{fi}(\mathrm{t})\right) x_f(\mathrm{t})\end{aligned} \tag{4}$$

$x_f(0) = x_{f0}$, where x_{f0} is the continuous initial vector function, $x_f(\mathrm{t}) \in R^n$ is the filter state vector, the estimated signal vector $z(\mathrm{t})$ is $z_f(\mathrm{t})$, and A_{fi}, B_{fi}, C_{fi}, $i = 1, 2, 3, \ldots, r$ are the filter parameters. $\Delta A_{fi}(\mathrm{t})$, $\Delta B_{fi}(\mathrm{t})$, $\Delta C_{fi}(\mathrm{t})$ represent the gain variations.

The multiplicative gain uncertainties are defined as

$$\begin{aligned}\Delta A_{fi}(\mathrm{t}) &= A_{fi} M_{1i} K_A(\mathrm{t}) N_{1i} \\ \Delta B_{fi}(\mathrm{t}) &= B_{fi} M_{2i} K_B(\mathrm{t}) N_{2i} \\ \Delta C_{fi}(\mathrm{t}) &= C_{fi} M_{3i} K_C(\mathrm{t}) N_{3i}\end{aligned} \tag{5}$$

where M_{1i}, N_{1i}, M_{2i}, N_{2i}, M_{3i}, N_{3i} are constant matrices with appropriate dimensions and $K_A(\mathrm{t})$, $K_B(\mathrm{t})$, $K_C(\mathrm{t})$ are uncertain matrices bounded, such that

$$\begin{aligned}K_A^T(\mathrm{t}) K_A(\mathrm{t}) &< I, \\ K_B^T(\mathrm{t}) K_B(\mathrm{t}) &< I, \\ K_C^T(\mathrm{t}) K_C(\mathrm{t}) &< I.\end{aligned} \tag{6}$$

By combining (2) with (4), we can obtain the following filtering error system:

$$\begin{aligned}\dot{\xi}(\mathrm{t}) &= \overline{A}(\mathrm{t})\xi(\mathrm{t}) + \overline{A}_\tau(\mathrm{t})\xi(\mathrm{t} - \tau(\mathrm{t})) + \overline{B}(\mathrm{t})\omega(\mathrm{t}) \\ e(\mathrm{t}) &= z(\mathrm{t}) - z_f(\mathrm{t}) = \overline{E}(\mathrm{t})\xi(\mathrm{t})\end{aligned} \tag{7}$$

where

$$\xi(\mathrm{t}) = \left[x^T(\mathrm{t}) \;\; x_f^T(\mathrm{t})\right]^T$$

$$\begin{aligned}\overline{A}(\mathrm{t}) &= \widehat{A}(\mathrm{t}) + \Delta\widehat{A}(\mathrm{t}) \\ &= \begin{bmatrix} A(\mathrm{t}) & 0 \\ B_f(\mathrm{t}) C(\mathrm{t}) & A_f(\mathrm{t}) \end{bmatrix} \\ &\quad + \begin{bmatrix} 0 & 0 \\ \Delta B_f(\mathrm{t}) C(\mathrm{t}) & \Delta A_f(\mathrm{t}) \end{bmatrix}\end{aligned}$$

$$\begin{aligned}\overline{A}_\tau(\mathrm{t}) &= \widehat{A}_\tau(\mathrm{t}) + \Delta\widehat{A}_\tau(\mathrm{t}) \\ &= \begin{bmatrix} A_\tau(\mathrm{t}) & 0 \\ B_f(\mathrm{t}) C_\tau(\mathrm{t}) & 0 \end{bmatrix} + \begin{bmatrix} 0 & 0 \\ \Delta B_f(\mathrm{t}) C_\tau(\mathrm{t}) & 0 \end{bmatrix}\end{aligned}$$

$$\begin{aligned}\overline{B}(\mathrm{t}) &= \widehat{B}(\mathrm{t}) + \Delta\widehat{B}(\mathrm{t}) \\ &= \begin{bmatrix} B(\mathrm{t}) \\ B_f(\mathrm{t}) D(\mathrm{t}) \end{bmatrix} + \begin{bmatrix} 0 \\ \Delta B_f(\mathrm{t}) D(\mathrm{t}) \end{bmatrix}\end{aligned}$$

$$\begin{aligned}\overline{E}(\mathrm{t}) &= \widehat{E}(\mathrm{t}) + \Delta\widehat{E}(\mathrm{t}) \\ &= \left[E(\mathrm{t}) \;\; -C_f(\mathrm{t})\right] + \left[0 \;\; -\Delta C_f(\mathrm{t})\right]\end{aligned}$$

$$\widehat{A}(t) = \sum_{i=1}^{r}\sum_{j=1}^{r} h_i h_j \begin{bmatrix} A_j & 0 \\ B_{fi} C_j & A_{fi} \end{bmatrix} = \begin{bmatrix} A(t) & 0 \\ B_f(t) C(t) & A_f(t) \end{bmatrix}$$

$$\widehat{A}_\tau(t) = \sum_{i=1}^{r}\sum_{j=1}^{r} h_i h_j \begin{bmatrix} A_{\tau j} & 0 \\ B_{fi} C_{\tau j} & 0 \end{bmatrix} = \begin{bmatrix} A_\tau(t) & 0 \\ B_f(t) C_\tau(t) & 0 \end{bmatrix}$$

$$\widehat{B}(t) = \sum_{i=1}^{r}\sum_{j=1}^{r} h_i h_j \begin{bmatrix} B_j \\ B_{fi} D_j \end{bmatrix} = \begin{bmatrix} B(t) \\ B_f(t) D(t) \end{bmatrix}$$

$$\widehat{E}(t) = \sum_{i=1}^{r}\sum_{j=1}^{r} h_i h_j \left[E_j \;\; -C_{fi}\right] = \left[E(t) \;\; -C_f(t)\right]$$

$$\Delta\widehat{A}(t) = \sum_{i=1}^{r}\sum_{j=1}^{r} h_i h_j \begin{bmatrix} 0 & 0 \\ \Delta B_{fi} C_j & \Delta A_{fi} \end{bmatrix} = \begin{bmatrix} 0 & 0 \\ \Delta B_f(t) C(t) & \Delta A_f(t) \end{bmatrix}$$

$$\Delta\widehat{A}_\tau(t) = \sum_{i=1}^{r}\sum_{j=1}^{r} h_i h_j \begin{bmatrix} 0 & 0 \\ \Delta B_{fi} C_{\tau j} & 0 \end{bmatrix} = \begin{bmatrix} 0 & 0 \\ \Delta B_f(t) C_\tau(t) & 0 \end{bmatrix}$$

$$\Delta\widehat{B}(t) = \sum_{i=1}^{r}\sum_{j=1}^{r} h_i h_j \begin{bmatrix} 0 \\ \Delta B_{fi} D_j \end{bmatrix} = \begin{bmatrix} 0 \\ \Delta B_f(t) D(t) \end{bmatrix}$$

$$\Delta\widehat{E}(t) = \sum_{i=1}^{r}\sum_{j=1}^{r} h_i h_j \begin{bmatrix} 0 & -\Delta C_{fi} \end{bmatrix} = \begin{bmatrix} 0 & -\Delta C_f(t) \end{bmatrix} \tag{8}$$

In this paper, our purpose is to design the fuzzy H_∞ filter in the form of (3), meanwhile, satisfying the following requirements.

(1) The filtering error system (7) with $\omega(t) = 0$ is said to be asymptotic stability for any initial condition

(2) For a given positive scalar $\gamma > 0$, the filtering error system (7) is said to be asymptotically stable with guaranteed H_∞ performance γ, if it is asymptotic stability and the filtering error $e(\mathrm{t})$ satisfies

$$\int_0^L \|e(t)\|^2 dt \le \gamma^2 \int_0^L \|\omega(t)\|^2 dt \tag{9}$$

for all $L > 0$ and nonzero $\omega(t) \in L_2[0, \infty)$ subject to the zero initial condition.

3. Stability and H_∞ Filtering Performance Analysis

The purpose of this paper is to design nonfragile H_∞ filter such that the filtering error system (7) is asymptotically stable with H_∞ performance index. A sufficient condition is presented in the following theorem to guarantee the existence of the filter in form of (3).

Lemma 1. *Let X, Y, and K be real matrices with appropriate dimensions and $K_i^T(\mathrm{t})K_i(\mathrm{t}) < I$. Then, for any scalar $\delta > 0$,*

$$XK(\mathrm{t})Y + Y^T K(\mathrm{t}) X^T \le \varepsilon XX^T + \varepsilon^{-1} Y^T Y \tag{10}$$

Lemma 2. *For any vectors $x, y \in R^n$ and any scalar $\varepsilon > 0$, matrices D, F, E are real matrices of appropriate dimensions with $F^T(\mathrm{t})F(\mathrm{t}) < I$; then the following inequalities hold:*

$$2xDF(\mathrm{t})Ey \le \varepsilon x^T DD^T x + \varepsilon^{-1} y^T EE^T y \tag{11}$$

Lemma 3. *Let V, H, E, Q, and F be real matrices of appropriate dimensions such that $Q > 0$ and $F^T F \le I$. Then, for any scalar $\varepsilon > 0$ such that $Q^{-1} - \varepsilon HH^T > 0$, we have*

$$\begin{aligned} &(V + HFE)^T Q (V + HFE) \\ &\quad \le V^T \left(Q^{-1} - \varepsilon HH^T\right)^{-1} V + \varepsilon^{-1} E^T E \end{aligned} \tag{12}$$

Lemma 4. *Let $P > 0$ and A_i, A_l be any real matrices of appropriate dimensions. Then*

$$A_i^T P A_l + A_l^T P A_i \le A_i^T P A_i + A_l^T P A_l \tag{13}$$

Lemma 5 (Jenson's inequality). *Suppose $\tau_1 \le \tau(\mathrm{t}) \le \tau_2$ and $x(\mathrm{t}) \in \mathfrak{R}^n$; for any positive matrix $R \in \mathfrak{R}^{n\times n}$, the following inequality holds:*

$$\begin{aligned} &-(\tau_2 - \tau_1)\int_{t-\tau_2}^{t-\tau_1} \dot{x}^T(\mathrm{s}) R \dot{x}(\mathrm{s})\, ds \\ &\quad \le \begin{bmatrix} x(t-\tau_1) \\ x(t-\tau_2) \end{bmatrix}^T \begin{bmatrix} -R & R \\ R & -R \end{bmatrix} \begin{bmatrix} x(t-\tau_1) \\ x(t-\tau_2) \end{bmatrix} \end{aligned} \tag{14}$$

Theorem 6. *For nonlinear systems (1) and the filtering error system (7), the given positive scalar H_∞ performance γ and the filtering error system (7) are asymptotically stable with H_∞ performance γ if there exist symmetric positive scalars $\varepsilon_2 > 0$, $\varepsilon_6 > 0$, $\varepsilon_{10} > 0$, $\varepsilon_{29} > 0$, $\varepsilon_{15} > 0$, $\varepsilon_{25} > 0$, $\varepsilon_{20} > 0$, $\varepsilon_{21} > 0$, $\varepsilon_{22} > 0$, $\varepsilon_{11} > 0$, $\varepsilon_{12} > 0$ and symmetric positive definite matrices $\widehat{P} > 0$, $\widehat{Q}_1 > 0$, $\widehat{Q}_2 > 0$, $\widehat{Q}_3 > 0$, $\widehat{R}_1 > 0$, $\widehat{R}_2 > 0$ such that we have the following inequality.*

$$\begin{bmatrix} I & \widetilde{M}_3 \\ * & \varepsilon_{20}^{-1} \end{bmatrix} > 0 \tag{15}$$

$$\begin{bmatrix} \widehat{R}_1^{-1} & \widetilde{M}_2 \\ * & \varepsilon_{1k}^{-1} \end{bmatrix} > 0, \quad (k = 5, 9) \tag{16}$$

$$\begin{bmatrix} \widehat{R}_2^{-1} & \widetilde{M}_2 \\ * & \varepsilon_{2k}^{-1} \end{bmatrix} > 0, \quad (k = 5, 9) \tag{17}$$

$$\begin{bmatrix} \widehat{R}_1^{-1} & \alpha_{11}\widetilde{M}_1 & \alpha_{12}\widetilde{M}_2 \\ * & I & 0 \\ * & * & I \end{bmatrix} > 0 \tag{18}$$

$$\begin{bmatrix} \widehat{R}_2^{-1} & \alpha_{21}\widetilde{M}_1 & \alpha_{22}\widetilde{M}_2 \\ * & I & 0 \\ * & * & I \end{bmatrix} > 0 \tag{19}$$

$$\Phi = \begin{bmatrix} \Phi_{11} & \Phi_{12} & \widehat{R}_1 & 0 & \Phi_{15} \\ * & \Phi_{22} & 0 & 0 & 0 \\ * & * & \Phi_{33} & 0 & 0 \\ * & * & * & \Phi_{44} & 0 \\ * & * & * & * & \Phi_{55} \end{bmatrix} < 0 \tag{20}$$

$$\begin{aligned} \Phi_{11} &= \widehat{P}\widehat{A}(\mathrm{t}) + \widehat{A}^T(\mathrm{t})\widehat{P} + \widehat{Q}_1 + \widehat{Q}_2 + \widehat{Q}_3 - \widehat{R}_1 \\ &\quad + \widehat{E}^T(\mathrm{t})\left[I - \varepsilon_{20}\widetilde{M}_3\widetilde{M}_3^T\right]^{-1}\widehat{E}(\mathrm{t}) + \alpha_4^2\widehat{P}\widetilde{M}_2\widetilde{M}_2^T\widehat{P} \\ &\quad + \alpha_3^2\widehat{P}\widetilde{M}_1\widetilde{M}_1^T\widehat{P} + \alpha_5^2\widetilde{N}_1\widetilde{N}_1 + \alpha_6^2\widetilde{N}_2\widetilde{N}_2 \end{aligned}$$

$$
\begin{aligned}
&+\beta_1^2\widehat{A}^T(t)\left[\widehat{R}_1^{-1}-\varepsilon_{11}\widetilde{M}_1\widetilde{M}_1^T-\varepsilon_{12}\widetilde{M}_2\widetilde{M}_2^T\right]^{-1}\widehat{A}(t)\\
&+\beta_2^2\widehat{A}^T(t)\left[\widehat{R}_2^{-1}-\varepsilon_{21}\widetilde{M}_1\widetilde{M}_1^T-\varepsilon_{22}\widetilde{M}_2\widetilde{M}_2^T\right]^{-1}\widehat{A}(t)\\
&+\varepsilon_{20}^{-1}\widetilde{N}_3^T\widetilde{N}_3\\
\Phi_{12}&=\widehat{P}\widehat{A}_\tau(t),\\
\Phi_{15}&=\widehat{P}\widehat{B}(t),\\
\Phi_{33}&=-\widehat{Q}_2-\left(\widehat{R}_1+\widehat{R}_2\right),\\
\Phi_{44}&=-\widehat{Q}_3-\widehat{R}_2,\\
\Phi_{22}&\\
&=-(1-d)\widehat{Q}_1+\alpha_2^2\widetilde{N}_{2\tau}^T\widetilde{N}_{2\tau}\\
&+\beta_1^2\widehat{A}_\tau^T(t)\left[\widehat{R}_1^{-1}-\varepsilon_{15}\widetilde{M}_2\widetilde{M}_2^T\right]^{-1}\widehat{A}_\tau(t)\\
&+\beta_2^2\widehat{A}_\tau^T(t)\left[\widehat{R}_2^{-1}-\varepsilon_{25}\widetilde{M}_2\widetilde{M}_2^T\right]^{-1}\widehat{A}_\tau(t),\\
\Phi_{55}&\\
&=\alpha_1^2\widetilde{N}_{2D}^T\widetilde{N}_{2D}-\gamma^2 I\\
&+\beta_1^2\widehat{B}_\tau^T(t)\left[\widehat{R}_1^{-1}-\varepsilon_{19}\widetilde{M}_2\widetilde{M}_2^T\right]^{-1}\widehat{B}_\tau(t)\\
&+\beta_2^2\widehat{B}_\tau^T(t)\left[\widehat{R}_2^{-1}-\varepsilon_{29}\widetilde{M}_2\widetilde{M}_2^T\right]^{-1}\widehat{B}_\tau(t)\\
\widetilde{M}_1&=\begin{bmatrix}0\\A_f(t)M_1\end{bmatrix},\\
\widetilde{M}_2&=\begin{bmatrix}0\\B_f(t)M_2\end{bmatrix},\\
\widetilde{M}_3&=M_3,\\
\widetilde{N}_1&=\begin{bmatrix}0 & N_1\end{bmatrix},\\
\widetilde{N}_2&=\begin{bmatrix}N_2C(t) & 0\end{bmatrix},\\
\widetilde{N}_{2\tau}&=\begin{bmatrix}N_2C_\tau(t) & 0\end{bmatrix},\\
\widetilde{N}_{2\tau}&=\begin{bmatrix}N_2C_\tau(t) & 0\end{bmatrix},\\
\widetilde{N}_{2D}&=N_2D(t),\\
\widetilde{N}_3&=\begin{bmatrix}0 & -N_3C_f(t)\end{bmatrix},\\
\beta_1&=\sqrt{3\tau_1^2},\\
\beta_2&=\sqrt{3\left(\tau_2^2-\tau_1^2\right)},\\
\alpha_1&=\sqrt{\beta_1^2\varepsilon_{19}^{-1}+\beta_2^2\varepsilon_{29}^{-1}+\varepsilon_{10}^{-1}},\\
\alpha_2&=\sqrt{\beta_1^2\varepsilon_{15}^{-1}+\beta_2^2\varepsilon_{25}^{-1}+\varepsilon_6^{-1}},\\
\alpha_3&=\sqrt{\varepsilon_{21}},\\
\alpha_4&=\sqrt{\varepsilon_2+\varepsilon_6+\varepsilon_{10}},\\
\alpha_5&=\sqrt{\varepsilon_{21}^{-1}+\beta_1^2\varepsilon_{11}^{-1}+\beta_2^2\varepsilon_{22}^{-1}},\\
\alpha_6&=\sqrt{\beta_1^2\varepsilon_{12}^{-1}+\beta_2^2\varepsilon_{22}^{-1}}
\end{aligned}
\tag{21}
$$

Proof. We construct a novel Lyapunov-Krasovskii function as follows:

$$
\begin{aligned}
V(\xi(t))&=\xi^T(t)\widehat{P}\xi(t)+\int_{t-\tau(t)}^{t}\xi^T(s)\widehat{Q}_1\xi(s)\,ds\\
&+\int_{t-\tau_1}^{t}\xi^T(s)\widehat{Q}_2\xi(s)\,ds\\
&+\int_{t-\tau_2}^{t}\xi^T(s)\widehat{Q}_3\xi(s)\,ds\\
&+\tau_1\int_{-\tau_1}^{0}\int_{t+\theta}^{t}\dot{\xi}^T(s)\widehat{R}_1\dot{\xi}(s)\,ds\,d\theta\\
&+(\tau_2-\tau_1)\int_{-\tau_2}^{-\tau_1}\int_{t+\theta}^{t}\dot{\xi}^T(s)\widehat{R}_2\dot{\xi}(s)\,ds\,d\theta
\end{aligned}
\tag{22}
$$

$$
\begin{aligned}
\dot{V}&=2\xi^T(t)\widehat{P}\overline{A}(t)\xi(t)\\
&+2\xi^T(t)\widehat{P}\overline{A}_\tau(t)\xi(t-\tau(t))\\
&+2\xi^T(t)\widehat{P}\overline{B}(t)\omega(t)\\
&+\xi^T(t)\left(\widehat{Q}_1+\widehat{Q}_2+\widehat{Q}_3\right)\xi(t)\\
&-(1-\dot{\tau}(t))\xi^T(t-\tau(t))\widehat{Q}_1\xi(t-\tau(t))\\
&-\xi^T(t-\tau_1)\widehat{Q}_2\xi(t-\tau_1)\\
&-\xi^T(t-\tau_2)\widehat{Q}_3\xi(t-\tau_2)\\
&+\tau_1^2\dot{\xi}^T(t)\widehat{R}_1\dot{\xi}(t)\\
&+(\tau_2-\tau_1)^2\dot{\xi}^T(t)\widehat{R}_2\dot{\xi}(t)\\
&-\tau_1\int_{t-\tau_1}^{t}\dot{\xi}^T(s)\widehat{R}_1\dot{\xi}(s)\,ds\\
&-(\tau_2-\tau_1)\int_{t-\tau_1}^{t}\dot{\xi}^T(s)\widehat{R}_2\dot{\xi}(s)\,ds\\
\dot{V}&\le 2\xi^T(t)\widehat{P}\widehat{A}(t)\dot{\xi}(t)+2\xi^T(t)\widehat{P}\Delta\widehat{A}(t)\xi(t)\\
&+2\xi^T(t)\widehat{P}(t)\widehat{A}_\tau(t)\xi(t-\tau(t))\\
&+\xi^T(t)\left(\widehat{Q}_1+\widehat{Q}_2+\widehat{Q}_3\right)\xi(t)\\
&+2\xi^T(t)\widehat{P}\Delta\widehat{B}(t)\omega(t)
\end{aligned}
\tag{23}
$$

$$
\begin{aligned}
&+ 2\xi^T(t)\,\widehat{P}(t)\,\Delta\widehat{A}_\tau(t)\,\xi(t-\tau(t))\\
&- (1-d)\,\xi^T(t-\tau(t))\,\widehat{Q}_1\xi(t-\tau(t))\\
&- \xi^T(t-\tau_1)\,\widehat{Q}_2\xi(t-\tau_1)\\
&+ 2\xi^T(t)\,\widehat{P}\widehat{B}(t)\,\omega(t)\\
&- \xi^T(t-\tau_2)\,\widehat{Q}_3\xi(t-\tau_2)\\
&+ \tau_1^2\dot{\xi}^T(t)\,\widehat{R}_1\dot{\xi}(t)\\
&+ (\tau_2-\tau_1)^2\,\dot{\xi}^T(t)\,\widehat{R}_2\dot{\xi}(t)\\
&- \tau_1\int_{t-\tau_1}^{t}\dot{\xi}^T(s)\,\widehat{R}_1\dot{\xi}(s)\,ds\\
&- (\tau_2-\tau_1)\int_{t-\tau_2}^{t-\tau_1}\dot{\xi}^T(s)\,\widehat{R}_2\dot{\xi}(s)\,ds
\end{aligned}
\tag{24}
$$

By Lemma 2, for $\forall\varepsilon_2>0$, $\forall\varepsilon_{21}>0$, we can obtain

$$
\begin{aligned}
2\xi^T(t)\,\widehat{P}\Delta\widehat{A}(t)\,\xi(t) &= 2\xi^T(t)\,\widehat{P}\left[\widetilde{M}_{2i}K_i(t)\,\widetilde{N}_{2i}\right.\\
&\left.+\widetilde{M}_{1i}K_i(t)\,\widetilde{N}_{1i}\right]\xi(t) \le \xi^T(t)\left[\varepsilon_2\widehat{P}\widetilde{M}_2\widetilde{M}_2^T\widehat{P}\right.\\
&\left.+\varepsilon_{21}\widehat{P}\widetilde{M}_1\widetilde{M}_1^T\widehat{P}+\varepsilon_2^{-1}\widetilde{N}_2^T\widetilde{N}_2+\varepsilon_{21}^{-1}\widetilde{N}_1^T\widetilde{N}_1\right]\xi(t)
\end{aligned}
\tag{25}
$$

Similar to (25), if there exists $\forall\varepsilon_{20}>0$, we can obtain

$$
\begin{aligned}
e^T(t)\,e(t) &= \xi^T(t)\,\overline{E}^T(t)\,\overline{E}(t)\,\xi(t)\\
&= \xi^T(t)\left(\widehat{E}(t)+\Delta\widehat{E}(t)\right)^T\left(\widehat{E}(t)+\Delta\widehat{E}(t)\right)\xi(t)\\
&\le \xi^T(t)\,\widehat{E}^T(t)\left(I-\varepsilon_{20}\widetilde{M}_3\widetilde{M}_3^T\right)^{-1}\widehat{E}(t)\,\xi(t)\\
&\quad+\varepsilon_{20}^{-1}\xi^T(t)\,\widetilde{N}_3^T\widetilde{N}_3\xi(t)
\end{aligned}
\tag{26}
$$

By Lemma 2, if there exists $\forall\varepsilon_6>0$, we can obtain

$$
\begin{aligned}
&2\xi^T(t)\,\widehat{P}\Delta\widehat{A}_\tau(t)\,\xi(t-\tau(t))\\
&\quad= 2\xi^T(t)\,\widehat{P}\left[\widetilde{M}_2K_i(t)\,\widetilde{N}_{2\tau}\right]\xi(t-\tau(t))\\
&\quad\le \xi^T(t)\left[\varepsilon_6\widehat{P}\widetilde{M}_2\widetilde{M}_2^T\widehat{P}\right]\xi(t)\\
&\qquad+\xi^T(t-\tau(t))\left[\varepsilon_6^{-1}\widetilde{N}_{2\tau}^T\widetilde{N}_{2\tau}\right]\xi(t-\tau(t))
\end{aligned}
\tag{27}
$$

Similar to (25), if there exists $\forall\varepsilon_{10}>0$, we can obtain

$$
\begin{aligned}
2\xi^T(t)\,\widehat{P}\Delta\widehat{B}(t)\,\omega(t) &= 2\xi^T(t)\,\widehat{P}\left[\widetilde{M}_2K_i(t)\,\widetilde{N}_{2D}\right]\omega(t)\\
&\le \xi^T(t)\left[\varepsilon_{10}\widehat{P}\widetilde{M}_2\widetilde{M}_2^T\widehat{P}\right]\xi(t)\\
&\quad+\omega^T(t)\left[\varepsilon_{10}^{-1}\widetilde{N}_{2D}^T\widetilde{N}_{2D}\right]\omega(t)
\end{aligned}
\tag{28}
$$

Combining with inequalities (25), (27), and (28) gives

$$
\begin{aligned}
&2\xi^T(t)\,\widehat{P}\Delta\widehat{A}(t)\,\xi(t)+2\xi^T(t)\,\widehat{P}\Delta\widehat{A}_\tau(t)\,\xi(t-\tau(t))\\
&\quad+2\xi^T(t)\,\widehat{P}\Delta\widehat{B}(t)\,\omega(t)\le\xi^T(t)\left[\varepsilon_2\widehat{P}\widetilde{M}_2\widetilde{M}_2^T\widehat{P}\right.\\
&\quad\left.+\varepsilon_2^{-1}\widetilde{N}_2\widetilde{N}_2^T+\varepsilon_{21}\widehat{P}\widetilde{M}_1\widetilde{M}_1^T\widehat{P}+\varepsilon_{21}^{-1}\widetilde{N}_1\widetilde{N}_1^T\right]\xi(t)\\
&\quad+\xi^T(t)\left[\varepsilon_{10}\widehat{P}\widetilde{M}_2\widetilde{M}_2^T\widehat{P}\right]\xi(t)+\xi^T(t)\left[\varepsilon_6\widehat{P}\widetilde{M}_2\widetilde{M}_2^T\widehat{P}\right]\\
&\quad\cdot\xi(t)+\xi^T(t-\tau(t))\left[\varepsilon_6^{-1}\widetilde{N}_{2\tau}^T\widetilde{N}_{2\tau}\right]\xi(t-\tau(t))\\
&\quad+\omega^T(t)\left[\varepsilon_{10}^{-1}\widetilde{N}_2^T\widetilde{N}_2\right]\omega(t)
\end{aligned}
\tag{29}
$$

Lemma 4 gives

$$
\begin{aligned}
\tau_1^2\dot{\xi}^T(t)\,\widehat{R}_1\dot{\xi}(t) &= \tau_1^2\left[\overline{A}(t)\,\xi(t)+\overline{A}_\tau(t)\,\xi(t-\tau(t))\right.\\
&\left.+\overline{B}(t)\,\omega(t)\right]^T\widehat{R}_1\left[\overline{A}(t)\,\xi(t)+\overline{A}_\tau(t)\,\xi(t-\tau(t))\right.\\
&\left.+\overline{B}(t)\,\omega(t)\right]\le 3\tau_1^2\xi^T(t)\,\overline{A}^T\widehat{R}_1\overline{A}(t)\,\xi(t)\\
&+3\tau_1^2\xi^T(t-\tau(t))\,\overline{A}_\tau^T(t-\tau(t))\,\widehat{R}_1\overline{A}_\tau(t-\tau(t))\,\xi(t\\
&-\tau(t))+3\tau_1^2\omega^T(t)\,\overline{B}^T(t)\,\widehat{R}_1\overline{B}(t)\,\omega(t)
\end{aligned}
\tag{30}
$$

where

$$
\begin{aligned}
\overline{A}^T(t)\,\widehat{R}_1\overline{A}(t) &= \left[\widehat{A}(t)+\Delta\widehat{A}(t)\right]^T\widehat{R}_1\left[\widehat{A}(t)+\Delta\widehat{A}(t)\right]\\
&= \left[\widehat{A}(t)+\widetilde{M}_2K_i(t)\,\widetilde{N}_2+\widetilde{M}_1K_i(t)\,\widetilde{N}_1\right]^T\\
&\cdot\widehat{R}_1\left[\widehat{A}(t)+\widetilde{M}_2K_i(t)\,\widetilde{N}_2+\widetilde{M}_1K_i(t)\,\widetilde{N}_1\right]
\end{aligned}
\tag{31}
$$

$$
\begin{aligned}
\overline{A}_\tau^T(t)\,\widehat{R}_1\overline{A}_\tau(t) &= \left[\widehat{A}_\tau(t)+\Delta\widehat{A}_\tau(t)\right]^T\\
&\cdot\widehat{R}_1\left[\widehat{A}_\tau(t)+\Delta\widehat{A}_\tau(t)\right]=\left[\widehat{A}_\tau(t)+\widetilde{M}_2K_i(t)\,\widetilde{N}_{2\tau}\right]^T\\
&\cdot\widehat{R}_1\left[\widehat{A}_\tau(t)+\widetilde{M}_2K_i(t)\,\widetilde{N}_{2\tau}\right]
\end{aligned}
\tag{32}
$$

$$
\begin{aligned}
\overline{B}^T(t)\,\widehat{P}\overline{B}(t) &= \left[\widehat{B}_\tau(t)+\Delta\widehat{B}(t)\right]^T\widehat{R}_1\left[\widehat{B}(t)+\Delta\widehat{B}(t)\right]\\
&= \left[\widehat{B}(t)+\widetilde{M}_2K_i(t)\,\widetilde{N}_{2D}\right]^T\\
&\cdot\widehat{R}_1\left[\widehat{B}_\tau(t)+\widetilde{M}_2K_i(t)\,\widetilde{N}_{2D}\right]
\end{aligned}
\tag{33}
$$

By Lemma 3, if there exist $\varepsilon_{11}>0$, $\varepsilon_{12}>0$ such that $\widehat{R}_1^{-1}-\varepsilon_{11}\widetilde{M}_1\widetilde{M}_1^T-\varepsilon_{12}\widetilde{M}_2\widetilde{M}_2^T>0$, from (31), it follows that

$$
\begin{aligned}
&\left[\widehat{A}(t)+\widetilde{M}_2K_i(t)\,\widetilde{N}_2+\widetilde{M}_1K_i(t)\,\widetilde{N}_1\right]^T\\
&\quad\cdot\widehat{R}_1\left[\widehat{A}(t)+\widetilde{M}_2K_i(t)\,\widetilde{N}_2+\widetilde{M}_1K_i(t)\,\widetilde{N}_1\right]
\end{aligned}
$$

$$\leq \left[\widehat{A}^T(t) + \widetilde{M}_2 K_i(t) \widetilde{N}_2\right]^T \left[\widehat{R}_1^{-1} - \varepsilon_{11}\widetilde{M}_1\widetilde{M}_1^T\right]^{-1} \cdot \left[\widehat{A}(t) + \widetilde{M}_2 K_i(t) \widetilde{N}_2\right] + \varepsilon_{11}^{-1}\widetilde{N}_1^T\widetilde{N}_1 \leq \widehat{A}^T(t) \cdot \left[\widehat{R}_1^{-1} - \varepsilon_{11}\widetilde{M}_1\widetilde{M}_1^T - \varepsilon_{12}\widetilde{M}_2\widetilde{M}_2^T\right]^{-1} \widehat{A}(t) + \varepsilon_{12}^{-1}\widetilde{N}_2^T\widetilde{N}_2 + \varepsilon_{11}^{-1}\widetilde{N}_1^T\widetilde{N}_1 \tag{34}$$

By Lemma 3, if there exist $\varepsilon_{15} > 0$, such that $\widehat{R}_1^{-1} - \varepsilon_{15}\widetilde{M}_2\widetilde{M}_2^T > 0$, from (32), it follows that

$$\left[\widehat{A}_\tau(t) + \widetilde{M}_2 K_i(t) \widetilde{N}_{2\tau}\right]^T \widehat{R}_1 \left[\widehat{A}_\tau(t) + \widetilde{M}_2 K_i(t) \widetilde{N}_{2\tau}\right] \leq \widehat{A}_\tau^T(t) \left[\widehat{R}_1^{-1} - \varepsilon_{15}\widetilde{M}_2\widetilde{M}_2^T\right]^{-1} \widehat{A}_\tau(t) + \varepsilon_{15}^{-1}\widetilde{N}_{2\tau}^T\widetilde{N}_{2\tau} \tag{35}$$

By Lemma 3, if there exist $\varepsilon_{19} > 0$ such that $\widehat{R}_1^{-1} - \varepsilon_{19}\widetilde{M}_2\widetilde{M}_2^T > 0$, from (33), we can get

$$\left[\widehat{B}(t) + \widetilde{M}_2 K_i(t) \widetilde{N}_{2D}\right]^T \widehat{R}_1 \left[\widehat{B}_\tau(t) + \widetilde{M}_2 K_i(t) \widetilde{N}_{2D}\right] \leq \widehat{B}^T(t) \left[\widehat{R}_1^{-1} - \varepsilon_{19}\widetilde{M}_2\widetilde{M}_2^T\right]^{-1} \widehat{B}(t) + \varepsilon_{19}^{-1}\widetilde{N}_{2D}^T\widetilde{N}_{2D} \tag{36}$$

Combining with formulas (31)~(36), from (30), we have

$$\tau_1^2\dot{\xi}^T(t)\widehat{R}_1\dot{\xi}(t) \leq \xi^T(t)\left\{3\tau_1^2\widehat{A}^T(t) \cdot \left[\widehat{R}_1^{-1} - \varepsilon_{11}\widetilde{M}_1\widetilde{M}_1^T - \varepsilon_{12}\widetilde{M}_2\widetilde{M}_2^T\right]^{-1}\widehat{A}(t) + \varepsilon_{12}^{-1}\widetilde{N}_2^T\widetilde{N}_2 + \varepsilon_{11}^{-1}\widetilde{N}_1^T\widetilde{N}_1\right\}\xi(t) + \xi^T(t-\tau(t)) \cdot \left[3\tau_1^2\widehat{A}^T{}_\tau(t)\left[\widehat{R}_1^{-1} - \varepsilon_{15}\widetilde{M}_2\widetilde{M}_2^T\right]\widehat{A}_\tau^T(t) + \varepsilon_{15}^{-1}\widetilde{N}_{2\tau}^T\widetilde{N}_{2\tau}\right]\xi^T(t-\tau(t)) + \omega^T(t)\left[3\tau_1^2\widehat{B}^T(t) \cdot \left[\widehat{R}_1^{-1} - \varepsilon_{19}\widetilde{M}_2\widetilde{M}_2^T\right]\widehat{B}(t) + \varepsilon_{19}^{-1}\widetilde{N}_{2D}^T\widetilde{N}_{2D}\right]\omega(t) \tag{37}$$

Similarly, for formula (30) we have

$$(\tau_2-\tau_1)^2\dot{\xi}^T(t)\widehat{R}_2\dot{\xi}(t) \leq \xi^T(t)\left[3(\tau_2-\tau_1)^2\widehat{A}^T(t) \cdot \left[\widehat{R}_2^{-1} - \varepsilon_{21}\widetilde{M}_1\widetilde{M}_1^T - \varepsilon_{22}\widetilde{M}_2\widetilde{M}_2^T\right]^{-1}\widehat{A}(t) + 3(\tau_2-\tau_1)^2\varepsilon_{22}^{-1}\widetilde{N}_2{}^T\widetilde{N}_2 + 3(\tau_2-\tau_1)^2 \cdot \varepsilon_{21}^{-1}\widetilde{N}_1{}^T\widetilde{N}_1\right]\xi(t) + \xi^T(t-\tau(t))\left[3(\tau_2-\tau_1)^2 \cdot \widehat{A}^T(t)\left[\widehat{R}_2^{-1} - \varepsilon_{25}\widetilde{M}_2\widetilde{M}_2^T\right]^{-1}\widehat{A}(t) + 3(\tau_2-\tau_1)^2 \cdot \varepsilon_{25}^{-1}\widetilde{N}_1{}^T\widetilde{N}_1\right]\xi(t-\tau(t)) + \omega^T(t)\left[3(\tau_2-\tau_1)^2 \cdot \widehat{B}^T(t)\left[\widehat{R}_2^{-1} - \varepsilon_{29}\widetilde{M}_2\widetilde{M}_2^T\right]^{-1}\widehat{B}(t) + 3(\tau_2-\tau_1)^2 \cdot \varepsilon_{29}^{-1}\widetilde{N}_{2D}^T\widetilde{N}_{2D}\right]\omega(t) \tag{38}$$

By Lemma 5, according to Jensen's inequality, we have that

$$-\tau_1\int_{t-\tau_1}^{t}\dot{\xi}^T(s)\widehat{R}_1\dot{\xi}(s)\,ds \leq \begin{bmatrix}\xi(t)\\ \xi(t-\tau_1)\end{bmatrix}^T\begin{bmatrix}-\widehat{R}_1 & \widehat{R}_1\\ * & -\widehat{R}_1\end{bmatrix}\begin{bmatrix}\xi(t)\\ \xi(t-\tau_1)\end{bmatrix} \tag{39}$$

$$-(\tau_2-\tau_1)\int_{t-\tau_2}^{t-\tau_1}\dot{\xi}^T(s)\widehat{R}_2\dot{\xi}(s)\,ds \leq \begin{bmatrix}\xi(t-\tau_1)\\ \xi(t-\tau_2)\end{bmatrix}^T\begin{bmatrix}-\widehat{R}_2 & \widehat{R}_2\\ * & -\widehat{R}_2\end{bmatrix}\begin{bmatrix}\xi(t-\tau_1)\\ \xi(t-\tau_2)\end{bmatrix} \tag{40}$$

Combining with formulas (25)~(30), from (23), we have

$$\dot{V}(\xi(t)) \leq \eta^T(t)\overline{\Phi}\eta(t) \tag{41}$$

where

$$\overline{\Phi} = \begin{bmatrix}\overline{\Phi}_{11} & \overline{\Phi}_{12} & \widehat{R}_1 & 0 & \overline{\Phi}_{15}\\ * & \overline{\Phi}_{22} & 0 & 0 & 0\\ * & * & \overline{\Phi}_{33} & 0 & 0\\ * & * & * & \overline{\Phi}_{44} & 0\\ * & * & * & * & \overline{\Phi}_{55}\end{bmatrix} < 0$$

$$\begin{aligned}\overline{\Phi}_{11} &= \widehat{P}\widehat{A}(t) + \widehat{A}^T(t)\widehat{P} + \widehat{Q}_1 + \widehat{Q}_2 + \widehat{Q}_3 - \widehat{R}_1 + \alpha_4^2\widehat{P}\widetilde{M}_2\widetilde{M}_2^T\widehat{P} + \alpha_3^2\widehat{P}\widetilde{M}_1\widetilde{M}_1^T\widehat{P} + \alpha_5^2\widetilde{N}_1\widetilde{N}_1 + \alpha_6^2\widetilde{N}_2\widetilde{N}_2 + \beta_1^2\widehat{A}^T(t)\left[\widehat{R}_1^{-1} - \varepsilon_{11}\widetilde{M}_1\widetilde{M}_1^T - \varepsilon_{12}\widetilde{M}_2\widetilde{M}_2^T\right]^{-1}\widehat{A}(t) + \beta_2^2\widehat{A}^T(t)\left[\widehat{R}_2^{-1} - \varepsilon_{21}\widetilde{M}_1\widetilde{M}_1^T - \varepsilon_{22}\widetilde{M}_2\widetilde{M}_2^T\right]^{-1}\widehat{A}(t)\\ \overline{\Phi}_{12} &= \widehat{P}\widehat{A}_\tau(t),\\ \overline{\Phi}_{15} &= \widehat{P}\widehat{B}(t),\\ \overline{\Phi}_{33} &= -\widehat{Q}_2 - \left(\widehat{R}_1 + \widehat{R}_2\right),\\ \overline{\Phi}_{44} &= -\widehat{Q}_3 - \widehat{R}_2,\\ \overline{\Phi}_{22} &= -(1-d)\widehat{Q}_1 + \varepsilon_6^{-1}\widetilde{N}_{2\tau}^T\widetilde{N}_{2\tau} + \alpha_2^2\widetilde{N}_{1\tau}^T\widetilde{N}_{1\tau} + \beta_1^2\widehat{A}_\tau^T(t)\left[\widehat{R}_1^{-1} - \varepsilon_{15}\widetilde{M}_2\widetilde{M}_2^T\right]^{-1}\widehat{A}_\tau(t)\end{aligned}$$

$$+\beta_2^2\widehat{A}_\tau^T(t)\left[\widehat{R}_2^{-1}-\varepsilon_{25}\widetilde{M}_2\widetilde{M}_2^T\right]^{-1}\widehat{A}_\tau(t)$$

$$\overline{\Phi}_{55}$$

$$=\alpha_1^2\widetilde{N}_{2D}^T\widetilde{N}_{2D}+\beta_1^2\widehat{B}^T(t)\left[\widehat{R}_1^{-1}-\varepsilon_{19}\widetilde{M}_2\widetilde{M}_2^T\right]^{-1}\widehat{B}(t)$$

$$+\beta_2^2\widehat{B}^T(t)\left[\widehat{R}_2^{-1}-\varepsilon_{29}\widetilde{M}_2\widetilde{M}_2^T\right]^{-1}\widehat{B}(t) \tag{42}$$

By Schur complement and formula (26), we have

$$\dot{V}(\xi(t))+e^T(t)e(t)-\gamma^2\omega^T(t)\omega(t)\le\eta^T(t)\Phi\eta(t) \tag{43}$$

where

$$\eta^T(t)=\left[\xi^T(t)\ \ \xi^T(t-\tau(t))\ \ \xi^T(t-\tau_1)\ \ \xi^T(t-\tau_2)\ \ \omega^T(t)\right] \tag{44}$$

Consequently, it follows from inequality (20), $V(\xi(t))|_{t=0}=0$ and $V(\xi(t))|_{t=L}\ge 0$, and we have $\int_0^L(\|e(t)\|^2-\gamma^2\|\omega(t)\|^2)dt+V(\xi(t))|_{t=L}-V(\xi(t))|_{t=0}\le 0$, which implies that (9) holds.

Thus, H_∞ performance is verified. In addition, when the zero disturbance input $\omega(t)=0$, by Schur complement, we can obtain that the time derivative of Lyapunov-Krasovskii $\dot{V}(\xi(t))\le 0$; that means that the filtering error system (7) with $\omega(t)=0$ is asymptotically stable. □

4. Fuzzy H_∞ Filter Design

Theorem 6 provides a sufficient condition for H_∞ filter design with time delay and satisfied the H_∞ performance. However, there exist some coupled matrix variables in the matrix inequality (15); H_∞ filter parameter can not be calculated directly. In order to decouple the variables in (15), we will use decoupling technique. Using this method, inequality (15) can be equivalently expressed in another form; hence, we can obtain H_∞ filter parameter.

Theorem 7. *For given scalars $\delta>0$, $\varepsilon_{2i}>0$, $\varepsilon_{6i}>0$, $\varepsilon_{10i}>0$, $\varepsilon_{19i}>0$, $\varepsilon_{29i}>0$, $\varepsilon_{15i}>0$, $\varepsilon_{25i}>0$, $\varepsilon_{20i}>0$, $\varepsilon_{21i}>0$, $\varepsilon_{22i}>0$, $\varepsilon_{11i}>0$, and $\varepsilon_{12i}>0$, the filtering error system (6) is asymptotically stable as well as with the H_∞ performance level γ, if there exist matrices $\widehat{P}>0$, $\widehat{Q}_1>0$, $\widehat{Q}_2>0$, $\widehat{Q}_3>0$, $\widehat{R}_1>0$, $\widehat{R}_2>0$, A_{fi}, B_{fi}, and C_{fi} such that the following linear matrix inequalities are satisfied:*

$$\begin{bmatrix}\widehat{R}_1^{-1} & \widetilde{M}_{2i}\\ * & \varepsilon_{1ki}^{-1}\end{bmatrix}>0,\quad (k=5,9) \tag{45}$$

$$\begin{bmatrix}\widehat{R}_2^{-1} & \widetilde{M}_{2i}\\ * & \varepsilon_{2ki}^{-1}\end{bmatrix}>0,\quad (k=5,9) \tag{46}$$

$$\begin{bmatrix}\widehat{R}_1^{-1} & \alpha_{11i}\widetilde{M}_{1i} & \alpha_{12i}\widetilde{M}_{2i}\\ * & I & 0\\ * & * & I\end{bmatrix}>0 \tag{47}$$

$$\begin{bmatrix}\widehat{R}_2^{-1} & \alpha_{21i}\widetilde{M}_{1i} & \alpha_{22i}\widetilde{M}_{2i}\\ * & I & 0\\ * & * & I\end{bmatrix}>0 \tag{48}$$

$$\Psi_{ij}=\begin{bmatrix}\Psi_1 & \Psi_2\\ * & \Psi_4\end{bmatrix} \tag{49}$$

where

$$\Psi_1=\begin{bmatrix}\Psi_{111} & \Psi_{112} & \Psi_{113} & \Psi_{114} & 0 & \Psi_{115} & 0 & \Psi_{118}\\ * & -I & 0 & 0 & 0 & 0 & 0 & 0\\ * & * & \Psi_{133} & 0 & 0 & 0 & 0 & 0\\ * & * & * & \Psi_{144} & \Psi_{145} & 0 & 0 & 0\\ * & * & * & * & -I & 0 & 0 & 0\\ * & * & * & * & * & \Psi_{166} & \Psi_{167} & 0\\ * & * & * & * & * & * & -I & 0\\ * & * & * & * & * & * & * & -I\end{bmatrix}$$

$$\Psi_{111}=\begin{bmatrix}\psi_{11} & \psi_{12} & 0 & 0 & \psi_{15}\\ * & -(1-d)\widehat{Q}_1 & 0 & 0 & 0\\ * & * & -\widehat{Q}_2-\left(\widehat{R}_1+\widehat{R}_2\right) & 0 & 0\\ * & * & * & -\widehat{Q}_3-\widehat{R}_2 & 0\\ * & * & * & * & -\gamma^2 I\end{bmatrix}$$

$$\psi_{11} = \begin{bmatrix} P_{11}A_j + \overline{B}_{fi}C_j & \overline{A}_{fi} \\ P_{12}^T A_j + \overline{B}_{fi}C_j & \overline{A}_{fi} \end{bmatrix} + \begin{bmatrix} P_{11}A_j + \overline{B}_{fi}C_j & \overline{A}_{fi} \\ P_{12}^T A_j + \overline{B}_{fi}C_j & \overline{A}_{fi} \end{bmatrix}^T + \widehat{Q}_1 + \widehat{Q}_2 + \widehat{Q}_3 - \widehat{R}_1,$$

$$\psi_{12} = \begin{bmatrix} P_{11}A_{\tau j} + \overline{B}_{fi}C_{\tau j} & 0 \\ P_{12}^T A_{\tau j} + \overline{B}_{fi}C_{\tau j} & 0 \end{bmatrix},$$

$$\psi_{15} = \begin{bmatrix} P_{11}B_j + \overline{B}_{fi}D_j \\ P_{12}^T B_j + \overline{B}_{fi}D_j \end{bmatrix},$$

$$\Psi_{112} = \begin{bmatrix} \alpha_{4i}\widehat{P}\widetilde{M}_{2i} & \alpha_{3i}\widehat{P}\widetilde{M}_{1i} \\ 0 & 0 \end{bmatrix},$$

$$\Psi_{113} = \begin{bmatrix} \alpha_{5i}\widetilde{N}_{1i}^T & \alpha_{6i}\widetilde{N}_{2i}^T & \alpha_{20i}\widetilde{N}_{3i}^T & \widehat{E}_j^T \\ 0 & 0 & 0 & 0 \end{bmatrix},$$

$$\Psi_{114} = \begin{bmatrix} \beta_{2i}\widehat{A}_j^T\widehat{P} \\ 0 \end{bmatrix},$$

$$\Psi_{115} = \begin{bmatrix} \beta_{2i}\widehat{A}_j^T\widehat{P} \\ 0 \end{bmatrix},$$

$$\Psi_{118} = \begin{bmatrix} 0 \\ \alpha_{7i}\widetilde{N}_{2\tau i}^T \\ 0 \\ 0 \\ 0 \end{bmatrix},$$

$$\Psi_{133} = -\mathrm{diag}\left(I, I, I, I - \alpha_{20i}^2\widetilde{M}_{3i}\widetilde{M}_{3i}^T\right),$$

$$\Psi_{144} = -2\delta\widehat{P} + \delta^2\widehat{R}_1,$$

$$\Psi_{145} = \left[\alpha_{11i}\widehat{P}\widetilde{M}_{1i} \quad \alpha_{12i}\widehat{P}\widetilde{M}_{2i}\right],$$

$$\Psi_{166} = -2\delta\widehat{P} + \delta^2\widehat{R}_2,$$

$$\Psi_{167} = \left[\alpha_{21i}\widehat{P}\widetilde{M}_{1i} \quad \alpha_{22i}\widehat{P}\widetilde{M}_{2i}\right],$$

$$\Psi_2 = \begin{bmatrix} \Psi_{211} & 0 & \Psi_{213} & 0 & \Psi_{215} & \Psi_{216} & 0 & \Psi_{218} & 0 \\ 0 & 0 & 0 & 0 & 0 & 0 & 0 & 0 & 0 \\ 0 & 0 & 0 & 0 & 0 & 0 & 0 & 0 & 0 \\ 0 & 0 & 0 & 0 & 0 & 0 & 0 & 0 & 0 \\ 0 & 0 & 0 & 0 & 0 & 0 & 0 & 0 & 0 \\ 0 & 0 & 0 & 0 & 0 & 0 & 0 & 0 & 0 \\ 0 & 0 & 0 & 0 & 0 & 0 & 0 & 0 & 0 \\ 0 & 0 & 0 & 0 & 0 & 0 & 0 & 0 & 0 \end{bmatrix},$$

$$\Psi_{211} = \begin{bmatrix} 0 \\ \beta_{1i}\widehat{A}_j^T\widehat{P} \\ 0 \\ 0 \\ 0 \end{bmatrix},$$

$$\Psi_{213} = \begin{bmatrix} 0 \\ \beta_{2i}\widehat{A}_{ij}^T\widehat{P} \\ 0 \\ 0 \\ 0 \end{bmatrix},$$

$$\Psi_{215} = \begin{bmatrix} 0 \\ 0 \\ 0 \\ 0 \\ \alpha_{1i}\widetilde{N}_{2Di}^T \end{bmatrix},$$

$$\Psi_{216} = \begin{bmatrix} 0 \\ 0 \\ 0 \\ 0 \\ \beta_{1i}\widehat{B}_j^T\widehat{P} \end{bmatrix},$$

$$\Psi_{218} = \begin{bmatrix} 0 \\ 0 \\ 0 \\ 0 \\ \beta_{2i}\widehat{B}_j^T\widehat{P} \end{bmatrix},$$

$$\Psi_4 = \begin{bmatrix} \Psi_{411} & \alpha_{15i}\widehat{P}\widetilde{M}_{2i} & 0 & 0 & 0 & 0 & 0 & 0 & 0 \\ * & -I & 0 & 0 & 0 & 0 & 0 & 0 & 0 \\ * & * & \Psi_{433} & \alpha_{25i}\widehat{P}\widetilde{M}_{2i} & 0 & 0 & 0 & 0 & 0 \\ * & * & * & -I & 0 & 0 & 0 & 0 & 0 \\ * & * & * & * & -I & 0 & 0 & 0 & 0 \\ * & * & * & * & * & \Psi_{466} & \alpha_{19i}\widehat{P}\widetilde{M}_{2i} & 0 & 0 \\ * & * & * & * & * & * & -I & 0 & 0 \\ * & * & * & * & * & * & * & \Psi_{488} & \alpha_{29i}\widehat{P}\widetilde{M}_{2i} \\ * & * & * & * & * & * & * & * & -I \end{bmatrix}$$

$$\Psi_{411} = -2\delta\widehat{P} + \delta^2\widehat{R}_1,$$

$$\Psi_{433} = -2\delta\widehat{P} + \delta^2\widehat{R}_2,$$

$$\Psi_{466} = -2\delta\widehat{P} + \delta^2\widehat{R}_1,$$

$$\Psi_{488} = -2\delta\widehat{P} + \delta^2\widehat{R}_2,$$

$$\widetilde{M}_{2i} = \begin{bmatrix} 0 \\ B_{fi}M_{2i} \end{bmatrix},$$

$$\widetilde{M}_{1i} = \begin{bmatrix} 0 \\ A_{fi}M_{1i} \end{bmatrix},$$

$$\widetilde{M}_{3i} = M_{3i},$$

$$\widetilde{N}_{1i} = \begin{bmatrix} 0 & N_{1i} \end{bmatrix},$$

$$\widetilde{N}_{2i} = \begin{bmatrix} N_{2i}C_j & 0 \end{bmatrix},$$

$$\widetilde{N}_{2\tau i} = \begin{bmatrix} N_{2i}C_{\tau j} & 0 \end{bmatrix},$$

$$\widetilde{N}_{2Di} = N_{2i}C_{Dj},$$

$$\widetilde{N}_{3i} = \begin{bmatrix} 0 & -N_{3i}C_{fi} \end{bmatrix} \tag{50}$$

We can obtain the filter parameters as follows:

$$\begin{aligned} A_{fi} &= P_{12}^{-1}\overline{A}_{fi}, \\ B_{fi} &= P_{12}^{-1}\overline{B}_{fi}, \\ C_{fi} &= \overline{C}_{fi} \end{aligned} \tag{51}$$

Proof. By Schur complement formula, the matrix inequality conditions (20) in Theorem 6 can be described as the following matrix inequalities:

$$\Gamma = \begin{bmatrix} \Gamma_1 & \Gamma_2 \\ * & \Gamma_4 \end{bmatrix} \tag{52}$$

where

$$\Gamma_1 = \begin{bmatrix} \Gamma_{111} & \Gamma_{112} & \Gamma_{113} & \Gamma_{114} & 0 & \Gamma_{115} & 0 & \Gamma_{118} \\ * & -I & 0 & 0 & 0 & 0 & 0 & 0 \\ * & * & \Gamma_{133} & 0 & 0 & 0 & 0 & 0 \\ * & * & * & -\widehat{R}_1^{-1} & \Gamma_{145} & 0 & 0 & 0 \\ * & * & * & * & -I & 0 & 0 & 0 \\ * & * & * & * & * & -\widehat{R}_2^{-1} & \Gamma_{167} & 0 \\ * & * & * & * & * & * & -I & 0 \\ * & * & * & * & * & * & * & -I \end{bmatrix}$$

$$\Gamma_{111} = \begin{bmatrix} \widehat{P}\widehat{A}(t) + \widehat{A}^T(t)\widehat{P} + \widehat{Q}_1 + \widehat{Q}_2 + \widehat{Q}_3 & \widehat{P}\widehat{A}_\tau(t) & 0 & 0 & \widehat{P}\widehat{B}(t) \\ * & -(1-d)\widehat{Q}_1 & 0 & 0 & 0 \\ * & * & -\widehat{Q}_2 & 0 & 0 \\ * & * & * & -\widehat{Q}_3 & 0 \\ * & * & * & * & -\gamma^2 I \end{bmatrix}$$

$$\Gamma_{112} = \begin{bmatrix} \alpha_4\widehat{P}\widetilde{M}_2 & \alpha_3\widehat{P}\widetilde{M}_1 \\ 0 & 0 \end{bmatrix},$$

$$\Gamma_{114} = \begin{bmatrix} \beta_1 \widehat{A}^T(t)\,\widehat{P} \\ 0 \end{bmatrix},$$

$$\Psi_{113} = \begin{bmatrix} \alpha_5 \widetilde{N}_1^T & \alpha_6 \widetilde{N}_2^T & \alpha_{20} \widetilde{N}_3^T & \widehat{E}^T \\ 0 & 0 & 0 & 0 \end{bmatrix},$$

$$\Gamma_{115} = \begin{bmatrix} \beta_2 \widehat{A}^T(t)\,\widehat{P} \\ 0 \end{bmatrix},$$

$$\Gamma_{118} = \begin{bmatrix} 0 \\ \alpha_7 \widetilde{N}_{2\tau}^T \\ 0 \\ 0 \\ 0 \end{bmatrix},$$

$$\Gamma_{133} = -\mathrm{diag}\left(I, I, I, I - \alpha_{20}^2 \widetilde{M}_3 \widetilde{M}_3^T\right),$$

$$\Gamma_{145} = \left[\alpha_{11} \widehat{P} \widetilde{M}_1 \quad \alpha_{12} \widehat{P} \widetilde{M}_2\right],$$

$$\Gamma_{167} = \left[\alpha_{21} \widehat{P} \widetilde{M}_1 \quad \alpha_{22} \widehat{P} \widetilde{M}_2\right],$$

$$\Gamma_2 = \begin{bmatrix} \Gamma_{211} & 0 & \Gamma_{213} & 0 & \Gamma_{215} & \Gamma_{216} & 0 & \Gamma_{218} & 0 \\ 0 & 0 & 0 & 0 & 0 & 0 & 0 & 0 & 0 \\ 0 & 0 & 0 & 0 & 0 & 0 & 0 & 0 & 0 \\ 0 & 0 & 0 & 0 & 0 & 0 & 0 & 0 & 0 \\ 0 & 0 & 0 & 0 & 0 & 0 & 0 & 0 & 0 \\ 0 & 0 & 0 & 0 & 0 & 0 & 0 & 0 & 0 \\ 0 & 0 & 0 & 0 & 0 & 0 & 0 & 0 & 0 \\ 0 & 0 & 0 & 0 & 0 & 0 & 0 & 0 & 0 \end{bmatrix},$$

$$\Gamma_{211} = \begin{bmatrix} 0 \\ \beta_1 \widehat{A}^T(t)\,\widehat{P} \\ 0 \\ 0 \\ 0 \end{bmatrix},$$

$$\Gamma_{213} = \begin{bmatrix} 0 \\ \beta_2 \widehat{A}_\tau^T(t)\,\widehat{P} \\ 0 \\ 0 \\ 0 \end{bmatrix},$$

$$\Gamma_{215} = \begin{bmatrix} 0 \\ 0 \\ 0 \\ 0 \\ \alpha_1 \widetilde{N}_{2D}^T \end{bmatrix},$$

$$\Gamma_{216} = \begin{bmatrix} 0 \\ 0 \\ 0 \\ 0 \\ \beta_1 \widehat{B}^T(t)\widehat{P} \end{bmatrix},$$

$$\Gamma_{218} = \begin{bmatrix} 0 \\ 0 \\ 0 \\ 0 \\ \beta_2 \widehat{B}^T(t)\widehat{P} \end{bmatrix},$$

$$\Gamma_4 = \begin{bmatrix} \Gamma_{411} & \alpha_{15}\widehat{P}\widetilde{M}_2 & 0 & 0 & 0 & 0 & 0 & 0 & 0 \\ * & -I & 0 & 0 & 0 & 0 & 0 & 0 & 0 \\ * & * & \Gamma_{433} & \alpha_{25}\widehat{P}\widetilde{M}_2 & 0 & 0 & 0 & 0 & 0 \\ * & * & * & -I & 0 & 0 & 0 & 0 & 0 \\ * & * & * & * & -I & 0 & 0 & 0 & 0 \\ * & * & * & * & * & \Gamma_{466} & \alpha_{19}\widehat{P}\widetilde{M}_2 & 0 & 0 \\ * & * & * & * & * & * & -I & 0 & 0 \\ * & * & * & * & * & * & * & \Gamma_{488} & \alpha_{29}\widehat{P}\widetilde{M}_2 \\ * & * & * & * & * & * & * & * & -I \end{bmatrix}$$

$$\begin{aligned} \Gamma_{411} &= -2\delta\widehat{P} + \delta^2\widehat{R}_1, \\ \Gamma_{433} &= -2\delta\widehat{P} + \delta^2\widehat{R}_2, \\ \Gamma_{466} &= -2\delta\widehat{P} + \delta^2\widehat{R}_1, \\ \Gamma_{488} &= -2\delta\widehat{P} + \delta^2\widehat{R}_2. \end{aligned} \tag{53}$$

Let $\widehat{P} = \begin{bmatrix} P_{11} & P_{12} \\ * & P_{12} \end{bmatrix}$, $\widehat{P}\widehat{A}(t) = \begin{bmatrix} P_{11}A(t)+\overline{B}_f(t)C(t) & \overline{A}_f(t) \\ P_{12}^T A(t)+\overline{B}_f(t)C(t) & \overline{A}_f(t) \end{bmatrix}$, $\widehat{P}\widehat{A}_\tau(t) = \begin{bmatrix} P_{11}A_\tau(t)+\overline{B}_f(t)C_\tau(t) & 0 \\ P_{12}^T A_\tau(t)+\overline{B}_f(t)C_\tau(t) & 0 \end{bmatrix}$, $\widehat{P}\widehat{B}(t) = \begin{bmatrix} P_{11}B(t)+\overline{B}_f(t)D(t) \\ P_{12}^T B(t)+\overline{B}_f(t)D(t) \end{bmatrix}$, $\beta_1 = \sqrt{3\tau_1^2}$, $\beta_2 = \sqrt{3(\tau_2^2-\tau_1^2)}$, $\alpha_1 = \sqrt{\beta_1^2\varepsilon_{19}^{-1} + \beta_2^2\varepsilon_{29}^{-1} + \varepsilon_{10}^{-1}}$, $\alpha_2 = \sqrt{\beta_1^2\varepsilon_{15}^{-1} + \beta_2^2\varepsilon_{25}^{-1} + \varepsilon_6^{-1}}$, $\alpha_3 = \sqrt{\varepsilon_{21}}$, $\alpha_4 = \sqrt{\varepsilon_2 + \varepsilon_6 + \varepsilon_{10}}$, $\alpha_5 = \sqrt{\varepsilon_{21}^{-1} + \beta_1^2\varepsilon_{11}^{-1} + \beta_2^2\varepsilon_{22}^{-1}}$, $\alpha_6 = \sqrt{\beta_1^2\varepsilon_{12}^{-1} + \beta_2^2\varepsilon_{22}^{-1}}$, $\alpha_7 = \sqrt{\varepsilon_6}$, $\alpha_{11} = \sqrt{\varepsilon_{11}}$, $\alpha_{12} = \sqrt{\varepsilon_{12}}$, $\alpha_{15} = \sqrt{\varepsilon_{15}}$, $\alpha_{25} = \sqrt{\varepsilon_{25}}$, $\alpha_{19} = \sqrt{\varepsilon_{19}}$, $\alpha_{20} = \sqrt{\varepsilon_{20}}$, $\alpha_{21} = \sqrt{\varepsilon_{21}}$, $\alpha_{22} = \sqrt{\varepsilon_{22}}$, $\alpha_{29} = \sqrt{\varepsilon_{29}}$, $\Delta(t) = \sum_{i=1}^{r} h_i(\theta(t))\Delta_i(t)$, where $\Delta = A, B, D, A_\tau, \overline{A}_f, \overline{B}_f, \overline{C}_f$.

According to $(\delta\widehat{R} - \widehat{P})\widehat{R}^{-1}(\delta\widehat{R} - \widehat{P}) \geq 0$, we have that $-\widehat{P}\widehat{R}^{-1}\widehat{P} \leq -2\delta\widehat{P} + \delta^2\widehat{R}$ holds for any scalar $\delta > 0$. The filter parameters in (3) can be designed as (51). This completes the proof. □

5. Simulation Example

Consider the following nonlinear systems with time-varying delays:

$$\begin{aligned} \dot{x}(t) &= \sum_{i=1}^{2} h_i \left[A_i x(t) + A_{\tau i} x(t-\tau(t)) + B_i \omega(t)\right] \\ y(t) &= \sum_{i=1}^{2} h_i \left[C_i x(t) + C_{\tau i} x(t-\tau(t)) + D_i \omega(t)\right] \\ z(t) &= \sum_{i=1}^{2} h_i \left[E_i x(t)\right] \end{aligned} \tag{54}$$

where

$$A_1 = \begin{bmatrix} -2.1 & 0.1 \\ 1 & -2 \end{bmatrix},$$

$$A_2 = \begin{bmatrix} -1.9 & 0 \\ -0.2 & -1.1 \end{bmatrix},$$

$$A_{\tau 1} = \begin{bmatrix} -1.1 & 0.1 \\ -0.8 & -0.9 \end{bmatrix},$$

$$
\begin{aligned}
A_{\tau 1} &= \begin{bmatrix} -0.9 & 0.1 \\ -1.1 & -1.2 \end{bmatrix}, \\
B_1 &= \begin{bmatrix} 1 \\ -0.2 \end{bmatrix}, \\
B_1 &= \begin{bmatrix} 0.3 \\ 0.1 \end{bmatrix}, \\
D_1 &= 0.3, \\
D_2 &= -0.6, \\
C_1 &= \begin{bmatrix} 1 & 0 \end{bmatrix}, \\
C_2 &= \begin{bmatrix} 0.5 & 0.6 \end{bmatrix} \\
C_{\tau 1} &= \begin{bmatrix} -0.8 & 0.6 \end{bmatrix}, \\
C_{\tau 2} &= \begin{bmatrix} -0.2 & 1 \end{bmatrix}, \\
E_1 &= \begin{bmatrix} 1 & -0.5 \end{bmatrix}, \\
E_2 &= \begin{bmatrix} -0.2 & 0.3 \end{bmatrix}
\end{aligned} \tag{55}
$$

The known matrices in (5) are given by

$$
\begin{aligned}
M_{11} &= M_{12} = \begin{bmatrix} 0.5 & 0.4 \\ 0.3 & 0.2 \end{bmatrix}, \\
M_{21} &= M_{22} = \begin{bmatrix} 0.5 & 0.3 \end{bmatrix}, \\
M_{31} &= M_{32} = \begin{bmatrix} 0.08 \\ 0.02 \end{bmatrix}, \\
N_{11} &= N_{12} = \begin{bmatrix} 0.3 & 0.6 \\ 0.2 & 0.1 \end{bmatrix}, \\
N_{21} &= N_{22} = \begin{bmatrix} 0.1 \\ -0.2 \end{bmatrix}, \\
N_{31} &= N_{32} = \begin{bmatrix} 0.2 & 0.3 \end{bmatrix}, \\
K_l(\mathrm{t}) &= \sin(\mathrm{t}), \quad \text{where } l = A, B, C.
\end{aligned} \tag{56}
$$

The disturbance signal $\omega(\mathrm{t})$ is given as follows:

$$
\omega(\mathrm{t}) = \begin{cases} \sin(\mathrm{t}), & 0 < \mathrm{t} < 15 \\ 0 & other. \end{cases} \tag{57}
$$

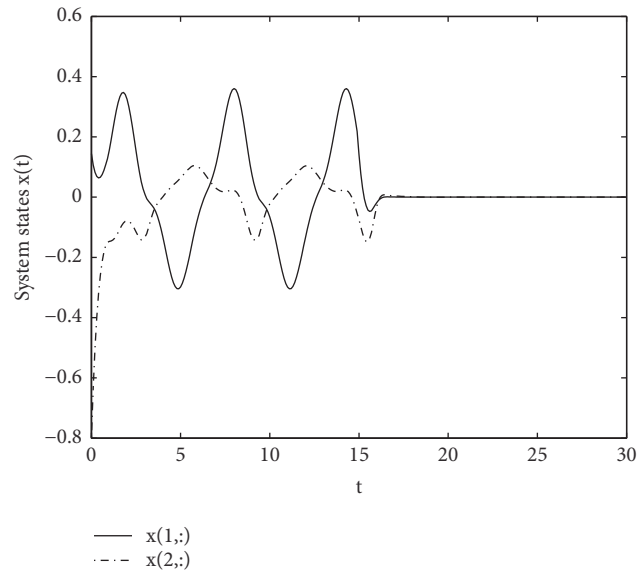

Figure 1: The response curve of system states x_1, x_2.

We can get the desired nonfragile filter by solving LMIS (45)-(49) in Theorem 7; the nonfragile parameter matrices are given as follows:

$$
\begin{aligned}
A_{f1} &= \begin{bmatrix} -3.1329 & 6.2268 \\ 0.7361 & -7.4593 \end{bmatrix}, \\
A_{f2} &= \begin{bmatrix} -2.7553 & 7.6590 \\ -0.8303 & -8.3416 \end{bmatrix}, \\
B_{f1} &= \begin{bmatrix} -0.4755 \\ -1.1658 \end{bmatrix}, \\
B_{f2} &= \begin{bmatrix} -0.2459 \\ -1.2213 \end{bmatrix}, \\
C_{f1} &= \begin{bmatrix} -0.2031 & 0.2124 \end{bmatrix}, \\
C_{f2} &= \begin{bmatrix} 0.2231 & -0.3065 \end{bmatrix}
\end{aligned} \tag{58}
$$

In addition, the new method provides less conservative design result; we can obtain a smaller $\gamma = 0.4996$. Figures 1 and 2 show the response of system's states $x(\mathrm{t})$ and filter's states $x_f(\mathrm{t})$, respectively. Figure 3 shows the trajectories of $z(\mathrm{t})$ and its estimates $z_f(\mathrm{t})$. The estimation error $e(\mathrm{t})$ is depicted in Figure 4.

The random disturbance signal is given as follows:

$$
\omega(\mathrm{t}) = \begin{cases} \alpha(\mathrm{t}) \sin(\mathrm{t}), & 0 < \mathrm{t} < 15 \\ 0 & other, \end{cases} \tag{59}
$$

where $\alpha(\mathrm{t})$ denotes Bernoulli's random event. The simulation results are obtained as shown in Figures 5–9.

The stochastic variables $\alpha(\mathrm{t})$ are Bernoulli-distributed white sequences; Figure 5 shows the event occurrence

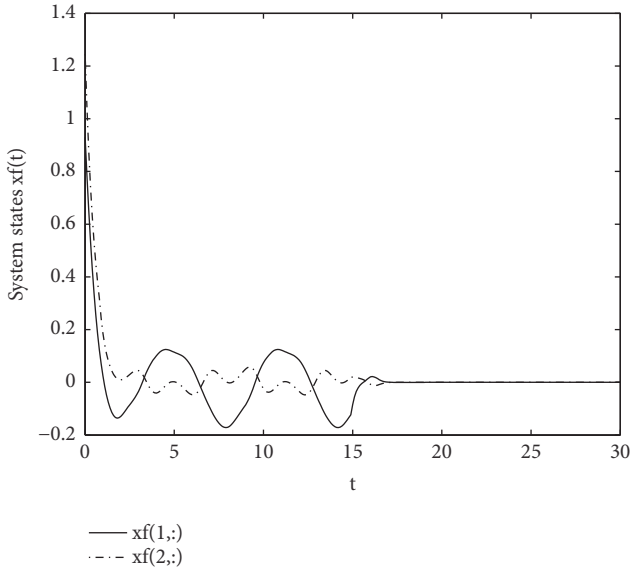

Figure 2: The response curve of system states x_{f1}, x_{f2}.

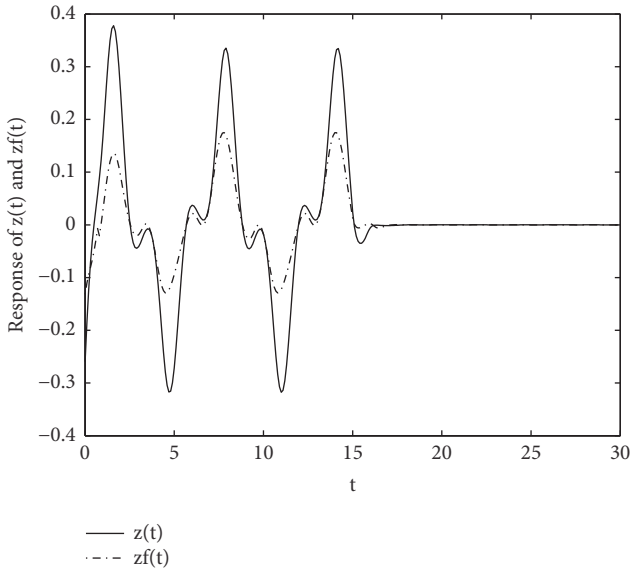

Figure 3: The response curve of vector $z(t)$, $z_f(t)$.

probability. Figures 6 and 7 show the response of system's states $x_1(t), x_2(t)$ and filter's states $x_{f1}(t), x_{f2}(t)$, respectively. Figure 8 shows the trajectories of $z(t)$ and its estimates $z_f(t)$. The system error $e(t)$ is depicted in Figure 9.

The results show that the H_∞ nonfragile filter can make the system have good stability. The system generates small overshoot; this filter can efficiently reduce the influence of external disturbance and uncertainty; it can enhance control precision and dynamic qualities of the system.

6. Conclusions

This paper studied the fuzzy nonfragile H_∞ filter design problem for a class of nonlinear systems with an interval

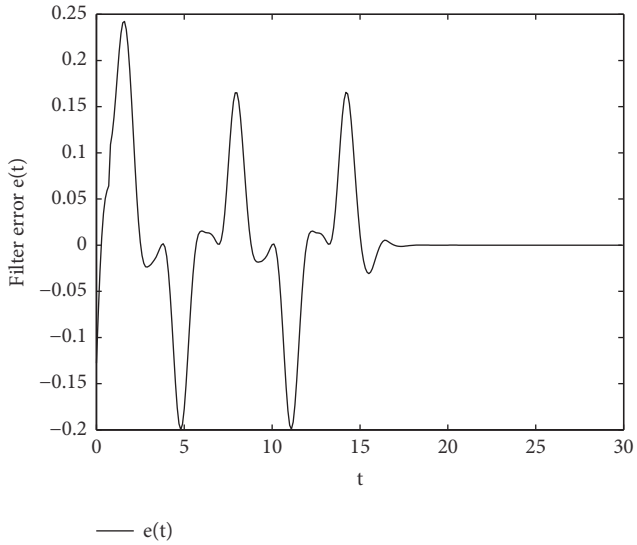

Figure 4: The response curve of vector $e(t)$.

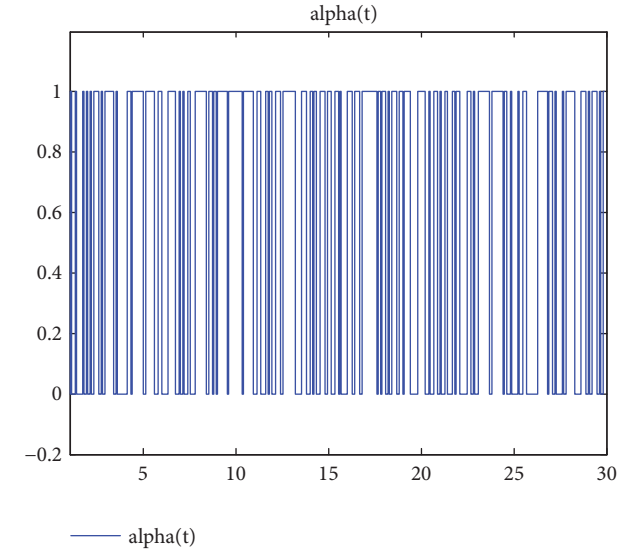

Figure 5: The event occurrence probability $\alpha(t)$.

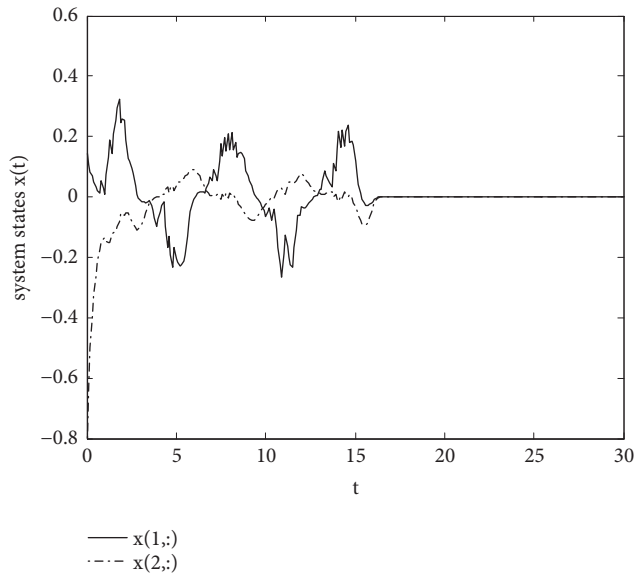

Figure 6: The response curve of system states x_1, x_2.

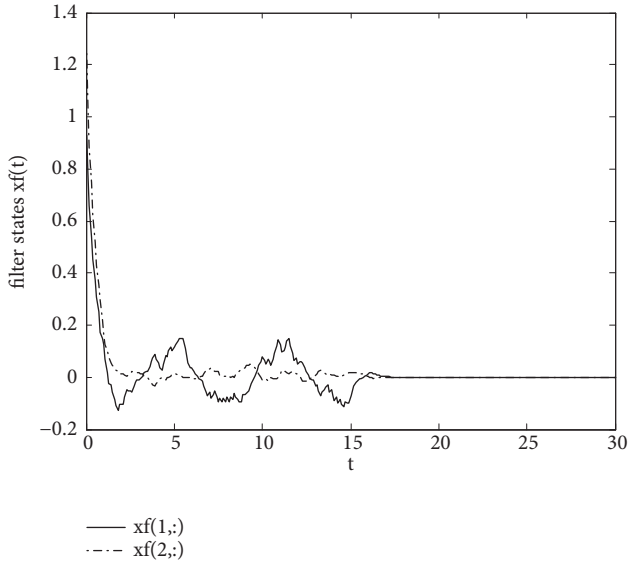

Figure 7: The response curve of system states x_{f1}, x_{f2}.

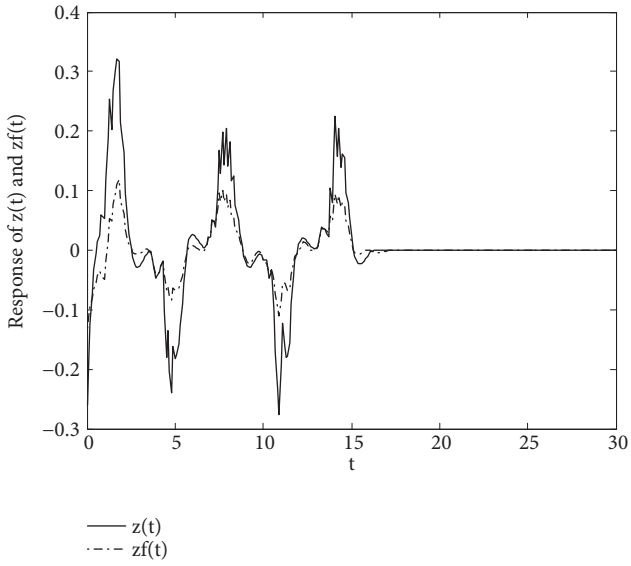

Figure 8: The response curve of vector $z(t)$, $z_f(t)$.

time-varying delays; meanwhile, the designing H_∞ filter with multiplicative gain variations was considered. By constructing a new Lyapunov-Krasovskii functional, we obtained a sufficient condition for designing the nonfragile H_∞ filter such that the filtering error system is asymptotically stable and satisfied the given H_∞ performance index. This nonfragile filter design method enhances the nonfragility of the filter and reduces some conservatism. A numerical example has shown the effectiveness of the proposed method. Future research includes event-triggered nonfragile H_∞ filter design for nonlinear system considering packet dropout and interval time-varying delays. Moreover, type 2 fuzzy filter design for nonlinear system with time-varying delays also can be further considered for the future investigation.

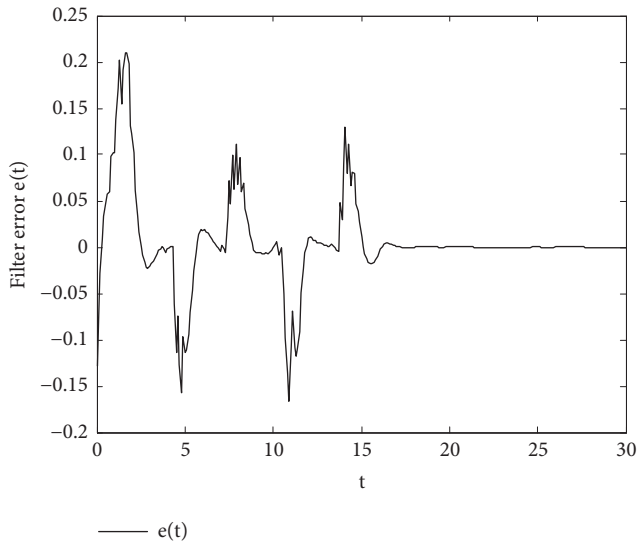

Figure 9: The response curve of vector $e(t)$.

Data Availability

The data used to support this study are currently under embargo while the research findings are commercialized. Requests for data, 12 months after initial publication, will be considered by the corresponding author.

Conflicts of Interest

The authors declare that there are no conflicts of interest regarding the publication of this paper.

Acknowledgments

This work was supported in part by Science and Technology project of State Grid corporation of China (SGTYHT/13-JS-175).

References

[1] T. Zhongda, L. Shujiang, W. Yanhong, and W. Xiangdong, "Scheduling method for networked control system with resource constraints based on fuzzy feedback priority and variable sampling period," *Transactions of the Institute of Measurement and Control*, vol. 40, no. 4, pp. 1136–1149, 2018.

[2] Z. Tian, S. Li, Y. Wang, and B. Gu, "Priority scheduling of networked control system based on fuzzy controller with self-tuning scale factor," *IAENG International Journal of Computer Science (IJCS)*, vol. 44, no. 3, pp. 308–315, 2017.

[3] Z. Tian, S. Li, and Y. Wang, "T-S fuzzy neural network predictive control for burning zone temperature in rotary kiln with improved hierarchical genetic algorithm," *International Journal of Modelling, Identification and Control*, vol. 25, no. 4, pp. 323–334, 2016.

[4] Z. Tian, S. Li, Y. Wang, X. Wang, and Q. Zhang, "The time-delay compensation method for networked control system based on improved fast implicit GPC," *International Journal of Control and Automation*, vol. 9, no. 1, pp. 231–240, 2016.

[5] T. Youssef, M. Chadli, H. R. Karimi, and R. Wang, "Actuator and sensor faults estimation based on proportional integral observer for TS fuzzy model," *Journal of The Franklin Institute*, vol. 354, no. 6, pp. 2524–2542, 2017.

[6] M. Wang, J. Qiu, M. Chadli, and M. Wang, "A Switched System Approach to Exponential Stabilization of Sampled-Data T–S Fuzzy Systems With Packet Dropouts," *IEEE Transactions on Cybernetics*, vol. 46, no. 12, pp. 3145–3156, 2016.

[7] J. An, G. Wen, and W. Xu, "Improved Results on Fuzzy Filter Design for T-S Fuzzy Systems," *Discrete Dynamics in Nature and Society*, vol. 21, 392915 pages, 2010.

[8] J. An, G. Wen, C. Lin, and R. Li, "New Results on a Delay-Derivative-Dependent Fuzzy H∞ Filter Design for T–S Fuzzy Systems," *IEEE Transactions on Fuzzy Systems*, vol. 19, no. 4, pp. 770–779, 2011.

[9] D. Zhang, W. Cai, L. Xie, and Q. Wang, "Non-fragile distributed filtering for T-S fuzzy systems in sensor networks," *IEEE Transactions on Fuzzy Systems*, 2014.

[10] H.-B. Zeng, J. H. Park, J.-W. Xia, and S.-P. Xiao, "Improved delay-dependent stability criteria for T-S fuzzy systems with time-varying delay," *Applied Mathematics and Computation*, vol. 235, pp. 492–501, 2014.

[11] C. Lin, Q. Wang, T. H. Lee, and B. Chen, "H_∞ filter design for nonlinear systems with time-delay through T-S fuzzy model approach," *IEEE Transactions on Fuzzy Systems*, vol. 16, no. 3, pp. 739–746, 2008.

[12] L. K. Wang, J. L. Peng, and X. D. Liu, "H∞ filtering design for continuous-time Takagi-Sugeno fuzzy model with immeasurable premise variables," *Neurocomputing*, vol. 173, pp. 2090–2096, 2016.

[13] Y. Su, Q. Zhou, and F. Gao, "A new delay-range-dependent H∞ filter design for T-S nonlinear systems," *Journal of The Franklin Institute*, vol. 351, no. 6, pp. 3305–3321, 2014.

[14] Y. Li, W. Xiao, J. Li, and L. Jiao, "H∞ filtering for discrete-time fuzzy stochastic neural networks with mixed time-delays," *Applied Mathematics and Computation*, vol. 52, no. 1-2, pp. 1–26, 2016.

[15] Y.-Q. Wu, H. Su, and Z.-G. Wu, "H∞ filtering for discrete fuzzy stochastic systems with randomly occurred sensor nonlinearities," *Signal Processing*, vol. 108, pp. 288–296, 2014.

[16] Z. Lu, G. Ran, G. Zhang, and F. Xu, "Event-Triggered H∞ Fuzzy Filtering for Networked Control Systems With Quantization and Delays," *IEEE Access*, vol. 6, pp. 20231–20241, 2018.

[17] Z. Li, Y. M. Chu, and S. Y. Xu, "Delay-dependent nonfragile robust H∞ filtering of T-S fuzzy time-delay systems," *Circuits, Systems and Signal Processing*, vol. 29, no. 3, pp. 361–375, 2010.

[18] X. Chang and G. Yang, "Non-fragile fuzzyHss filter design for nonlinear continuous-time systems with D stability constraints," *Signal Processing*, vol. 92, no. 2, pp. 575–586, 2012.

[19] D. Ding W, X. Li, Z. Shi, and X. Guo, "Nonfragile H∞ filtering for discrete-time T-S fuzzy systems," in *Proceedings of the Control Conference (CCC)*, vol. 201, pp. 3552–3557, 2012.

[20] X.-H. Chang and G.-H. Yang, "Nonfragile H∞ Filter Design for T–S Fuzzy Systems in Standard Form," *IEEE Transactions on Industrial Electronics*, vol. 61, no. 7, pp. 3448–3458, 2014.

[21] G.-H. Yang and W.-W. Che, "Non-fragile H∞ filter design with additive gain variations," in *Proceedings of the 45th IEEE Conference on Decision and Control (CDC '06)*, pp. 4775–4780, San Diego, Calif, USA, December 2006.

[22] S. Zhang, Z. Wang, D. Ding, H. Dong, F. E. Alsaadi, and T. Hayat, "Nonfragile H∞Fuzzy Filtering with Randomly Occurring Gain Variations and Channel Fadings," *IEEE Transactions on Fuzzy Systems*, vol. 24, no. 3, pp. 504–518, 2016.

[23] G. Yang and W. Che, "Non-fragile filter design for linear continuous-time systems," *Automatica*, vol. 44, no. 11, pp. 2849–2856, 2008.

[24] Z. Li, F. Gu, Y. He, and W. Hao, "Nonfragile Robust Filter Design for a Class of Fuzzy Stochastic Systems with Stochastic Input-to-State Stability," *Mathematical Problems in Engineering*, vol. 2015, Article ID 896574, 10 pages, 2015.

Hindawi
Journal of Control Science and Engineering
Volume 2018, Article ID 2572846, 10 pages
https://doi.org/10.1155/2018/2572846

Research Article

Event-Triggered H_∞ Filtering for Multiagent Systems with Markovian Switching Topologies

Jiahao Li, Tingting Zhang, Jinfeng Gao, and Ping Wu

Faculty of Mechanical Engineering and Automation, Zhejiang Sci-Tech University, Hangzhou 310018, China

Correspondence should be addressed to Jinfeng Gao; gaojf163@163.com

Received 11 May 2018; Revised 1 July 2018; Accepted 12 July 2018; Published 14 August 2018

Academic Editor: Cui-Qin Ma

This paper is concerned with the problem of event-triggered H_∞ filtering for multiagent systems with Markovian switching topologies and network-induced delay. An event-triggered mechanism is given to ease the information transmission. Consider that the network topology is directed in this paper, which represents the communication links among agents. Due to the existence of network-induced delay, the time-delay approach is adopted, which can effectively deal with filtering error system. By constructing a Lyapunov-Krasovskii functional and employing linear matrix inequality technique, sufficient conditions are established to ensure the filtering error system to achieve asymptotically stable with H_∞ performance index. A simulation example is given to illustrate the effectiveness of the proposed method.

1. Introduction

Recently, multiagent systems (MASs) have received much interest due to their widespread applications in various fields such as formation control [1, 2], sensor network [3], synchronization [4], and flocking [5, 6]. Due to the fact that communication networks consist of lots of agents, their states are usually not fully available in network outputs. Hence, filtering or state estimation problem is to estimate the states of the agent by the available output measurement, which is very important both in theory and in practice. In the past decades, the consensus-based filtering or estimation problem for a special multiagent system, i.e., the multi-sensor networked system, has received much attention. For example, Kalman filters are the filters primarily proposed in [7, 8] for multi-sensor networked systems, while H_∞ filters are given in [9] for sensor networks with multiple missing measurements. In most existing literatures, the study of multiagent systems has been investigated in the ideal situation without considering external interference. However, in practical engineering, the existence of external disturbances cannot be ignored, which may have a great impact on agent dynamics. Furthermore, the research history of multiagent systems on H_∞ filtering or state estimation is very short; there are many problems which need to be studied extensively. Thus, it is necessary to study the H_∞ filtering problem of multiagent systems with many practical factors.

The exchange of information between agents on a communication network is usually completed on the basis of sampled packets. Many articles have presented more and more methods based on rapid development of the theory of sampling data systems. In the early results, time-triggered communication is a common way to transfer every sampled signal to the controller and update control signal periodically, which wastes a lot of network bandwidth resources and increases network load. Compared with the widely used time-triggered sampling scheme [10–13], event-triggered communication schemes [14–16] can avoid the unnecessary transmission and reduce the release times of the sensor and the burden of communication network. Event-triggered filtering/estimation for different systems has received considerable attention in the past few years [17–22]. Paper [17] addresses event-triggered state estimation problem for a class of complex networks with mixed time delays and [20] presents H_∞ filter design for a class of neural network systems with quantization. The filtering problem for discrete-time networked control system (NCS) under event-triggered scheme is proposed in [18, 19, 21]. Paper [22] designs the H_∞

fuzzy filter for a class of nonlinear networked control system based on event-triggered communication scheme.

In the real world, because of the uncertainty of the network, the communication topology may change. Hence, it is significant to design a filtering network with time-varying and switching topology to estimate or monitor a target; see [23–28]. Event-based H_∞ filtering for discrete-time and continue-time Markov jump system with network-induced delay is investigated in [23, 24], respectively. Paper [25, 26] addresses asynchronous $l_2 - l_\infty$ filtering with sensor nonlinearity and delay-dependent robust H_∞ control and filtering with parameter uncertainties, respectively. Paper [27] investigates the problem of H_∞ estimation for a class of discrete-time Markov jump systems with time-varying transition probabilities. The problem of distributed state estimation about vehicle formation with time-varying measurement topology is discussed in [28]. To the best of our knowledge, there is no article that considers H_∞ filtering problem for multiagent systems with Markovian switching topologies and network-induced delay based on event-triggered strategy. The theoretical results of such systems will be attractive and have extensive practical applications, which inspired the research presented in this paper.

In the view of the above discussion, this paper addresses the event-triggered H_∞ filtering for multiagent systems with Markovian switching topologies and network-induced delay. The main contributions are summarized as follows: (1) different from the general event-triggered sampled-data strategy, this paper takes into account the effect of network-induced delay and Markovian switching topologies. A distributed event-triggered scheme is presented to release the load of the network. (2) By employing the time-delay system method, H_∞ filtering performance is derived, the co-design method of the event-triggered condition and the filter design are also given. (3) The Laplacian matrices of switching topologies are not required to be symmetric.

The rest of this paper is organized as follows. In Section 2, we give some preliminaries and present the problem formulation. The main results for stability analysis and event-triggered H_∞ filter design are elaborated in Section 3. In Section 4, a numerical example is provided to illustrate the feasibility and effectiveness of the proposed method. Finally, conclusions are drawn in Section 5.

Notations. R^n represents the n-dimension Euclidean space and $R^{n\times m}$ denotes the set of $n \times m$ real matrices. Let I_N represent the $N \times N$ identity matrix and $\mathbf{0}$ denote zero matrix with an appropriate dimension. The superscripts -1 and T stand for the inverse and the transpose of a matrix, respectively. We use the notation $\otimes$ and $*$ to represent Kronecker product and the elements below the main diagonal of some symmetric matrix, respectively. The real matrix $P > 0$ shows that P is positive definite.

2. Problem Formulation

2.1. Graph Theory. Let $G = (V, \xi, A)$ denote a directed weighted graph of N order, where the set of nodes is denotes by $V = \{v_1, v_2, \ldots, v_n\}$ and the set of edges is denoted by $\xi \subseteq V \times V$. An edge in graph G is described by (v_j, v_i), $i, j \in 1, 2, \ldots, n$ which represents that the jth agent transmit information to the ith agent. Matrix $A = [a_{ij}]_{n\times n}$ is called weighted adjacency matrix. The set of neighbors of agent i is denoted as $N_i = \{j \mid (v_j, v_i) \in \xi\}$. If $j \in N_i$, $a_{ij} > 0$; otherwise, $a_{ij} = 0$. The diagonal matrix $D = \text{diag}\{d_1, d_2, \ldots, d_N\} \in R^{N\times N}$ is called the degree matrix of graph G with diagonal elements $d_i = \Sigma_{j\in N_i} a_{ij}$. The Laplacian matrix of G is defined as $L = D - A = [l_{ij}] \in R^{N\times N}$, where $l_{ii} = \sum_{j\in N_i} a_{ij}$ and $l_{ij} = -a_{ij}$ for $i \neq j$.

2.2. System Description. We consider MASs composed of N interconnected agents in this paper, where each agent is assumed to have the following state-space description:

$$\begin{aligned} \dot{x}_i(t) &= Ax_i(t) + Bw_i(t) \\ y_i(t) &= C_2 \Sigma_{j\in N_i} a_{ij}^{r(t)} \left(x_i(t) - x_j(t)\right) + Dw_i(t) \\ z_i(t) &= C_1 \Sigma_{j\in N_i} a_{ij}^{r(t)} \left(x_i(t) - x_j(t)\right) \end{aligned} \tag{1}$$

for $i = 1, 2, \ldots, N$, where $x_i(t)$, $y_i(t)$, and $z_i(t)$ are the state, the measured output, and the signal to be estimated of agent i. $w_i(t)$ denotes the external disturbance which belongs to $L_2[0, \infty)$.

The switching communication topologies are described by $G_{r(t)} \in \{G_1, G_2, \ldots, G_q\}$, where $r(t)$ represents the continuous process of Markov chain. Furthermore, it takes values in a given finite set $S = \{1, 2, \ldots, q\}$. We define the transition probability as follows:

$$prob\{r(t + \Delta t) = s \mid r(t) = r\} = \begin{cases} \pi_{rs}\Delta t + o(\Delta t), & r \neq s \\ 1 + \pi_{rr}\Delta t + o(\Delta t), & r = s \end{cases} \tag{2}$$

where $\lim_{\Delta t \to 0}(o(\Delta t)/\Delta t) = 0, \Delta t > 0$, and the transition probability satisfies $\pi_{rs} > 0$ when $r, s \in S$ and $\pi_{rr} = -\sum_{s=1, s\neq r}^{q} \pi_{rs}$.

For MASs (1), we design the following full-order filter to estimate signal $z_i(t)$:

$$\begin{aligned} \dot{x}_{fi}(t) &= A_{fr}x_{fi}(t) + B_{fr}y_{fi}(t) \\ z_{fi}(t) &= C_{fr}x_{fi}(t) \end{aligned} \tag{3}$$

where $x_{fi}(t)$ represents the state of the ith filtering subsystem, $z_{fi}(t)$ is the estimation signal of $z_i(t)$, and A_{fr}, B_{fr}, C_{fr} are filter parameters to be determined.

2.3. Event-Triggered Scheme. In order to reduce the communication network burden, event-triggered scheme is adopted in this paper. The sampler is assumed to be time-driven; the zero-order-hold (ZOH) is event-driven. Then, we construct the following event-triggered strategy.

$$\begin{aligned} t_{k+1}^i h = t_k^i h + \min_{l_i > 1} \{ & l_i h \mid \chi_i^T \left(t_k^i h + l_i h\right) \phi_r \chi_i \left(t_k^i h + l_i h\right) \\ & \geq \sigma_r y_i^T \left(t_k^i h + l_i h\right) \phi_r y_i \left(t_k^i h + l_i h\right) \} \end{aligned} \tag{4}$$

where $l_i \in N$, $\chi_i(t_k^i h + l_i h) \triangleq y_i(t_k^i h + l_i h) - y_i(t_k^i h)$ is the threshold error, $t_k^i h$ represents the latest kth triggering instant of the ith agent, $t_k^i h + l_i h$ denotes the currently sampled instant, and $t_{k+1}^i h$ denotes the next broadcast instant. Then $\sigma_r > 0$ represents the threshold and $\phi_r > 0$ stands for a symmetric positive definite matrix.

Remark 1. From the event-triggered strategy (4), we can automatically exclude Zeno behavior.

Proof. Zeno behavior in the event-triggered communication framework is defined as the infinite number of communication in a finite time. Due to the fact that each agent's state is periodically sampled and the sampling time sequence is $\{0, h, 2h, \ldots\}$, we can obtain that the event-triggered time sequence is a subsequence of the sampling time sequence, namely, $\{t_0^i h, t_1^i h, t_2^i h, \ldots\} \subseteq \{0, h, 2h, \ldots\}$, which means that the minimum interevent time $\min_k\{t_{k+1}^i h - t_k^i h\}$, $\forall i$, is lower bounded by the sampling period h. Since the number of agents is finite, the communication events in any finite time cannot be infinite. Therefore, the event-triggered strategy (4) can rule out Zeno behavior automatically. □

Remark 2. Different from traditional filtering problem, due to the existence of network-induced delays, taking the property of ZOH into account, we get

$$y_{fi}(t) = y_i\left(t_k^i h\right) \tag{5}$$

Substituting (5) into (3), we have

$$\begin{aligned} \dot{x}_{fi}(t) &= A_{fr} x_{fi}(t) + B_{fr} y_i\left(t_k^i h\right) \\ z_{fi}(t) &= C_{fr} x_{fi}(t), \\ & t \in \left[t_k^i h + \tau\left(t_k^i\right), t_{k+1}^i h + \tau\left(t_{k+1}^i\right)\right) \end{aligned} \tag{6}$$

Remark 3. Suppose that the network delay is bounded, i.e., $0 < \tau_m \le \tau_k^i \le \overline{\tau}$, where τ_m and $\overline{\tau}$ denote the lower and upper bound of $\tau(t)$, respectively. It is worth noting that when $\sigma_r = 0$, all the sampled signals are transmitted, the event-triggered strategy (4) reduces to a periodic time-triggered scheme.

2.4. Time-Delay Modeling. Using the same technique as in [29], we assume that there is a integer $q > 0$, which satisfies $t_{k+1}^i = t_k^i + q + 1$. Hence, we can obtain the following equality:

$$\left[t_k^i h + \tau\left(t_k^i\right), t_{k+1}^i h + \tau\left(t_{k+1}^i\right)\right) = \bigcup_{n=0}^{q} \Omega_n \tag{7}$$

with $\Omega_n = [t_k^i h + nh + \tau(t_k^i + n), t_k^i h + (n+1)h + \tau(t_k^i + n + 1))$, $t_{k+1}^i = t_k^i + n + 1$.

For convenience, we define

$$\tau(t) = t - t_k^i h - nh, \quad t \in \Omega_n \tag{8}$$

Then, we can know that

$$0 < \tau_m \le \tau(t) \le h + \overline{\tau} = \tau_M \tag{9}$$

To show the effect of the event-triggered scheme (4) in deriving system stability and stabilization criterion, we define a new variable $e_{ki}(t)$, which satisfies the following equality:

$$e_{ki}(t) = y_i\left(t_k^i h\right) - y_i\left(t_k^i h + nh\right), \quad t \in \Omega_n \tag{10}$$

Substituting (8), (10) into (6), we have

$$\begin{aligned} \dot{x}_{fi}(t) &= A_{fr} x_{fi}(t) + B_{fr}\left[y_i(t - \tau(t)) + e_{ki}(t)\right] \\ z_{fi}(t) &= C_{fr} x_{fi}(t) \end{aligned} \tag{11}$$

From (10) and (4), we can obtain

$$e_{ki}^T(t)\phi_r e_{ki}(t) \le \sigma_r y_i^T(t - \tau(t))\phi_r y_i(t - \tau(t)) \tag{12}$$

where $t \in [t_k^i h + \tau(t_k^i), t_{k+1}^i h + \tau(t_{k+1}^i))$.

2.5. Event-Triggered H_∞ Filter Problem. By defining $\xi_i^T(t) = \left[x_i^T(t) \;\; x_{fi}^T(t)\right]$, $\widehat{w}_i(t) = \left[w_i^T(t) \;\; w_i^T(t - \tau(t))\right]^T$, and $e_i(t) = z_i(t) - z_{fi}(t)$, we can obtain the following filtering error system:

$$\begin{aligned} \dot{\xi}_i(t) &= \overline{A}\xi_i(t) + \Sigma_{j\in N_i} a_{ij}\overline{B}H\xi_i(t - \tau(t)) + \overline{E}e_{ki}(t) \\ &\quad + \overline{D}\widehat{w}_i(t) \\ e_i(t) &= \overline{C}_1\xi_i(t) + \Sigma_{j\in N_i} a_{ij}\overline{C}_2\left(\xi_i(t) - \xi_j(t)\right) \end{aligned} \tag{13}$$

where

$$\begin{aligned} \overline{A} &= \begin{bmatrix} A & 0 \\ 0 & A_{fr} \end{bmatrix}, \\ \overline{B} &= \begin{bmatrix} 0 \\ B_{fr}C_2 \end{bmatrix}, \\ H &= \begin{bmatrix} I_n & 0 \end{bmatrix}, \\ \overline{D} &= \begin{bmatrix} B & 0 \\ 0 & B_{fr}D \end{bmatrix}, \\ \overline{C}_1 &= \begin{bmatrix} 0 & -C_{fr} \end{bmatrix}, \\ \overline{C}_2 &= \begin{bmatrix} C_1 & 0 \end{bmatrix} \\ \overline{E} &= \begin{bmatrix} 0 \\ B_{fr} \end{bmatrix} \end{aligned} \tag{14}$$

Then, we define some new augment variables to compact system:

$$\begin{aligned} \xi(t) &= \left[\xi_1^T(t) \;\; \xi_2^T(t) \;\; \ldots \;\; \xi_N^T(t)\right]^T, \\ e(t) &= \left[e_1^T(t) \;\; e_2^T(t) \;\; \ldots \;\; e_N^T(t)\right]^T, \\ \widehat{w}(t) &= \left[\widehat{w}_1^T(t) \;\; \widehat{w}_2^T(t) \;\; \ldots \;\; \widehat{w}_N^T(t)\right]^T, \\ e_k(t) &= \left[e_{k1}^T(t) \;\; e_{k2}^T(t) \;\; \ldots \;\; e_{kN}^T(t)\right]^T \end{aligned} \tag{15}$$

Therefore, the filtering error system can be rewritten as follows:

$$\begin{aligned}\dot{\xi}(t) &= \left(I_N \otimes \overline{A}\right)\xi(t) + \left(L \otimes \overline{B}H\right)\xi(t-\tau(t)) \\ &\quad + \left(I_N \otimes \overline{E}\right)e_k(t) + \left(I_N \otimes \overline{D}\right)\widehat{w}(t) \\ e(t) &= \left(I_N \otimes \overline{C}_1 + L \otimes \overline{C}_2\right)\xi(t)\end{aligned} \tag{16}$$

Definition 4. The filtering error system (16) with $w(t) = 0$ is asymptotically stable in mean square, if for any initial conditions, such that

$$\lim_{t\longrightarrow+\infty} \left\|\xi(t)\right\|^2 = 0 \tag{17}$$

Definition 5. Given a positive scalar γ, and for all nonzero $w(t) \in L_2[0,\infty)$, the filtering error system (16) is asymptotically stable in mean square with a guaranteed H_∞ performance γ if the filtering error $e(t)$ satisfies

$$E\left\{\int_0^\infty e^T(t)\,e(t)\,dt\right\} \le \gamma^2 E\left\{\int_0^\infty w^T(t)\,w(t)\,dt\right\} \tag{18}$$

Before proceeding further, we introduce the following lemmas that will be helpful for deriving the following results.

Lemma 6 (see [30]). *Given scalar $\tau > 0$, matrix $M > 0$, and vector function w, $[0,\tau] \longrightarrow R^n$ satisfy the following inequality:*

$$\begin{aligned}&\left(\int_0^\tau w(s)\,ds\right)^T M \left(\int_0^\tau w(s)\,ds\right) \\ &\quad \le \tau\left(\int_0^\tau w^T(s) M w(s)\,ds\right).\end{aligned} \tag{19}$$

Lemma 7 (see [31]). *Suppose that $f_1(t), f_2(t), \ldots, f_N(t) : \mathbf{R}^m \longmapsto \mathbf{R}^n$ is positive values, which satisfies*

$$\min \sum_{i=1}^N \frac{1}{\alpha_i} f_i(t) = \sum_{i=1}^N f_i(t) + \max \sum_{i=1}^N \sum_{j=1, j\neq i}^N g_{i,j}(t) \tag{20}$$

subject to

$$\left\{g_{i,j} : \mathbf{R}^m \longmapsto \mathbf{R}^n,\ g_{j,i}(t) \equiv g_{i,j}(t),\ \begin{bmatrix} f_i(t) & g_{i,j} \\ g_{i,j} & f_i(t)\end{bmatrix} \ge 0\right\} \tag{21}$$

3. Main Results

3.1. Asymptotical Stability Analysis

Theorem 8. *For given scalars $\sigma_r > 0$, $\tau_M > \tau_m > 0$, the filtering error system (16) without external disturbance can achieve mean square stable under Definition 4 if there exist appropriate dimensional matrices $P_r > 0$, $Q_1 > 0$, $Q_2 > 0$, $R_1 > 0$, $R_2 > 0$, $\phi_r > 0$ and S_1 such that the following LMIs hold:*

$$\begin{bmatrix} R_2 & S_1 \\ * & R_2\end{bmatrix} > 0 \tag{22}$$

$$\begin{bmatrix} \Pi & \tau_m \Gamma^T \widehat{H}^T R_1 & (\tau_M - \tau_m)\Gamma^T \widehat{H}^T R_2 \\ * & -R_1 & 0 \\ * & * & -R_2\end{bmatrix} < 0 \tag{23}$$

$$\sum_{s=1}^q \pi_{rs} P_s \le P_r \tag{24}$$

where

$$\begin{aligned}\Pi &= \begin{bmatrix} \Xi_{11} & \Xi_{12} & \Xi_{13} & 0 & \Xi_{15} \\ * & \Xi_{22} & \Xi_{23} & \Xi_{24} & 0 \\ * & * & \Xi_{33} & \Xi_{34} & 0 \\ * & * & * & \Xi_{44} & 0 \\ * & * & * & * & -\widehat{\phi}_r\end{bmatrix} \\ \Gamma &= \begin{bmatrix} I_N \otimes \overline{A} & L \otimes \overline{B} & 0 & 0 & I_N \otimes \overline{E}\end{bmatrix} \\ \Xi_{11} &= \left(I_N \otimes \overline{A}\right)^T P_r + P_r\left(I_N \otimes \overline{A}\right) + P_r + \widehat{H}^T Q_1 \widehat{H} \\ &\quad + \widehat{H}^T Q_2 \widehat{H} - \widehat{H}^T R_1 \widehat{H} \\ \Xi_{12} &= P_r\left(L \otimes \overline{B}\right) \\ \Xi_{13} &= \widehat{H}^T R_1 \\ \Xi_{15} &= P_r\left(I_N \otimes \overline{E}\right) \\ \Xi_{22} &= \sigma_r\left(L \otimes C_2\right)^T \widehat{\phi}_r\left(L \otimes C_2\right) - 2R_2 + S_1 + S_1^T \\ \Xi_{23} &= -S_1^T + R_2 \\ \Xi_{24} &= -S_1 + R_2 \\ \Xi_{33} &= -Q_1 - R_1 - R_2 \\ \Xi_{34} &= S_1 \\ \Xi_{44} &= -Q_2 - R_2 \\ \widehat{H} &= I_N \otimes H, \\ \widehat{H}_2 &= I_N \otimes H_2, \\ \widehat{\phi}_r &= I_N \otimes \phi_r, \\ H_2 &= \begin{bmatrix} 0 & I_n\end{bmatrix}\end{aligned} \tag{25}$$

Proof. Consider that there is no external disturbance, i.e., $w(t) = 0$. We construct the following Lyapunov functional:

$$V\left(t,\xi(t),\dot{\xi}(t),r(t)\right) = \sum_{i=1}^5 V_i\left(t,\xi(t),\dot{\xi}(t),r(t)\right) \tag{26}$$

where

$$V_1\left(t,\xi(t),\dot{\xi}(t),r(t)\right) = \xi^T(t) P_r \xi(t)$$

$$V_2\left(t,\xi(t),\dot{\xi}(t)\right) = \int_{t-\tau_m}^t \xi^T(s)\widehat{H}^T Q_1 \widehat{H}\xi(s)\,ds$$

$$V_3\left(t,\xi(t),\dot{\xi}(t)\right) = \int_{t-\tau_M}^t \xi^T(s)\widehat{H}^T Q_2 \widehat{H}\xi(s)\,ds$$

$$
\begin{aligned}
&V_4\left(t,\xi(t),\dot{\xi}(t)\right)\\
&\quad=\tau_m\int_{-\tau_m}^{0}\int_{t+\theta}^{t}\dot{\xi}^T(s)\,\widehat{H}^T R_1\widehat{H}\dot{\xi}(s)\,ds\,d\theta\\
&V_5\left(t,\xi(t),\dot{\xi}(t)\right)\\
&\quad=\left(\tau_M-\tau_m\right)\int_{-\tau_M}^{-\tau_m}\int_{t+\theta}^{t}\dot{\xi}^T(s)\,\widehat{H}^T R_2\widehat{H}\dot{\xi}(s)\,ds\,d\theta
\end{aligned}
\tag{27}
$$

then its derivative along system (16) with $w(t)=0$ is

$$
\begin{aligned}
\dot{V}_1&=\dot{\xi}^T(t)\,P_r\xi(t)+\xi^T(t)\,P_r\dot{\xi}(t)\\
&\quad+\xi^T(t)\left\{\sum_{s=1}^{q}\pi_{rs}P_s\right\}\xi(t)\\
\dot{V}_2&=\xi^T(t)\,\widehat{H}^T Q_1\widehat{H}\xi(t)\\
&\quad-\xi^T\left(t-\tau_m\right)\widehat{H}^T Q_1\widehat{H}\xi\left(t-\tau_m\right)\\
\dot{V}_3&=\xi^T(t)\,\widehat{H}^T Q_2\widehat{H}\xi(t)\\
&\quad-\xi^T\left(t-\tau_M\right)\widehat{H}^T Q_2\widehat{H}\xi\left(t-\tau_M\right)
\end{aligned}
$$

$$
\begin{aligned}
\dot{V}_4&=\tau_m^2\dot{\xi}^T(t)\,\widehat{H}^T R_1\widehat{H}\dot{\xi}(t)\\
&\quad-\tau_m\int_{t-\tau_m}^{t}\dot{\xi}^T(s)\,\widehat{H}R_1\widehat{H}\dot{\xi}(s)\,ds\\
\dot{V}_5&=\left(\tau_M-\tau_m\right)^2\dot{\xi}^T(t)\,\widehat{H}^T R_2\widehat{H}\dot{\xi}(t)\\
&\quad-\left(\tau_M-\tau_m\right)\int_{t-\tau(t)}^{t-\tau_m}\dot{\xi}^T(s)\,\widehat{H}R_2\widehat{H}\dot{\xi}(s)\,ds\\
&\quad-\left(\tau_M-\tau_m\right)\int_{t-\tau_M}^{t-\tau(t)}\dot{\xi}^T(s)\,\widehat{H}R_2\widehat{H}\dot{\xi}(s)\,ds
\end{aligned}
\tag{28}
$$

Applying Lemmas 6 and 7 to deal with the integral items and combining the event-triggered scheme (12), we have

$$
\begin{aligned}
&\dot{V}\left(t,\xi(t),\dot{\xi}(t),r(t)\right)\\
&\quad\le\sum_{i=1}^{5}V_i\left(t,\xi(t),\dot{\xi}(t),r(t)\right)-e_k^T(t)\,\hat{\phi}_r e_k(t)\\
&\qquad+\sigma_r y^T\left(t-\tau(t)\right)\hat{\phi}_r y\left(t-\tau(t)\right)=\zeta^T(t)\,\psi\,\zeta(t)
\end{aligned}
\tag{29}
$$

where

$$
\begin{aligned}
\zeta^T(t)&=\left[\xi^T(t)\;\;\xi^T\left(t-\tau(t)\right)\widehat{H}^T\;\;\xi^T\left(t-\tau_m\right)\widehat{H}^T\;\;\xi^T\left(t-\tau_M\right)\widehat{H}^T\;\;e_k^T(t)\right]\\
\psi&=\Pi+\tau_m^2\Gamma^T\widehat{H}^T R_1\widehat{H}\Gamma+\left(\tau_M-\tau_m\right)^2\Gamma^T\widehat{H}^T R_2\widehat{H}\Gamma
\end{aligned}
\tag{30}
$$

By employing the Schur complement, we can find easily that (23) ensures $\psi<0$. According to Definition 4, the filtering error system (16) is asymptotically stable in mean square under the event-triggered scheme (12) if (22), (23), and (24) hold. The proof is completed. □

3.2. H_∞ Performance Analysis

Theorem 9. *For given scalars $\sigma_r>0$, $\tau_M>\tau_m>0$, considering the existence of external disturbance, the filtering error system (16) can achieve being asymptotically stable with an H_∞ performance index γ under Definition 5 if there exist appropriate dimensional matrices $P_r>0$, $Q_1>0$, $Q_2>0$, $R_1>0$, $R_2>0$, $\phi_r>0$ and S_1 such that the following LMIs hold:*

$$
\begin{bmatrix}R_2 & S_1\\ * & R_2\end{bmatrix}>0
\tag{31}
$$

$$
\begin{bmatrix}
\Theta & \tau_m\Gamma_1^T\widehat{H}^T R_1 & \left(\tau_M-\tau_m\right)\Gamma_1^T\widehat{H}^T R_2 & \Gamma_2^T\\
* & -R_1 & 0 & 0\\
* & * & -R_2 & 0\\
* & * & * & -I
\end{bmatrix}<0
\tag{32}
$$

$$
\sum_{s=1}^{q}\pi_{rs}P_s\le P_r
\tag{33}
$$

where

$$
\begin{aligned}
\Theta&=\begin{bmatrix}
\Xi_{11} & \Xi_{12} & \Xi_{13} & 0 & \Xi_{15} & \Xi_{16}\\
* & \Xi_{22} & \Xi_{23} & \Xi_{24} & 0 & \Xi_{26}\\
* & * & \Xi_{33} & \Xi_{34} & 0 & 0\\
* & * & * & \Xi_{44} & 0 & 0\\
* & * & * & * & -\hat{\phi}_r & \\
* & * & * & * & * & \Xi_{66}
\end{bmatrix}\\
\Gamma_1&=\left[I_N\otimes\overline{A}\;\;L\otimes\overline{B}\;\;0\;\;0\;\;I_N\otimes\overline{E}\;\;I_N\otimes\overline{D}\right]\\
\Gamma_2&=\left[I_N\otimes\overline{C}_1+L\otimes\overline{C}_2\;\;0\;\;0\;\;0\;\;0\;\;0\right]\\
\Xi_{16}&=P_r\left(I_N\otimes\overline{D}\right)\\
\Xi_{26}&=\sigma_r\left(L\otimes C_2\right)^T\hat{\phi}_r\left(I_N\otimes D\right)\widehat{H}_2\\
\Xi_{66}&=-\gamma^2 I+\sigma_r\widehat{H}_2^T\left(I_N\otimes D\right)^T\hat{\phi}_r\left(I_N\otimes D\right)\widehat{H}_2
\end{aligned}
\tag{34}
$$

and the other parameters are defined as in Theorem 8.

Proof. Consider the existence of external disturbance, i.e., $w(t) \neq 0$, and choose the same Lyapunov functional like Theorem 8; we have

$$\begin{aligned}
&\dot{V}\left(t,\xi(t),\dot{\xi}(t),r(t)\right)\\
&\quad=\dot{V}\left(t,\xi(t),\dot{\xi}(t),r(t)\right)+e^T(t)\,e(t)\\
&\qquad-\gamma^2\widehat{w}^T(t)\,\widehat{w}(t)-e^T(t)\,e(t)+\gamma^2\widehat{w}^T(t)\,\widehat{w}(t)\\
&\quad=\eta^T(t)\,\Omega\eta(t)-e^T(t)\,e(t)+\gamma^2\widehat{w}^T(t)\,\widehat{w}(t)
\end{aligned} \tag{35}$$

where

$$\begin{aligned}
\eta^T(t)&=\left[\zeta^T(t)\quad\widehat{w}^T(t)\right]\\
\Omega&=\Theta+\tau_m^2\Gamma_1^T\widehat{H}^TR_1\widehat{H}\Gamma_1\\
&\quad+\left(\tau_M-\tau_m\right)^2\Gamma_1^T\widehat{H}^TR_2\widehat{H}\Gamma_1+\Gamma_2^T\Gamma_2
\end{aligned} \tag{36}$$

By using the Schur complement, we can find easily that (32) guarantees $\Omega < 0$. According to Definition 5, the filtering error system (16) is asymptotically stable with H_∞ norm bound γ if (31), (32), and (33) are satisfied. The proof is completed. □

3.3. Filter Design

Theorem 10. *For given scalars $\sigma_r > 0$, $\tau_M > \tau_m > 0$ and H_∞ performance index γ, the filtering error system (16) under the event-triggered scheme (12) is asymptotically stable in mean square for $w(t) = 0$ and satisfies the H_∞ performance constraint (18) for all nonzero $w(t) \in L_2[0,+\infty)$ under the zero initial condition if there exist real matrices $P_r > 0$, $W_r > 0$, $\phi_r > 0$ ($r \in S$), $Q_1 > 0$, $Q_2 > 0$, $R_1 > 0$, $R_2 > 0$ and matrices $S_1, \overline{A}_{fr}, \overline{B}_{fr}, \overline{C}_{fr}$ ($r \in S$) with appropriate dimension such that the following LMIs hold:*

$$\begin{bmatrix} R_2 & S_1 \\ * & R_2 \end{bmatrix} > 0, \tag{37}$$

$$\begin{bmatrix} \phi_{11} & \phi_{12} & \phi_{13} & \phi_{14} \\ * & -R_1 & 0 & 0 \\ * & * & -R_2 & 0 \\ * & * & * & -I \end{bmatrix} < 0, \tag{38}$$

$$\sum_{s=1}^{q}\pi_{rs}\left(U_{1s}-W_s\right)\le U_{1r}-W_r \tag{39}$$

where

$$\phi_{11}=\begin{bmatrix} \widehat{\Xi}_{11} & \widehat{\Xi}_{12} & \widehat{\Xi}_{13} & 0 & \widehat{\Xi}_{15} & \widehat{\Xi}_{16} \\ * & \Xi_{22} & \Xi_{23} & \Xi_{24} & 0 & \Xi_{26} \\ * & * & \Xi_{33} & \Xi_{34} & 0 & 0 \\ * & * & * & \Xi_{44} & 0 & 0 \\ * & * & * & * & -\widehat{\phi}_r & 0 \\ * & * & * & * & * & \Xi_{66} \end{bmatrix}$$

$$\begin{aligned}
\phi_{12}&=\left[\tau_mR_1\left(I_N\otimes A\right)\widehat{H}\;\;0\;\;0\;\;0\;\;0\;\;\tau_mR_1\left(I_N\otimes B\right)\widehat{H}\right]^T,\\
\phi_{13}&=\left[\left(\tau_M-\tau_m\right)R_2\left(I_N\otimes A\right)\widehat{H}\;\;0\;\;0\;\;0\;\;0\;\;\left(\tau_M-\tau_m\right)R_2\left(I_N\otimes B\right)\widehat{H}\right]^T,\\
\phi_{14}&=\left[\left(I_N\otimes-\overline{C}_{fr}\right)\widehat{H}_2+\left(L\otimes C_1\right)\widehat{H}\;\;0\;\;0\;\;0\;\;0\;\;0\right]^T,\\
\widehat{\Xi}_{11}&=I_N\otimes\begin{bmatrix} U_{1r}+A^TU_{1r}+U_{1r}A & W_r+\overline{A}_{fr}+A^TW_r \\ * & W_r+\overline{A}_{fr}+\overline{A}_{fr}^T \end{bmatrix}+\widehat{H}^T\left(Q_1+Q_2-R_1\right)\widehat{H},\\
\widehat{\Xi}_{12}&=L\otimes\begin{bmatrix}\overline{B}_{fr}C_2\\ \overline{B}_{fr}C_2\end{bmatrix},\\
\widehat{\Xi}_{13}&=\widehat{H}^TR_1,\\
\widehat{\Xi}_{15}&=I_N\otimes\begin{bmatrix}\overline{B}_{fr}\\ \overline{B}_{fr}\end{bmatrix},\\
\widehat{\Xi}_{16}&=I_N\otimes\begin{bmatrix}U_{1r}B & \overline{B}_{fr}D\\ W_rB & \overline{B}_{fr}D\end{bmatrix}
\end{aligned} \tag{40}$$

Moreover, if the above conditions are feasible, the parameter matrices of the filter are given by

$$\begin{aligned} A_{fr} &= W_r^{-1}\overline{A}_{fr} \\ B_{fr} &= W_r^{-1}\overline{B}_{fr} \\ C_{fr} &= \overline{C}_{fr} \end{aligned} \tag{41}$$

Proof. Let $P_r = I_N \otimes U_r$ for conditions (32) in Theorem 8. Let matrix U_r be partitioned as

$$U_r = \begin{bmatrix} U_{1r} & U_{2r} \\ * & U_{3r} \end{bmatrix} \tag{42}$$

where $U_{1r} > 0$, U_{2r}, and U_{3r} are nonsingular matrices, satisfying $W_r = U_{2r}U_{3r}^{-1}U_{2r}^T$. By Schur complement, we can obtain that $U_r > 0$ is equivalent to $U_{1r} - W_r > 0$. Define the following invertible matrix:

$$J_1 = \begin{bmatrix} I & 0 \\ 0 & U_{2r}U_{3r}^{-1} \end{bmatrix} \tag{43}$$

Then, pre- and postmultiply (32) by J_2 and J_2^T, respectively, where $J_2 = \text{diag}\{J_1, \underbrace{I, \ldots, I}_{8}\}$ and define new variables:

$$\begin{aligned} \overline{A}_{fr} &= U_{2r}A_{fr}U_{3r}^{-1}U_{2r}^T \\ \overline{B}_{fr} &= U_{2r}B_{fr} \\ \overline{C}_{fr} &= C_{fr}U_{3r}^{-1}U_{2r}^T \end{aligned} \tag{44}$$

By the linear transformation above, we can find easily that (32) is equivalent to (38). Therefore, we can obtain (41). The proof is completed. □

Remark 11. Comparing with the previous results [32], lower bounds theorem [31] is adopted in this paper, which not only achieves performance behavior identical to approaches based on the integral inequality lemma, but also decreases the number of decision variables dramatically.

4. Simulation

The parameters of MASs (1) are given as follows:

$$\begin{aligned} A &= \begin{bmatrix} -1 & 1 \\ 0.8 & -4 \end{bmatrix}, \\ B &= \begin{bmatrix} 0.5 \\ 0.1 \end{bmatrix} \\ C1 &= \begin{bmatrix} 0.1 & 0 \end{bmatrix}, \\ C2 &= \begin{bmatrix} 0.2 & 0 \end{bmatrix}, \\ D &= 0.1 \end{aligned} \tag{45}$$

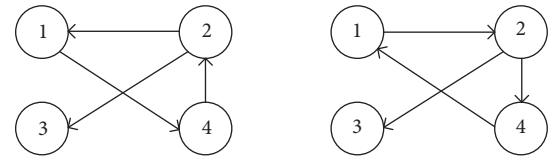

G1 G2

Figure 1: Directed communication topology graphs.

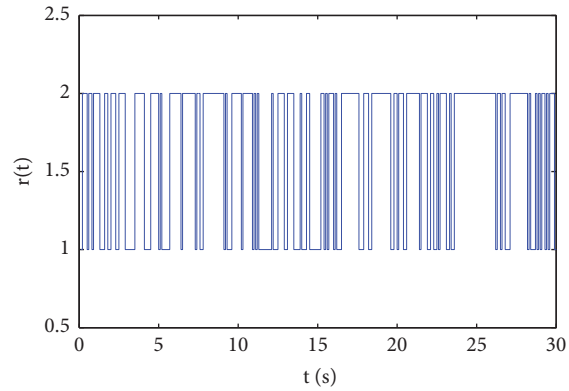

Figure 2: Evolution of Markov chain.

In addition, the external disturbances of MASs (1) are defined as follows:

$$w_i(t) = 0.4e^{-0.2t}\cos(0.6t). \tag{46}$$

All the possible information transmission relationships among agents are shown in Figure 1. Then, the corresponding Laplacian matrices are given as follows, respectively.

$$\begin{aligned} L_1 &= \begin{bmatrix} 1 & -1 & 0 & 0 \\ 0 & 1 & 0 & -1 \\ 0 & -1 & 1 & 0 \\ -1 & 0 & 0 & 1 \end{bmatrix}, \\ L_2 &= \begin{bmatrix} 1 & 0 & 0 & -1 \\ -1 & 1 & 0 & 0 \\ 0 & -1 & 1 & 0 \\ 0 & -1 & 0 & 1 \end{bmatrix} \end{aligned} \tag{47}$$

Figure 2 shows the switching of two modes in a Markov chain. Suppose that the probability transition matrix is defined as

$$\Pi = \begin{bmatrix} -5 & 5 \\ 2 & -2 \end{bmatrix} \tag{48}$$

Given that $h = 0.1$, $\sigma_1 = 0.1$, $\sigma_2 = 0.2$, minimum allowable delay $\tau_m = 0.1$ and the maximum allowable delay $\tau_M = 0.5$. Let the initial states $x_1(0) = [3; -1]$, $x_2(0) = [1; -1]$, $x_3(0) = [1; -3]$, $x_4(0) = [-3; 3]$. By solving LMIs in

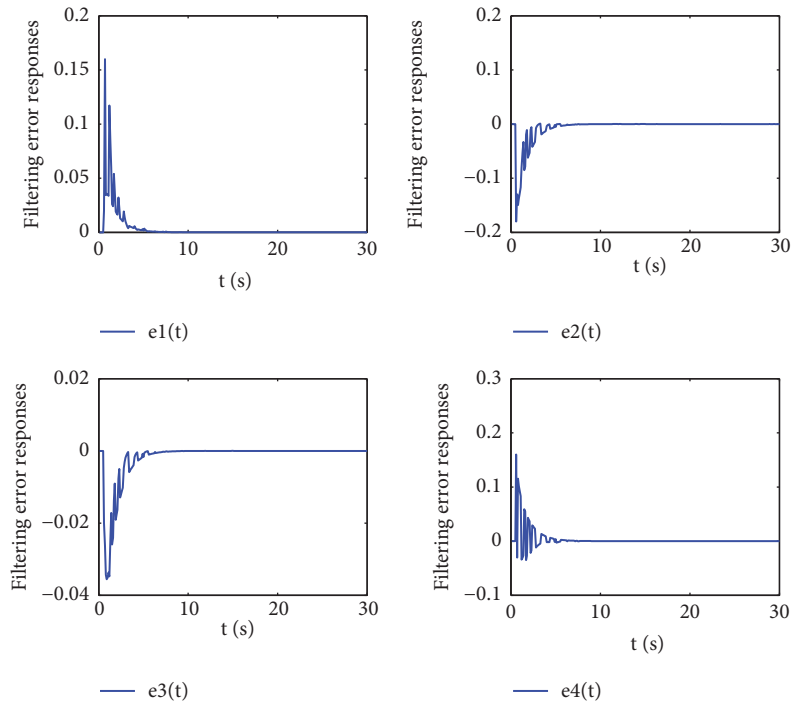

Figure 3: Filtering error response.

Theorem 9, we can obtain parameters of the designed filter (3),

$$
\begin{aligned}
A_{f1} &= \begin{bmatrix} -24.8840 & 52.462 \\ -9.6761 & 20.1822 \end{bmatrix}, \\
B_{f1} &= \begin{bmatrix} -0.6878 \\ -0.2918 \end{bmatrix} \\
C_{f1} &= \begin{bmatrix} -1.3535 & 0.0581 \end{bmatrix} \\
A_{f2} &= \begin{bmatrix} -58.5910 & 137.6004 \\ -22.9133 & 53.7343 \end{bmatrix}, \\
B_{f2} &= \begin{bmatrix} 0.8893 \\ 0.3558 \end{bmatrix} \\
C_{f2} &= \begin{bmatrix} -0.1373 & -0.0623 \end{bmatrix} \times 10^{-5},
\end{aligned} \tag{49}
$$

and the event-triggered parameters,

$$
\begin{aligned}
\phi_1 &= 15.5816, \\
\phi_2 &= 7.9041
\end{aligned} \tag{50}
$$

In Figure 3, it shows the filtering error of agent i ($i = 1, 2, 3, 4$). In Figure 4, it depicts the state curves of $z_i(t)$ and estimation signal $z_{fi}(t)$ ($i = 1, 2, 3, 4$). The event-triggered release instants and intervals of agent i ($i = 1, 2, 3, 4$) are shown in Figure 5. Letting the simulation time t=30, we can get that agent 1 triggers 84 times, agent 2 triggers 36 times, agent 3 triggers 40 times, and agent 4 triggers 92 times. If $\sigma_r = 0$ (time-triggered), there are 300 times transmitted. We can find clearly that the event-triggered control strategy (12) efficiently saves the network resources.

5. Conclusion

In this paper, we study the problem of H_∞ filtering for MASs with Markovian switching topologies. Considering the effect of switching topologies and network-induced delay, we adopt a reasonable event-triggered mechanism to reduce the amount of network transmission. By employing Lyapunov stability theory and LMI technique, some sufficient conditions are obtained which can ensure filtering error system to achieve mean square stable with an H_∞ norm bound. Finally, a numerical example is provided to show that the method we proposed is feasible and effective.

Data Availability

(i) The system parameters A, B, C1, C2, D used to support the findings of this study are included within the article. (ii) The external disturbance wi(t) used to support the findings of this study titled "Event-triggered H_∞ Filtering for Discrete-Time Neural Networks with Missing Measurements" is available from the corresponding author upon request. (iii) The initial states $x1(0)$, $x2(0)$, $x3(0)$, $x4(0)$ used to support the findings of this study are included within the article. (iv) The Laplacian matrices $L1$, $L2$ and probability transition matrix Π used to support the findings of this study are included within the article. (v) The filter parameters $Af1, Af2, Bf1, Bf2, Cf1, Cf2$ and event-triggered parameters $\Phi1$, $\Phi2$ used to support the findings of this study are derived by solving LMIs, which are included in the article.

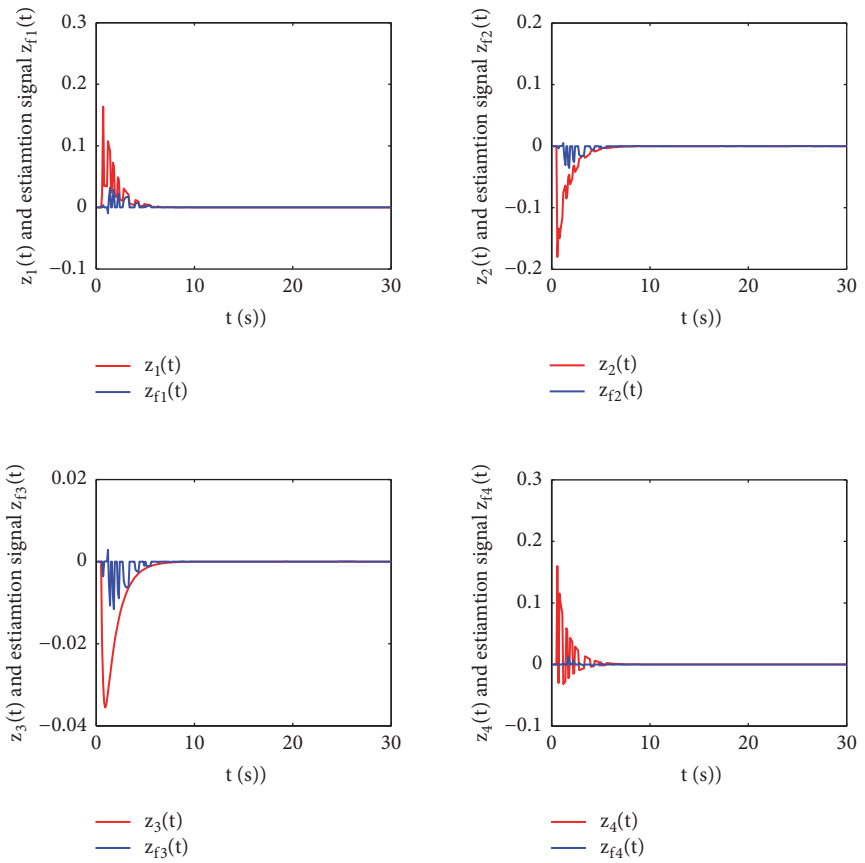

FIGURE 4: $z_i(t)$ and their estimation $z_{fi}(t)$.

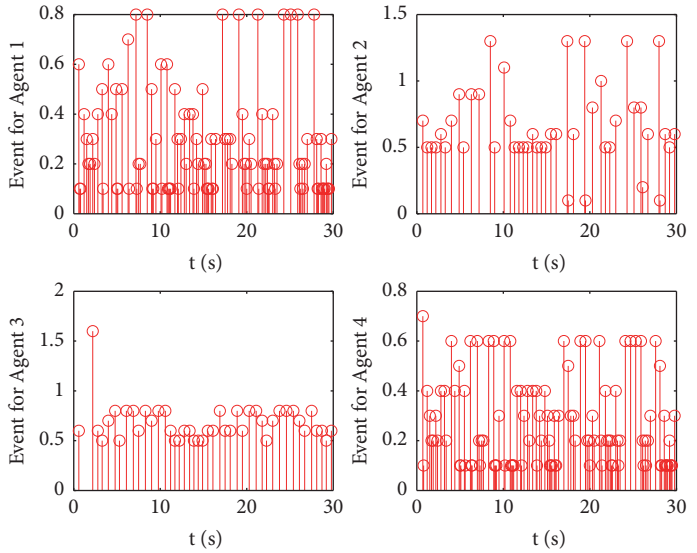

FIGURE 5: The release instants and release interval of each agent.

Conflicts of Interest

The authors declare that they have no conflicts of interest.

Acknowledgments

This work was supported by the National Natural Science Foundation of China (61374083 and 61703371).

References

[1] X. Ge and Q.-L. Han, "Distributed Formation Control of Networked Multi-Agent Systems Using a Dynamic Event-Triggered Communication Mechanism," *IEEE Transactions on Industrial Electronics*, vol. 64, no. 10, pp. 8118–8127, 2017.

[2] T. Han, Z. H. Guan, M. Chi, B. Hu, T. Li, and X. H. Zhang, "Multi-formation control of nonlinear leader-following multi-agent systems," *ISA Transactions®*, vol. 69, pp. 140–147, 2017.

[3] X. Ge and Q.-L. Han, "Distributed event-triggered H_∞ filtering over sensor networks with communication delays," *Information Sciences*, vol. 291, pp. 128–142, 2015.

[4] C. P. Bechlioulis and G. A. Rovithakis, "Decentralized robust synchronization of unknown high order nonlinear multi-agent systems with prescribed transient and steady state performance," *IEEE Transactions on Automatic Control*, vol. 62, no. 1, pp. 123–134, 2017.

[5] J. Gao, X. Xu, N. Ding, and E. Li, "Flocking motion of multi-agent system by dynamic pinning control," *IET Control Theory & Applications*, vol. 11, no. 5, pp. 714–722, 2017.

[6] L. Zhou and S. Li, "Distributed model predictive control for multi-agent flocking via neighbor screening optimization," *International Journal of Robust and Nonlinear Control*, vol. 27, no. 9, pp. 1690–1705, 2017.

[7] R. Olfati-Saber, "Distributed Kalman filtering for sensor networks," in *Proceedings of the 46th IEEE Conference on Decision and Control*, pp. 5492–5498, December 2007.

[8] R. Olfati-Saber, "Kalman-consensus filter: optimality, stability, and performance," in *Proceedings of the 48th IEEE Conference on Decision and Control Held Jointly with the 28th Chinese Control Conference (CDC/CCC '09)*, pp. 7036–7042, IEEE, Shanghai, China, December 2009.

[9] B. Shen, Z. Wang, and Y. S. Hung, "Distributed H_∞-consensus filtering in sensor networks with multiple missing measurements: the finite-horizon case," *Automatica*, vol. 46, no. 10, pp. 1682–1688, 2010.

[10] Y. Xu, H. Y. Su, Y. J. Pan, and Z. Wu, "Robust H_∞ filtering for networked stochastic systems with randomly occurring sensor nonlinearities and packet dropouts," *Signal Processing*, vol. 93, no. 7, pp. 1794–1803, 2013.

[11] X. Ge, Q. Han, D. Ding, X. Zhang, and B. Ning, "A survey on recent advances in distributed sampled-data cooperative control of multi-agent systems," *Neurocomputing*, vol. 275, pp. 1684–1701, 2018.

[12] R. Yang, P. Shi, G. P. Liu, and H. Gao, "Network-based feedback control for systems with mixed delays based on quantization and dropout compensation," *Automatica*, vol. 47, no. 12, pp. 2805–2809, 2011.

[13] Z. G. Wu, P. Shi, H. Y. Su, and J. Chu, "Network-based robust passive control for fuzzy systems with randomly occurring uncertainties," *IEEE Transactions on Fuzzy Systems*, vol. 21, no. 5, pp. 966–971, 2013.

[14] Y. Wu, R. Lu, P. Shi, H. Su, and Z. Wu, "Sampled-Data Synchronization of Complex Networks With Partial Couplings and T–S Fuzzy Nodes," *IEEE Transactions on Fuzzy Systems*, vol. 26, no. 2, pp. 782–793, 2018.

[15] Y. Wu, R. Lu, P. Shi, H. Su, and Z. Wu, "Analysis and Design of Synchronization for Heterogeneous Network," *IEEE Transactions on Cybernetics*, vol. 48, no. 4, pp. 1253–1262, 2018.

[16] Y. Wu and R. Lu, "Event-based control for network systems via integral quadratic constraints," *IEEE Transactions on Circuits and Systems I: Regular Papers*, vol. 65, no. 4, pp. 1386–1394, 2018.

[17] L. Zou, Z. Wang, H. Gao, and X. Liu, "Event-triggered state estimation for complex networks with mixed time delays via sampled data information: The continuous-time case," *IEEE Transactions on Cybernetics*, vol. 45, no. 12, pp. 2804–2815, 2015.

[18] J. Hu, Z. Wang, J. Liang, and H. Dong, "Event-triggered distributed state estimation with randomly occurring uncertainties and nonlinearities over sensor networks: a delay-fractioning approach," *Journal of The Franklin Institute*, vol. 352, no. 9, pp. 3750–3763, 2015.

[19] S. Hu and D. Yue, "Event-based H_∞ filtering for networked system with communication delay," *Signal Processing*, vol. 92, no. 9, pp. 2029–2039, 2012.

[20] J. Liu, J. Tang, and S. Fei, "Event-triggered H∞ filter design for delayed neural network with quantization," *Neural Networks*, vol. 82, pp. 39–48, 2016.

[21] S. Li, D. Sauter, and B. Xu, "Fault isolation filter for networked control system with event-triggered sampling scheme," *Sensors*, vol. 11, no. 1, pp. 557–572, 2011.

[22] H. Wang, P. Shi, and J. Zhang, "Event-triggered fuzzy filtering for a class of nonlinear networked control systems," *Signal Processing*, vol. 113, pp. 159–168, 2015.

[23] H. Wang, A. Xue, J. Wang, and R. Lu, "Event-based H∞ filtering for discrete-time markov jump systems with network-induced delay," *Journal of The Franklin Institute*, vol. 354, no. 14, pp. 6170–6189, 2017.

[24] H. Wang, D. Zhang, and R. Lu, "Event-triggered H∞ filter design for markovian jump systems with quantization," *Nonlinear Analysis: Hybrid Systems*, vol. 28, pp. 23–41, 2018.

[25] Z. G. Wu, P. Shi, H. Su, and J. Chu, "Asynchronous l_2-l_∞ filtering for discrete-time stochastic Markov jump systems with randomly occurred sensor nonlinearities," *Automatica*, vol. 50, no. 1, pp. 180–186, 2014.

[26] S. Xu, J. Lam, and X. Mao, "Delay-dependent H_∞ control and filtering for uncertain Markovian jump systems with time-varying delays," *IEEE Transactions on Circuits and Systems I: Regular Papers*, vol. 54, no. 9, pp. 2070–2077, 2007.

[27] L. X. Zhang, "H_∞ estimation for discrete-time piecewise homogeneous Markov jump linear systems," *Automatica*, vol. 45, no. 11, pp. 2570–2576, 2009.

[28] D. Viegas, P. Batista, P. Oliveira, C. Silvestre, and C. L. Chen, "Distributed state estimation for linear multi-agent systems with time-varying measurement topology," *Automatica*, vol. 54, pp. 72–79, 2015.

[29] D. Yue, E. Tian, and Q. Han, "A delay system method for designing event-triggered controllers of networked control systems," *IEEE Transactions on Automatic Control*, vol. 58, no. 2, pp. 475–481, 2013.

[30] K. Gu, "An integral inequality in the stability problem of time-delay systems," in *Proceedings of the 39th IEEE Confernce on Decision and Control*, pp. 2805–2810, Sydney, Australia, December 2000.

[31] P. G. Park, J. W. Ko, and C. Jeong, "Reciprocally convex approach to stability of systems with time-varying delays," *Automatica*, vol. 47, no. 1, pp. 235–238, 2011.

[32] H. Y. Shao, "New delay-dependent stability criteria for systems with interval delay," *Automatica*, vol. 45, no. 3, pp. 744–749, 2009.

Hindawi
Journal of Control Science and Engineering
Volume 2018, Article ID 1630402, 11 pages
https://doi.org/10.1155/2018/1630402

Research Article

Superresolution Reconstruction of Electrical Equipment Incipient Fault

Manran Wang, Li Guo, Jinhao Chen, Bingqi Lv, and Yang Yang

Hubei University for Nationalities, Hubei, Enshi 445000, China

Correspondence should be addressed to Li Guo; 411985846@qq.com

Received 10 May 2018; Accepted 12 July 2018; Published 7 August 2018

Academic Editor: Yun-Bo Zhao

With the rapid development of industry and technology, the electrical power system becomes more complex and the electrical equipment becomes more diverse. Defective equipment is often the cause of industrial accidents and electrical injuries, which can result in serious injuries, such as electrocution, burns, and electrical shocks. In some cases, electrical equipment fault may result in death. However, in some special situation, some fault is very small even invisible, such as equipment aging, holes, and cracks, so the detection of these incipient faults is difficult or even impossible. These potential incipient faults become the biggest hidden danger in the electrical equipment and electricity power system. For these reasons, this paper proposes a superresolution reconstruction method for electrical equipment incipient fault to ensure complete detection in electrical equipment, which aims to guarantee the security of electrical power system operation and industry production. Experimental results show that this method can get a state-of-the-art reconstruction effect of incipient fault, so as to provide reliable fault detection of electrical power system.

1. Introduction

In the electrical power system, there is no doubt that the safety of electrical equipment is the basis for ensuring the stability and reliability [1]. Aging and fine lines of electrical equipment components can be characterized as incipient fault of electrical equipment. In power system, fault of electrical equipment components may manifest themselves as abnormal deviations in system behavior and operation. However, due to their very slow evolution, their effects may be confused with noise and uncertainty, which constitutes the characteristic that incipient fault is difficult to detect. Because it is not easy to be discovered, incipient fault is often regarded as precursors in significant accidents. Earlier detected type and exact location of the fault can cause faster detection and repairing of the fault, which is very important for the stable operation of the power system [2]. In recent years, there are many researchers who focus on fault detection of the electrical power system. Huang D et al. developed a transformer fault information pattern recognition and diagnosis model using the objective entropy weight method [3]. Taha I B M et al. designed a conditional probability scheme to inspect transformer incipient fault [4]. And Huang D et al. presented an improved hidden Markov model (HMM) algorithm for fault diagnosis of urban rail transit motors equipment; they also used a back-propagation neural network for multiple fault of complex equipment bearings [5, 6]. However, these methods can only be targeted at minor devices, failing to accurately determine potential incipient fault, which is a limitation in fault detection application. At present, it seems that few works are concerned with the topic of incipient fault detection [7–9]. In view of the above situation, this paper proposes a preprocessing method based on superresolution (SR) reconstruction, which can helpfully detect the incipient fault by improving the resolution of the electrical equipment image. In this method, a deep network structure is combined with sparse prior information, so as to obtain the high-resolution (HR) version by mapping from low-resolution (LR) input. Finally the SR reconstruction result of incipient fault can be obtained to improve the subjective visual effect, which can help detect and analyze the electrical equipment fault.

This paper is organized as follows. The basic framework and methods of SR are discussed in Section 2. In Section 3,

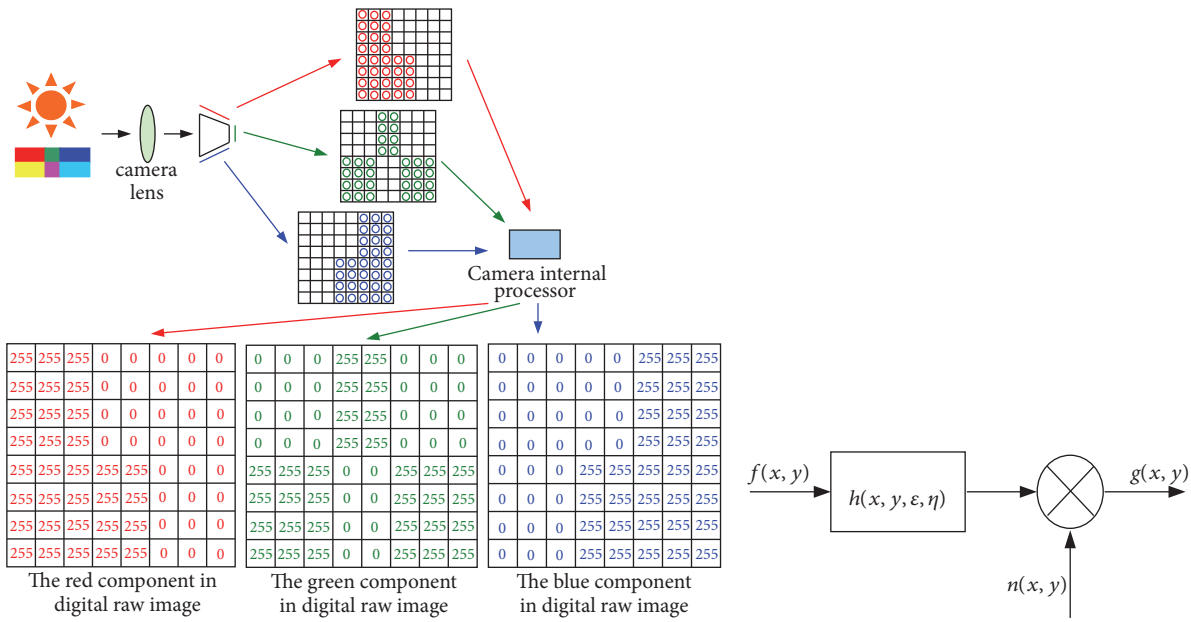

(a) The colorful imaging process of a natural scene

(b) The image degraded model

FIGURE 1: Imaging process and image degraded model.

we evaluate our model on some electrical equipment images containing electrical fault and give a detailed analysis of these results. Finally, Section 4 draws a conclusion.

2. SR Reconstruction Method of Electrical Equipment Incipient Fault

2.1. Basic Framework of SR. In some special electrical situations where it is difficult to produce HR monitoring video (images), SR reconstruction is an efficient method to improve the resolution of the captured monitoring video (images). SR is a problem of obtaining a HR image from multiple or single LR images [10], which is an inverse problem of imaging process. In imaging process, the LR image is acquired through various imaging devices which are corrupted by noise and other degraded effect [11–13], and the imaging process is shown in Figure 1(a). It is worthwhile to improve the resolution of LR images in some special situations. The observation model of imaging process is mathematized as (1) and shown in Figure 1(b).

$$g(x, y) = h(x, y, \varepsilon, \eta) \cdot f(x, y) + n(x, y) \quad (1)$$

where $\mathbf{f}(\mathbf{x},\mathbf{y})$ represents the original real HR continuous natural scene, $\mathbf{g}(\mathbf{x},\mathbf{y})$ is the output digital LR image, $\mathbf{h}(\mathbf{x},\mathbf{y},\boldsymbol{\varepsilon},\boldsymbol{\eta})$ is the point-spread function (PSF), which represents blurring matrices and downsampling matrices, and $\mathbf{n}(\mathbf{x},\mathbf{y})$ is the additive noise from different environment and device [14]. From this observation model, SR is an ill-posed inverse problem of reconstructing a HR image from an observed LR image.

Figure 1(a) is the basic illustration of the colorful imaging process of a natural scene, which can obtain R, G, and B channel of an image, respectively, by CCD array. Figure 1(b) is the image degraded model; it corresponds to (1). SR is an inverse process of Figure 1(b), so it is an ill-posed inverse problem which estimates a HR version closed to an original real HR scene.

In recent image processing area, the type of SR reconstruction can be divided into single-image SR, single-video SR, and multiple-video SR. This paper focuses on single-image SR; it is more useful in the incipient fault detection of electrical equipment. Single-image SR also can be divided into classical method [15, 16] and learning-based method [17–19]. Figure 2(a) shows the classical multiframe image to achieve single-image SR; there are 4 LR images with subpixel translation; the complementary information can be fused to reconstruct a HR image with higher resolution. In Figure 2(a), all of the small circulars, rhombuses and triangles represent subpixel different sample points in HR grid, respectively.

The other recently popular method is learning-based SR reconstruction, one of which is illustrated in Figure 2(b) [20]. All of these methods use single-scale or multiscale information to get learning network, so as to achieve HR reconstruction from LR input. In this paper, we adopt the second SR framework to reconstruct detailed information of incipient fault on electrical equipment.

2.2. SR Reconstruction Method for Incipient Fault Detection. For what is detailed above, in order to accurately detect the incipient fault and guarantee safety of electricity power system, improving the resolution of monitoring images of electrical equipment is an effective pathway. A SR reconstruction method is introduced in this paper, which adopt the idea of deep learning network model [21] shown in Figure 3. This model combines the traditional sparse coding model

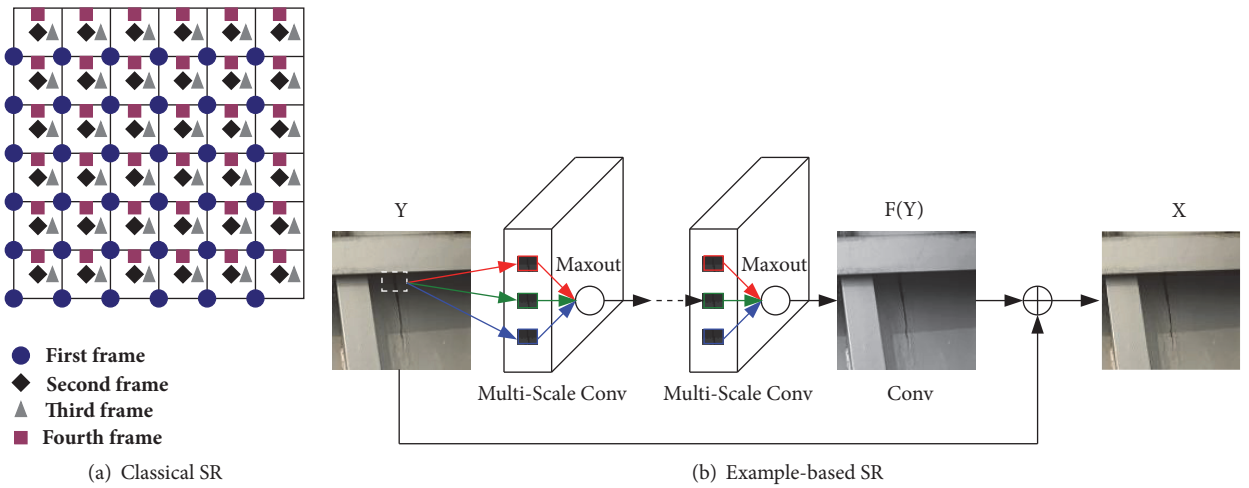

(a) Classical SR (b) Example-based SR

FIGURE 2: The relation of LR samples mapped on HR grid.

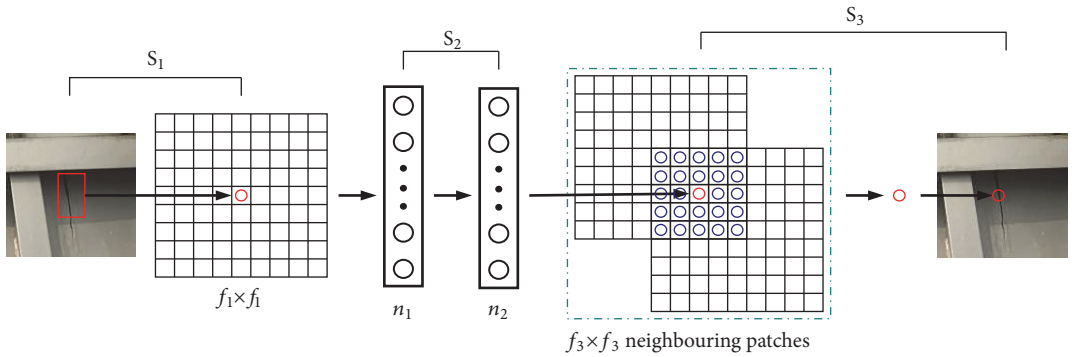

FIGURE 3: Illustration of sparse coding combined neural network SR reconstruction [21].

into deep learning so as to obtain HR result, which extends the conventional sparse coding model using several key ideas from deep learning, and complements large learning capacity to improve SR reconstruction performance.

Firstly, we implement a feed-forward neural network whose layers strictly correspond to each step in the processing flow of sparse coding based image SR; the framework is shown in Figure 3. In this way, the sparse representation prior is effectively encoded in our deep network structure; all the coded components are trained jointly through back-propagation. This method includes three stages as shown in Figure 3. The first stage $\mathbf{S_1}$ is a convolutional process, which is patch extraction and representation. LR image $\mathbf{I_y}$ is the Bicubic-upscaled version of input real LR image, and this layer extracts feature for each LR patch of size $\mathbf{5 \times 5}$. In this stage, the size of our input patch $\mathbf{y}$ must be the same as the filter spatial size as $\mathbf{s_y \times s_y}$. This process can be represented as $\mathbf{S_1(y)} = \max(\mathbf{0}, \mathbf{w_1} * \mathbf{y} + \mathbf{b_1})$; here $\mathbf{w_1}$ and $\mathbf{b_1}$ are convolution filter and deviation, respectively. In this paper, we extract 100-dimension feature in this stage. The middle stage of this model $\mathbf{S_2}$ is a high-dimension mapping process, which includes three linear layers shown in Figure 4 [22]. The sparse code $\boldsymbol{\alpha}$ is multiplied with HR dictionary $\mathbf{D_x}$ in the last linear layer to reconstruct HR patch. This stage is

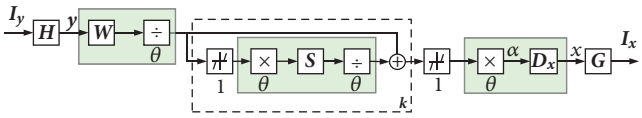

FIGURE 4: Process of middle mapping stage $\mathbf{S_2}$ [22].

equal to a filter with simple spatial support $\mathbf{1 \times 1}$; it also can be mathematized as $\mathbf{S_2(y)} = \max[\mathbf{0}, \mathbf{w_2} * \mathbf{S_1(y)} + \mathbf{b_2}]$. Here $\mathbf{w_2}$ and $\mathbf{b_2}$ are also filter and deviation, respectively, just like in stage $\mathbf{S_1}$. The final stage $\mathbf{S_3}$ in this model is reconstruction, which is also a convolution similar to $\mathbf{S_1}$. In this stage, all the recovered patches are placed back to the corresponding positions in the HR grid through a convolutional filter, so as to get the HR output result. This model combined with the focal points of sparse coding and the strong points of deep learning to achieve SR reconstruction. As a result, HR version of the incipient fault on electrical equipment can be more visible and helpful in achieving easier fault detection. The recurrent middle stage adopted the idea referred in [22], which is mathematized as Eq. (2)

$$Z_{k+1} = h_\theta(Wy + Sz_k) \tag{2}$$

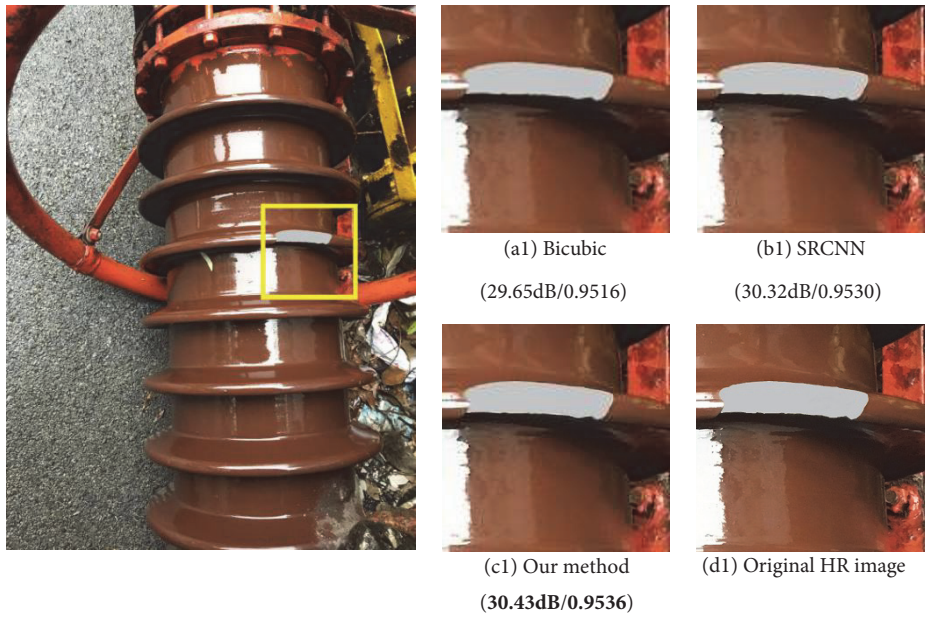

Figure 5: Simulated gaps fault in the ceramic insulators.

where $\mathbf{y}$ is the input signal and $\mathbf{h}_\theta$ is an coordinate-wise shrinkage function defined as $[\mathbf{h}_\theta(\boldsymbol{\alpha})]_i = \text{sign}(\boldsymbol{\alpha}_i)\boldsymbol{\theta}_i(|\boldsymbol{\alpha}_i|/\boldsymbol{\theta}_i - \mathbf{1})_+ = \boldsymbol{\theta}_i\mathbf{h}_1(\boldsymbol{\alpha}_i/\boldsymbol{\theta}_i)$ with positive threshold $\boldsymbol{\theta}$. $\mathbf{W}$ is the transpose of the dictionary matrix $\mathbf{D}_y$, and $\mathbf{S}$ is $\mathbf{D}_Y{}^T \cdot \mathbf{D}_y$. The matrices $\mathbf{W}$ and $\mathbf{S}$ are learned so as to minimize the approximation error to the optimal sparse coding on a given dataset. The final convolution stage $\mathbf{S}_3$ producing HR reconstruction result is described as $\mathbf{S}_3(\mathbf{y}) = \mathbf{w}_3 * \mathbf{S}_2(\mathbf{y}) + \mathbf{b}_3$, $\mathbf{b}_3$ is a vector, and $\mathbf{w}_3$ project the coefficients to image spatial domain to get averaged HR result [22, 23].

On the other hand, loss function is also needed in this model, which can be obtained by minimizing reconstruction result $\mathbf{S}_3(\mathbf{y})$ and corresponding original HR version $\mathbf{I}_x$. In this paper, mean squared error (MSE) is adopted as loss function in this model, which is shown in

$$MSE = \frac{SSE}{n} = \frac{1}{n}\sum i = w_i \left(I_i - y_i\right)^2 \tag{3}$$

Here SSE is the sum of squared error, $\mathbf{n}$ is the number of samples, weight $\mathbf{w}_i > 0$, $\mathbf{I}_i$ is the original HR image, and $\mathbf{y}_i$ is the estimated SR reconstruction HR result.

3. Experiment

In order to show the efficiency of the proposed method for incipient fault SR reconstruction of electrical equipment, we give two experiments to straightly verify the effective result. One is simulation incipient fault image SR, and some good electrical equipment is manually added and some incipient fault on the surface. The other is electrical equipment images with real incipient fault on the surface.

In these experiments, we firstly perform incipient fault extraction on images captured by high-definition (HD) camera, and then a degraded processing is applied to change the resolution to be $256 * 256$, which is referred to as original HR image. For SR model, the resolution of LR input is $128 * 128$ by Bicubic interpolation. In our SR reconstruction process, the upscaling factor is 2. In order to clearly show the efficiency of the detailed method in this paper, the result of Bicubic interpolation, SR reconstruction of SRCNN [24], SR result by proposed method in this paper, and the ground-truth HR image are all provided to give a complete subjective comparable effect. At the same time, we also provide the objective quantitative metric peak-signal-noise-ratio (PSNR) [25, 26] and structural similarity index metric (SSIM) [25, 27] to evaluate all of these results, so as to further validate efficiency of the detailed method in this section. PSNR is a classical objective metric for image quality evaluation, which is widely used in many real applications. SSIM is a popular image quality assessment based on computing the structure similarity; it also provides superior performance.

3.1. Simulation Incipient Fault Experiment. In the following simulation experiment, we simulate the incipient fault of common four types of electrical equipment in substations. In Figures 5–8, we simulate the gaps and the oil pillow's leakage of insulator marked by gray part; we also simulate the 35kv transformer's crack with a black broken line, and a painted brown part on the circuit breaker is the simulated rust stain. All of these artificially added parts are simulated fault on the electrical equipment, which are very small or invisible in natural scene, because the size of electrical equipment is usually large or huge. Note that, in order to better display the visual results, we select detailed information of the fault for each image and enlarge them to show better display. All the following experiments also follow this rule.

From the different SR reconstruction results in Figures 5–8, the details of Bicubic reconstruction in Figures a1-a4 are the most obscured and ambiguous. Although the results of SRCNN shown in Figures b1-b4 are slightly clear, the detailed

(a2) Bicubic (27.02dB/ 0.8715)

(b2) SRCNN (28.67dB/0.8756)

(c2) Our method (**28.95dB/0.8793**)

(d2) Original HR image

Figure 6: Simulated oil leaking in the transformer's oil pillow.

(a3) Bicubic (23.85dB/0.8231)

(b3) SRCNN (25.01dB/0.8318)

(c3) Our method (**25.18dB/0.8327**)

(d3) Original HR image

Figure 7: Simulated cracks in the 35 kv transformer.

information is not sufficient enough to make accurate fault judgments. It is clearly shown that the image c1-c4 has a fine edge structure; the image feature structure is closer to the HR image (d1-d4). In the image detected by our method, the edge portion of the electrical device has more zigzag texture, and the image sharpening effect is better, so that the shape and angle of the notch and crack can be clearly observed to help diagnose electrical equipment incipient fault. All of the objective evaluation values are included in Table 1, which also proves the efficient SR reconstruction of the proposed method in this paper.

3.2. Real Incipient Fault Experiment. Although the simulation incipient fault SR experiment is effective and credible, we further provide real incipient fault SR experiment to validate the proposed method. Similar to the above experiments, we detect the actual fault commonly found in substations. In the same way, we also give objective evaluation and subjective

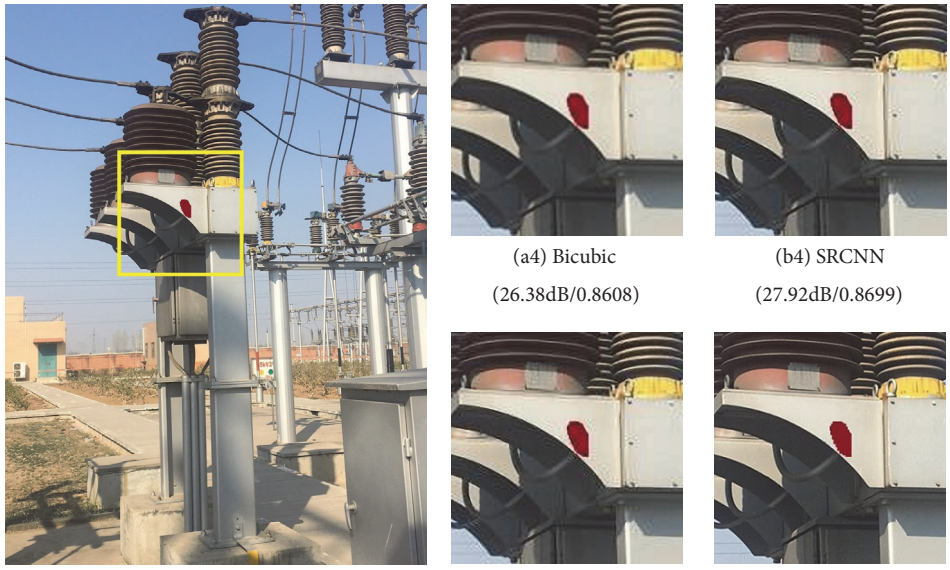

Figure 8: Simulating the rust in the circuit breaker.

Table 1: The objective comparison (PSNR / SSIM) of simulation incipient fault by three methods. Bold indicates the best performance.

	Figure 5	Figure 6	Figure 7	Figure 8
Bicubic	(29.65 dB/0.9516)	(27.02 dB/ 0.8715)	(23.85 dB/0.8231)	(26.38 dB/0.8608)
SRCNN	(30.32 dB/0.9530)	(28.67 dB/0.8756)	(25.01 dB/0.8318)	(27.92 dB/0.8699)
Our method	(**30.43 dB/0.9536**)	(**28.95 dB/0.8793**)	(**25.18 dB/0.8327**)	(**28.19 dB/0.8735**)

Table 2: The objective comparison (PSNR / SSIM) of actual incipient fault by three methods. Bold indicates the best performance.

	Figure 9	Figure 10	Figure 11	Figure 12
Bicubic	(29.12 dB/0.8541)	(25.63 dB/ 0.8554)	(33.45 dB/0.9388)	(31.95 dB/0.8828)
SRCNN	(29.30 dB/**0.8543**)	(26.91 dB/0.8664)	(34.26 dB/0.9400)	(32.62 dB/0.8852)
Our method	(**29.37 dB/0.8543**)	(**27.07 dB/0.8669**)	(**34.51 dB/0.9415**)	(**32.76 dB/0.8856**)

evaluation indicators based on human vision in this SR reconstruction experiment.

In the power system, once incipient fault such as cracks and gaps occur in electrical equipment, which are difficult to be discovered by human, they even lead to a huge accident crisis for the whole system. In Figures 9–12, the Bicubic interpolation reconstruction (a5-a8) has the most blurring fault edge information and the highest distortion, which is helpless for the detection of incipient fault. The SR reconstruction results (b5-b8) by SRCNN are relatively acceptable. In Table 2 and Figure 13 (average value of these three methods of PSNR and SSIM), the results of the proposed method in this paper (c5-c8) are absolutely superior to Bicubic and SRCNN, the edges and lines of the fault are more clear, and the crack length and shape are more obvious. So it is shown that the proposed method is the effective way to make the incipient fault more visible.

3.3. Low-Resolution Actual Incipient Fault Experiment. In this subsection, the incipient fault images are captured by LR imaging device (such as cellphone with LR shot camera); some of them are also captured in special conditions such as dim environments. In this case, the original LR image is 128 ∗ 128, and the upscaled factor is 2. Because there is not a HR version for objective quality evaluation, the blind image quality metric (BRISQUE) [28, 29] is adopted in this experiment. BRISQUE is a widespread no-reference image quality metric; it extracts mean subtracted contrast normalized (MSCN) coefficients to fit asymmetric generalized Gaussian distribution (AGGD), so as to estimate the image quality.

Figures 14 and 15 are electrical equipment LR images captured in a dim environment; most of the incipient fault is difficult to detect under such circumstance. The burr sparked by insulator in Figure 14 and the soldering position on the switch blade in Figure 15 are easy to be recognized by SR reconstruction. Comparable fine structure SR results in Figure c9-10 are more vivid than other results. Furthermore, the objective evaluation metric of BRISQUE also proves the proposed method is higher than the SR results by other

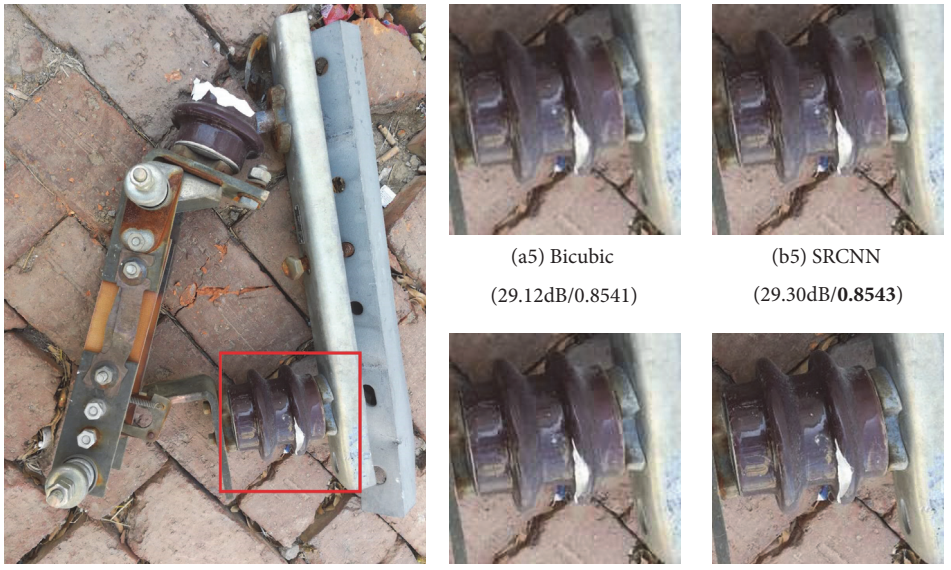

(a5) Bicubic (29.12dB/0.8541)

(b5) SRCNN (29.30dB/**0.8543**)

(c5) Our method (**29.37dB/0.8543**)

(d5) Original HR image

Figure 9: Insulators on low voltage knife gates.

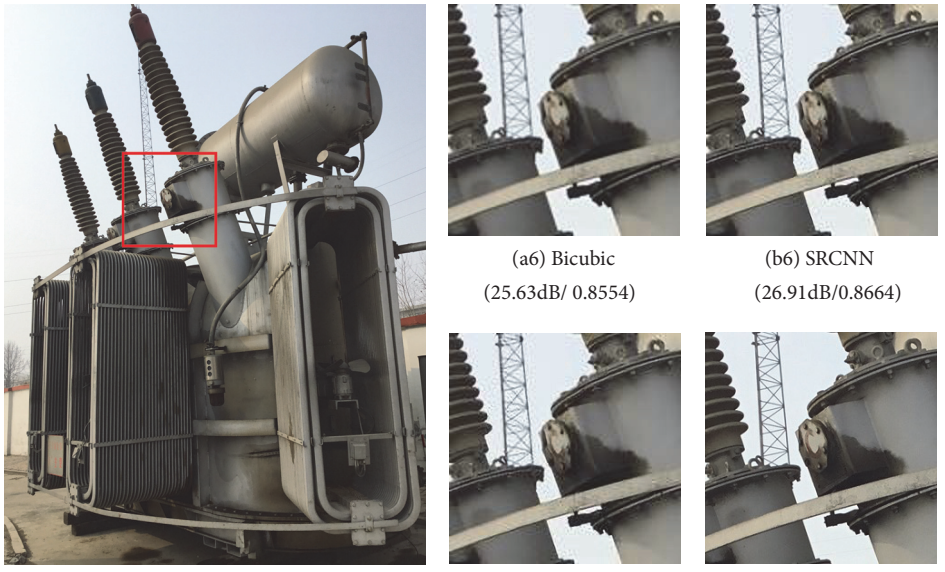

(a6) Bicubic (25.63dB/ 0.8554)

(b6) SRCNN (26.91dB/0.8664)

(c6) Our method (**27.07dB/0.8669**)

(d6) Original HR image

Figure 10: Oil leak in the transformer's oil pillow.

methods (lower BRISQUE value means more quality or higher resolution of the image) in Table 3.

4. Conclusion

A SR reconstruction method combining sparse coding and deep learning is used in this paper, so as to achieve pre-processing for accurate incipient fault detecting of electrical equipment. It can be seen from the subjective and objective results compared with other methods that the proposed SR method in this paper achieved significant visual improvement in image resolution. Through the above-mentioned

Table 3: The objective comparison (BRISQUE) of actual incipient fault by three methods. Bold indicates the best performance.

	Figure 14	Figure 15
Bicubic	(0.5378)	(0.5039)
SRCNN	(0.5037)	(0.4604)
Our method	(**0.4904**)	(**0.4539**)

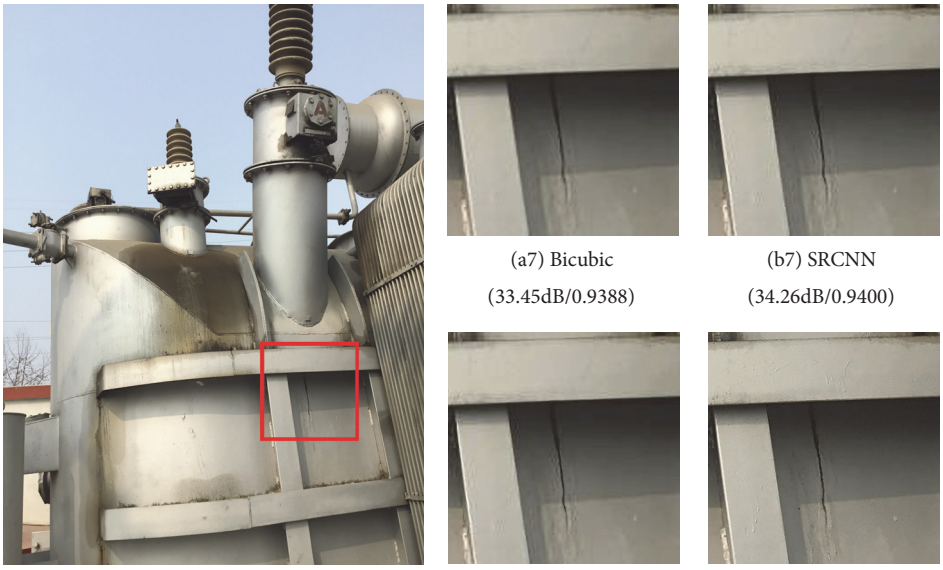

(a7) Bicubic (33.45dB/0.9388)

(b7) SRCNN (34.26dB/0.9400)

(c7) Our method (**34.51dB/0.9415**)

(d7) Original HR image

Figure 11: Cracks on the body of transformer.

(a8) Bicubic (31.95dB/0.8828)

(b8) SRCNN (32.62dB/0.8852)

(c8) Our method (**32.76dB/0.8856**)

(d8) Original HR image

Figure 12: Rusts on the circuit breaker.

detection of a series of initial defect incipient fault, such as incompleteness, cracks, and blemishes, this method can obtain relatively clear effect and retain most of fine edge information. Applying this method for practical incipient fault detection can improve fault resolution and achieve accurate fault location and judgment, so as to ensure the safe operation of electrical equipment and electricity power system. For actual application, our further work will combine this method in fault diagnosis and other areas, to ensure the reliability of electrical system operation.

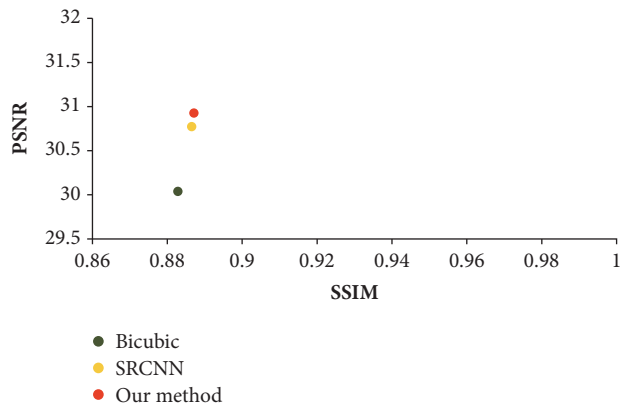

Figure 13: Average value of PSNR and SSIM of actual fault detection by three methods. Red indicates the best performance.

(a9) Bicubic (0.5378)

(b9) SRCNN (0.5037)

(c9) Our method (**0.4904**)

Figure 14: Insulators on poles.

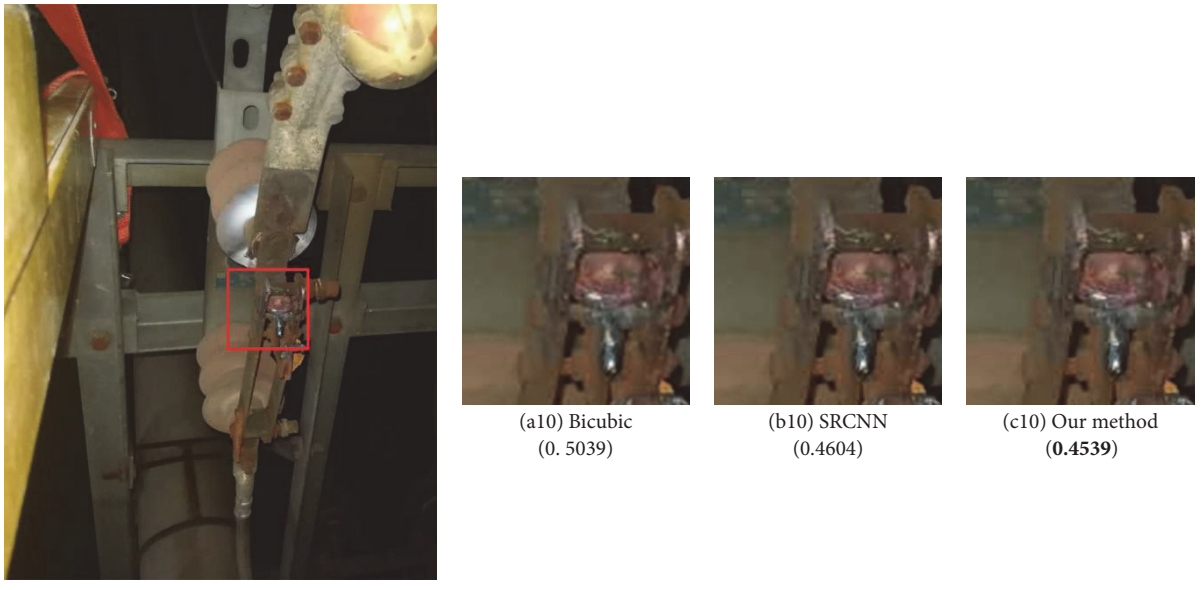

(a10) Bicubic (0. 5039)

(b10) SRCNN (0.4604)

(c10) Our method (**0.4539**)

Figure 15: Switch knife.

Data Availability

The data used to support the findings of this study are available from the corresponding author upon request.

Conflicts of Interest

The authors declare that they have no conflicts of interest.

Acknowledgments

This work is supported by National Natural Science Foundation of China (61663008), Natural Science Foundation of Hubei Province (2015CFC781, 2014CFB612), Foundation of CSC (China Scholar Council), and PhD Technology Program (MY2014B018).

References

[1] E. Zio and L. R. Golea, "Analyzing the topological, electrical and reliability characteristics of a power transmission system for identifying its critical elements," *Reliability Engineering & System Safety*, vol. 101, pp. 67–74, 2012.

[2] N. Ismail, F. H. Nordin, and A. A. Alkahtani, "Detection of the source of the incipient faults produced by single phase inverter using feed- forward back-propagation neural network," *Indian Journal of Science and Technology*, vol. 9, no. 48, 2017.

[3] D. Huang, C. Chen, G. Sun, and L. Zhao, "Recognition and Diagnosis Method of Objective Entropy Weight for Power Transformer Fault," *Dianli Xitong Zidonghua/Automation of Electric Power Systems*, vol. 41, no. 12, pp. 206–211, 2017.

[4] I. B. M. Taha, D.-E. A. Mansour, S. S. M. Ghoneim, and N. I. Elkalashy, "Conditional probability-based interpretation of dissolved gas analysis for transformer incipient faults," *IET Generation, Transmission & Distribution*, vol. 11, no. 4, pp. 943–951, 2017.

[5] D. Huang, L. Ke, X. Chu et al., "Fault diagnosis for the motor drive system of urban transit based on improved hidden markov model," *Microelectronics Reliability*, vol. 82, pp. 179–189, 2018.

[6] D.-R. Huang, C.-S. Chen, G.-X. Sun, L. Zhao, and B. Mi, "Linear Discriminant Analysis and Back Propagation Neural Network Cooperative Diagnosis Method for Multiple Faults of Complex Equipment Bearings," *Acta Armamentarii*, vol. 38, no. 8, pp. 1649–1657, 2017.

[7] G. Rigatos, P. Siano, and A. Piccolo, "Incipient fault detection for electric power transformers using neural modeling and the local statistical approach to fault diagnosis," in *Proceedings of the IEEE Sensors Applications Symposium, SAS '12*, pp. 32–37, Italy, February 2012.

[8] T. Escobet, V. Puig, J. Quevedo, and D. Garcia, "A methodology for incipient fault detection," in *Proceedings of the IEEE Conference on Control Applications, CCA '14*, pp. 104–109, France, October 2014.

[9] W. Ge, J. Wang, J. Zhou, H. Wu, and Q. Jin, "Incipient fault detection based on fault extraction and residual evaluation," *Industrial & Engineering Chemistry Research*, vol. 54, no. 14, pp. 3664–3677, 2015.

[10] K. Zhang, X. Gao, D. Tao, and X. Li, "Single image super-resolution with non-local means and steering kernel regression," *IEEE Transactions on Image Processing*, vol. 21, no. 11, pp. 4544–4556, 2012.

[11] I. E. Mourabit, M. E. Rhabi, A. Hakim, A. Laghrib, and E. Moreau, "A new denoising model for multi-frame super-resolution image reconstruction," *Signal Processing*, vol. 132, pp. 51–65, 2017.

[12] P. Purkait and B. Chanda, "Super resolution image reconstruction through Bregman iteration using morphologic regularization," *IEEE Transactions on Image Processing*, vol. 21, no. 9, pp. 4029–4039, 2012.

[13] L. Yue, H. Shen, J. Li, Q. Yuan, H. Zhang, and L. Zhang, "Image super-resolution: The techniques, applications, and future," *Signal Processing*, vol. 128, pp. 389–408, 2016.

[14] R. Kolte and A. Arora, "Image super-resolution," *Lap Lambert Academic Publishing*, vol. 3, no. 10, pp. 7195–7199, 2013.

[15] A. R. A. Nazren, S. N. Yaakob, R. Ngadiran, M. B. Hisham, and N. M. Wafi, "Improving iterative back projection super resolution model via anisotropic diffusion edge enhancement," in *Proceedings of the International Conference on Robotics, Automation and Sciences, ICORAS '16*, Malaysia, November 2016.

[16] X. Liu, D. Song, C. Dong et al., "MAP-based image super-resolution reconstruction," *International Journal of Computer and Information Engineering*, vol. 27, pp. 208–211, 2008.

[17] W. T. Freeman, T. R. Jones, and E. C. Pasztor, "Example-based super-resolution," *IEEE Computer Graphics and Applications*, vol. 22, no. 2, pp. 56–65, 2002.

[18] W. T. Freeman, E. C. Pasztor, and O. T. Carmichael, "Learning low-level vision," *International Journal of Computer Vision*, vol. 40, no. 1, pp. 25–47, 2000.

[19] J. Yang, J. Wright, T. S. Huang, and Y. Ma, "Image super-resolution via sparse representation," *IEEE Transactions on Image Processing*, vol. 19, no. 11, pp. 2861–2873, 2010.

[20] X. Du, X. Qu, Y. He, and D. Guo, "Single Image Super-Resolution Based on Multi-Scale Competitive Convolutional Neural Network," *Sensors*, vol. 18, no. 3, p. 789, 2018.

[21] C. Dong, C. Loy, K. He, and X. Tang, "Learning a deep convolutional network for image super-resolution," in *Computer Vision-ECCV*, vol. 8692 of *Lecture Notes in Computer Science*, pp. 184–199, Springer, New York, NY, USA, 2014.

[22] Z. Wang, D. Liu, J. Yang, W. Han, and T. Huang, "Deep networks for image super-resolution with sparse prior," in *Proceedings of the 15th IEEE International Conference on Computer Vision, ICCV '15*, pp. 370–378, Chile, December 2015.

[23] K. Gregor and Y. LeCun, "Learning fast approximations of sparse coding," in *Proceedings of the 27th International Conference on Machine Learning, ICML 2010*, pp. 399–406, Israel, June 2010.

[24] K. I. Kim and Y. Kwon, "Example-based learning for single-image super-resolution," in *Pattern Recognition*, vol. 5096 of *Lecture Notes in Computer Science*, pp. 456–465, Springer, Berlin, 2008.

[25] A. Horé and D. Ziou, "Image quality metrics: PSNR vs. SSIM," in *Proceedings of the 20th International Conference on Pattern Recognition (ICPR '10)*, pp. 2366–2369, Istanbul, Turkey, August 2010.

[26] Q. Huynh-Thu and M. Ghanbari, "Scope of validity of PSNR in image/video quality assessment," *IEEE Electronics Letters*, vol. 44, no. 13, pp. 800-801, 2008.

[27] P. Zhao, Y. Liu, J. Liu, A. Argyriou, and S. Ci, "SSIM-based error-resilient cross-layer optimization for wireless video streaming," *Signal Processing: Image Communication*, vol. 40, pp. 36–51, 2016.

[28] A. Mittal, A. K. Moorthy, and A. C. Bovik, *BRISQUE Software Release*, 2011, http://live.ece.utexas.edu/research/quality/BRISQUE_release.zip.

[29] A. Mittal, A. K. Moorthy, and A. . Bovik, "No-reference image quality assessment in the spatial domain," *IEEE Transactions on Image Processing*, vol. 21, no. 12, pp. 4695–4708, 2012.

Hindawi
Journal of Control Science and Engineering
Volume 2018, Article ID 4215147, 9 pages
https://doi.org/10.1155/2018/4215147

Research Article

Dynamic Output Feedback Control of Discrete Markov Jump Systems based on Event-Triggered Mechanism

Zhen Zhao, Jinfeng Gao, and Tingting Zhang

Faculty of Mechanical Engineering and Automation, Zhejiang Sci-Tech University, Hangzhou, Zhejiang 310018, China

Correspondence should be addressed to Jinfeng Gao; gaojf163@163.com

Received 11 May 2018; Accepted 3 July 2018; Published 1 August 2018

Academic Editor: Cui-Qin Ma

This paper is devoted to the co-design strategy of event-triggered scheme and dynamic output feedback controller for a class of discrete-time networked control systems (NCSs) with random time delay. An event-triggered mechanism is given to ease the information transmission. Both the sensor and controller are set with mode-dependent quantizers in the system. A Markov process is used to model the time delay which is used to describe the quantization density. By employing the Lyapunov-Krasovskii functional and linear matrix inequality (LMI), sufficient conditions are obtained for the system. A specific example is given to demonstrate the proposed approach.

1. Introduction

In recent years, a boom of computer science and technology has led to the increasing role of network control in industry. Nevertheless, main problems in the network such as time delay, disorder, packet loss, and the occupation of network bandwidth cannot be ignored.

The issue of time delay is usually treated as the major cause of deterioration of system performance which has been dealt with by quite a few researchers, and they proposed a variety of approaches to these problems; see [1–5]. In [6], the authors propose sequential measurement fusion and state fusion estimation methods to deal with delayed data for clustered sensor networks, since they can handle the data that are available sequentially. In order to save network resources, some literatures have proposed time-triggered mechanism (such as [7–9]); this scheme transfers each sample data which reduces the utilization of network bandwidth. The event-triggering mechanism proposed in the 1990s is more advantageous than the time-triggered scheme (see [10–13]), which means that the data will not be transmitted unless condition set in advance is satisfied, and then it will reduce the time of accessing network and save the network resources. In [14], the event-triggered scheme is applied to the fault detection to guarantee the fault detection accuracy. Furthermore, an event-triggered scheme with an adaptive threshold would subserve the quality of the control; see [15, 16].

Quantization also has become a research hotspot these years, paper [17] notes that quantization process plays an important role in the networked control systems, an adaptive quantizer can help to alleviate network congestion and maintain system stability, paper [18] proposes a quantized state feedback strategy for global and asymptotical stabilization of the networked control systems, papers [19, 20] address the problem of output feedback control for networked control systems with limited information, it should be noted that the impact of quantification cannot be ignored, and, in [18, 19, 21], the quantization deviation is disposed as an uncertainty. Papers [20, 22, 23] design dynamic quantizer to reduce the impact of the quantization error.

Markov jump system is a random system with multimodes which has attracted much attention in the past few decades (see [24–26]); the jump transition of the system in each mode is determined by a Markov chain so it can be applied to the multimodes in many kinds of systems. In [4, 27, 28], the Markov process is applied to modeling the time delay, in [10, 20], the time delay is used to describe the quantization density in the form of function and the authors investigate the dynamic quantization output feedback controller; in [10], the author also takes into account an event-triggered scheme to

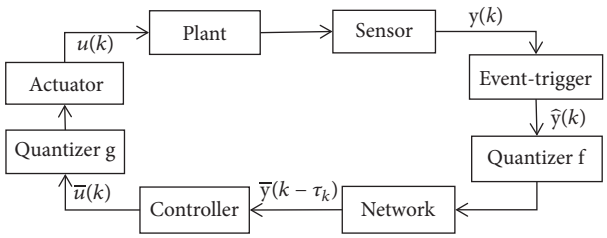

Figure 1: The structure of NCS with event-trigger and quantizers.

the aforementioned systems. Nevertheless, no article has considered a system with a dynamic output feedback controller and two quantizers based on event-triggered scheme.

In the view of the aforementioned analysis, in this paper, we aim to investigate the co-design strategy of the event-triggered scheme and dynamic output feedback controller. An adaptive event-triggered mechanism is presented to reduce the information transmission. A Markov chain is applied to modeling the time delay which is used to describe quantization density as a function to ease bandwidth usage. Methods utilizing Lyapunov-Krasovskii functional and linear matrix inequality (LMI) are presented to develop the sufficient conditions of stochastic stability. An event-triggered scheme based dynamic output feedback controller is adopted to guarantee the performance of the closed-loop system. Finally, an example demonstrates the proposed method in detail.

The remainder of this paper is organized as follows. The system description and formulation are provided in **Section 2**. The sufficient condition of stochastic stability and the co-design strategy are presented in **Section 3**. In **Section 4**, a simulation example is presented to demonstrate the feasibility of the proposed approach. The conclusion is given in **Section 5**.

2. Problem Formulation

The plant of NCS is considered as a discrete-time model

$$\begin{aligned} x(k+1) &= Ax(k) + Bu(k) \\ y(k) &= Cx(k) \end{aligned} \tag{1}$$

where $x(k) \in R^n$ is the system state, $u(k) \in R^m$ is the control input, and $y(k) \in R^n$ is the output, A, B, and C are constant matrices of appropriate dimensions, and the structure of our concerned NCS is shown as in Figure 1.

Throughout the paper, some assumptions as follows are needed for the considered NCS.

Assumption 1. Both the controller and actuator are event-driven, while the sensor is time-driven with a sampling period h.

Assumption 2. The data communication in the network is assumed to be single packet transmission without packet dropout.

Assumption 3. The network-induced delay is smaller than one sampling period and bounded by $0 \le \underline{\tau} \le \tau_k \le \overline{\tau}$.

The event-triggered scheme is shown as follows:

$$e^{\mathrm{T}}(k)\, e(k) \ge \sigma(k)\, y^{\mathrm{T}}(k)\, y(k) \tag{2}$$

where k is the sampling instant and $k = 0, 1, 2, \cdots$. $e(k)$ is the quantization error and defined as

$$e(k) = y(k) - \hat{y}(k-1) \tag{3}$$

where $\hat{y}(k-1)$ is the latest transmitted signal and $y(k)$ is the signal which is to be transmitted. Based on [10], $\sigma(k)$ is the adaptive threshold and defined as

$$\sigma(k) = \begin{cases} \sigma_1, & if\ e^{\mathrm{T}}(k-1)\, e(k-1) \ge \Delta \\ \sigma_2, & if\ e^{\mathrm{T}}(k-1)\, e(k-1) \le \Delta \end{cases} \tag{4}$$

and $\alpha(k)$ is defined as

$$\alpha(k) = \begin{cases} 1, & if\ (2)\ is\ satisfied \\ 0, & otherwise \end{cases} \tag{5}$$

and

$$\hat{y}(k) = \alpha(k)\, y(k) + (1 - \alpha(k))\, \hat{y}(k-1) \tag{6}$$

The quantization density in this paper is designed as a function of time delay $\tau_k = \tau(k)$, which is modeled as a discrete homogeneous Markov chain $\{r_k, k\}$, with a finite number of states $\omega = \{1, 2, \ldots, s\}$, and the transition probability of this Markov chain from mode i to mode j at time $k+1$ is

$$p_{ij} = Prob\{r_{k+1} = j \mid r_k = i\} \tag{7}$$

where $i, j \in \omega$ and $0 \le p_{ij} \le 1$.

The quantizer f is described as follows:

$$f(y_j, i) = \begin{cases} \rho^h(i), & if\ \dfrac{\rho^h(i)}{1+\delta(i)} < y_j < \dfrac{\rho^h(i)}{1-\delta(i)}, \\ & y_j > 0,\ h = 0, \pm 1, \pm 2, \cdots \\ 0, & if\ y_j = 0 \\ -f(-y_j, i), & if\ y_j < 0 \end{cases} \tag{8}$$

where $j = 1, 2, \ldots, s$, and the relation between $\delta_f(i)$ and $\rho_f(i)$ is

$$\delta_f(i) = \frac{1 - \rho_f(i)}{1 + \rho_f(i)} \tag{9}$$

and the quantized set is

$$\zeta = \left\{ \pm \rho^h(i), h = 0, \pm 1, \pm 2, \cdots \right\} \tag{10}$$

Based on [21], $\Delta_f \in [-\delta_f(i), \delta_f(i)]$, and then

$$f\left(y_j, i\right) = \left(1 + \Delta_f\right) \widehat{y}\left(k\right) \tag{11}$$

The quantized density and quantized set of the quantizer g is similar to the quantizer f, and it can be expressed as follows:

$$g\left(u_r, i\right) = \left(1 + \Delta_g\right) \overline{u}\left(k\right) \tag{12}$$

where $r = 1, 2, \cdots, m$ and $\Delta_g \in [-\delta_r(i), \delta_r(i)]$.

According to the above statement, the dynamic output feedback controller is designed as

$$\begin{aligned} \widehat{x}\left(k+1\right) &= A_c\left(i\right)\widehat{x}\left(k\right) + B_c\left(i\right)\overline{y}\left(k-\tau_k\right) \\ \overline{u}\left(k\right) &= C_c\left(i\right)\widehat{x}\left(k\right) \end{aligned} \tag{13}$$

Combining (11) and (12), the closed-loop system of (1) can be represented as follows:

$$\begin{aligned} x\left(k+1\right) &= Ax\left(k\right) + B\left(1+\Delta_g\right)C_c\left(i\right)\widehat{x}\left(k\right) \\ \widehat{x}\left(k+1\right) &= A_c\left(i\right)\widehat{x}\left(k\right) + B_c\left(i\right)\left(1+\Delta_f\right)Cx\left(k-\tau_k\right) \\ &\quad - B_c\left(i\right)\left(1+\Delta_f\right)\left(1-\alpha\left(k\right)\right)e\left(k\right) \\ e\left(k+1\right) &= \left(CA-C\right)x\left(k\right) + CBC_c\left(i\right)\left(1+\Delta_g\right)\widehat{x}\left(k\right) \\ &\quad + \left(1-\alpha\left(k\right)\right)e\left(k\right) \end{aligned} \tag{14}$$

Define an augmented vector

$$\eta\left(k\right) = \left[x^{\mathrm{T}}\left(k\right) \;\; \widehat{x}^{\mathrm{T}}\left(k\right) \;\; e^{\mathrm{T}}\left(k\right)\right]^{\mathrm{T}} \tag{15}$$

and then

$$\begin{aligned} &\eta\left(k+1\right) \\ &\quad = \left(\Phi_{1\alpha(k)}\left(i\right) + \Phi_2\left(i\right) + \Phi_3\left(i\right)\left(1+\Delta_g\right)\right)\eta\left(k\right) \\ &\qquad + \Phi_{4\alpha(k)}\left(i\right)\left(1+\Delta_f\right)\eta\left(k-\tau_k\right) \end{aligned} \tag{16}$$

where

$$\Phi_{1\alpha(k)}\left(i\right) = \begin{bmatrix} A & 0 & 0 \\ 0 & 0 & 0 \\ CA-C & 0 & \left(1-\alpha\left(k\right)\right)I \end{bmatrix}$$

$$\Phi_2\left(i\right) = \begin{bmatrix} 0 & 0 & 0 \\ 0 & A_c\left(i\right) & 0 \\ 0 & 0 & 0 \end{bmatrix}$$

$$\Phi_3\left(i\right) = \begin{bmatrix} 0 & BC_c\left(i\right) & 0 \\ 0 & 0 & 0 \\ 0 & CBC_c\left(i\right) & 0 \end{bmatrix}$$

$$\Phi_{4\alpha(k)}\left(i\right) = \begin{bmatrix} 0 & 0 & 0 \\ B_c\left(i\right)C & 0 & -\left(1-\alpha\left(k\right)\right)B_c\left(i\right) \\ 0 & 0 & 0 \end{bmatrix} \tag{17}$$

We define

$$J = \sum_{k=0}^{\infty} \begin{pmatrix} x\left(k\right) \\ u\left(k\right) \end{pmatrix}^{\mathrm{T}} Q' \begin{pmatrix} x\left(k\right) \\ u\left(k\right) \end{pmatrix} \tag{18}$$

as the cost function for system (16), where $Q' = \mathrm{diag}\{Q_1', Q_2'\} \in R^{2n\times 2n}$, $Q_1' \in R^{n\times n}$, and $Q_2' \in R^{n\times n}$.

3. Main Results

The stabilization of the closed-loop system (16) will be considered in this section, and, before going any further, a lemma and a definition are introduced, which will be helpful for deriving the following results.

Lemma 4 (see [10]). *Let $\overline{x}(k) = x(k+1) - x(k)$,*

$$\begin{aligned} &\widetilde{\eta}\left(k\right) \\ &\quad = \left[\eta^{\mathrm{T}}\left(k\right) \;\; \eta^{\mathrm{T}}\left(k\right)\Delta_g^{\mathrm{T}} \;\; \eta^{\mathrm{T}}\left(k-\tau_k\right) \;\; \eta^{\mathrm{T}}\left(k-\tau_k\right)\Delta_f^{\mathrm{T}}\right]^{\mathrm{T}}, \end{aligned} \tag{19}$$

and $\widetilde{\eta}(k) \in R^l$, for any matrices $E \in R^{n\times n}$, $M \in R^{n\times l}$, and $Z \in R^{l\times l}$ satisfying

$$\begin{bmatrix} E & M \\ M^{\mathrm{T}} & Z \end{bmatrix} \geq 0 \tag{20}$$

Then the following inequality holds:

$$-\sum_{i=k-\tau}^{k-1} \overline{x}\left(i\right)^{\mathrm{T}} E\overline{x}\left(i\right) \leq \widetilde{\eta}^{\mathrm{T}}\left(k\right)\left\{\gamma + \gamma^{T} + \overline{\tau}Z\right\}\widetilde{\eta}\left(k\right) \tag{21}$$

where

$$\gamma = M^{\mathrm{T}}\left[\mathrm{diag}\left\{I, 0, 0\right\} \;\; 0 \;\; \mathrm{diag}\left\{-I, 0, 0\right\} \;\; 0\right] \tag{22}$$

Proof is given in the Appendix.

Definition 5 (see [20]). The closed-loop systems given in (23) is stochastically stable; i.e., there exists a constant $0 \leq \alpha \leq \infty$, such that $E\{\sum_{l=0}^{\infty} \eta^{\mathrm{T}}(l)\eta(l)\} < \alpha$ for any initial states $x(0)$ and r_0.

Theorem 6. *For given matrices $A_c(i)$, $B_c(i)$, and $C_c(i)$, positive constants $\overline{\tau}$, $\underline{\tau}$, and quantization density values $\rho_f(i)$ and $\rho_g(i)$, if there exists a set of positive definite matrices $E_{\alpha(k)}(i)$, $Z_{\alpha(k)}(i)$, Q', $P_0(i)$, $P_1(i)$, $W_0(i)$, $W_1(i)$, $Q_0(i)$, $Q_1(i)$, $T(i)$, $N(i)$, and $M(i)$ of appropriate dimensions the following inequalities hold:*

$$min \quad tr\left(P_1\left(r_0\right)\right) \tag{23}$$

$$s.t. \quad \begin{bmatrix} E_{\alpha(i)}(i) & M(i) \\ * & Z_{\alpha(i)} \end{bmatrix} \geq 0 \tag{24}$$

$$\Lambda_0(i) + \Gamma_{10}^{\mathrm{T}}(i)\widetilde{P}_0(i)\Gamma_{10}(i) + \overline{\tau}Z_0(i) + \Gamma_2^{\mathrm{T}}(i)\overline{\tau}E_0(i)\Gamma_2(i) + \gamma(i) + \gamma^{\mathrm{T}}(i) + \sigma(i)I_1^{\mathrm{T}}C^{\mathrm{T}}CI_1 - I_2^{\mathrm{T}}I_2 < 0 \tag{25}$$

$$\Lambda_1(i) + \Gamma_{11}^{\mathrm{T}}(i)\widetilde{P}_1(i)\Gamma_{11}(i) + \overline{\tau}Z_1(i) + \Gamma_2^{\mathrm{T}}(i)\overline{\tau}E_1(i)\Gamma_2(i) + \gamma(i) + \gamma^{\mathrm{T}}(i) + I_2^{\mathrm{T}}I_2 - \sigma(i)I_1^{\mathrm{T}}C^{\mathrm{T}}CI_1 < 0 \tag{26}$$

$$\begin{aligned}
&\Gamma_{1\alpha(k)} = \left[\Phi_{1\alpha}(i) + \Phi_2(i) + \Phi_3(i) \;\; \Phi_3(i) \;\; \Phi_{4\alpha(k)}(i)\,\Phi_{4\alpha(k)}(i)\right] \\
&\Gamma_2 = \left[\overline{A} \;\; \overline{B} \;\; 0 \;\; 0\right] \\
&\overline{A} = \left[A - I \;\; BC_c(i) \;\; 0\right] \\
&I_1 = \left[\mathrm{diag}\{I, 0, 0\} \;\; 0 \;\; 0 \;\; 0\right] \\
&I_2 = \left[\mathrm{diag}\{0, 0, I\} \;\; 0 \;\; 0 \;\; 0\right] \\
&\gamma = M^{\mathrm{T}}\left[\mathrm{diag}\{I, 0, 0\} \;\; 0 \;\; \mathrm{diag}\{-I, 0, 0\} \;\; 0\right] \\
&\Lambda_0(i) = \mathrm{diag}\left\{\left(\overline{\tau} - \underline{\tau} + 1\right)Q - P_0(i) - T(i) - N(i) + \Psi^{\mathrm{T}}(i)Q'\Psi(i), -W_0(i), \delta^2(i)W_1(i) - Q_0, -W_1(i)\right\} \\
&\Lambda_1(i) = \mathrm{diag}\left\{\left(\overline{\tau} - \underline{\tau} + 1\right)Q - P_1(i) - T(i) - N(i) + \Psi^{\mathrm{T}}(i)Q'\Psi(i), -W_2(i), \delta^2(i)W_3(i) - Q_1, -W_3(i)\right\} \\
&\widetilde{P}_0(i) = \sum_{j=1}^{s} p_{ij}P_0(i)(j) \\
&\widetilde{P}_1(i) = \sum_{j=1}^{s} p_{ij}P_1(i)(j) \\
&\Psi(i) = \begin{bmatrix} I & 0 & 0 \\ 0 & C_c(i) & 0 \end{bmatrix}
\end{aligned} \tag{27}$$

Then the closed-loop system (16) is stochastically stable with the dynamic feedback controller.

Proof. Based on **Lemma 4**, (16) can be represented as follows:

$$\widetilde{\eta}(k+1) = \Gamma_{1\alpha(k)}(r_k)\widetilde{\eta}(k) \tag{28}$$

where

$$\begin{aligned}
\Gamma_{1\alpha(k)} = &\left[\Phi_{1\alpha}(r_k) + \Phi_2(r_k)\right. \\
&\left. + \Phi_3(r_k) \;\; \Phi_3(r_k) \;\; \Phi_{4\alpha(k)}(r_k)\,\Phi_{4\alpha(k)}(r_k)\right]
\end{aligned} \tag{29}$$

Then select Lyapunov-Krasovskii functional as

$$\begin{aligned}
V(k, r_k) = &V_1(k, r_k) + V_2(k, r_k) + V_3(k, r_k) \\
&+ V_4(k, r_k) + V_5(k, r_k)
\end{aligned} \tag{30}$$

where

$$\begin{aligned}
&V_1(k, r_k) = \eta_k^{\mathrm{T}}P(r_k)\eta_k, \\
&V_2(k, r_k) = \sum_{l=-\overline{\tau}}^{-1}\sum_{j=k+l}^{k-1}\overline{x}_j^{\mathrm{T}}E(r_k)\overline{x}_j, \\
&V_3(k, r_k) = \eta_k^{T}T(r_k)\eta_k, \\
&V_4(k, r_k) = \sum_{l=k-\tau_k}^{k-1}\eta_k^{\mathrm{T}}Q(r_k)\eta_k \\
&\qquad + \sum_{l=-\overline{\tau}+2}^{-\tau+1}\sum_{j=k+l-1}^{k-1}\eta_j^{\mathrm{T}}Q(r_k)\eta_j, \\
&V_5(k, r_k) = \eta_k^{\mathrm{T}}T(r_k)\eta_k,
\end{aligned} \tag{31}$$

Let

$$\begin{aligned}
E_{\alpha(k+1)}(r_{k+1}) &= E_0(r_k) \\
Q_{\alpha(k+1)}(r_{k+1}) &= Q_0(r_k)
\end{aligned} \tag{32}$$

Then we can obtain the following equalities and inequalities:

$$\begin{aligned}
\Delta V_1(k, r_k) &= \widetilde{\eta}_k^{\mathrm{T}} \Gamma_{1\alpha(k)}^{\mathrm{T}} \widetilde{P}(r_k) \Gamma_{1\alpha(k)} \widetilde{\eta}_k - \eta_k^{\mathrm{T}} P(r_k) \eta_k, \\
\Delta V_2(k, r_k) &= \overline{x}_k^{\mathrm{T}} \overline{\tau} E_0(r_k) \overline{x}_k - \sum_{l=k-\overline{\tau}}^{k-1} \overline{x}_k^{\mathrm{T}} E_0(r_k) \overline{x}_k \\
&\leq \widetilde{\eta}(k) \left[\Gamma_2^{\mathrm{T}}(r_k) \overline{\tau} E_0(r_k) \Gamma_2(r_k) + \gamma(r_k) + \gamma^{\mathrm{T}}(r_k) \right. \\
&\quad \left. + \overline{\tau} Z(r_k) \right] \widetilde{\eta}, \\
\Delta V_3(k, r_k) &= \widetilde{\eta}_k^{\mathrm{T}} \Gamma_{1\alpha(k)}^{\mathrm{T}}(r_k) T_0(r_k) \Gamma_{1\alpha(k)} \widetilde{\eta}(k) \\
&\quad - \eta_k^{\mathrm{T}} T_0(r_k) \eta_k, \\
\Delta V_4(k, r_k) &\leq (\overline{\tau} - \underline{\tau} + 1) \eta_k^{\mathrm{T}} Q_0(r_k) \eta_k - \eta_{k-\tau_k}^{\mathrm{T}} Q_0(r_k) \\
&\quad \cdot \eta_{k-\tau_k}, \\
\Delta V_5(k, r_k) &= \widetilde{\eta}_k^{\mathrm{T}} \Gamma_{1\alpha(k)}^{\mathrm{T}}(r_k) N_0(r_k) \Gamma_{1\alpha(k)} \widetilde{\eta}(k) \\
&\quad - \eta_k^{\mathrm{T}} N_0(r_k) \eta_k, \\
\Delta V(k, r_k) &\leq \widetilde{\eta}_k^{\mathrm{T}} \left[\Gamma_{1\alpha(k)}^{\mathrm{T}} \left(\widetilde{P}(r_k) + T_0(r_k) + N_0(r_k) \right) \Gamma_{1\alpha(k)} \right. \\
&\quad + \Gamma_2^{\mathrm{T}}(r_k) \overline{\tau} E_0(r_k) \Gamma_2(r_k) + \gamma(r_k) + \gamma^{\mathrm{T}}(r_k) \\
&\quad \left. + \overline{\tau} Z(r_k) \right] \widetilde{\eta}_k + \eta_k^{\mathrm{T}} \left((\overline{\tau} - \underline{\tau} + 1) Q_0(r_k) - P(r_k) \right. \\
&\quad \left. - T_0(r_k) - N_0(r_k) \right) \eta_k - \eta_{k-\tau_k}^{\mathrm{T}} Q_0(r_k) \eta_{k-\tau_k}
\end{aligned} \tag{33}$$

Let

$$\begin{aligned}
J' &= \begin{pmatrix} x(k) \\ u(k) \end{pmatrix}^{\mathrm{T}} Q' x \begin{pmatrix} x(k) \\ u(k) \end{pmatrix} \\
&= \eta_k^{\mathrm{T}} \Psi^{\mathrm{T}}(r_k) Q' \Psi(r_k) \eta_k
\end{aligned} \tag{34}$$

according to (6), we know $\alpha(k) = 0$ means that $e^{\mathrm{T}}(k)e(k) < \sigma(k) y^{\mathrm{T}}(k) y(k)$, then, adding $\eta_k^{\mathrm{T}} \Delta_g^{\mathrm{T}} W_0(r_k) \Delta_g \eta_k$ and subtracting $\eta_{k-\tau_k}^{\mathrm{T}} \Delta_f^{\mathrm{T}} W_1(r_k) \Delta_f \eta_{k-\tau_k}$ to (33),

$$\begin{aligned}
\Delta V(k, r_k) + J' &\leq \widetilde{\eta}_k^{\mathrm{T}} \left[\Lambda_0(i) \right. \\
&\quad + \Gamma_{10}^{\mathrm{T}}(i) \left(\widetilde{P}(r_k) + T_0(r_k) + N_0(r_k) \right) \Gamma_{10}(i) \\
&\quad \left. + \Gamma_2^{\mathrm{T}}(i) \overline{\tau} E \Gamma_2(i) + \gamma(i) + \gamma^{\mathrm{T}}(i) + \overline{\tau} Z_0(i) \right] \widetilde{\eta}_k
\end{aligned} \tag{35}$$

and, according to (25), $\Delta V(k, r_k) + J' \leq 0$. When $\alpha(k) = 1$, namely, (2) is satisfied, then, adding $\eta_k^{\mathrm{T}} \Delta_g^{\mathrm{T}} W_2(r_k) \Delta_g \eta_k$ and subtracting $\eta_{k-\tau_k}^{\mathrm{T}} \Delta_f^{\mathrm{T}} W_3(r_k) \Delta_f \eta_{k-\tau_k}$ to (35), in a similar way, $\Delta V(k, r_k) + J' \leq 0$ is obtained, and then

$$\Delta V(k, r_k) \leq -J' = -\begin{pmatrix} x(k) \\ u(k) \end{pmatrix}^{\mathrm{T}} Q' x \begin{pmatrix} x(k) \\ u(k) \end{pmatrix} \tag{36}$$

Then take expectation on both sides of it, and we obtain

$$\begin{aligned}
&E\{V(\infty, r_\infty)\} - E\{V(0, r_0)\} \leq -\beta_0 E \left\{ \sum_{k=0}^{\infty} \eta_k^{\mathrm{T}} \eta_k \right\} \\
&E \left\{ \sum_{k=0}^{\infty} \eta_k^{\mathrm{T}} \eta_k \right\} < \frac{1}{\beta_0} E\{V(0, r_k)\} - \frac{1}{\beta_0} E\{V(\infty, r_\infty)\} \\
&< \beta
\end{aligned} \tag{37}$$

where $\beta_0 = \inf\{\lambda_{min}(-\Psi^{\mathrm{T}}(r_k) Q' \Psi(r_k))\}$. It can be concluded from **Definition 5** that the system is stochastically stable, and the proof is completed. □

Theorem 7. *For given matrices $A_c(i)$, $B_c(i)$, and $C_c(i)$, positive constants $\overline{\tau}$, $\underline{\tau}$, and quantization density values $\rho_f(i)$ and $\rho_g(i)$, if there exists a set of positive definite matrices $E_{\alpha(k)}(i)$, $Z_{\alpha(k)}(i)$, $\overline{Q}$, $P_0(i)$, $P_1(i)$, $W_0(i)$, $W_1(i)$, $Q_0(i)$, $Q_1(i)$, $T(i)$, $N(i)$, and $M(i)$ of appropriate dimensions and constant $0 < \mu < 1$ the following inequalities hold:*

$$min \quad tr(P_1(r_0)) \tag{38}$$

$$s.t. \quad \begin{bmatrix} E_{\alpha(i)}(i) & M(i) \\ * & Z_{\alpha(i)} \end{bmatrix} \geq 0 \tag{39}$$

$$\Pi_0 = \begin{bmatrix} \Pi_{10} & \Gamma_{10}^{\mathrm{T}}(i) & \Gamma_2^{\mathrm{T}}(i) & \Psi^{\mathrm{T}}(i) \\ * & \overline{P_0} & 0 & 0 \\ * & * & \overline{E_0} & 0 \\ * & * & * & \overline{Q} \end{bmatrix} < 0 \tag{40}$$

$$\Pi_1 = \begin{bmatrix} \Pi_{11} & \Gamma_{11}^{\mathrm{T}}(i) & \Gamma_2^{\mathrm{T}}(i) & \Psi^{\mathrm{T}}(i) \\ * & \overline{P_1} & 0 & 0 \\ * & * & \overline{E_1} & 0 \\ * & * & * & \overline{Q} \end{bmatrix} < 0 \tag{41}$$

where

$$\begin{aligned}
\Pi_{10} &= \Theta_0(i) + \gamma(i) + \gamma^{\mathrm{T}}(i) + \overline{\tau} Z_0(i) + \mu I_1^{\mathrm{T}} C^{\mathrm{T}} C I_1 \\
&\quad - I_2^{\mathrm{T}} I_2, \\
\Pi_{11} &= \Theta_1(i) + \gamma(i) + \gamma^{\mathrm{T}}(i) + \overline{\tau} Z_1(i) + I_2^{\mathrm{T}} I_2 \\
&\quad - \mu I_1^{\mathrm{T}} C^{\mathrm{T}} C I_1, \\
\Theta_0(i) &= \mathrm{diag}\left\{ (\overline{\tau} - \underline{\tau} + 1) Q - P_0(i) - T(i) - N(i), \right. \\
&\quad \left. - W_0(i), \delta^2(i) W_1(i) - Q_0, -W_1(i) \right\} \\
\Theta_1(i) &= \mathrm{diag}\left\{ (\overline{\tau} - \underline{\tau} + 1) Q - P_1(i) - T(i) - N(i), \right. \\
&\quad \left. - W_2(i), \delta^2(i) W_3(i) - Q_1, -W_3(i) \right\}
\end{aligned}$$

$$\begin{aligned}
&\Gamma_{1\alpha(k)} = \left[\Phi_{1\alpha}(i) + \Phi_2(i) \right.\\
&\quad \left. + \Phi_3(i) \;\; \Phi_3(i) \;\; \Phi_{4\alpha(k)}(i) \;\; \Phi_{4\alpha(k)}(i)\right]\\
&\Gamma_2 = \left[\overline{A} \;\; \overline{B} \;\; 0 \;\; 0\right]\\
&\overline{A} = \left[A - I \;\; BC_c(i) \;\; 0\right]\\
&I_1 = \left[\operatorname{diag}\{I, 0, 0\} \;\; 0 \;\; 0 \;\; 0\right]\\
&I_2 = \left[\operatorname{diag}\{0, 0, I\} \;\; 0 \;\; 0 \;\; 0\right]\\
&\gamma = M^{\mathrm{T}}\left[\operatorname{diag}\{I, 0, 0\} \;\; 0 \;\; \operatorname{diag}\{-I, 0, 0\} \;\; 0\right]\\
&\overline{P}_0(i) = -\left(\sum_{j=1}^{s} p_{ij} P_0(i)(j)\right)^{-1}\\
&\overline{P}_1(i) = -\left(\sum_{j=1}^{s} p_{ij} P_1(i)(j)\right)^{-1}\\
&\overline{E}_0(i) = -\left(\overline{\tau} E_0(i)\right)^{-1}\\
&\overline{E}_1(i) = -\left(\overline{\tau} E_1(i)\right)^{-1}\\
&\Psi(i) = \begin{bmatrix} I & 0 & 0 \\ 0 & C_c(i) & 0 \end{bmatrix}\\
&\widetilde{Q} = \left(-Q'\right)^{-1}
\end{aligned} \tag{42}$$

Proof. $\widetilde{P}_0(i) = \sum_{j=1}^{s} p_{ij} P_0(j)$ and $\widetilde{P}_1(i) = \sum_{j=1}^{s} p_{ij} P_1(j)$ have been proposed in **Theorem 6**, let $\mu = \sigma$, and then the Schur complement lemma to (25) and (40) is obtained. In a similar way, (41) can be obtained from (26), and then the proof is completed. □

4. Simulation

Consider a system as follows:

$$\begin{aligned}
x(k+1) &= \begin{bmatrix} 0 & 2 \\ -2 & -3 \end{bmatrix} x(k) + \begin{bmatrix} 0 \\ 0.1 \end{bmatrix} u(k)\\
y(k) &= \begin{bmatrix} 0 & 1 \end{bmatrix} x(k)
\end{aligned} \tag{43}$$

The time delay is bounded as $0.01 \le \tau_k \le 0.09$ and modeled by a Markov chain $\omega = \{1, 2\}$, which is corresponded to mode 1 and mode 2, assume that $\delta_f = \delta_g = 0.023$, $x(0) = \begin{bmatrix} 1 & 0 \end{bmatrix}^T$, and the quantization density of each mode is defined as $\delta(1) = 0.02$ and $\delta(2) = 0.03$, $\mu = 0.0195$ is chosen as threshold, and the transition probability matrix is as follows:

$$p = \begin{bmatrix} 0.42 & 0.58 \\ 0.46 & 0.54 \end{bmatrix} \tag{44}$$

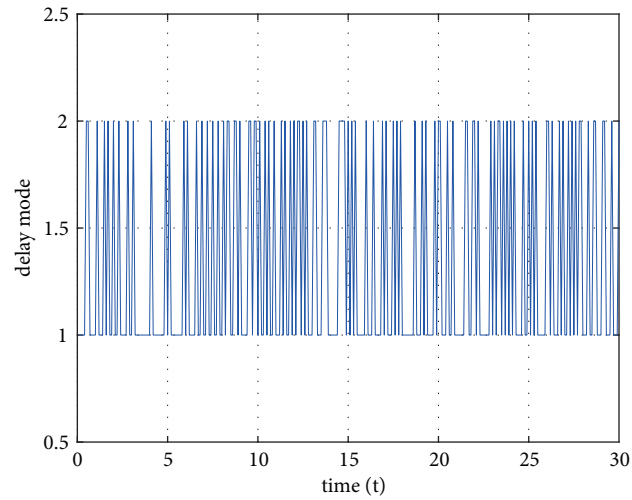

Figure 2: Group 1: the mode of time delay.

The linear matrix inequality is utilized and the matrices of controller are obtained as follows:

$$\begin{aligned}
A_c(1) &= \begin{bmatrix} -1.600 & 0.8703 \\ -0.6204 & -1.5032 \end{bmatrix}\\
A_c(2) &= \begin{bmatrix} -1.4306 & 0.3010 \\ 1.3071 & 0 \end{bmatrix}\\
B_c(1) &= \begin{bmatrix} 0.0012 & 0.1203 \end{bmatrix}^{\mathrm{T}}\\
B_2(2) &= \begin{bmatrix} -0.0210 & -0.0013 \end{bmatrix}^{\mathrm{T}}\\
C_c(1) &= \begin{bmatrix} -3.2122 & -0.0013 \end{bmatrix}\\
C_c(2) &= \begin{bmatrix} -3.5421 & -0.0009 \end{bmatrix}
\end{aligned} \tag{45}$$

and we take two groups parameters to make a comparison:

Group 1. $\sigma_1 = 0.01; \sigma_2 = 0.023$.

Group 2. $\sigma_1 = 0.01; \sigma_2 = 0.0195$.

Remark 8. Figures 2 and 5 show the switching of two modes of the time delay in a Markov chain, and the switching is determined by the transition probability. Figures 3 and 6 show the curves of the state response which eventually tend to be stable. The event-triggered release instants and intervals are shown in Figures 4 and 7, and the numbers of triggers in two figures are 79 and 73, which are much less than the number of the traditional sampling, which means that the network resources are greatly saved.

Remark 9. In literature [10], the structure of its system based on event-triggered scheme contains one quantizer, and the event-triggered release instants and interval are 74 and 84 while the sampling time is 10s. Comparing with [10], the method proposed in this article can save the network resources better.

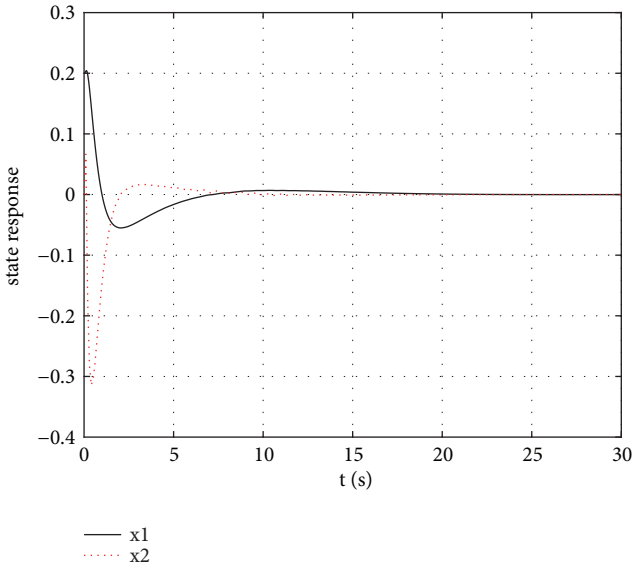

Figure 3: Group 1: the response of state.

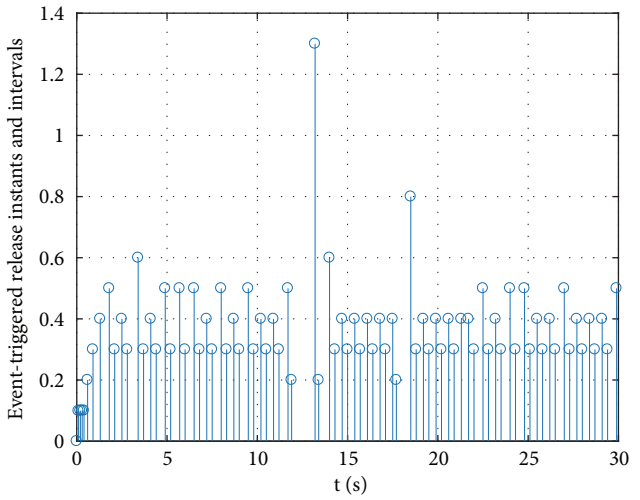

Figure 4: Group 1: the event-triggered release instants and intervals.

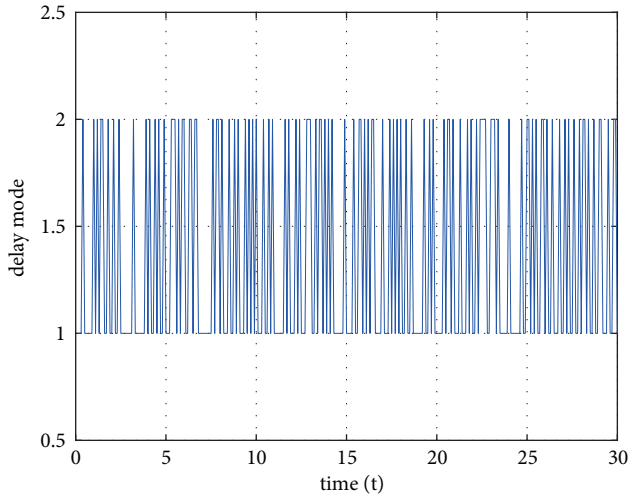

Figure 5: Group 2: the mode of time delay.

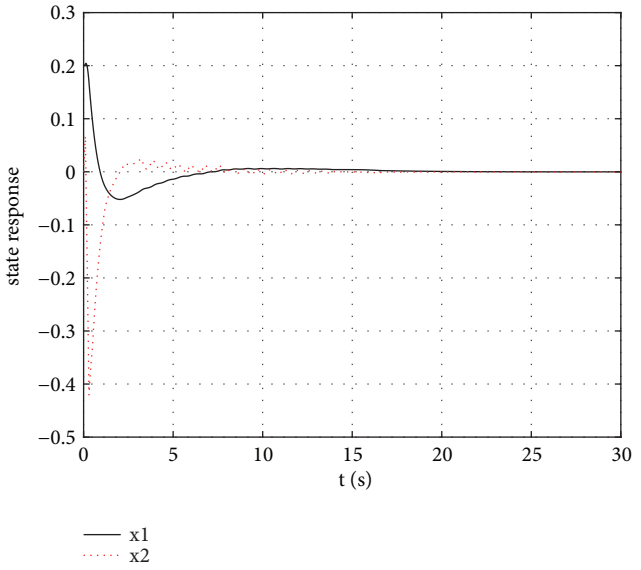

Figure 6: Group 2: the response of state.

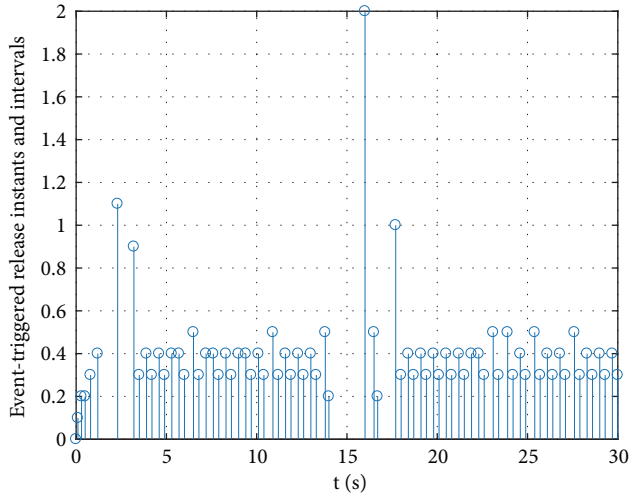

Figure 7: Group 2: the event-triggered release instants and intervals.

5. Conclusion

A co-design of event-triggered scheme and dynamic output feedback controller for a class of NCSs with random time delay is presented. Two mode-dependent quantizers are set to balance the network congestion and quantization error. A Markov process is used to model the time delay which is used to describe the quantization density as a function. Lyapunov-Krasovskii functional and LMI are used to derive the stability sufficient conditions. A numerical example is given to illustrate the proposed approach.

Appendix

Proof of Lemma 4 . From (20), we learn that

$$\sum_{i=k-\overline{\tau}}^{k-1} \begin{bmatrix} \overline{x}(i) \\ \widetilde{\eta}(i) \end{bmatrix}^{\mathrm{T}} \begin{bmatrix} E & M \\ M^{\mathrm{T}} & Z \end{bmatrix} \begin{bmatrix} \overline{x}(i) \\ \widetilde{\eta}(i) \end{bmatrix} \geq 0 \qquad \text{(A.1)}$$

Then

$$\begin{aligned}
&\sum_{i=k-\overline{\tau}}^{k-1}\left[\overline{x}^{\mathrm{T}}(i)E\overline{x}(i)+\widetilde{\eta}^{\mathrm{T}}(k)M^{\mathrm{T}}\overline{x}(i)+\overline{x}^{\mathrm{T}}(i)M\widetilde{\eta}(k)\right.\\
&\quad\left.+\widetilde{\eta}^{\mathrm{T}}(k)Z\widetilde{\eta}(k)\right]\geq 0,\\
&\sum_{i=k-\overline{\tau}}^{k-1}\widetilde{\eta}^{\mathrm{T}}(k)M^{\mathrm{T}}\overline{x}(i)+\sum_{i=k-\overline{\tau}}^{k-1}\overline{x}^{\mathrm{T}}(i)M\widetilde{\eta}(k)\\
&\quad+\sum_{i=k-\overline{\tau}}^{k-1}\widetilde{\eta}^{\mathrm{T}}(k)Z\widetilde{\eta}(k)\geq-\sum_{i=k-\overline{\tau}}^{k-1}\overline{x}^{\mathrm{T}}(i)E\overline{x}(i),\\
&\widetilde{\eta}^{\mathrm{T}}(k)M^{\mathrm{T}}\{x(k)-x(k-\overline{\tau})\}+\{x(k)-x(k-\overline{\tau})\}^{\mathrm{T}}\\
&\quad\cdot M\widetilde{\eta}(k)+\overline{\tau}\widetilde{\eta}^{\mathrm{T}}(k)Z\widetilde{\eta}(k)\geq-\sum_{i=k-\overline{\tau}}^{k-1}\overline{x}^{\mathrm{T}}(i)E\overline{x}(i),
\end{aligned}\tag{A.2}$$

Let

$$\begin{aligned}
&x(k)-x(k-\overline{\tau})\\
&\quad=\left[diag\{I,0,0\}\ \ 0\ \ diag\{-I,0,0\}\ \ 0\right]\widetilde{\eta}(k)\\
&\gamma=M^{\mathrm{T}}\left[diag\{I,0,0\}\ \ 0\ \ diag\{-I,0,0\}\ \ 0\right]
\end{aligned}\tag{A.3}$$

Then (21) is obtained. □

Data Availability

The data used to support the findings of this study are available from the corresponding author upon request.

Conflicts of Interest

The authors declare that they have no conflicts of interest.

Acknowledgments

This work is supported by the National Natural Science Foundation of China under Grant (61374083) and the National Funds for Distinguished Young Scientists of China (61425009).

References

[1] W.-A. Zhang, A. Liu, and K. Xing, "Stability analysis and stabilization of aperiodic sampled-data systems based on a switched system approach," *Journal of The Franklin Institute*, vol. 353, no. 4, pp. 955–970, 2016.

[2] A. Liu, W. Zhang, L. Yu, S. Liu, and M. Z. Chen, "New results on stabilization of networked control systems with packet disordering," *Automatica*, vol. 52, pp. 255–259, 2015.

[3] P. Antsaklis and J. Baillieul, "Special issue on technology of networked control systems," *Proceedings of the IEEE*, vol. 95, no. 1, pp. 5–8, 2007.

[4] D. Huang and S. K. Nguang, "State feedback control of uncertain networked control systems with random time-delays," in *Proceedings of the IEEE Conference on Decision and Control*, pp. 3964–3969, 2007.

[5] L. Zhou and G. Lu, "Quantized feedback stabilization for networked control systems with nonlinear perturbation," *International Journal of Innovative Computing, Information and Control*, vol. 6, no. 6, pp. 2485–2495, 2010.

[6] W.-A. Zhang and L. Shi, "Sequential fusion estimation for clustered sensor networks," *Automatica*, vol. 89, pp. 358–363, 2018.

[7] R. Yang, P. Shi, G. P. Liu, and H. Gao, "Network-based feedback control for systems with mixed delays based on quantization and dropout compensation," *Automatica*, vol. 47, no. 12, pp. 2805–2809, 2011.

[8] Y. Xia, J. Yan, P. Shi, and M. Fu, "Stability analysis of discrete-time systems with quantized feedback and measurements," *IEEE Transactions on Industrial Informatics*, vol. 9, no. 1, pp. 313–324, 2013.

[9] Z. G. Wu, P. Shi, H. Y. Su, and J. Chu, "Network-based robust passive control for fuzzy systems with randomly occurring uncertainties," *IEEE Transactions on Fuzzy Systems*, vol. 21, no. 5, pp. 966–971, 2013.

[10] J. He, Q. Ma, J. Guo, and C. Zhou, "Event-triggered mechanism based dynamic quantized output feedback controller for networked control systems," in *Proceedings of the 29th Chinese Control and Decision Conference, CCDC 2017*, pp. 2569–2574, May 2017.

[11] P. Tabuada, "Event-triggered real-time scheduling of stabilizing control tasks," *IEEE Transactions on Automatic Control*, vol. 52, no. 9, pp. 1680–1685, 2007.

[12] S. Hu, Y. Zhang, and Z. Du, "Network-based H∞ tracking control with event-triggering sampling scheme," *Control Theory and Applications Iet*, vol. 6, no. 4, pp. 533–544, 2012.

[13] B. Wang, X. Meng, and T. Chen, "Event based pulse-modulated control of linear stochastic systems," *Institute of Electrical and Electronics Engineers Transactions on Automatic Control*, vol. 59, no. 8, pp. 2144–2150, 2014.

[14] K. Peng, M. Wang, and J. Dong, "Event-triggered fault detection framework based on subspace identification method for the networked control systems," *Neurocomputing*, vol. 239, pp. 257–267, 2017.

[15] H. Xu, A. Sahoo, and S. Jagannathan, "Stochastic adaptive event-triggered control and network scheduling protocol co-design for distributed networked systems," *IET Control Theory & Applications*, vol. 8, no. 18, pp. 2253–2265, 2014.

[16] J. Zhang, C. Peng, D. Du, and M. Zheng, "Adaptive event-triggered communication scheme for networked control systems with randomly occurring nonlinearities and uncertainties," *Neurocomputing*, vol. 174, pp. 475–482, 2016.

[17] N. Elia and S. K. Mitter, "Stabilization of linear systems with limited information," *IEEE Transactions on Automatic Control*, vol. 46, no. 9, pp. 1384–1400, 2002.

[18] C. Peng and Y. Tian, "Networked H_∞ control of linear systems with state quantization," *Information Sciences*, vol. 177, no. 24, pp. 5763–5774, 2007.

[19] E. Tian, D. Yue, and C. Peng, "Quantized output feedback control for networked control systems," *Information Sciences*, vol. 178, no. 12, pp. 2734–2749, 2008.

[20] F. Rasool, D. Huang, and S. K. Nguang, "Robust H∞ output feedback control of discrete-time networked systems with limited information," *Systems and Control Letters*, vol. 60, no. 10, pp. 845–853, 2011.

[21] M. Fu and L. Xie, "The sector bound approach to quantized feedback control," *IEEE Transactions on Automatic Control*, vol. 50, no. 11, pp. 1698–1711, 2005.

[22] K. Liu, E. Fridman, and K. H. Johansson, "Dynamic quantization of uncertain linear networked control systems," *Automatica*, vol. 59, pp. 248–255, 2015.

[23] G. Gu and L. Qiu, "Networked control systems for multi-input plants based on polar logarithmic quantization," *Systems & Control Letters*, vol. 69, pp. 16–22, 2014.

[24] Y. Kao, J. Xie, C. Wang, and H. R. Karimi, "A sliding mode approach to H∞ mathcontainer loading mathjax non-fragile observer-based control design for uncertain markovian neutral-type stochastic systems," *Automatica*, vol. 52, pp. 218–226, 2015.

[25] J. Cheng, J. H. Park, Y. Liu, Z. Liu, and L. Tang, "Finite-time H ∞ fuzzy control of nonlinear Markovian jump delayed systems with partly uncertain transition descriptions," *Fuzzy Sets and Systems*, vol. 314, pp. 99–115, 2016.

[26] L. Zha, J. A. Fang, X. Li, and X. Liu, "Event-triggered output feedback H∞ mathcontainer loading mathjax control for networked markovian jump systems with quantizations," *Nonlinear Analysis Hybrid Systems*, vol. 24, pp. 146–158, 2017.

[27] Y. Shi and B. Yu, "Output feedback stabilization of networked control systems with random delays modeled by Markov chains," *IEEE Transactions on Automatic Control*, vol. 54, no. 7, pp. 1668–1674, 2009.

[28] S. Chae, F. Rasool, S. K. Nguang, and A. Swain, "Robust mode delay-dependent H∞ control of discrete-time systems with random communication delays," *Control Theory and Applications Iet*, vol. 4, no. 6, pp. 936–944, 2010.

Hindawi
Journal of Control Science and Engineering
Volume 2018, Article ID 3975373, 10 pages
https://doi.org/10.1155/2018/3975373

Research Article

An Improved Defogging Algorithm Based on Dark Color Theory Combined with Self-Adaptive Threshold Mechanism

Aixing Li,[1] Zhou Fang ,[2] and Bo Mi[1]

[1]*College of Information Science and Engineering, Chongqing Jiaotong University, Chongqing 400074, China*
[2]*College of Information Science and Engineering, Chaohu University, Chaohu 23800, China*

Correspondence should be addressed to Zhou Fang; 054050@chu.edu.cn

Received 10 May 2018; Accepted 28 June 2018; Published 1 August 2018

Academic Editor: Yun-Bo Zhao

Defogging algorithms based on dark channel prior have color shift in light color areas because of inaccurate estimation of transmittance. To resolve this problem, a novel improved image clearness method is proposed. Based on the dark channel prior, the essential causes of color shift are analyzed, with two important factors summarized. Then, transmission map is calculated by using 3∗3 fixed region, and the restoration module based on self-adaptive threshold mechanism for transmission map is provided. Some experiments are carried out to determine parameters in restoration module to correct the transmission map. According to the corrected transmission map, a transmission restoration algorithm is constructed based on the self-adaptive threshold mechanism to improve the performance of the fog-free image. The experiment results show that this method can resolve the color shift in light color areas effectively and guarantee the overall framework of defogging method based on dark color theory unchanged.

1. Introduction

In fog weather, due to the influence of atmospheric scattering, image taken by outdoor surveillance system would get serious degradation problems in the color and contrast fidelity. It not only directly affects the safety of sea, land, and air transportation by making the outdoor surveillance system abnormal [1, 2], but also hinders images feature extraction, which causes some monitoring systems based on feature extraction ineffective, such as production monitoring system [3, 4].

Currently, most of image defogging algorithms are based on image restoration, the core idea of which is as follows: firstly, an imaging mode should be established; secondly, the degraded part of the imaging model is compensated and the interferential part of it is filtered; thirdly, the clear image is restored [5–17]. Theoretically, the defogging effect of these algorithms can be ideal; however, most of the existing imaging models are dependent on the image depth information; unfortunately, they cannot be accurately calculated using a single image. Therefore, how to obtain the accurate image depth information is a bottleneck in image restoration field.

In 2009, Professor Kaiming He proposed a dark channel prior (DCP) theory on CVPR conference [8]. According to his theory, image depth information can be accurately acquired, which makes breakthrough progress in image restoration field. The defogging algorithm based on DCP is simple and effective; however, the inaccurate estimates of transmission would lead to distortion of the image, such as halo artifacts and overly enhanced restoration in light color areas, and also the optimization algorithm of transmission has high spatial complexity. Therefore, some improved methods have been proposed [9–17] based on DCP. Li et al. [11] proposed an edge-preserving decomposition method to estimate transmission map. This method removes haze effectively and overcomes halo artifacts. However, the result of dehazing partly depends on the accuracy of haze level estimation and the algorithm cannot do that at present. Song et al. [12] estimate the transmission by using small patch size dark channel (DC), and several gray images as guided filter (GF) are used to optimize the transmission. This method has excellent performance in edge maintenance and halo reduction; nevertheless, the dehazing effect of it is not so outstanding because of the limitation of DC size. Yang et al. [13] proposed a edge of alternative method to refine transmission map, which could overcome halo artifacts effectively. Chen et al. [14] proposed a dehazing-parameter

adaptive method to adjust the degree of haze removal, and an iteration method based on GF is used to optimize transmission. Experimental results show that this algorithm performs well in different levels of haze conditions. However, the optimization method of transmission is replaced by an approximate scheme to reduce high computation.

Other methods are proposed and also have an outstanding effect on dehazing. Zhu et al. [18] exploited the characteristics of brightness and saturation of the pixels in hazy image, proposing a new linear model and learning the parameters of the model by using a supervised learning method to estimate the depth information. Their experimental results indicated that dehazing effects are good and efficient, but the insufficient estimation of transmission map is still an unsolved problem.

Based on DCP, this paper proposes an improved algorithm combined with self-adaptive threshold mechanism (STM), which enhances the transmittance in light color area. The remaining parts of this paper are arranged as follows: in Section 2, atmospheric scattering model will be introduced briefly; in Section 3, the original defogging algorithm based on dark channel prior theory will be described in detail; Section 4 performs a detailed analysis of the color shift problem and construct an improved algorithm combined with self-adaptive threshold mechanism (STM). In Section 5, the comparison of the experiment results between our defogging algorithm and other algorithms will be used to illustrate the validity of the improved algorithm. And then, Section 6 summarizes our work and discusses the future direction.

2. Introduction of Atmospheric Scattering Model

In image restoration filed, the following mathematical model is widely used to describe the imaging process of fogging image:

$$I(x) = J(x)\,t(x) + A\,(1 - t(x)) \tag{1}$$

where $I(x)$ is the fogging image light intensity acquired by visual system (i.e., input image); $J(x)$ presents the light intensity reflected at the surface of the scene (i.e., needed fog-free image); x is used to mark the two-dimensional location of the pixels in image; and A describes the atmospheric light coming from infinity (skylight), which is usually assumed as a global constant. In other words, there is no relationship between location parameter x and A . $t(x)$ denotes the transmission map of the image, which reflects the depth information of the scene, and it can be expressed as follows:

$$t(x) = e^{-\beta(\lambda)d(x)} \tag{2}$$

where β is scattering coefficient of the atmosphere and d describes the distance between the target scene and the observer. In general, the atmosphere is uniform.

Formula (1) is widely used in image defogging field [8–15] at present, which describes the imaging process of fogging image and gives us the tip about the core idea of image defogging algorithm, i.e., eliminating the atmospheric light participated in imaging, and compensating for the lost reflected light of scene caused by atmospheric scattering.

3. Imaging Defogging Algorithm Based on Dark Channel Prior Theory

3.1. Basic Concept of Dark Channel Prior Theory. After observing large numbers of outdoor fog-free images, empirical statistical regularity called dark channel prior theory is proposed by Professor Kaiming He in [8]. It points out that any local regions of vast majority outdoor clear images contain some pixels, which has very low intensity values in at least one color channel. This intensity value that belongs to local area is called dark channel value and we can use the following formula to calculate the dark channel values:

$$J^{dark}(x) = \min_{c\subset\{r,g,b\}} \left\{ \min_{y\subset\Omega(x)} \left(J^c(y)\right) \right\} \tag{3}$$

where J^c represents one color channel of image J and $\Omega(x)$ is local area of image, which is centered on x meaning two-dimensional position. Generally, these dark channel values always exist in object shadow, dark object, and object with bright colors.

3.2. Image Defogging Algorithm Based on Dark Channel Prior Theory. Due to the fact that dark channel values of the fogging image are always close to zero in fog weather, the dark channel values obtain certain brightness at the process of imaging. Notice that the dark channel values may be calculated at both sides of (1), and then the first term at the right of (1) is set to zero. Thus, formula (1) could be rewritten as follows:

$$I^{dark} = A\,(1 - t(x)). \tag{4}$$

According to (4), the image depth information $t(x)$ can be expressed as follows formula.

$$t(x) = 1 - \frac{I^{dark}}{A} \tag{5}$$

There are two unknown parameters in formula (5): dark channel values I^{dark} which can be calculated by using formula (3) and atmospheric light A. Unfortunately, we do not know how to acquire atmospheric light A. To solve the problem, Professor Kaiming He sorted these dark channel values and extracted the 10% brightest dark channel values and then took the mean of these 10% brightest dark channel values as the value of atmospheric light A in [8].

In fact, atmospheric scattering exists even in a cloudless day. Particles are suspended in air, so the vague area of image will appear when we observe distant objects. On the other hand, images have depth because of atmospheric scattering. If we remove atmospheric light thoroughly, the restoring image may tend to look fake and unnatural. For solving the problem, Professor He introduces parameter $w(0 < w \leq 1)$ to keep a small amount of atmospheric light for distant objects in [8]. And formula (5) is adapted as

$$t(x) = 1 - w\left(\frac{I^{dark}}{A}\right). \tag{6}$$

Figure 1: Original images without obvious light color areas.

Meanwhile, the defogging model of images may get combined with imaging model (1).

$$J(x) = \frac{I(x) - A}{t(x)} + A \tag{7}$$

Therefore, once the transmission map $t(x)$ is calculated using formula (6), the clear fog-free image can be restored. Notice that the clear fog-free image restored by defogging algorithm based on dark channel prior theory is always darker than atmospheric light, so the parameter t_0 is introduced to enhance and increase the intensity of the image in [8]. Therefore, formula (7) may be adapted as follows:

$$J(x) = \frac{I(x) - A}{\max\left(t(x), t_0\right)} + A. \tag{8}$$

In practice sense, the value of t_0 is set according to the requirements of real application. For example, the value of t_0 has been set as 0.1 in [8].

3.3. Insufficiency of Defogging Algorithm Based on Dark Channel Prior Theory. Generally speaking, if the fogging images acquired by outdoor surveillance system contain no obvious light color areas, they can obtain a satisfactory defogging effect by defogging algorithm based on dark channel prior theory. This is because the vast majority of the pixels in these images meet dark channel prior theory; i.e., there has to be at least one color channel whose value is close to 0 among these pixels. For example, the original fogging images are shown as Figure 1 and the defogging images processed by dark channel prior theory are shown as Figure 2.

In a real world situation, however, some fogging images may always contain obvious light color areas shown as Figure 3.

In this case, if we use the defogging method based on dark channel prior theory to restore these fogging images, the color shift problem should appear in light color areas. This is due to the fact that the pixel values in three color channels are very high for all pixels in the light color area, and then the defogging algorithm based on dark channel prior theory is invalid in these light color areas. It is illustrated as Figure 4.

Notice that, in Figure 4, the restored images look too saturated when we calculate the dark channel values by using 3∗3 fixed region. In this paper, our main purpose is how to restore the invalid image caused by the dark channel prior theory in these light areas.

To solve the color shift problem, we will first analyze the characteristics of original fogging image and restored image and then figure out the essential cause of image color shift problem. Based on this, a repaired model of inaccurate transmission map in light color is constructed directionally.

4. Improved Image Defogging Algorithm Based on Dark Channel Prior Theory and Self-Adaptive Threshold Mechanism

4.1. Cause Analysis of Color Shift in Light Color Areas. In order to analyze the characteristics of original fogging image and restored image, find out the essential cause of image color shift problem; the Histograms of dark channel values between images containing obvious light color areas and images containing no obvious light areas are shown in

Figure 2: Clearness images restored from original images without obvious light color areas.

(a) (b) (c)

Figure 3: Original images with obvious light color areas.

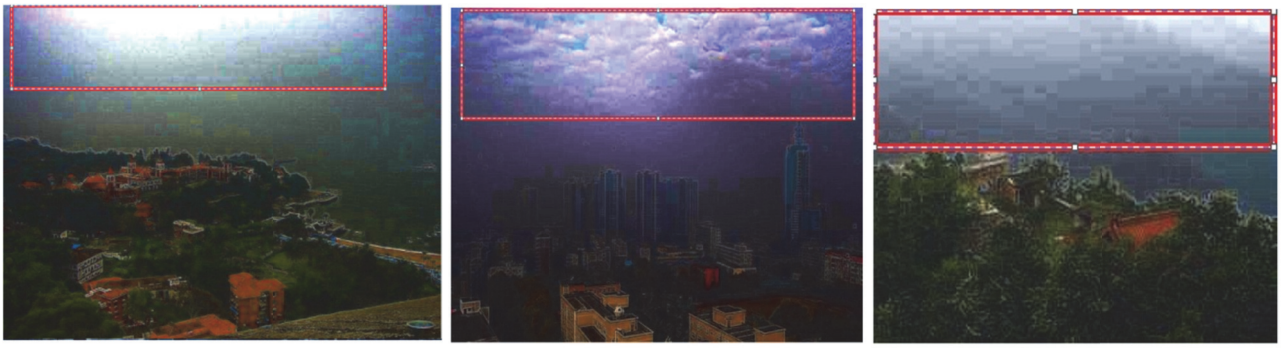

Figure 4: Clearness images restored from images with light color areas.

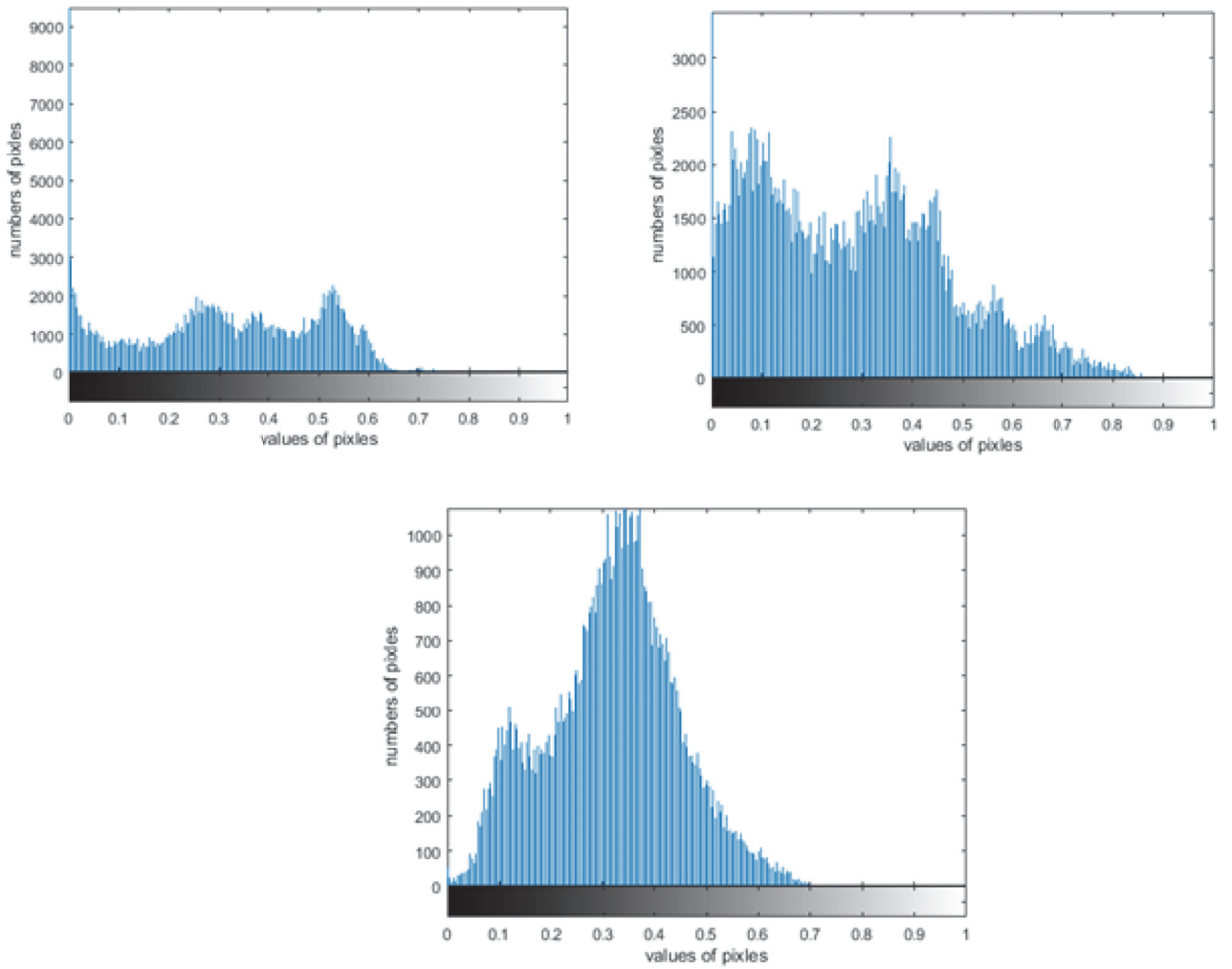

Figure 5: Histogram of dark channel values without obvious light color areas.

Figures 2 and 4. The corresponding statistical comparison results are illustrated in Figures 5 and 6.

From Figure 5, it can be found that the histogram of dark channel values of fogging images which contain no obvious light color areas is darker and its statistical values are close to zero as a whole. In contrast, we can find from Figure 6 that some inconsistent larger dark channel values exist in the images that contain obvious light color areas. This indicated that the dark channel value may be inexistent in these light color areas; i.e., the dark channel prior theory has failed in these areas of image.

However, how do these larger incorrect dark channel values affect the final defogging effect? For answering this question, we rewrite formula (7) according to formula (6) and (8) as follows:

$$J(x) = \frac{I(x) - A}{\max\left(\left(1 - w\left(I^{dark}/A\right)\right), t_0\right)} + A \tag{9}$$

where $J(x)$ and $I(x)$ denote restored fog-free image and original fogging image, respectively. As every image has three color channels as R, G, or B, formula (9) may also be remarked as follows:

$$J^c(x) = \frac{I^c(x) - A}{\max\left(\left(1 - w\left(I^{dark}/A\right)\right), t_0\right)} + A \tag{10}$$

where c presents color channels of image. Obviously, three color channels of image $J^c(x)$ can be marked as J^R, J^G, andJ^B, analogously, and those of original image $I^c(x)$ can be described as I^R, I^G, and I^B.

Notice that the dark channel value I^{dark} is usually larger in light color area, which will result in transmittance $t(x)$ tending to be smaller directly. In this fact, even if the pixel values of three color channels are quite close, their difference will become larger while they are divided by a small transmittance value, which can lead to significant change of color values of these pixels essentially. At this point, the color shift happens.

To better analyze the problem, the maximum difference of three channels between original fogging images and restored free-fog images by dark channel prior theory is experimented.

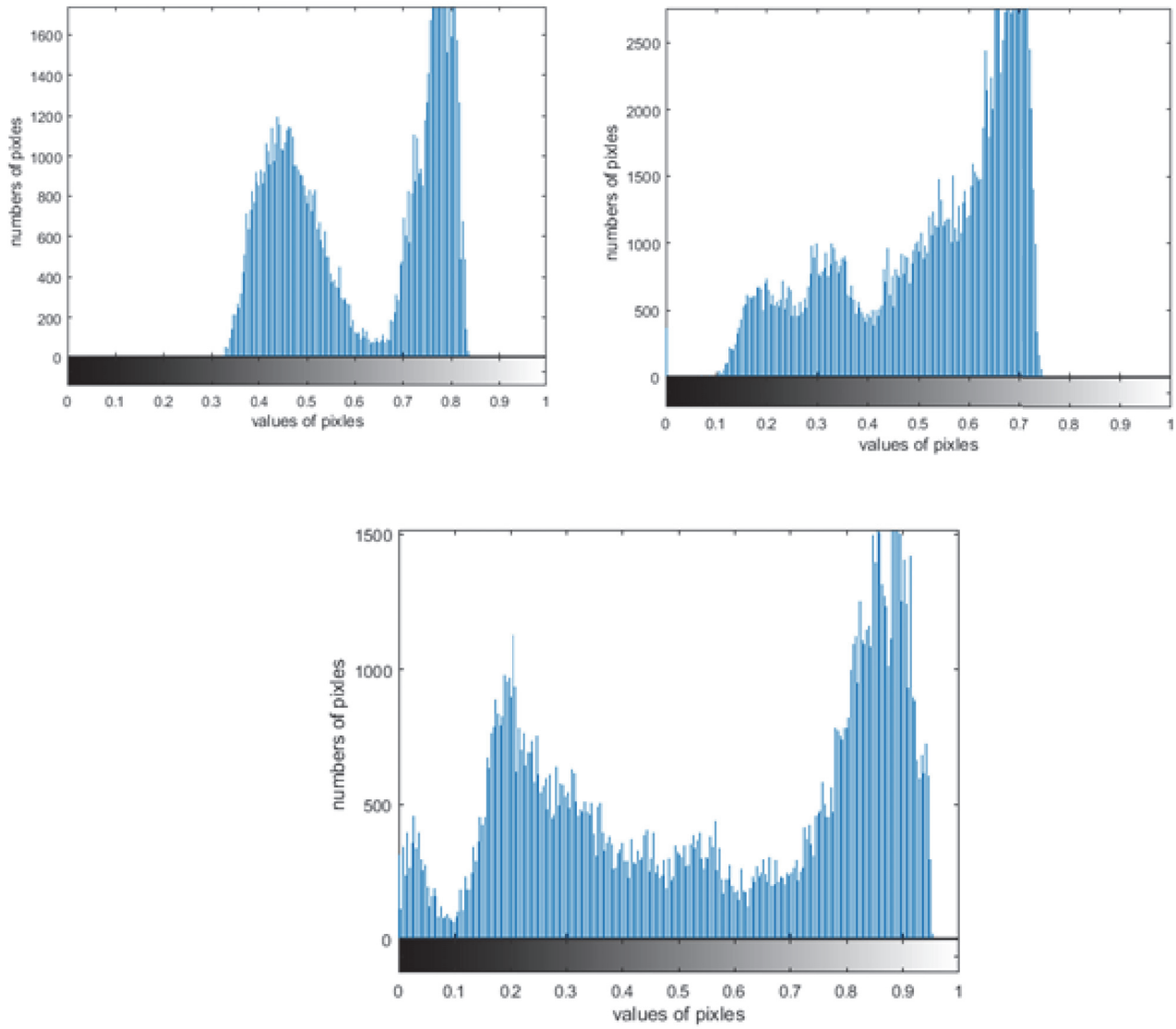

Figure 6: Histogram of dark channel values with obvious light color areas.

Figure 7 describes three color channels' maximum difference of each pixel with obvious light color areas.

It can be clearly found that vast majority of three color channels' maximum difference values of pixels have to be increased several times, which brings a great change for the original color of these pixels, after using defogging algorithm based on dark channel prior theory. To precisely locate these pixels in primary images, the three color channels' maximum difference values are presented in image form shown as Figure 8.

Obviously, the distribution of these maximum difference values and that of light color areas are coincidental. This indicates that the conclusion is reasonable and fit in with facts. Next, we need to find a method to solve these types of problems.

4.2. Transmittance Restored Algorithm Based on Self-Adaptive Threshold Mechanism. According to the analysis in previous section, the essential reason of color shift problem in light color areas is the incorrect smaller transmittances generated by the larger dark channel values that come from incorrect calculations. Therefore, the original defogging algorithm can be improved by optimizing these incorrect smaller transmittances. Firstly, we assume that the optimized transmittance and primary transmittance satisfy the following relationship:

$$t^{after} = \begin{cases} k \cdot \max\left(t^{before}(x), t_0\right) & x \text{ located at light color areas} \\ 1 \cdot \max\left(t^{before}(x), t_0\right) & x \text{ not located at light color areas.} \end{cases} \tag{11}$$

In other words, the transmittance can be optimized in light color areas by multiplying a weight coefficient $k(k > 1)$ and can be kept in other areas. The parameter t_0 is used to enhance the intensity of the image in defogging algorithm based on dark channel prior theory. Therefore, the key of

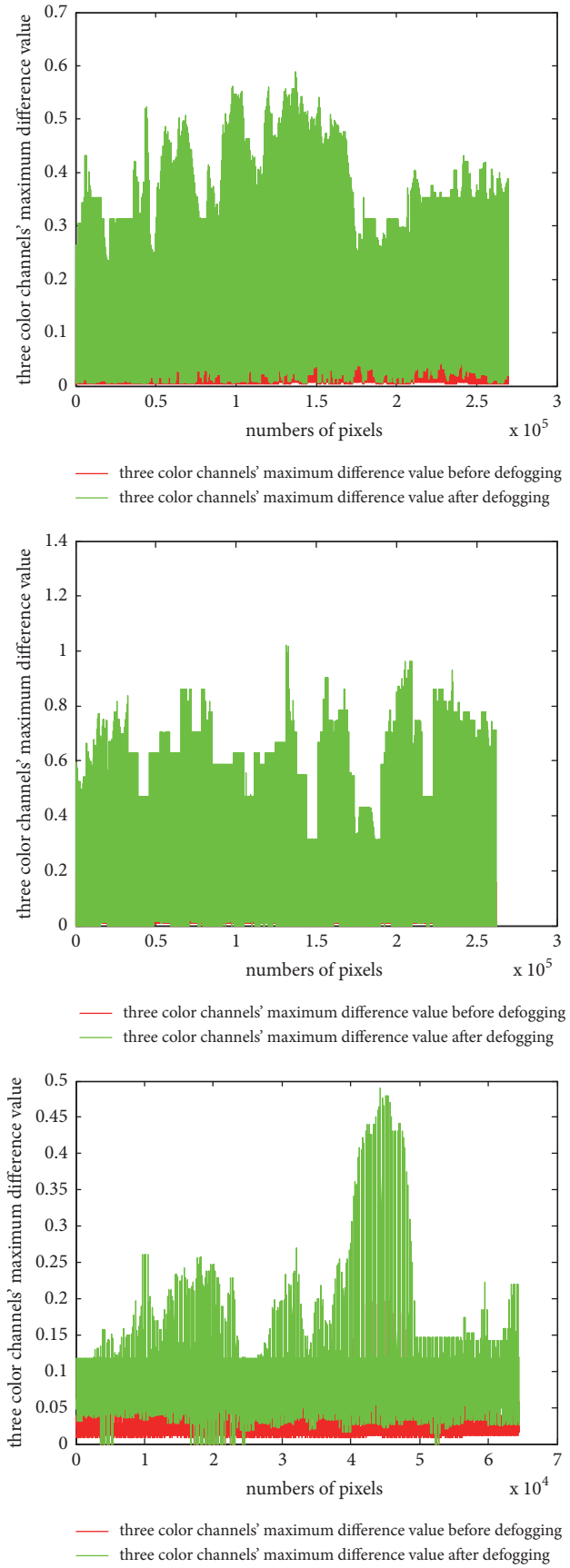

Figure 7: Numerical form of three color channels' maximum difference values.

improving defogging algorithm is how to locate light color area and estimate parameter k.

To improve the effect, Professor Jiang proposed an improvement model to calculate the parameter k and improve original transmittance in [10]. They assumed that all pixel values in three color channels are close to atmospheric light in light color area. Based on the assumption, the improved formula of transmittance is set as follows:

$$t^{after} = \min\left(\max\left(\frac{cons\tan t}{I^c(x) - A}, 1\right) \cdot \max\left(t^{before}, t_0\right), 1\right). \tag{12}$$

For simplicity, let $cons\tan t = 50$ in [10].

Unfortunately, according to the analysis of the pixels in light color area in Figures 7 and 8, the pixels in light color area have another characteristic yet; i.e., the maximum difference values of three color channels are smaller which can be found by the red curve in Figure 7. These indicate that the following two characteristics are true in practice:

(1) The maximum difference values of three color channels are smaller, which can be found by the red curve in Figure 7.

(2) All pixel values in three color channels are close to atmospheric light.

Obviously, Jiang only considered second feature of the light color area, so formula (12) cannot satisfy the dynamical need for restoring image and the algorithm has poor robustness.

To better improve the effect of restored images and meet the dynamical need, the expression of k could be assumed combining the above two characteristics as follows:

$$k = \frac{\max(\Delta(x))}{I^c(x) - A} \tag{13}$$

where

x indicates the two-dimension coordinate of the pixels in image;

Δ presents the difference values of three color channel in original fogging image;

I^c denotes the value of pixel of the original fogging image in c color channel;

c can be selected as R, G, B.

In reality, $\max(\Delta(x))$ is calculated as the value located at the 99% position in ascending order of Δ because of the existence of noise.

According to the analysis above, the following formula can be used to optimize the primary transmittance:

$$t^{after} = \min\left(\max\left(\frac{\max(\Delta(x))}{I^c(x) - A}, 1\right) \cdot \max\left(t^{before}, t_0\right), 1\right). \tag{14}$$

In addition, there have been cases where the primary fogging image is dim on the whole. Meanwhile, the pixel values in different color channels are close; i.e., the vast

Figure 8: Image form of three color channels' maximum difference values.

majority of three color channels' maximum difference values of pixels are close to zero. However, the light color areas still exist relatively. In this case, the weight coefficient k computed by formula (13) is too small that the improved effect of transmittance cannot be achieved. Therefore, the following method is proposed to solve the problem brought by the situation.

The concrete processing steps are as follows.

(1) Locating this situation. Observing the statistical result, it is found that Δ_{mean} which presents the mean of Δ is small and most of values in Δ are smaller than Δ_{mean}. Thus, the characteristic could be described using the following model:

$$\Delta_{mean} \leq \Delta_{thread},$$
$$\frac{count_{lower\_mean}}{count_{higer\_mean}} > 1 \tag{15}$$

where Δ_{thread} is a self-adaptive fault-tolerant threshold. In particular, experiments have shown that when threshold value Δ_{thread} is set to be 0.1, almost this situation can be successfully located. $count_{lower\_mean}$ is the number of pixels whose three color channels' maximum difference values are less than Δ_{mean}. And $count_{higer\_mean}$ presents the number of pixels whose three color channels' maximum difference values are greater than Δ_{mean}.

(2) Recalculation for weight coefficient k. Considering the fact that even though the vast majority of color channels' maximum difference values are close to zero, the differences among them exist still. Therefore, the original Δ can be processed using linear stretch algorithm to increase these differences:

$$\Delta^*(x) = \Delta(x) \cdot \left(\frac{(\Delta(x) - \Delta_{\min})}{(\Delta_{\max} - \Delta(x))} \right) \tag{16}$$

where $\Delta_{\min}$, $\Delta_{\max}$ represent the maximum value and minimum value of Δ, respectively

As a result, it not only retains the relative difference of color channels' maximum difference values, but also increases their absolute difference values. Then we could get a new maximum value $\max(\Delta^*(x))$ by using the linear stretch formula (16).

To guarantee the improvement effect of transmittance, the self-adaptive maximum value model of Δ is constructed combining the primary maximum value $\max(\Delta(x))$ and linear stretch maximum $\max(\Delta^*(x))$.

$$\max_f(\Delta(x)) = \frac{\max(\Delta^*(x)) + \max(\Delta(x))}{2} \tag{17}$$

Based on this information, a final $\max(\Delta(x))$ could be calculated again by using the stretch difference value Δ^* and the original difference value Δ. Further, the weight coefficient k could be gotten by formula (13) and formula (17).

5. Experimental Simulation and Analysis

For verifying the availability of our algorithm, in this section, we will compare it with experimental results of DCP algorithm and Improved DCP algorithm in two ways: subjective visual evaluation and objective quality of defogging images. Here the original images containing large light color areas, which are shown as Figure 3, are used as the experimental images.

5.1. Subjective Visual Evaluation. The fogging images are restored by using DCP algorithm shown as Figure 4; serious color shift problem exists in light color areas. Improved DCP algorithm and STM algorithm that we proposed could improve the insufficiency well. Two different visual results are shown as Figure 9.

According to formula (12), the improvement effect of transmittance of Improved DCP algorithm relies mainly on the selection of $cons\tan t$. In actual engineering, if these images have different characteristics, $cons\tan t$ should be selected as different value. However, [10] overlooked the problem and $cons\tan t$ had been selected as a constant value 50. We can find out from Figure 9(a) that although the algorithm proposed by Professor Jiang solved the color shift problem, it has poor robustness. This is mainly because the different constant value may result in different optimized effects for different images.

In comparison, the algorithm proposed in this paper prevents artificial arbitrariness of selection for $cons\tan t$ and changes adaptively weight coefficient k according to color channels' maximum difference values. The defogging images shown as Figure 9(b), which are restored by our algorithm, would have more robustness.

5.2. Objective Evaluation. Considering the limitation of subjective evaluation coming from human visual system, here,

(a) Clearness images obtained by Improved DCP algorithm

(b) Clearness images obtained by STM algorithm

Figure 9: Visual comparison of clearness images.

we introduce image's standard deviation that can reflect the contrast of an image to evaluate the quality of restored images defogging by different algorithms. The computing model is as follows:

$$H = -\sum_{i=0}^{255} p(i) \log p(i), \quad i \in (0, 255) \tag{18}$$

where i indicates gray value of different pixel and $p(i)$ represents the probability of i in images.

Meanwhile, the information entropy, which represents the amount of information in an image, is used to evaluate the quality of restored images defogging by different algorithms. And the computing model is as follows:

$$\sigma = \sqrt{\sum_{i=0}^{255} (i - mean)^2 \cdot p(i)}, \quad i \in (0, 255) \tag{19}$$

where i and $p(i)$ are the same as described in formula (18). The symbol *mean* denotes the statistical mean of gray value of the whole image. The formula is shown as follows:

$$mean = \sum_{i=0}^{255} i \cdot p(i), \quad i \in (0, 255). \tag{20}$$

Normally, if the size of image block is too large, it will result in overly enhanced restoration and then the following problems of restored images arise: image is so saturated that some image details are lost. In addition, our goal is to improve the insufficiency of defogging method based on dark channel prior theory used in light color areas, so a 3∗3 image block is used to calculate the dark channel values for better comparison.

It is generally known that a fogging image always has a low contrast and less depth information. Therefore, the better the algorithm is, the bigger the standard deviation and entropy of the defogging image are. Thus, the performance comparison of quality of defogging images, restored by three algorithms, is listed in Table 1 from (18)-(20).

Observing the above table, we can find that all the algorithms can increase the standard deviation and entropy of the images, i.e., improving the objective quality of images. STM algorithm makes more contribution for standard deviation and entropy of the images, when compared with DCP and Improved DCP algorithm. These results in Table 1 show that STM algorithm/model is effective.

6. Conclusion

In this paper, a new improved defogging algorithm based on dark color theory is presented combined with self-adaptive threshold mechanism. First we make a detailed analysis and experimental verification for characteristics of the light color area in image, and then the invalidity of dark channel prior theory in light color is discussed in detail. Based on the dynamical need for defogging image in light color areas, a self-adaptive threshold mechanism is proposed to optimize transmittance. The optimized transmission helps to avoid color shift problem in light color areas. The experiments indicate that our algorithm is in line with practical situation.

On the other hand, we do not consider the situation in which dark prior channel theory is out of work when image contains large range of white objects. It would be worth studying in the future.

Data Availability

The data used to support the findings of this study are available from the corresponding author upon request.

Table 1: Comparison of clearness images quality.

	Figure 3(a)			
	Original image	DCP algorithm	Improved DCP algorithm	STM algorithm
Standard deviation	0.2636	0.2878	0.3317	0.3454
Entropy	7.6276	7.0131	7.4399	7.5828
	Figure 3(b)			
	Original image	DCP algorithm	Improved DCP algorithm	STM algorithm
Standard deviation	0.1616	0.2498	0.2665	0.2696
Entropy	7.0704	6.8523	7.2481	7.3115
	Figure 3(c)			
	Original image	DCP algorithm	Improved DCP algorithm	STM algorithm
Standard deviation	0.1495	0.2507	0.3044	0.3076
Entropy	6.6060	6.7186	6.9363	6.9744

Note. Figures 3(a), 3(b), and 3(c) above correspond to the images shown as Figures 3(a)–3(c), respectively.

Conflicts of Interest

The authors declare that they have no conflicts of interest.

Acknowledgments

The research was sponsored by Natural Science Foundation of China (NSFC) under Grants 61573076, 61663008, and 61703063; the Scientific Research Foundation for the Returned Overseas Chinese Scholars and Program for Excellent Talents of Chongqing Higher School under Grant 2015-49; the Program for Excellent Talents of Chongqing Higher School under Grant 2014-18; Science and Technology Project under Grants KJ1705121 and KJ1705139; and the Chongqing Natural Science Foundation of China under Grant CSTC2017jcyjA1665.

References

[1] D. Huang, Z. Fang, L. Zhao, and X. Chu, "An improved image clearness algorithm based on dark channel prior," in *Proceedings of the 33rd Chinese Control Conference*, pp. 7350–7355, 2014.

[2] D.-R. Huang, Z. Fang, and L. Zhao, "An improved defogging algorithm combined with edge detection," *Journal of Shanghai Jiaotong University*, vol. 49, no. 6, pp. 861–867, 2015 (Chinese).

[3] K. Zhang, H. Hao, Z. Chen, S. X. Ding, and K. X. Peng, "A comparison and evaluation of key performance indicator-based multivariate statistics process monitoring approaches," *Journal of Process Control*, vol. 33, no. 3, pp. 112–126, 2015.

[4] K. Zhang, K. Peng, and J. Dong, "A common and individual feature extraction-based multimode process monitoring method with application to the finishing mill process," *IEEE Transactions on Industrial Informatics*, pp. 1551–3203, 2018.

[5] Y.-K. Wang and C.-T. Fan, "Single image defogging by multiscale depth fusion," *IEEE Transactions on Image Processing*, vol. 23, no. 11, pp. 4826–4837, 2014.

[6] M. Ding and R. Tong, "Efficient dark channel based image dehazing using quadtrees," *Science China Information Sciences*, vol. 56, no. 9, pp. 1–9, 2013.

[7] R. T. Tan, "Visibility in bad weather from a single image," in *Proceedings of the IEEE Conference on Computer Vision and Pattern Recognition*, pp. 1–8, June 2008.

[8] K. He and J. Sun, "Single image haze removal using dark channel prior," in *Proceedings of the IEEE Conference on Computer Vision and Pattern Recognition*, pp. 1956–1963, IEEE Computer Society, New York, NY, USA, June 2009.

[9] K. He, J. Sun, and X. Tang, "Guided image filtering," in *Proceedings of the 11th European Conference on Computer Vision*, pp. 1–14, 2010.

[10] J. Jiang and T. Hou, "Improved defogging algorithm based on dark channel prior theory," *Journal of Circuits and Systems*, vol. 16, no. 2, pp. 7–12, 2011.

[11] Z. Li and J. Zheng, "Edge-preserving decomposition-based single image haze removal," *IEEE Transactions on Image Processing*, vol. 24, no. 12, pp. 5432–5441, 2015.

[12] Y. Song, H. Luo, B. Hui, and Z. Chang, "An improved image dehazing and enhancing method using dark channel prior," in *Proceedings of the 27th Chinese Control and Decision Conference, CCDC '15*, pp. 5840–5845, May 2015.

[13] L. Yang, H. Bian, J. Feng et al., "Optimized design of fast single image dehazing algorithm," in *Proceedings of the 14th International Computer Conference on Wavelet Active Media Technology and Information Processing (ICCWAMTIP)*, pp. 171–174, December 2017.

[14] C. Chen, J. Li, and S. Deng, "An adaptive image dehazing algorithm based on dark channel prior," *IEEE Control and Decision Conference*, pp. 7472–7477, 2017.

[15] L. Feng and Y. Canmei, "A fast method for single image dehazing using dark channel prior," in *Proceedings of the IEEE International Conference on Signal Processing, Communications and Computing*, pp. 483–486, 2014.

[16] Y. Li, Q. Fu, F. Ye, and H. Shouno, "Dark channel prior based blurred image restoration method using total variation and morphology," *Journal of Systems Engineering and Electronics*, vol. 26, no. 2, pp. 359–366, 2015.

[17] Y. Kumar and A. Gupta, "Single image dehazing using improved dark channel prior," in *Proceedings of the 2nd International Conference on Signal Processing and Integrated Networks*, pp. 564–569, Feburary 2015.

[18] Q. Zhu, J. Mai, and L. Shao, "A fast single image haze removal algorithm using color attenuation prior," *IEEE Transactions on Image Processing*, vol. 24, no. 11, pp. 3522–3533, 2015.

Hindawi
Journal of Control Science and Engineering
Volume 2018, Article ID 4541586, 15 pages
https://doi.org/10.1155/2018/4541586

Research Article

Event-Based Nonfragile $H\infty$ Filter Design for Networked Control Systems with Interval Time-Varying Delay

Zhongda Lu,[1,2] **Guangtao Ran**,[1] **Guoliang Zhang**,[1] **and Fengxia Xu**[1]

[1]*School of Computer and Control Engineering, Qiqihar University, Qiqihar 161006, China*
[2]*College of Computer Science and Technology, Harbin University of Science and Technology, Harbin 150080, China*

Correspondence should be addressed to Zhongda Lu; luzhongda@163.com

Received 26 February 2018; Accepted 7 May 2018; Published 12 June 2018

Academic Editor: Yun-Bo Zhao

This paper first investigates the event-triggered nonfragile H_∞ filter design for a class of nonlinear NCSs with interval time-varying delay. An event-triggered scheme is addressed to determine sampled data to be transmitted so that network communication resource can be saved significantly. The nonfragile filter design is assumed to include multiplicative gain variations according to the filter's implement. Under the event-triggered scheme, the filtering error system is modeled as a system with interval time-varying delay. By constructing a new Lyapunov-Krasovskii functional and employing Wirtinger inequality, a sufficient condition is derived, which guarantees that the filtering error system is asymptotically stable with the prescribed H_∞ performance. The nonfragile filter parameters are obtained by solving a set of linear matrix inequalities. Two numerical examples are given to show the usefulness and the effectiveness of the proposed method.

1. Introduction

During the past several years, Takagi-Sugeno (T-S) fuzzy model approach has got considerable attention due to its great merits on modeling for nonlinear networked control systems (NCSs) [1]. Many efforts have been proposed based on T-S fuzzy model for nonlinear systems [2–5]. On one hand, some state variables cannot be directly measured in practical system; therefore, the filtering problem attracted the attention of many researchers to estimate the unmeasured states. In comparison with traditional Kalman filtering, the H_∞ filter does not require statistical assumptions on the exogenous signals. Thus, the H_∞ filtering theory has got considerable development. The phenomenon of H_∞ filter design with time-varying delays, sensor faults, and packet dropouts was studied for nonlinear systems [6]. The authors in [7] proposed new results on a delay-derivative-dependent fuzzy H_∞ filter.

It should be mentioned that all the above works are based on accuracy assumptions that filter can be implemented exactly. However, inaccuracies or uncertainties do occur in filter implementation, which will reduce the performance of systems and lead the filter system to be fragile. Thus, a nonfragile filter must be designed to handle uncertainties and maintain the performance of systems. Up to now, a few results on the nonfragile filter have been proposed. Recently, the nonfragile H_∞ filtering problem for a class of discrete-time Takagi-Sugeno fuzzy systems with both randomly occurring gain variations and channel fading was investigated in [8]. Based on vertex theory and probabilistic algorithm, deterministic and randomised filtering algorithms are proposed in [9]. Aiming at the fuzzy stochastic systems, the authors in [10] proposed a nonfragile robust H_∞ filter design and a desired H_∞ performance level. It should be pointed out that the nonfragile H_∞ filtering problem has not been fully studied, which is one of motivations of this paper.

On the other hand, one topic that has been increasingly important is how to mitigate the network bandwidth while guaranteeing the stability and other desired performance of systems [11–15]. In traditional time-triggered control systems, the sample data will be transmitted into controller via network communication whatever the data are desired or not, which leads to network resource waste and low efficiency. Therefore, an event-triggered scheme was proposed to reduce data transmission and improve the effective utilities

of network resource. Recently, a novel discrete model for networked control systems was introduced in [16], which contained trigger parameters, dynamic quantization, and fault detection. In [17], event-triggering load frequency control was employed in multiarea power systems. It should be noted that although the works on event-triggered NCSs are rich, the limitations still remain and there still exist some problems to be handled [18–20]. To the best of our knowledge, there are no works that investigate how to use the event-triggered scheme in nonfragile H_∞ filtering systems, which is another motivation of this paper.

According to the above discussion, we first consider the problem of the event-triggered nonfragile H_∞ filter design for a class of nonlinear networked control systems. Our main contributions of this paper are summarized as follows:

(1) An event-triggered communication scheme is proposed to save network resource significantly. By considering the event-triggered scheme, filter's multiplicative gain variations, and interval time-varying delays, a novel filtering error system is established.

(2) Different from some existing works, the Wirtinger inequality is used to tackle the integral items of the derivative of Lyapunov-Krasovskii; a more relaxed H_∞ performance stability criterion is derived.

The rest of this paper is organized as follows. The problem formulation is given in Section 2; under the event-triggered scheme, the filtering error system is modeled as a system with interval time-varying delay. Stability analysis for filtering error system is presented in Section 3. The nonfragile H_∞ filter design method is first addressed in Section 4. Numerical examples are provided in Section 5 to demonstrate the effectiveness of the proposed method.

Notations. Throughout this paper, R^n denote the n-dimensional Euclidean space and $R^{n\times m}$ is the set of $n\times m$ real matrices. Superscript $(\bullet)^T$ stands for the matrix transposition, I represents the identity matrix, and diag$\{\cdots\}$ denotes the block-diagonal matrix. The notation $P > 0$ means that the matrix P is a real symmetric positive define matrix. In symmetric block matrices, "$*$" is used as ellipsis for terms induced by symmetry.

2. Problem Formulation

2.1. T-S Fuzzy System. Consider the following nonlinear system, which can be described by T-S fuzzy model with i plant rules:

Plant Rule i

$$\begin{aligned}&\text{IF } \varsigma_1(t) \text{ is } M_{i1}, \varsigma_2(t) \text{ is } M_{i2}, \ldots, \text{and } \varsigma_r(t) \text{ is } M_{ip},\\ &\quad \text{THEN}\end{aligned} \tag{1}$$

$$\begin{aligned}\dot{x}(t) &= A_i x(t) + B_i \omega(t)\\ z(t) &= C_i x(t)\\ y(t) &= D_i x(t),\end{aligned} \tag{2}$$

where M_{ij} are the fuzzy sets, $i = 1, 2, \ldots, r$, and $j = 1, 2, \ldots, p$ is the number of IF-THEN rules. $\varsigma_1(t), \varsigma_2(t) \cdots \varsigma_r(t)$ are the premise variables. $x(t) \in R^n$ and $y(t) \in R^m$ are the system state vector and the measured output, respectively. $\omega(t) \in R^q$ is the external disturbance and $\omega(t) \in l_2[0, \infty)$. $z(t) \in R^p$ is the signal vector to be estimated; A_i, B_i, C_i, and D_i are known parameter matrices with appropriate dimensions.

By using center-average defuzzifier, product inference, and a singleton fuzzifier, the T-S fuzzy system (2) can be rewritten as follows:

$$\begin{aligned}\dot{x}(t) &= \sum_{i=1}^{r} \mu_i(\varsigma(t)) \left[A_i x(t) + B_i \omega(t)\right]\\ z(t) &= \sum_{i=1}^{r} \mu_i(\varsigma(t)) C_i x(t)\\ y(t) &= \sum_{i=1}^{r} \mu_i(\varsigma(t)) D_i x(t)\end{aligned} \tag{3}$$

where $\varsigma = [\varsigma_1, \ldots, \varsigma_r]^T$; the fuzzy basis functions are given by

$$\begin{aligned}\mu_i(\varsigma(t)) &= \frac{h_i(\varsigma(t))}{\sum_{i=1}^{r} h_i(\varsigma(t))},\\ h_i(\varsigma(t)) &= \prod_{j=1}^{p} M_{ij}\left(\varsigma_j(t)\right).\end{aligned} \tag{4}$$

$M_{ij}(\varsigma_j(t))$ represents the grade of membership for $\varsigma_j(t)$ in M_{ij}; $0 \le \mu_i(\varsigma(t)) \le 1$, $(i = 1, 2, \ldots, r)$, $\sum_{i=1}^{r} \mu_i(\varsigma(t)) > 0$.

Therefore, we have

$$\sum_{i=1}^{r} \mu_i(\varsigma(t)) = 1, \quad \mu_i(\varsigma(t)) \ge 0 \ \ (i = 1, 2, \ldots, r). \tag{5}$$

2.2. Event-Triggered Scheme. In this section, we consider the communication networks with limited bandwidth; an event generator under the event-triggered scheme is employed. Inspired by the method in [12], the event-triggered scheme is adopted as follows:

$$t_{k+1}h = t_k h + \min_{j\ge 1} \left\{\Delta\left(t_k h + jh\right)\right\} \tag{6}$$

for $\Delta(t_k h + jh) = e_k(t_k h + jh)^T \psi e_k(t_k h + jh) \ge \lambda y(t_k h)^T \psi y(t_k h)$, where $e_k(t_k h + jh) = y(t_k h + jh) - y(t_k h)$ is the threshold error among the current sampling data and the last transmitted data. ψ and λ are the triggering parameters.

Remark 1. It should be mentioned that the current sampling data will be transmitted only when the condition proposed in (6) is satisfied. Therefore, in comparison with periodic transmission communication scheme, the event-triggered mechanism can reduce the transmission rate and utilize the limited bandwidth effectively.

2.3. Nonfragile Fuzzy Filter. In some previous results of filter design, the implicit assumption is made that there are no multiplicative gain uncertainties. However, in fact,

there inevitably exist filter parameter uncertainties in filter implementation. Therefore, in this section, we consider a full-order nonfragile fuzzy filter with gain variations as follows:

Plant Rule j

$$\begin{aligned} &\text{IF } \varsigma_1(t_k h) \text{ is } W_{i1}, \\ &\quad \varsigma_2(t_k h) \text{ is } W_{i2}, \ldots, \text{and } \varsigma_r(t_k h) \text{ is } W_{ip}, \text{THEN} \end{aligned} \tag{7}$$

$$\dot{x}_f(t) = \left(A_{fj} + \Delta A_{fj}(t)\right) x_f(t) + \left(B_{fj} + \Delta B_{fj}(t)\right) \cdot y_f(t) \tag{8}$$

$$z_f(t) = \left(C_{fj} + \Delta C_{fj}(t)\right) x_f(t),$$

where $x_f(t) \in R^n$ is the filter state vector, $y_f(t) \in R^n$ is the real input of the filter, $z_f(t)$ is the estimated signal vector of $z(t)$, and A_{fj}, B_{fj}, and C_{fj} are the filter parameters to be designed.

Similarly, we represent the nonfragile fuzzy filter as

$$\begin{aligned} \dot{x}_f(t) &= \sum_{j=1}^{r} \mu_j(\varsigma(t_k h)) \left[\left(A_{fj} + \Delta A_{fj}(t)\right) x_f(t) \right. \\ &\quad \left. + \left(B_{fj} + \Delta B_{fj}(t)\right) y_f(t)\right] \\ z_f(t) &= \sum_{j=1}^{r} \mu_j(\varsigma(t_k h)) \left(C_{fj} + \Delta C_{fj}(t)\right) x_f(t), \end{aligned} \tag{9}$$

where ΔA_{fj}, ΔB_{fj}, and ΔC_{fj} are the multiplicative gain uncertainties, which can be defined as

$$\begin{aligned} \Delta A_{fj}(t) &= A_{fj} M_{1j} K_A(t) N_{1j} \\ \Delta B_{fj}(t) &= B_{fj} M_{2j} K_B(t) N_{2j} \\ \Delta C_{fj}(t) &= C_{fj} M_{3j} K_C(t) N_{3j}, \end{aligned} \tag{10}$$

where M_{ij} and N_{ij} $(i = 1, 2, 3)$ are constant matrices with appropriate dimension. $K_A(t), K_B(t), K_C(t)$ are uncertain bounded matrices:

$$\begin{aligned} K_A^T(t) K_A(t) &\le I, \\ K_B^T(t) K_B(t) &\le I, \\ K_C^T(t) K_C(t) &\le I. \end{aligned} \tag{11}$$

Next, consider the effect of the logic ZOH; the last transmission data instant is maintained with the holding interval as follows:

$$y_z = y(t_k h), \quad t \in \left[t_k h + \tau_{t_k}, t_{k+1} h + \tau_{t_{k+1}}\right) \tag{12}$$

In order to facilitate analysis, the holding interval can be represented by the following subsets:

$$\left[t_k h + \tau_{t_k}, t_{k+1} h + \tau_{t_{k+1}}\right) = \bigcup_{l=0}^{m} \Omega_l, \tag{13}$$

where

$$\Omega_i = \left[t_k h + lh + \tau_{t_{k+i}}, t_k h + lh + h + \tau_{t_{k+i+1}}\right), \quad l = 0, 1, \ldots, m. \tag{14}$$

Then, we define the function of the interval time-varying delays as follows:

$$\tau(t) = \begin{cases} (1 - \Delta t_0)\, t & t \in \Omega_0 \\ (1 - \Delta t_1)\, t & t \in \Omega_1 \\ \vdots & \vdots \\ (1 - \Delta t_m)\, t & t \in \Omega_m, \end{cases} \tag{15}$$

where $\Delta t_m = \alpha t = t_k h + lh$, $0 \le \alpha < 1$. Therefore, we can easily derive

$$\begin{aligned} 0 < \tau_1 \le \tau(t) \le \tau_2, \\ \dot{\tau}(t) \le 1 - \alpha = d \le 1, \end{aligned} \tag{16}$$

where τ_1 and τ_2 are lower bound and upper bound of the delays, respectively. d is the bound of the delay variation.

To summarize, the inputs of the filter are described as

$$y_f(t) = y_z(t) = y(t - \tau(t)) - e_k(t - \tau(t)) \tag{17}$$

2.4. Fuzzy Filtering Error System. For simplicity, we let μ_i represent $\mu_i(\varsigma(t))$ and let μ_j represent $\mu_j(\varsigma(t_k h))$, and

$$\begin{aligned} \xi(t) &= \operatorname{col}\left\{x(t), x_f(t)\right\}, \\ e_f(t) &= z(t) - z_f(t). \end{aligned} \tag{18}$$

By combining (3), (9), and (17), we can obtain the following filtering error system:

$$\begin{aligned} \dot{\xi}(t) &= \sum_{i=1}^{r}\sum_{j=1}^{r} \left\{\overline{A}_{ij}(t)\, \xi(t) + \overline{B}_{ij1}(t)\, \xi(t - \tau(t)) \right. \\ &\quad \left. + \overline{B}_{ij2}(t)\, e_k(t - \tau(t)) + \overline{B}_{wij}(t)\, \omega(t)\right\} \\ e_f(t) &= \sum_{i=1}^{r}\sum_{j=1}^{r} \overline{C}_{ij}(t)\, \xi(t), \end{aligned} \tag{19}$$

where

$$\begin{aligned} \overline{A}_{ij}(t) &= \widetilde{A}_{ij} + \Delta\widehat{A}_{ij}(t), \\ \overline{B}_{ij1}(t) &= \widetilde{B}_{ij1} + \Delta\widehat{B}_{ij1}(t), \\ \overline{B}_{ij2}(t) &= \widetilde{B}_{ij2} + \Delta\widehat{B}_{ij2}(t), \\ \overline{C}_{ij}(t) &= \widetilde{C}_{ij} + \Delta\widehat{C}_{ij}(t), \\ \widetilde{A}_{ij} &= \sum_{i=1}^{r}\sum_{j=1}^{r} \mu_i \mu_j \begin{bmatrix} A_i & 0 \\ 0 & A_{fj} \end{bmatrix}, \end{aligned}$$

$$\Delta\widehat{A}_{ij}(t) = \sum_{i=1}^{r}\sum_{j=1}^{r}\mu_i\mu_j\begin{bmatrix}0 & 0\\ 0 & \Delta A_{fj}(t)\end{bmatrix},$$

$$\widetilde{B}_{ij1} = \sum_{i=1}^{r}\sum_{j=1}^{r}\mu_i\mu_j\begin{bmatrix}0 & 0\\ 0 & B_{fj}D_i\end{bmatrix},$$

$$\Delta\widehat{B}_{ij1} = \sum_{i=1}^{r}\sum_{j=1}^{r}\mu_i\mu_j\begin{bmatrix}0 & 0\\ 0 & \Delta B_{fj}(t)D_i\end{bmatrix},$$

$$\widetilde{B}_{ij2} = \sum_{i=1}^{r}\sum_{j=1}^{r}\mu_i\mu_j\begin{bmatrix}0\\ -B_{fj}\end{bmatrix},$$

$$\Delta\widehat{B}_{ij2} = \sum_{i=1}^{r}\sum_{j=1}^{r}\mu_i\mu_j\begin{bmatrix}0\\ -\Delta B_{fj}(t)\end{bmatrix},$$

$$\widetilde{C}_{ij} = \sum_{i=1}^{r}\sum_{j=1}^{r}\mu_i\mu_j\begin{bmatrix}C_i & -C_{fj}\end{bmatrix},$$

$$\Delta\widehat{C}_{ij} = \sum_{i=1}^{r}\sum_{j=1}^{r}\mu_i\mu_j\begin{bmatrix}0 & -\Delta C_{fj}(t)\end{bmatrix},$$

$$\widetilde{B}_{wij} = \sum_{i=1}^{r}\sum_{j=1}^{r}\mu_i\mu_j\begin{bmatrix}B_i\\ 0\end{bmatrix}. \tag{20}$$

Before the end of this section, the following definitions and lemmas are needed for the fuzzy filtering error system.

Definition 2. The fuzzy filtering error system is asymptotically stable with an H_∞ performance, if the following holds:

(1) The filtering error system (19) is asymptotically stable when $\omega(t) = 0$.

(2) The filtering error system (19) has a prescribed $H\infty$ performance γ; under zero initial condition,

$$\int_0^L \|e(t)\|^2\,dt \le \gamma^2\int_0^L \|\omega(t)\|^2\,dt \tag{21}$$

is satisfied for any nonzero $\omega(t) \in L_2[0,\infty)$.

Lemma 3 (see [21]). *Let X, Y, and G be real matrices with appropriate dimensions and $G_i^T(t)G_i(t) \le I$. Then, for any constant $\varepsilon > 0$, one has*

$$XG(t)Y + Y^TG(t)X^T \le \varepsilon XX^T + \varepsilon^{-1}Y^TY \tag{22}$$

Lemma 4 (see [22]). *For any vectors $x, y \in R^n$ and any scalar $\varepsilon > 0$, matrices D, F, and E are real matrices of appropriate dimensions with $F^T(t)F(t) \le I$; then the following inequalities hold:*

$$2xDF(t)Ey \le \varepsilon x^TDD^Tx + \varepsilon^{-1}y^TEE^Ty \tag{23}$$

Lemma 5 (see [23]). *Let V, H, E, Q, and F be real matrices of appropriate dimensions such that $Q > 0$ and $F^TF \le I$. Then, for any scalar $\varepsilon > 0$ such that $Q - \varepsilon DD^T > 0$, one has*

$$\begin{aligned}&(V + HFE)^TQ(V + HFE)\\ &\quad\le V^T\left(Q^{-1} - \varepsilon HH^T\right)V + \varepsilon^{-1}E^TE\end{aligned} \tag{24}$$

Lemma 6 (see [24]). *Let $P > 0$ and let A_i and A_l be any real matrices of appropriate dimensions. Then*

$$A_i^TPA_l + A_l^TPA_i \le A_i^TPA_i + A_l^TPA_l \tag{25}$$

Lemma 7 (Seuret and Gouaisbaut [25]). *For a given symmetric and positive matrix $R > 0$ of appropriate dimensions and different signal x in $[a,b] \to R^n$, the following inequality holds:*

$$\begin{aligned}&-\int_a^b \dot{\xi}^T(s)R\dot{\xi}(s)\,ds\\ &\quad\le -\frac{1}{b-a}\begin{bmatrix}\xi(b)\\ \xi(a)\\ v\end{bmatrix}^T\begin{bmatrix}a_1R & a_2R & a_3R\\ * & a_1R & a_3R\\ * & * & a_4R\end{bmatrix}\begin{bmatrix}\xi(b)\\ \xi(a)\\ v\end{bmatrix},\end{aligned} \tag{26}$$

where

$$\begin{aligned}v &= \frac{1}{b-a}\int_a^b \xi(s)\,ds\\ a_1 &= \frac{\pi^2}{4} + 1,\\ a_2 &= \frac{\pi^2}{4} - 1,\\ a_3 &= -\frac{\pi^2}{2},\\ a_4 &= \pi^2.\end{aligned} \tag{27}$$

3. Stability Analysis

In this section, we first present the H_∞ performance analysis for the filtering error system (19) under event-triggered scheme. The following results are established to guarantee that the filtering error system (19) is asymptotically stable.

Theorem 8. *For given positive parameters τ_1, τ_2, $d \le 1$, $\gamma > 0$, $\varepsilon_i > 0$, $(i = 1,2,\ldots,10)$, and $0 < \lambda < 1$, the filtering error system in (19) is asymptotically stable with H_∞ performance γ under the event-triggered scheme (16), if there exist matrices $Q_i > 0$, $(i = 1,2,3)$, $\psi > 0$, $R_i > 0$ $(i = 1,2)$, $a_i > 0$ $(i = 1,2,3,4)$, and $P > 0$ and A_{fj}, B_{fj}, and C_{fj} with appropriate dimensions such that the following matrix inequalities hold:*

$$\begin{bmatrix}I & \widetilde{M}_3\\ * & \varepsilon_{10}^{-1}\end{bmatrix} > 0 \tag{28}$$

$$\begin{bmatrix}R_1^{-1} & \widetilde{M}_1\\ * & \varepsilon_4^{-1}\end{bmatrix} > 0,$$

$$\begin{bmatrix}R_2^{-1} & \widetilde{M}_1\\ * & \varepsilon_7^{-1}\end{bmatrix} > 0 \tag{29}$$

$$\begin{bmatrix} R_1^{-1} & \widetilde{M}_{21} \\ * & \varepsilon_5^{-1} \end{bmatrix} > 0,$$
$$\begin{bmatrix} R_2^{-1} & \widetilde{M}_{21} \\ * & \varepsilon_8^{-1} \end{bmatrix} > 0 \tag{30}$$
$$\begin{bmatrix} R_1^{-1} & \widetilde{M}_{22} \\ * & \varepsilon_6^{-1} \end{bmatrix} > 0,$$
$$\begin{bmatrix} R_2^{-1} & \widetilde{M}_{22} \\ * & \varepsilon_9^{-1} \end{bmatrix} > 0 \tag{31}$$
$$\Pi = \begin{bmatrix} \Lambda_{11} & \Lambda_{12} \\ * & \Lambda_{22} \end{bmatrix} < 0 \tag{32}$$

for

$$\Lambda_{11} = \begin{bmatrix} \Pi_{11} & \Pi_{12} & \Pi_{13} & 0 & \Pi_{15} \\ * & \Pi_{22} & \Pi_{23} & 0 & \Pi_{25} \\ * & * & \Pi_{33} & \Pi_{34} & 0 \\ * & * & * & \Pi_{44} & 0 \\ * & * & * & * & \Pi_{55} \end{bmatrix},$$
$$\Lambda_{12} = \begin{bmatrix} 0 & 0 & \Pi_{18} & \Pi_{19} \\ \Pi_{26} & 0 & 0 & 0 \\ \Pi_{36} & \Pi_{37} & 0 & 0 \\ 0 & \Pi_{47} & 0 & 0 \\ 0 & 0 & 0 & 0 \end{bmatrix}, \tag{33}$$
$$\Lambda_{22} = \begin{bmatrix} \Pi_{66} & 0 & 0 & 0 \\ * & \Pi_{77} & 0 & 0 \\ * & * & \Pi_{88} & 0 \\ * & * & * & \Pi_{99} \end{bmatrix},$$

where

$$\begin{aligned} \Pi_{11} &= P\widetilde{A}_{ij} + \widetilde{A}_{ij}^T P + Q_1 + Q_2 + Q_3 - a_1 R_1 \\ &\quad + \varepsilon_1 P\widetilde{M}_1\widetilde{M}_1^T P + \varepsilon_1^{-1}\widetilde{N}_1^T\widetilde{N}_1 \\ &\quad + \varepsilon_2 P\widetilde{M}_{21}\widetilde{M}_{21}^T P + \varepsilon_3 P\widetilde{M}_{22}\widetilde{M}_{22}^T P \\ &\quad + \varepsilon_{10}^{-1}\widetilde{N}_3^T\widetilde{N}_3 \\ &\quad + \alpha_1^2\widetilde{A}_{ij}^T\left[R_1^{-1} - \varepsilon_4\widetilde{M}_1\widetilde{M}_1^T\right]^{-1}\widetilde{A}_{ij} \\ &\quad + \alpha_1^2\varepsilon_4^{-1}\widetilde{N}_1^T\widetilde{N}_1 \\ &\quad + \alpha_2^2\widetilde{A}_{ij}^T\left[R_2^{-1} - \varepsilon_7\widetilde{M}_1\widetilde{M}_1^T\right]^{-1}\widetilde{A}_{ij} \\ &\quad + \alpha_2^2\varepsilon_7^{-1}\widetilde{N}_1^T\widetilde{N}_1 + \widetilde{C}_{ij}^T\left[I - \varepsilon_{10}\widetilde{M}_3\widetilde{M}_3^T\right]^{-1}\widetilde{C}_{ij}, \\ \Pi_{12} &= -a_2 R_1, \\ \Pi_{13} &= P\widetilde{B}_{ij1}, \\ \Pi_{15} &= -a_3 R_1, \\ \Pi_{18} &= P\widetilde{B}_{ij2}, \\ \Pi_{19} &= P\widetilde{B}_{wij}, \\ \Pi_{22} &= -Q_2 - a_1 R_1 - a_1 R_2, \\ \Pi_{23} &= -a_2 R_2, \\ \Pi_{25} &= -a_3 R_1, \\ \Pi_{26} &= -a_3 R_2, \\ \Pi_{33} &= -(1-d)Q_1 + \varepsilon_2^{-1}\widetilde{N}_{21}^T\widetilde{N}_{21} + \lambda D_i^T\psi D_i - 2a_1 R_2 \\ &\quad + \alpha_1^2\varepsilon_5^{-1}\widetilde{N}_{21}^T\widetilde{N}_{21} + \alpha_2^2\varepsilon_8^{-1}\widetilde{N}_{21}^T\widetilde{N}_{21} \\ &\quad + \alpha_1^2 B_{ij1}^T\left[R_1^{-1} - \varepsilon_5\widetilde{M}_{21}\widetilde{M}_{21}^T\right]^{-1}B_{ij1} \\ &\quad + \alpha_2^2 B_{ij1}^T\left[R_2^{-1} - \varepsilon_8\widetilde{M}_{21}\widetilde{M}_{21}^T\right]^{-1}B_{ij1}, \\ \Pi_{34} &= -a_2 R_2, \\ \Pi_{36} &= -a_3 R_2, \\ \Pi_{37} &= -a_3 R_2, \\ \Pi_{44} &= -Q_3 - a_1 R_2, \\ \Pi_{47} &= -a_3 R_2, \\ \Pi_{55} &= -a_4 R_1, \\ \Pi_{66} &= -a_4 R_2, \\ \Pi_{77} &= -a_4 R_2, \\ \Pi_{88} &= \varepsilon_3^{-1}\widetilde{N}_{22}^T\widetilde{N}_{22} + (\lambda - 1)\psi + \alpha_1^2\varepsilon_6^{-1}\widetilde{N}_{22}^T\widetilde{N}_{22} \\ &\quad + \alpha_2^2\varepsilon_9^{-1}\widetilde{N}_{22}^T\widetilde{N}_{22} \\ &\quad + \alpha_1^2 B_{ij2}^T\left[R_1^{-1} - \varepsilon_6\widetilde{M}_{22}\widetilde{M}_{22}^T\right]^{-1}B_{ij2} \\ &\quad + \alpha_2^2 B_{ij2}^T\left[R_2^{-1} - \varepsilon_9\widetilde{M}_{22}\widetilde{M}_{22}^T\right]^{-1}B_{ij2}, \\ \Pi_{99} &= \alpha_1^2\widetilde{B}_{wij}^T R_1\widetilde{B}_{wij} + \alpha_2^2\widetilde{B}_{wij}^T R_2\widetilde{B}_{wij} - \gamma^2 I_n, \\ \widetilde{M}_1 &= \begin{bmatrix} 0 \\ A_{fj}M_{1j} \end{bmatrix}, \\ \widetilde{M}_{21} &= \begin{bmatrix} 0 \\ B_{fj}M_{2j} \end{bmatrix}, \\ \widetilde{M}_{22} &= \begin{bmatrix} 0 \\ -B_{fj}M_{2j} \end{bmatrix}, \\ \widetilde{M}_3 &= C_{fj}M_{3j}, \end{aligned}$$

$$\begin{aligned}
\widetilde{N}_1 &= \begin{bmatrix} 0 & N_{1j} \end{bmatrix}, \\
\widetilde{N}_{21} &= \begin{bmatrix} 0 & N_{2j} D_i \end{bmatrix}, \\
\widetilde{N}_{22} &= \begin{bmatrix} 0 & N_{2j} \end{bmatrix}, \\
\widetilde{N}_3 &= \begin{bmatrix} 0 & N_{3j} \end{bmatrix}, \\
a_1 &= \frac{\pi^2}{4} + 1, \\
a_2 &= \frac{\pi^2}{4} - 1, \\
a_3 &= -\frac{\pi^2}{2}, \\
a_4 &= \pi^2, \\
\alpha_1 &= 2\tau_1, \\
\alpha_2 &= 2\left(\tau_2 - \tau_1\right).
\end{aligned} \tag{34}$$

Proof. We construct a candidate of Lyapunov-Krasovskii function as follows:

$$V\left(t, \xi_t\right) = \sum_{j=1}^{3} V_j\left(t, \xi_t\right), \tag{35}$$

where

$$\begin{aligned}
V_1\left(t, \xi_t\right) &= \xi^T(t) P \xi(t), \\
V_2\left(t, \xi_t\right) &= \int_{t-\tau(t)}^{t} \xi^T(s) Q_1 \xi(s)\, ds \\
&\quad + \int_{t-\tau_1}^{t} \xi^T(s) Q_2 \xi(s)\, ds \\
&\quad + \int_{t-\tau_2}^{t} \xi^T(s) Q_3 \xi(s)\, ds, \\
V_3\left(t, \xi_t\right) &= \tau_1 \int_{-\tau_1}^{0} \int_{t+\theta}^{t} \dot{\xi}^T(s) R_1 \dot{\xi}(s)\, ds\, d\theta \\
&\quad + \left(\tau_2 - \tau_1\right) \int_{-\tau_2}^{-\tau_1} \int_{t+\theta}^{t} \dot{\xi}^T(s) R_2 \dot{\xi}(s)\, ds\, d\theta.
\end{aligned} \tag{36}$$

Taking the time derivation of $V(t)$ for t, we have

$$\dot{V}\left(t, \xi_t\right) = \dot{V}_1\left(t, \xi_t\right) + \dot{V}_2\left(t, \xi_t\right) + \dot{V}_3\left(t, \xi_t\right), \tag{37}$$

where

$$\begin{aligned}
\dot{V}_1\left(t, \xi_t\right) &= 2\xi^T(t) P \overline{A}_{ij}(t) \xi(t) \\
&\quad + 2\xi^T(t) P \overline{B}_{ij1}(t) \xi\left(t - \tau(t)\right) \\
&\quad + 2\xi^T(t) P \overline{B}_{ij2}(t) e_k\left(t - \tau(t)\right) \\
&\quad + 2\xi^T(t) P \overline{B}_{wij}(t) \omega(t) \\
&= 2\xi^T(t) P \widetilde{A}_{ij} \xi(t) + 2\xi^T(t) P \Delta \widehat{A}_{ij}(t) \xi(t) \\
&\quad + 2\xi^T(t) P \widetilde{B}_{ij1} \xi\left(t - \tau(t)\right) \\
&\quad + 2\xi^T(t) P \Delta \widehat{B}_{ij1}(t) \xi\left(t - \tau(t)\right) \\
&\quad + 2\xi^T(t) P \widetilde{B}_{ij2} e_k\left(t - \tau(t)\right) \\
&\quad + 2\xi^T(t) P \Delta \widehat{B}_{ij2}(t) e_k\left(t - \tau(t)\right) \\
&\quad + 2\xi^T(t) P \overline{B}_{wij}(t) \omega(t)
\end{aligned} \tag{38}$$

$$\begin{aligned}
\dot{V}_2\left(t, \xi_t\right) &= \xi^T(t)\left(Q_1 + Q_2 + Q_3\right)\xi(t) \\
&\quad - \left(1 - \dot{\tau}(t)\right)\xi^T\left(t - \tau(t)\right) Q_1 \xi\left(t - \tau(t)\right) \\
&\quad - \xi^T\left(t - \tau_1\right) Q_2 \xi\left(t - \tau_1\right) \\
&\quad - \xi^T\left(t - \tau_2\right) Q_3 \xi\left(t - \tau_2\right) \\
&\le \xi^T(t)\left(Q_1 + Q_2 + Q_3\right)\xi(t) \\
&\quad - (1 - d)\,\xi^T\left(t - \tau(t)\right) Q_1 \xi\left(t - \tau(t)\right) \\
&\quad - \xi^T\left(t - \tau_1\right) Q_2 \xi\left(t - \tau_1\right) \\
&\quad - \xi^T\left(t - \tau_2\right) Q_3 \xi\left(t - \tau_2\right)
\end{aligned} \tag{39}$$

$$\begin{aligned}
\dot{V}_3\left(t, \xi_t\right) &= \tau_1^2 \dot{\xi}^T(t) R_1 \dot{\xi}(t) + \left(\tau_2 - \tau_1\right)^2 \dot{\xi}^T(t) R_2 \dot{\xi}(t) \\
&\quad - \tau_1 \int_{t-\tau_1}^{t} \dot{\xi}^T(s) R_1 \dot{\xi}(s)\, ds \\
&\quad - \left(\tau_2 - \tau_1\right) \int_{t-\tau_2}^{t-\tau_1} \dot{\xi}^T(s) R_2 \dot{\xi}(s)\, ds
\end{aligned} \tag{40}$$

By Lemma 3, for $\forall \varepsilon_1 > 0$, we can obtain

$$\begin{aligned}
2\xi^T(t) P \Delta \widehat{A}_{ij}(t) \xi(t) &= 2\xi^T(t) P \left[\widetilde{M}_1 K_A(t) \widetilde{N}_1\right] \xi(t) \\
&\le \xi^T(t)\left(\varepsilon_1 P \widetilde{M}_1 \widetilde{M}_1^T P + \varepsilon_1^{-1} P \widetilde{N}_1^T \widetilde{N}_1 P\right) \xi(t)
\end{aligned} \tag{41}$$

By Lemma 4, if there exist $\forall \varepsilon_2 > 0$ and $\forall \varepsilon_3 > 0$, we have

$$\begin{aligned}
&2\xi^T(t) P \Delta \widehat{B}_{ij1}(t) \xi\left(t - \tau(t)\right) \\
&\quad = 2\xi^T(t) P \left[\widetilde{M}_{21} K_B(t) \widetilde{N}_{21}\right] \xi\left(t - \tau(t)\right) \\
&\quad \le \xi^T(t) \left[\varepsilon_2 P \widetilde{M}_{21} \widetilde{M}_{21}^T P\right] \xi(t) \\
&\qquad + \xi^T\left(t - \tau(t)\right) \left[\varepsilon_2^{-1} P \widetilde{N}_{21}^T \widetilde{N}_{21} P\right] \xi\left(t - \tau(t)\right)
\end{aligned} \tag{42}$$

$$\begin{aligned}
&2\xi^T(t) P \Delta \widehat{B}_{ij2}(t) e_k\left(t - \tau(t)\right) \\
&\quad = 2\xi^T(t) P \left[\widetilde{M}_{22} K_B(t) \widetilde{N}_{22}\right] e_k\left(t - \tau(t)\right) \\
&\quad \le \xi^T(t) \left[\varepsilon_3 P \widetilde{M}_{22} \widetilde{M}_{22}^T P\right] \xi(t) \\
&\qquad + e_k^T\left(t - \tau(t)\right) \left[\varepsilon_3^{-1} P \widetilde{N}_{22}^T \widetilde{N}_{22} P\right] e_k\left(t - \tau(t)\right)
\end{aligned} \tag{43}$$

From (41) to (43), we derive

$$\begin{aligned}
&2\xi^T(t)P\Delta\widehat{A}_{ij}(t)\xi(t)+2\xi^T(t)P\Delta\widehat{B}_{ij1}(t)\xi(t-\tau(t))\\
&\quad+2\xi^T(t)P\Delta\widehat{B}_{ij2}(t)e_k(t-\tau(t))\le\xi^T(t)\\
&\quad\cdot\left\{\varepsilon_1P\widetilde{M}_1\widetilde{M}_1^TP+\varepsilon_2P\widetilde{M}_{21}\widetilde{M}_{21}^TP+\varepsilon_1^{-1}P\widetilde{N}_1^T\widetilde{N}_1P\right.\\
&\quad\left.+\varepsilon_3P\widetilde{M}_{22}\widetilde{M}_{22}^TP\right\}\xi(t)+e_k^T(t-\tau(t))\\
&\quad\cdot\left[\varepsilon_3^{-1}P\widetilde{N}_{22}^T\widetilde{N}_{22}P\right]e_k(t-\tau(t))+\xi^T(t-\tau(t))\\
&\quad\cdot\left[\varepsilon_2^{-1}P\widetilde{N}_{21}^T\widetilde{N}_{21}P\right]\xi(t-\tau(t))
\end{aligned}\tag{44}$$

By using Lemmas 5 and 6, if there exists $\forall\varepsilon_i>0(i=4,5,6,7,8)$, we derive

$$\begin{aligned}
&\tau_1^2\dot{\xi}^T(t)R_1\dot{\xi}(t)=\tau_1{}^2\left[\overline{A}_{ij}(t)\xi(t)\right.\\
&\quad+\overline{B}_{ij1}(t)\xi(t-\tau(t))+\overline{B}_{ij2}(t)e_k(t-\tau(t))\\
&\quad\left.+\overline{B}_{wij}(t)w(t)\right]^TR_1\left[\overline{A}_{ij}(t)\xi(t)\right.\\
&\quad\left.+\overline{B}_{ij1}(t)\xi(t-\tau(t))+\overline{B}_{ij2}(t)e_k(t-\tau(t))\right.\\
&\quad\left.+\overline{B}_{wij}(t)w(t)\right]\le4\tau_1^2\xi^T(t)\\
&\quad\cdot\left\{\widetilde{A}_{ij}^T\left[R_1^{-1}-\varepsilon_4\widetilde{M}_1\widetilde{M}_1^T\right]^{-1}\widetilde{A}_{ij}+\varepsilon_4^{-1}\widetilde{N}_1^T\widetilde{N}_1\right\}\xi(t)\\
&\quad+4\tau_1^2\xi^T(t-\tau(t))\left\{\widetilde{B}_{ij1}^T\left[R_1^{-1}-\varepsilon_5\widetilde{M}_{21}\widetilde{M}_{21}^T\right]^{-1}\widetilde{B}_{ij1}\right.\\
&\quad\left.+\varepsilon_5^{-1}\widetilde{N}_{21}^T\widetilde{N}_{21}\right\}\xi(t-\tau(t))+4\tau_1^2e_k^T(t-\tau(t))\\
&\quad\cdot\left\{\widetilde{B}_{ij2}^T\left[R_1^{-1}-\varepsilon_6\widetilde{M}_{22}\widetilde{M}_{22}^T\right]^{-1}\widetilde{B}_{ij2}+\varepsilon_6^{-1}\widetilde{N}_{22}^T\widetilde{N}_{22}\right\}\\
&\quad\cdot e_k(t-\tau(t))+4\tau_1^2\omega^T(t)\overline{B}_{wij}^T(t)R_1\overline{B}_{wij}(t)\omega(t)
\end{aligned}\tag{45}$$

$$\begin{aligned}
&(\tau_2-\tau_1)^2\dot{\xi}^T(t)R_2\dot{\xi}(t)=(\tau_2-\tau_1)^2\left[\overline{A}_{ij}(t)\xi(t)\right.\\
&\quad+\overline{B}_{ij1}(t)\xi(t-\tau(t))+\overline{B}_{ij2}(t)e_k(t-\tau(t))\\
&\quad\left.+\overline{B}_{wij}(t)w(t)\right]^TR_1\left[\overline{A}_{ij}(t)\xi(t)\right.\\
&\quad\left.+\overline{B}_{ij1}(t)\xi(t-\tau(t))+\overline{B}_{ij2}(t)e_k(t-\tau(t))\right.\\
&\quad\left.+\overline{B}_{wij}(t)w(t)\right]\le4(\tau_2-\tau_1)^2\xi^T(t)\\
&\quad\cdot\left\{\widetilde{A}_{ij}^T\left[R_2^{-1}-\varepsilon_7\widetilde{M}_1\widetilde{M}_1^T\right]^{-1}\widetilde{A}_{ij}+\varepsilon_7^{-1}\widetilde{N}_1^T\widetilde{N}_1\right\}\xi(t)\\
&\quad+4(\tau_2-\tau_1)^2\xi^T(t-\tau(t))\\
&\quad\cdot\left\{\widetilde{B}_{ij1}^T\left[R_2^{-1}-\varepsilon_8\widetilde{M}_{21}\widetilde{M}_{21}^T\right]^{-1}\widetilde{B}_{ij1}+\varepsilon_8^{-1}\widetilde{N}_{21}^T\widetilde{N}_{21}\right\}\xi(t\\
&\quad-\tau(t))+4(\tau_2-\tau_1)^2e_k^T(t-\tau(t))\\
&\quad\cdot\left\{\widetilde{B}_{ij2}^T\left[R_2^{-1}-\varepsilon_9\widetilde{M}_{22}\widetilde{M}_{22}^T\right]^{-1}\widetilde{B}_{ij2}+\varepsilon_9^{-1}\widetilde{N}_{22}^T\widetilde{N}_{22}\right\}\\
&\quad\cdot e_k(t-\tau(t))+4(\tau_2-\tau_1)^2\omega^T(t)\overline{B}_{wij}^T(t)\\
&\quad\cdot R_2\overline{B}_{wij}(t)\omega(t)
\end{aligned}\tag{46}$$

By applying Lemma 5, if there exists $\forall\varepsilon_{10}>0$, we can obtain

$$\begin{aligned}
e_f^T(t)e_f(t)&=\xi^T(t)\overline{C}_{ij}^T(t)\overline{C}_{ij}\xi(t)\\
&=\xi^T(t)\left(\widetilde{C}_{ij}+\Delta\widehat{C}_{ij}(t)\right)^T\left(\widetilde{C}_{ij}+\Delta\widehat{C}_{ij}(t)\right)\xi(t)\\
&\le\xi^T(t)\widetilde{C}_{ij}^T\left(I-\varepsilon_{10}\widetilde{M}_3\widetilde{M}_3^T\right)^{-1}\widetilde{C}_{ij}\xi^T(t)\\
&\quad+\varepsilon_{10}^{-1}\xi^T(t)\widetilde{N}_3^T\widetilde{N}_3\xi(t)
\end{aligned}\tag{47}$$

Furthermore, we use Lemma 7 to deal with the integral items in (40); it follows that

$$\begin{aligned}
&-\tau_1\int_{t-\tau_1}^t\dot{\xi}^T(s)R_1\dot{\xi}(s)ds\le\begin{bmatrix}\xi(t)\\ \xi(t-\tau_1)\\ \upsilon_1\end{bmatrix}^T\\
&\quad\cdot\begin{bmatrix}a_1R_1 & a_2R_1 & a_3R_1\\ * & a_1R_1 & a_3R_1\\ * & * & a_4R_1\end{bmatrix}\begin{bmatrix}\xi(t)\\ \xi(t-\tau_1)\\ \upsilon_1\end{bmatrix}\\
&-(\tau_2-\tau_1)\int_{t-\tau_2}^{t-\tau_1}\dot{\xi}^T(s)R_2\dot{\xi}(s)ds=-(\tau_2-\tau_1)\\
&\quad\cdot\int_{t-\tau(t)}^{t-\tau_1}\dot{\xi}^T(s)R_2\dot{\xi}(s)ds-(\tau_2-\tau_1)\\
&\quad\cdot\int_{t-\tau_2}^{t-\tau(t)}\dot{\xi}^T(s)R_2\dot{\xi}(s)ds\le-\begin{bmatrix}\xi(t-\tau_1)\\ \xi(t-\tau(t))\\ \upsilon_2\end{bmatrix}^T\\
&\quad\cdot\begin{bmatrix}a_1R_2 & a_2R_2 & a_3R_2\\ * & a_1R_2 & a_3R_2\\ * & * & a_4R_2\end{bmatrix}\begin{bmatrix}\xi(t-\tau_1)\\ \xi(t-\tau(t))\\ \upsilon_2\end{bmatrix}\\
&\quad-\begin{bmatrix}\xi(t-\tau(t))\\ \xi(t-\tau_2)\\ \upsilon_3\end{bmatrix}^T\\
&\quad\cdot\begin{bmatrix}a_1R_2 & a_2R_2 & a_3R_2\\ * & a_1R_2 & a_3R_2\\ * & * & a_4R_2\end{bmatrix}\begin{bmatrix}\xi(t-\tau(t))\\ \xi(t-\tau_2)\\ \upsilon_3\end{bmatrix},
\end{aligned}\tag{48}$$

$$\begin{aligned}
&-\tau_1\int_{t-\tau_1}^t\dot{\xi}^T(s)R_1\dot{\xi}(s)ds\le\begin{bmatrix}\xi(t)\\ \xi(t-\tau_1)\\ \upsilon_1\end{bmatrix}^T\\
&\quad\cdot\begin{bmatrix}a_1R_1 & a_2R_1 & a_3R_1\\ * & a_1R_1 & a_3R_1\\ * & * & a_4R_1\end{bmatrix}\begin{bmatrix}\xi(t)\\ \xi(t-\tau_1)\\ \upsilon_1\end{bmatrix}\\
&-(\tau_2-\tau_1)\int_{t-\tau_2}^{t-\tau_1}\dot{\xi}^T(s)R_2\dot{\xi}(s)ds=-(\tau_2-\tau_1)\\
&\quad\cdot\int_{t-\tau(t)}^{t-\tau_1}\dot{\xi}^T(s)R_2\dot{\xi}(s)ds-(\tau_2-\tau_1)\\
&\quad\cdot\int_{t-\tau_2}^{t-\tau(t)}\dot{\xi}^T(s)R_2\dot{\xi}(s)ds\le-\begin{bmatrix}\xi(t-\tau_1)\\ \xi(t-\tau(t))\\ \upsilon_2\end{bmatrix}^T\\
&\quad\cdot\begin{bmatrix}a_1R_2 & a_2R_2 & a_3R_2\\ * & a_1R_2 & a_3R_2\\ * & * & a_4R_2\end{bmatrix}\begin{bmatrix}\xi(t-\tau_1)\\ \xi(t-\tau(t))\\ \upsilon_2\end{bmatrix}\\
&\quad-\begin{bmatrix}\xi(t-\tau(t))\\ \xi(t-\tau_2)\\ \upsilon_3\end{bmatrix}^T\\
&\quad\cdot\begin{bmatrix}a_1R_2 & a_2R_2 & a_3R_2\\ * & a_1R_2 & a_3R_2\\ * & * & a_4R_2\end{bmatrix}\begin{bmatrix}\xi(t-\tau(t))\\ \xi(t-\tau_2)\\ \upsilon_3\end{bmatrix},
\end{aligned}\tag{49}$$

where

$$\begin{aligned}
\upsilon_1&=\frac{1}{\tau_1}\int_{t-\tau_1}^t\xi(s)ds,\\
\upsilon_2&=\frac{1}{\tau(t)-\tau_1}\int_{t-\tau(t)}^{t-\tau_1}\xi(s)ds,\\
\upsilon_3&=\frac{1}{\tau_2-\tau(t)}\int_{t-\tau_2}^{t-\tau(t)}\xi(s)ds.
\end{aligned}\tag{50}$$

By combining (44) to (49), we obtain

$$\dot{V}(t,\xi_t)+e_f^T(t)e_f(t)-\gamma^2\omega^T(t)\omega(t)\le\widehat{\eta}^T(t)\Pi\widehat{\eta}(t)\tag{51}$$

where

$$\widehat{\eta}(t) = \operatorname{col}\{\xi(t), \xi(t-\tau_1), \xi(t-\tau(t)), \xi(t-\tau_2), \upsilon_1, \upsilon_2, \upsilon_3, e_k(t-\tau(t)), \omega(t)\}. \tag{52}$$

Then, from (28) to (32), under the zero initial condition, we integrate the right and left sides of (51) from 0 to L for all $L > 0$; we can easily derive

$$\int_0^L e_f^T(t)\, e_f(t)\, dt \le \gamma^2 \int_0^L \omega^T(t)\, \omega(t)\, dt \tag{53}$$

This completes the proof. □

4. Fuzzy $H\infty$ Filter Design

It is worth mentioning that the condition in (32) cannot be directly used for filter design. Therefore, in this section, we provide a sufficient condition for the fuzzy H_∞ filter design, and a suitable filter parameter matrix is obtained.

Theorem 9. *For given positive parameters τ_1, τ_2, $d \le 1$, $\gamma > 0$, $\delta > 0$, $\varepsilon_i > 0$, $(i = 1, 2, \ldots, 10)$, and $0 < \lambda < 1$, if there exist symmetric positive definite matrices $P > 0$, $Q_1 > 0$, $Q_2 > 0$, $Q_3 > 0$, $\psi > 0$, $R_1 > 0$, and $R_2 > 0$ and $\widetilde{A}_{fj}$, $\widetilde{B}_{fj}$, and $\widetilde{C}_{fj}$ with appropriate dimensions, the following hold:*

$$\begin{bmatrix} I & \widetilde{M}_3 \\ * & \varepsilon_{10}^{-1} \end{bmatrix} > 0 \tag{54}$$

$$\begin{bmatrix} R_1^{-1} & \widetilde{M}_1 \\ * & \varepsilon_4^{-1} \end{bmatrix} > 0, \qquad \begin{bmatrix} R_2^{-1} & \widetilde{M}_1 \\ * & \varepsilon_7^{-1} \end{bmatrix} > 0 \tag{55}$$

$$\begin{bmatrix} R_1^{-1} & \widetilde{M}_{21} \\ * & \varepsilon_5^{-1} \end{bmatrix} > 0, \qquad \begin{bmatrix} R_2^{-1} & \widetilde{M}_{21} \\ * & \varepsilon_8^{-1} \end{bmatrix} > 0 \tag{56}$$

$$\begin{bmatrix} R_1^{-1} & \widetilde{M}_{22} \\ * & \varepsilon_6^{-1} \end{bmatrix} > 0, \qquad \begin{bmatrix} R_2^{-1} & \widetilde{M}_{22} \\ * & \varepsilon_9^{-1} \end{bmatrix} > 0 \tag{57}$$

$$\widetilde{\Pi} = \begin{bmatrix} \widetilde{\Lambda}_{11} & \widetilde{\Lambda}_{12} \\ * & \widetilde{\Lambda}_{22} \end{bmatrix} < 0 \tag{58}$$

for

$$\widetilde{\Lambda}_{11} = \begin{bmatrix} \widetilde{\Pi}_{11} & \widetilde{\Pi}_{12} & \widetilde{\Pi}_{13} & 0 & \widetilde{\Pi}_{15} \\ * & \widetilde{\Pi}_{22} & \widetilde{\Pi}_{23} & 0 & \widetilde{\Pi}_{25} \\ * & * & \widetilde{\Pi}_{33} & \Pi_{34} & 0 \\ * & * & * & \Pi_{44} & 0 \\ * & * & * & * & \Pi_{55} \end{bmatrix},$$

$$\widetilde{\Lambda}_{12} = \begin{bmatrix} 0 & 0 & \widetilde{\Pi}_{18} & \widetilde{\Pi}_{19} \\ \widetilde{\Pi}_{26} & 0 & 0 & 0 \\ \Pi_{36} & \Pi_{37} & 0 & 0 \\ 0 & \Pi_{47} & 0 & 0 \\ 0 & 0 & 0 & 0 \end{bmatrix}, \tag{59}$$

$$\widetilde{\Lambda}_{22} = \begin{bmatrix} \Pi_{66} & 0 & 0 & 0 \\ * & \Pi_{77} & 0 & 0 \\ * & * & \widetilde{\Pi}_{88} & 0 \\ * & * & * & \widetilde{\Pi}_{99} \end{bmatrix},$$

where

$$\widetilde{\Pi}_{11} = \begin{bmatrix} \widetilde{\varphi}_{11} & \widetilde{\varphi}_{12} & \widetilde{N}_1^T & \widetilde{\varphi}_{14} & \widetilde{\varphi}_{15} & \widetilde{N}_3^T & \widetilde{\varphi}_{17} & \widetilde{\varphi}_{18} & \widetilde{C}_{ij}^T \\ * & -\varepsilon_1^{-1} & 0 & 0 & 0 & 0 & 0 & 0 & 0 \\ * & * & \widetilde{\varphi}_{33} & 0 & 0 & 0 & 0 & 0 & 0 \\ * & * & * & -\varepsilon_2^{-1} & 0 & 0 & 0 & 0 & 0 \\ * & * & * & * & -\varepsilon_3^{-1} & 0 & 0 & 0 & 0 \\ * & * & * & * & * & -\varepsilon_{10} & 0 & 0 & 0 \\ * & * & * & * & * & * & \widetilde{\varphi}_{77} & 0 & 0 \\ * & * & * & * & * & * & * & \widetilde{\varphi}_{88} & 0 \\ * & * & * & * & * & * & * & * & \widetilde{\varphi}_{99} \end{bmatrix},$$

$$\widetilde{\varphi}_{11} = \begin{bmatrix} P_{11}A_i & \widetilde{A}_{fj} \\ P_{12}^T A_i & \widetilde{A}_{fj} \end{bmatrix} + \begin{bmatrix} P_{11}A_i & \widetilde{A}_{fj} \\ P_{12}^T A_i & \widetilde{A}_{fj} \end{bmatrix}^T + Q_1 + Q_2 + Q_3 - a_1 R_1,$$

$$\widetilde{\varphi}_{12} = \begin{bmatrix} \widetilde{A}_{fj} M_{1j} \\ \widetilde{A}_{fj} M_{1j} \end{bmatrix},$$

$$\widetilde{\varphi}_{14} = \begin{bmatrix} \widetilde{B}_{fj} M_{2j} \\ \widetilde{B}_{fj} M_{2j} \end{bmatrix},$$

$$\widetilde{\varphi}_{15} = -\widetilde{\varphi}_{14},$$

$$\widetilde{\varphi}_{17} = \alpha_1 \begin{bmatrix} P_{11}A_i & \widetilde{A}_{fj} \\ P_{12}^T A_i & \widetilde{A}_{fj} \end{bmatrix}^T,$$

$$\widetilde{\varphi}_{18} = \alpha_2 \begin{bmatrix} P_{11}A_i & \widetilde{A}_{fj} \\ P_{12}^T A_i & \widetilde{A}_{fj} \end{bmatrix}^T,$$

$$\widetilde{\varphi}_{33} = -\left(\varepsilon_1^{-1} + \alpha_1^2\varepsilon_4^{-1} + \alpha_2^2\varepsilon_7^{-1}\right)^{-1},$$

$$\widetilde{\varphi}_{77} = \begin{bmatrix} -2\delta P + \delta^2 R_1 & \widetilde{\varphi}_{12} \\ * & -\varepsilon_4^{-1} \end{bmatrix},$$

$$\widetilde{\varphi}_{88} = \begin{bmatrix} -2\delta P + \delta^2 R_2 & \widetilde{\varphi}_{12} \\ * & -\varepsilon_7^{-1} \end{bmatrix},$$

$$\widetilde{\varphi}_{99} = \begin{bmatrix} I & \widetilde{M}_3 \\ * & -\varepsilon_{10}^{-1} \end{bmatrix},$$

$$\widetilde{\Pi}_{12} = -a_2 R_1,$$

$$\widetilde{\Pi}_{13} = \begin{bmatrix} 0 & \widetilde{B}_{fj}D_i \\ 0 & \widetilde{B}_{fj}D_i \end{bmatrix},$$

$$\widetilde{\Pi}_{15} = -a_3 R_1,$$

$$\widetilde{\Pi}_{18} = \begin{bmatrix} -\widetilde{B}_{fj} \\ -\widetilde{B}_{fj} \end{bmatrix},$$

$$\widetilde{\Pi}_{19} = \begin{bmatrix} P_{11}B_i \\ P_{12}^T B_i \end{bmatrix},$$

$$\widetilde{\Pi}_{22} = -Q_2 - a_1 R_1 - a_1 R_2,$$

$$\widetilde{\Pi}_{23} = -a_2 R_2,$$

$$\widetilde{\Pi}_{25} = -a_3 R_1,$$

$$\widetilde{\Pi}_{26} = -a_3 R_2,$$

$$\widetilde{\Pi}_{33} = \begin{bmatrix} \overline{\varphi}_{11} & \widetilde{N}_{21}^T & \overline{\varphi}_{13} & 0 & \overline{\varphi}_{15} & 0 \\ * & \overline{\varphi}_{22} & 0 & 0 & 0 & 0 \\ * & * & \overline{\varphi}_{33} & \overline{\varphi}_{34} & 0 & 0 \\ * & * & * & -\varepsilon_5^{-1} & 0 & 0 \\ * & * & * & * & \overline{\varphi}_{55} & \overline{\varphi}_{56} \\ * & * & * & * & * & -\varepsilon_8^{-1} \end{bmatrix},$$

$$\overline{\varphi}_{11} = -(1-d)Q_1 + \lambda D_i^T \psi D_i - 2a_1 R_2,$$

$$\overline{\varphi}_{13} = \begin{bmatrix} 0 & 0 \\ \alpha_1 D_i^T \widetilde{B}_{fj}^T & \alpha_1 D_i^T \widetilde{B}_{fj}^T \end{bmatrix},$$

$$\overline{\varphi}_{15} = \begin{bmatrix} 0 & 0 \\ \alpha_2 D_i^T \widetilde{B}_{fj}^T & \alpha_2 D_i^T \widetilde{B}_{fj}^T \end{bmatrix},$$

$$\overline{\varphi}_{22} = -\left(\varepsilon_2^{-1} + \alpha_1^2\varepsilon_5^{-1} + \alpha_2^2\varepsilon_8^{-1}\right)^{-1},$$

$$\overline{\varphi}_{33} = -2\delta P + \delta^2 R_1,$$

$$\overline{\varphi}_{34} = \overline{\varphi}_{56} = \begin{bmatrix} \widetilde{B}_{fj}M_{2j} \\ \widetilde{B}_{fj}M_{2j} \end{bmatrix},$$

$$\overline{\varphi}_{55} = -2\delta P + \delta^2 R_2,$$

$$\widetilde{\Pi}_{88} = \begin{bmatrix} (\lambda-1)\psi & \widetilde{N}_{22}^T & \widetilde{\kappa}_{13} & 0 & \widetilde{\kappa}_{15} & 0 \\ * & \widetilde{\kappa}_{22} & 0 & 0 & 0 & 0 \\ * & * & \widetilde{\kappa}_{33} & \widetilde{\kappa}_{34} & 0 & 0 \\ * & * & * & -\varepsilon_6^{-1} & 0 & 0 \\ * & * & * & * & \widetilde{\kappa}_{55} & \widetilde{\kappa}_{56} \\ * & * & * & * & * & -\varepsilon_9^{-1} \end{bmatrix},$$

$$\widetilde{\kappa}_{13} = \begin{bmatrix} -\alpha_1 B_{fj}^T & -\alpha_1 B_{fj}^T \end{bmatrix},$$

$$\widetilde{\kappa}_{15} = \begin{bmatrix} -\alpha_2 B_{fj}^T & -\alpha_2 B_{fj}^T \end{bmatrix},$$

$$\widetilde{\kappa}_{22} = -\left(\varepsilon_3^{-1} + \alpha_1^2\varepsilon_6^{-1} + \alpha_2^2\varepsilon_9^{-1}\right)^{-1},$$

$$\widetilde{\kappa}_{33} = -2\delta P + \delta^2 R_1,$$

$$\widetilde{\kappa}_{34} = \widetilde{\kappa}_{56} = \begin{bmatrix} -\widetilde{B}_{fj}M_{2j} \\ -\widetilde{B}_{fj}M_{2j} \end{bmatrix},$$

$$\widetilde{\kappa}_{55} = -2\delta P + \delta^2 R_2,$$

$$\widetilde{\Pi}_{99} = \begin{bmatrix} -\gamma^2 I & \overline{\kappa}_{12} & \overline{\kappa}_{13} \\ * & \overline{\kappa}_{22} & 0 \\ * & * & \overline{\kappa}_{33} \end{bmatrix},$$

$$\overline{\kappa}_{12} = \alpha_1 \begin{bmatrix} B_i^T P_{11}^T & B_i^T P_{12} \end{bmatrix},$$

$$\overline{\kappa}_{13} = \alpha_2 \begin{bmatrix} B_i^T P_{11}^T & B_i^T P_{12} \end{bmatrix},$$

$$\overline{\kappa}_{22} = -2\delta P + \delta^2 R_1,$$

$$\overline{\kappa}_{33} = -2\delta P + \delta^2 R_2. \tag{60}$$

Moreover, if inequality is feasible, the filter parameters can be obtained by

$$\begin{aligned} A_{fj} &= P_{12}^{-1}\widetilde{A}_{fj}, \\ B_{fj} &= P_{12}^{-1}\widetilde{B}_{fj}, \\ C_{fj} &= \widetilde{C}_{fj}. \end{aligned} \tag{61}$$

Proof. By applying Schur complement lemma, the matrix inequality conditions (32) in Theorem 8 can be rewritten as the following matrix inequality:

$$\widetilde{\Xi} = \begin{bmatrix} \Gamma_{11} & \Gamma_{12} \\ * & \Gamma_{22} \end{bmatrix} < 0 \tag{62}$$

for

$$\Gamma_{11} = \begin{bmatrix} \Theta_{11} & -a_2R_1 & P\widetilde{B}_{ij1} & 0 & -a_3R_1 \\ * & \Theta_{22} & -a_2R_2 & 0 & -a_3R_1 \\ * & * & \Theta_{33} & -a_2R_2 & 0 \\ * & * & * & -Q_3 - a_1R_2 & 0 \\ * & * & * & * & -a_4R_1 \end{bmatrix},$$

$$\Gamma_{12} = \begin{bmatrix} 0 & 0 & P\widetilde{B}_{ij2} & P\widetilde{B}_{wij} \\ -a_3R_2 & 0 & 0 & 0 \\ -a_3R_2 & -a_3R_2 & 0 & 0 \\ 0 & -a_4R_2 & 0 & 0 \\ 0 & 0 & 0 & 0 \end{bmatrix}, \quad (63)$$

$$\Gamma_{22} = \begin{bmatrix} -a_4R_2 & 0 & 0 & 0 \\ * & -a_4R_2 & 0 & 0 \\ * & * & \Theta_{88} & 0 \\ * & * & * & \Theta_{99} \end{bmatrix},$$

where

$$\Theta_{11} = \begin{bmatrix} \phi_{11} & P\widetilde{M}_1 & \widetilde{N}_1^T & P\widetilde{M}_{21} & -P\widetilde{M}_{21} & \widetilde{N}_3^T & \phi_{17} & \phi_{18} & \widetilde{C}_{ij}^T \\ * & -\varepsilon_1^{-1} & 0 & 0 & 0 & 0 & 0 & 0 & 0 \\ * & * & \phi_{33} & 0 & 0 & 0 & 0 & 0 & 0 \\ * & * & * & -\varepsilon_2^{-1} & 0 & 0 & 0 & 0 & 0 \\ * & * & * & * & -\varepsilon_3^{-1} & 0 & 0 & 0 & 0 \\ * & * & * & * & * & -\varepsilon_{10} & 0 & 0 & 0 \\ * & * & * & * & * & * & \phi_{77} & 0 & 0 \\ * & * & * & * & * & * & * & \phi_{88} & 0 \\ * & * & * & * & * & * & * & * & \phi_{99} \end{bmatrix},$$

$$\phi_{11} = P\widetilde{A}_{ij} + \widetilde{A}_{ij}^T P + Q_1 + Q_2 + Q_3 - a_1R_1,$$

$$\phi_{17} = \alpha_1\widetilde{A}_{ij}^T P,$$

$$\phi_{18} = \alpha_2\widetilde{A}_{ij}^T P,$$

$$\phi_{33} = -\left(\varepsilon_1^{-1} + \alpha_1^2\varepsilon_4^{-1} + \alpha_2^2\varepsilon_7^{-1}\right)^{-1},$$

$$\phi_{77} = \begin{bmatrix} -PR_1^{-1}P & P\widetilde{M}_1 \\ * & -\varepsilon_4^{-1} \end{bmatrix},$$

$$\phi_{88} = \begin{bmatrix} -PR_2^{-1}P & P\widetilde{M}_1 \\ * & -\varepsilon_4^{-1} \end{bmatrix},$$

$$\phi_{99} = \begin{bmatrix} I & \widetilde{M}_3 \\ * & -\varepsilon_{10}^{-1} \end{bmatrix},$$

$$\Theta_{22} = -Q_2 - a_1R_1 - a_1R_2,$$

$$\Theta_{33} = \begin{bmatrix} \overline{\phi}_{11} & \widetilde{N}_{21}^T & \alpha_1\widetilde{B}_{ij1}^T P & 0 & \alpha_2\widetilde{B}_{ij1}^T P & 0 \\ * & \overline{\phi}_{22} & 0 & 0 & 0 & 0 \\ * & * & -PR_1^{-1}P & P\widetilde{M}_{21} & 0 & 0 \\ * & * & * & -\varepsilon_5^{-1} & 0 & 0 \\ * & * & * & * & -PR_2^{-1}P & P\widetilde{M}_{21} \\ * & * & * & * & * & -\varepsilon_8^{-1} \end{bmatrix},$$

$$\overline{\phi}_{11} = -(1-d)Q_1 + \lambda D_i^T \psi D_i - 2a_1R_2,$$

$$\overline{\phi}_{22} = -\left(\varepsilon_2^{-1} + \alpha_1^2\varepsilon_5^{-1} + \alpha_2^2\varepsilon_8^{-1}\right)^{-1},$$

$$\Theta_{88} = \begin{bmatrix} (\lambda-1)\psi & \widetilde{N}_{22}^T & \alpha_1\widetilde{B}_{ij2}^T P & 0 & \alpha_2\widetilde{B}_{ij2}^T P & 0 \\ * & \widetilde{\kappa}_{22} & 0 & 0 & 0 & 0 \\ * & * & -PR_1^{-1}P & P\widetilde{M}_{22} & 0 & 0 \\ * & * & * & -\varepsilon_6^{-1} & 0 & 0 \\ * & * & * & * & -PR_2^{-1}P & P\widetilde{M}_{22} \\ * & * & * & * & * & -\varepsilon_9^{-1} \end{bmatrix},$$

$$\Theta_{99} = \begin{bmatrix} -\gamma^2 I & \alpha_1\widetilde{B}_{wij}^T P & \alpha_2\widetilde{B}_{wij}^T P \\ * & -PR_1^{-1}P & 0 \\ * & * & -PR_2^{-1}P \end{bmatrix}. \quad (64)$$

Then, we define the following matrices:

$$P = \begin{bmatrix} P_{11} & P_{12} \\ * & P_{12} \end{bmatrix},$$

$$\widetilde{A}_{fj} = P_{12}A_{fj}, \quad (65)$$

$$\widetilde{B}_{fj} = P_{12}B_{fj},$$

$$\widetilde{C}_{fj} = C_{fj}.$$

We have

$$P\widetilde{A}_{ij} = \begin{bmatrix} P_{11}A_i & \widetilde{A}_{fj} \\ P_{12}^T A_i & \widetilde{A}_{fj} \end{bmatrix},$$

$$P\widetilde{B}_{ij1} = \begin{bmatrix} 0 & \widetilde{B}_{fj}D_i \\ 0 & \widetilde{B}_{fj}D_i \end{bmatrix},$$

$$P\widetilde{B}_{ij2} = \begin{bmatrix} -\widetilde{B}_{fj} \\ -\widetilde{B}_{fj} \end{bmatrix},$$

$$P\widetilde{B}_{wij} = \begin{bmatrix} P_{11}B_i \\ P_{12}^T B_i \end{bmatrix},$$

$$P\widetilde{M}_1 = \begin{bmatrix} \widetilde{A}_{fj}M_1 \\ \widetilde{A}_{fj}M_1 \end{bmatrix},$$

$$P\widetilde{M}_{21} = \begin{bmatrix} \widetilde{B}_{fj}M_2 \\ \widetilde{B}_{fj}M_2 \end{bmatrix},$$

$$P\widetilde{M}_{22} = \begin{bmatrix} -\widetilde{B}_{fj}M_2 \\ -\widetilde{B}_{fj}M_2 \end{bmatrix}. \tag{66}$$

Moreover, we can derive $-PR^{-1}P \leq -2\delta P + \delta^2 R$ by the inequality $(\delta R - P)R^{-1}(\delta R - P) \geq 0$ for any scalar $\delta > 0$. Then, by applying Schur complement lemma and combining (32) and (62)–(66), we can easily derive inequality (58). This completes the proof. □

5. Simulation Results

In this section, we provide two examples to demonstrate the merit of the nonfragile H_∞ filter based event-triggered scheme.

Example 1. Consider the following fuzzy systems:

$$\begin{aligned} \dot{x}(t) &= \sum_{i=1}^{2} u_i \left[A_i x(t) + B_i \omega(t)\right] \\ z(t) &= \sum_{i=1}^{2} u_i C_i x(t) \\ y(t) &= \sum_{i=1}^{2} u_i D_i x(t), \end{aligned} \tag{67}$$

where

$$\begin{aligned} A_1 &= \begin{bmatrix} -2.1 & 0.1 \\ 1 & -2 \end{bmatrix}, \\ A_2 &= \begin{bmatrix} -1.9 & 0 \\ -0.2 & -1.1 \end{bmatrix}, \\ B_1 &= \begin{bmatrix} 1 \\ -0.2 \end{bmatrix}, \\ B_1 &= \begin{bmatrix} 0.3 \\ 0.1 \end{bmatrix}, \\ C_1 &= \begin{bmatrix} 1 & -0.5 \end{bmatrix}, \\ C_2 &= \begin{bmatrix} -0.2 & 0.3 \end{bmatrix}, \\ D_1 &= \begin{bmatrix} 1 & 0 \end{bmatrix}, \\ D_2 &= \begin{bmatrix} 0.5 & 0.6 \end{bmatrix}. \end{aligned} \tag{68}$$

And the parameter uncertainties are given as

$$\begin{aligned} M_{11} = M_{12} &= \begin{bmatrix} 0.05 \\ 0.04 \end{bmatrix}, \\ M_{21} = M_{22} &= 0.01, \\ M_{31} = M_{32} &= \begin{bmatrix} 0.02 \\ 0.01 \end{bmatrix}, \\ N_{11} = N_{12} &= \begin{bmatrix} 0.02 & 0.03 \end{bmatrix}, \\ N_{21} = N_{22} &= 0.05, \\ N_{31} = N_{32} &= \begin{bmatrix} 0.03 & 0.02 \end{bmatrix}, \\ K_g(t) &= \sin(t), \quad g = A, B, C. \end{aligned} \tag{69}$$

The membership function $u_i(t)$, $i = 1, 2$, and the external disturbance signal $\omega(t)$ are given as

$$\begin{aligned} u_1(t) &= \sin\left(t^2\right), \\ u_2(t) &= 1 - u_1(t), \\ \omega(t) &= \frac{1}{1 + 3t^2}. \end{aligned} \tag{70}$$

Consider the interval time-varying delay with $\tau_1 = 0.03$ and $\tau_2 = 0.2$. And choose $\lambda = 0.2, d = 0.2, \delta = 10$, and sample period $h = 20$ ms. By Theorem 9, we derive the desired nonfragile parameter as follows:

$$\begin{aligned} A_{f1} &= \begin{bmatrix} -17.4366 & 8.5268 \\ 7.7146 & -11.2453 \end{bmatrix}, \\ A_{f2} &= \begin{bmatrix} -16.9835 & 6.2715 \\ 7.0539 & -9.1581 \end{bmatrix}, \\ B_{f1} &= \begin{bmatrix} -0.4852 \\ -0.3343 \end{bmatrix}, \\ B_{f2} &= \begin{bmatrix} 0.2106 \\ -0.1013 \end{bmatrix}, \\ C_{f1} &= \begin{bmatrix} -2.4715 & 0.2475 \end{bmatrix}, \\ C_{f2} &= \begin{bmatrix} -1.8903 & 1.1024 \end{bmatrix}. \end{aligned} \tag{71}$$

Meanwhile, we obtain the event-triggered parameter $\psi = 23.6026$ and the minimum H_∞ performance level is $\gamma = 0.99$.

It is assumed that the initial condition is $x(0) = \begin{bmatrix} 1 & -1 \end{bmatrix}^T$. The responses of the original state and the filter state are shown in Figures 1 and 2. The system output signal is depicted in Figure 3. As depicted in Figure 4, we can clearly see that the response of the filtering error is stable after about three seconds, which demonstrates the effective of the proposed approach. Note that, in Figure 5, the transmission rate is mitigated from 100% to 7%, which demonstrates that the event-triggered scheme is effective in reducing data transmission and saving the network resource.

Example 2. To further demonstrate the effectiveness of the proposed method, in this example, we consider a truck-trailer

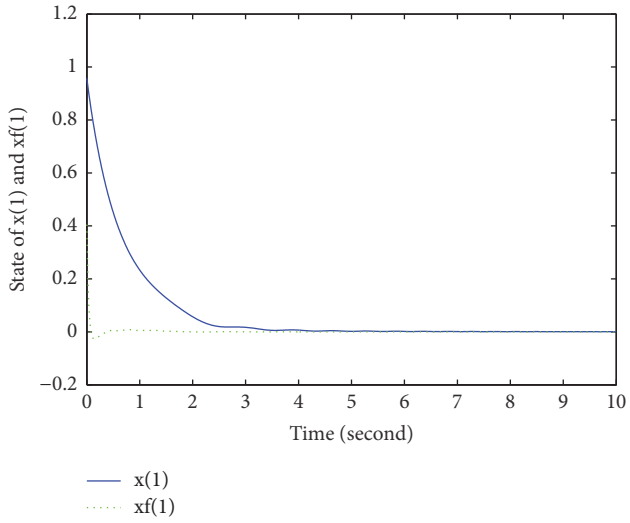

Figure 1: State trajectories of x_1.

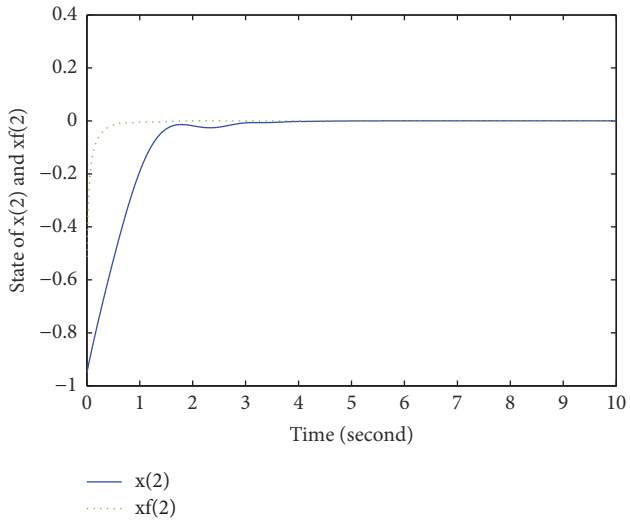

Figure 2: State trajectories of x_2.

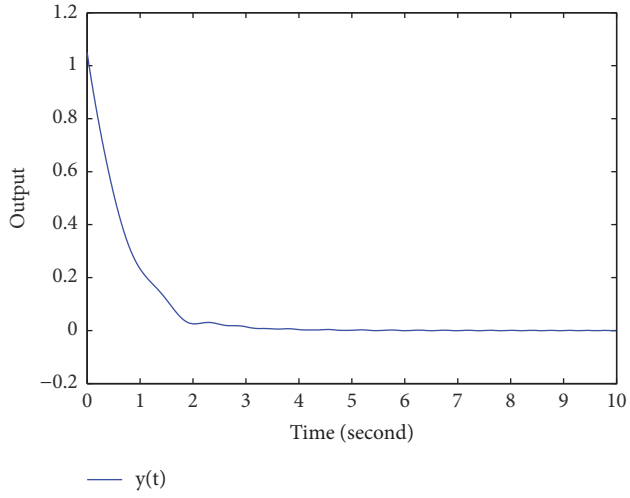

Figure 3: The trajectories of $y(t)$.

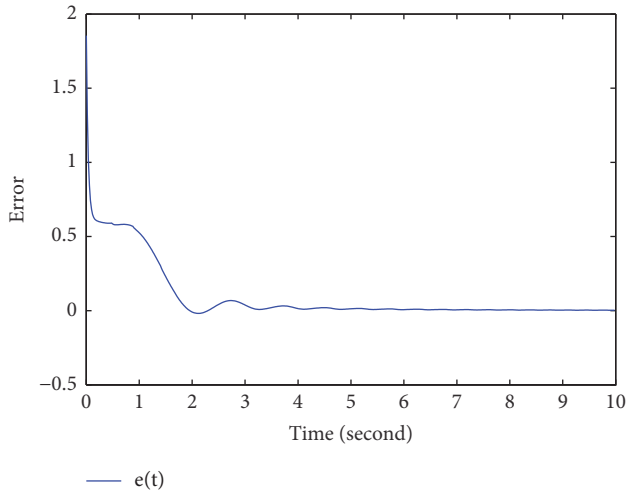

Figure 4: The trajectories of estimate error.

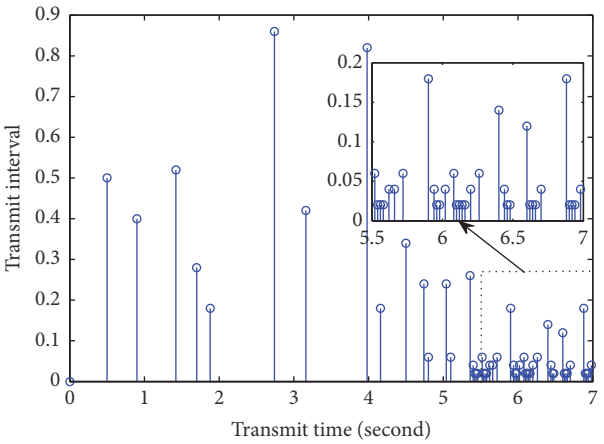

Figure 5: Release instant.

system; the practical example is borrowed from [26]. The system parameters are given as follows:

$$A_1 = \begin{bmatrix} -1.6371 & 0.5741 & -0.0157 \\ -0.5091 & 0 & 0 \\ 0.5091 & -4 & 0 \end{bmatrix},$$

$$A_2 = \begin{bmatrix} -1.6086 & 0.5284 & -0.0150 \\ -0.5091 & 0 & 0 \\ 0.0016 & -0.0127 & 0 \end{bmatrix},$$

$$B_1 = \begin{bmatrix} 1 \\ 0.5 \\ 0 \end{bmatrix},$$

$$B_2 = \begin{bmatrix} 1 \\ 0.5 \\ 0 \end{bmatrix},$$

$$C_1 = [0 \ \ 1 \ \ 0],$$
$$C_2 = [0 \ \ 1 \ \ 0],$$
$$D_1 = [4.9 \ \ -2 \ \ 0.04],$$
$$D_2 = [4.9 \ \ -2 \ \ 0.04]. \tag{72}$$

Then, we suppose that the parameter uncertainties are given by

$$M_{11} = M_{12} = \begin{bmatrix} 0.1 \\ 0.1 \\ 0.21 \end{bmatrix},$$
$$M_{21} = M_{22} = 0.1,$$
$$M_{31} = M_{32} = \begin{bmatrix} -0.2 \\ 0 \\ 0.2 \end{bmatrix}, \tag{73}$$
$$N_{11} = N_{12} = [0.2 \ \ 0.3 \ \ 0.1],$$
$$N_{21} = N_{22} = 0.5,$$
$$N_{31} = N_{32} = [-0.3 \ \ 0.2 \ \ 0.1],$$
$$K_l(t) = \sin(t), \quad l = A, B, C.$$

We assume that the lower bound and upper bound of the interval time-varying delay are $\tau_1 = 0.01$ and $\tau_2 = 0.25$, respectively. The derivative of the time delay is $d = 0.3$. Furthermore, we suppose that $\lambda = 0.2$ and $\delta = 0.1$. By solving the LMIs in Theorem 9, we obtain minimum performance level $\gamma = 1.1241$, which is less than previously studied $\gamma = 7.0948$ in [26]. Meanwhile, the event-triggered argument $\psi = 2.0069$ is obtained, and the corresponding filter parameters can be derived as follows:

$$A_{f1} = \begin{bmatrix} -8.1449 & 8.2655 & -0.6046 \\ -3.6646 & 3.5043 & -0.2331 \\ -2.3869 & 2.7130 & -1.5149 \end{bmatrix},$$
$$A_{f2} = \begin{bmatrix} -7.6655 & -8.2644 & -0.3039 \\ -3.2074 & 3.1396 & -0.1352 \\ -0.6803 & 0.6193 & -0.9489 \end{bmatrix},$$
$$B_{f1} = \begin{bmatrix} -0.0942 \\ -0.0503 \\ -0.1788 \end{bmatrix}, \tag{74}$$
$$B_{f2} = \begin{bmatrix} -0.0742 \\ -0.0360 \\ -0.2396 \end{bmatrix},$$
$$C_{f1} = [-0.9862 \ \ 0.8778],$$
$$C_{f2} = [-2.6857 \ \ 4.0130].$$

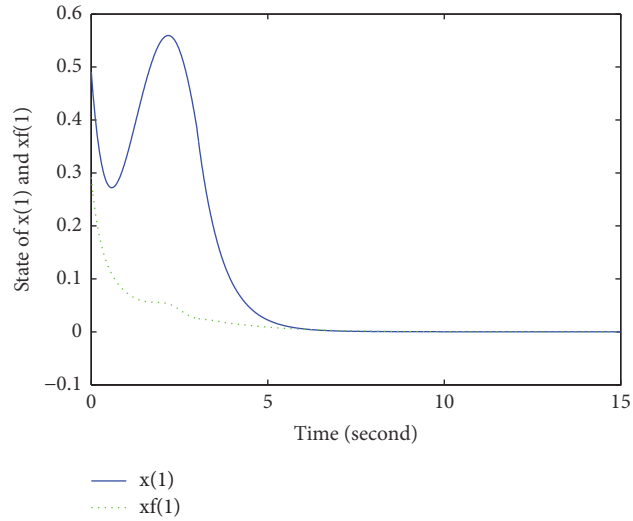

Figure 6: State trajectories of x_1.

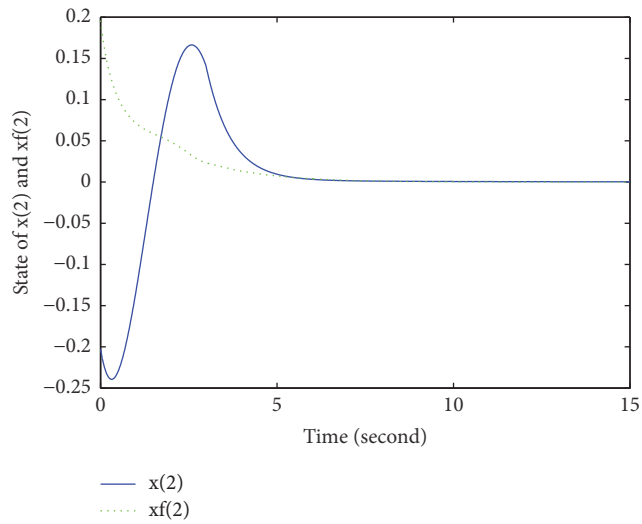

Figure 7: State trajectories of x_2.

Figures 6, 7, and 8 show the original state and the filter state; it is clear that the filter state is asymptotically stable. The curve of the system output signal is depicted in Figure 9.

The filtering error response is depicted in Figure 10, which shows that the designed nonfragile H_∞ filter is feasible.

Finally, we choose the sample period $h = 10$ ms; under the event-triggered scheme, it can be seen that Figure 11 shows that only 24 times in all 900 sampling instants are transmitted, which illustrates that the network bandwidth is greatly mitigated.

6. Conclusions

In this paper, the problem of the event-triggered fuzzy nonfragile H_∞ filter design has been investigated for nonlinear NCSs with interval time-varying delay. The resultant filtering error system has been modeled as a system with an

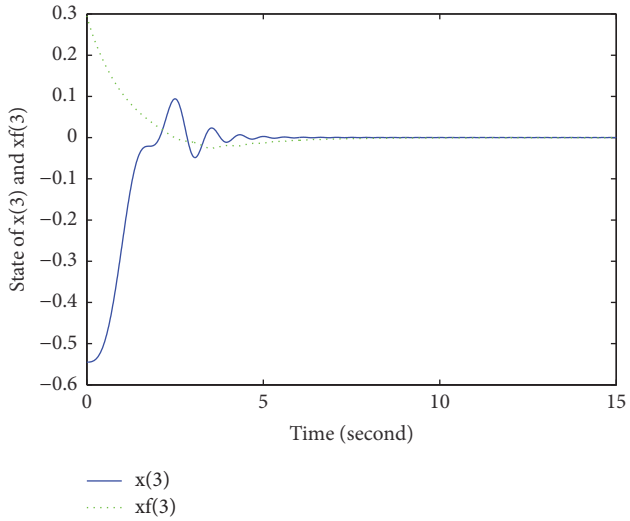

Figure 8: State trajectories of x_3.

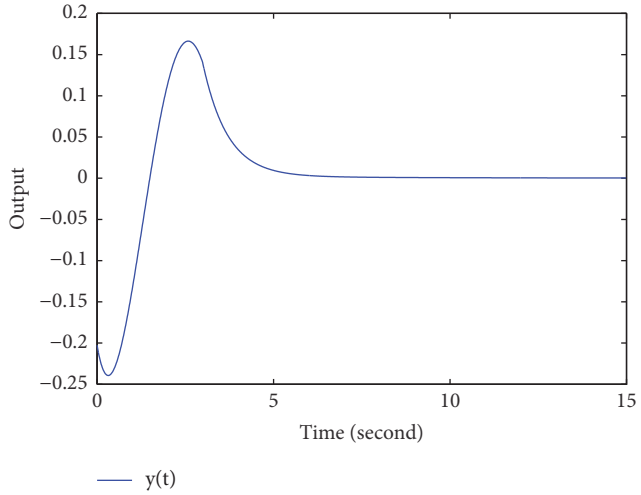

Figure 9: The trajectories of $y(t)$.

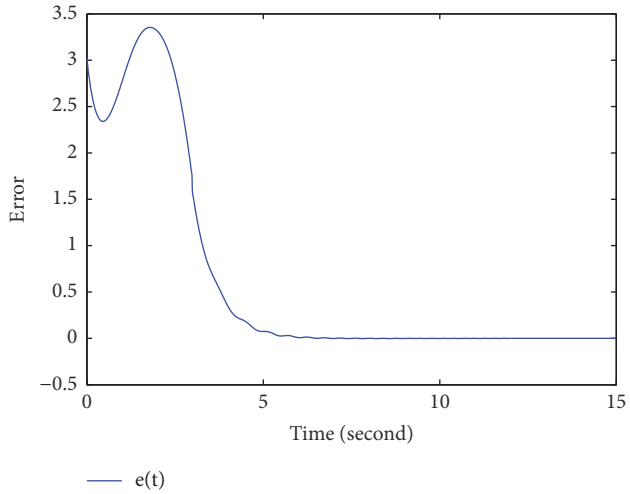

Figure 10: The trajectories of estimate error.

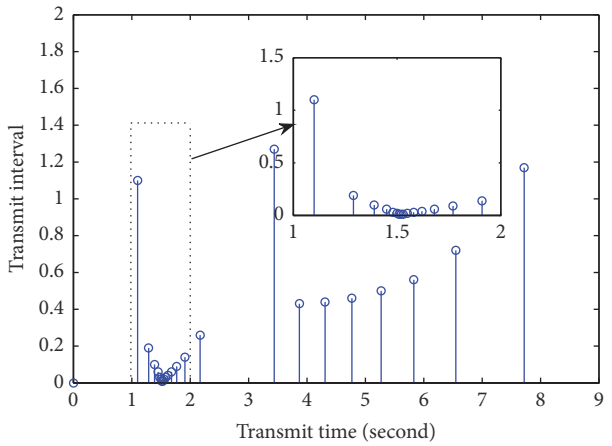

Figure 11: Release instant.

interval time-varying delay. By constructing a new Lyapunov-Krasovskii functional and employing Wirtinger inequality, we have obtained a sufficient condition for designing the fuzzy nonfragile H_∞ filter such that the fuzzy filtering error system is asymptotically stable with a prescribed H_∞ performance level. Two numerical examples have been given to demonstrate the effectiveness of the proposed method. Future research includes nonfragile fuzzy fault filter design for nonlinear control systems considering time-varying delays. In addition, type-2 nonfragile fuzzy filter design for NCSs with packet dropout also can be further considered for the future investigation.

Data Availability

The data used to support this study are currently under embargo, while the research findings are commercialized. Requests for data will be considered by the corresponding author.

Conflicts of Interest

The authors declare that there are no conflicts of interest regarding the publication of this paper.

Acknowledgments

This work was supported in part by Natural Science Foundation of Heilongjiang Province (Grant no. LC2015024) and the Fundamental Research Funds in Heilongjiang Provincial Universities (Grant no. 135109238).

References

[1] Y.-Q. Xia, Y.-L. Gao, L.-P. Yan, and M.-Y. Fu, "Recent progress in networked control systems — A survey," *International Journal of Automation and Computing*, vol. 12, no. 4, pp. 343–367, 2015.

[2] C. Han, L. Wu, H. K. Lam, and Q. Zeng, "Non-fragile control with guaranteed cost of T-S fuzzy singular systems based on

parallel distributed compensation," *IEEE Transactions on Fuzzy Systems*, 2013.

[3] C. Han, G. Zhang, L. Wu, and Q. Zeng, "Sliding mode control of T-S fuzzy descriptor systems with time-delay," *Journal of The Franklin Institute*, vol. 349, no. 4, pp. 1430–1444, 2012.

[4] H. K. Lam, "Stability analysis of T-S fuzzy control systems using parameter-dependent Lyapunov function," *IET Control Theory & Applications*, vol. 3, no. 6, pp. 750–762, 2009.

[5] H. K. Lam, "LMI-based stability analysis for fuzzy-model-based control systems using artificial TS fuzzy model," *IEEE Transactions on Fuzzy Systems*, vol. 19, no. 3, pp. 505–513, 2011.

[6] X. Xu, H. Yan, H. Zhang, and F. Yang, "H∞ filtering for T–S fuzzy networked systems with stochastic multiple delays and sensor faults," *Neurocomputing*, vol. 207, pp. 590–598, 2016.

[7] J. An, G. Wen, C. Lin, and R. Li, "New results on a delay-derivative-dependent fuzzy H∞ filter design for T-S fuzzy systems," *IEEE Transactions on Fuzzy Systems*, vol. 19, no. 4, pp. 770–779, 2011.

[8] S. Zhang, Z. Wang, D. Ding et al., "Non-fragile H8 fuzzy filtering with randomly occuring gain variations and channel fadings," *IEEE Transactions on Fuzzy Systems*, vol. 24, no. 33, pp. 505–518, 2016.

[9] D. W. Ding, X. L. Li, Y. Y. Wang, and Z. G. Shi, "Non-fragile H8 fuzzy filtering for discrete-time non-linear systems," *IET Control Theory and Applications*, vol. 7, no. 6, pp. 848–857, 2013.

[10] Z. Li, F. Gu, Y. Q. He, and W. J. Hao, "Nonfragile robust H∞ filter design for a class of fuzzy stochastic systems with stochastic input-to-state stability," *Mathematical Problems in Engineering*, vol. 2015, 10 pages, 2015.

[11] W. P. Heemels, M. C. Donkers, and A. R. Teel, "Periodic event-triggered control for linear systems," *Institute of Electrical and Electronics Engineers Transactions on Automatic Control*, vol. 58, no. 4, pp. 847–861, 2013.

[12] C. Peng, Q.-L. Han, and D. Yue, "To transmit or not to transmit: a discrete event-triggered communication scheme for networked takagi-sugeno fuzzy systems," *IEEE Transactions on Fuzzy Systems*, vol. 21, no. 1, pp. 164–170, 2013.

[13] P. J. Gawthrop and L. Wang, "Event-driven intermittent control," *International Journal of Control*, vol. 82, no. 12, pp. 2235–2248, 2009.

[14] J. Lunze and D. Lehmann, "A state-feedback approach to event-based control," *Automatica*, vol. 46, no. 1, pp. 211–215, 2010.

[15] X. Yin and D. Yue, "Event-triggered tracking control for heterogeneous multi-agent systems with Markov communication delays," *Journal of The Franklin Institute*, vol. 350, no. 5, pp. 1312–1334, 2013.

[16] K. Duan and W. Zhang, "Event-triggered fault-tolerant control for networked systems with dynamic quantiser," *IET Control Theory & Applications*, vol. 10, no. 9, pp. 1088–1096, 2016.

[17] S. Wen, X. Yu, and Z. Zeng, "Event-triggering load frequency control for multi-area power systems," *IEEE Transactions on Industrial Electronics*, vol. 63, no. 2, pp. 1308–1317, 2016.

[18] P. Shi, H. Wang, and C.-C. Lim, "Network-based event-triggered control for singular systems with quantizations," *IEEE Transactions on Industrial Electronics*, vol. 63, no. 2, pp. 1230–1238, 2016.

[19] Z. D. Lu, G. T. Ran, G. L. Zhang, and F. X. Xu, "Event-triggered H∞ fuzzy filtering for networked control systems with quantization and delays," *IEEE Access*, vol. 6, no. 1, pp. 20231–20241, 2018.

[20] C. Peng and J. Zhang, "Even-triggered output-feedback H∞ control for networked control systems with time-varying sampling," *IET Control Theory & Applications*, vol. 9, no. 9, pp. 1384–1391, 2015.

[21] I. R. Petersen, "A stabilization algorithm for a class of uncertain linear systems," *Systems & Control Letters*, vol. 8, no. 4, pp. 351–357, 1987.

[22] L. H. Xie, "Output feedback H∞ control of systems with parameter uncertainty," *International Journal of Control*, vol. 63, no. 4, pp. 741–750, 1996.

[23] Y. Y. Wang, L. H. Xie, and C. E. de Souza, "Robust control of a class of uncertain nonlinear systems," *Systems and Control Letters*, vol. 19, no. 2, pp. 139–149, 1992.

[24] S. Zhou, W. Ren, and J. Lam, "Stabilization for T-S model based uncertain stochastic systems," *Information Sciences*, vol. 181, no. 4, pp. 779–791, 2011.

[25] A. Seuret and F. Gouaisbaut, "On the use of the Wirtinger inequalities for time-delay systems," *IFAC Proceedings Volumes*, vol. 45, no. 14, pp. 260–265, 2012.

[26] Y. J. Liu, B. Z. Guo, and J. H. Park, "Non-fragile H8 filtering for delayed Takagi-Sugeno fuzzy systems with randomly occurring gain variations," *Fuzzy Sets and Systems*, vol. 316, no. 1, pp. 99–116, 2017.

Hindawi
Journal of Control Science and Engineering
Volume 2018, Article ID 7245872, 8 pages
https://doi.org/10.1155/2018/7245872

Research Article

Networked Closed-Loop Model for Smart On-Site Maintenance of Substation Equipment Using Mobile Networks

Zhenxin Feng,[1,2] Yi Jiang,[1,2] Yuting Luo,[3] Kun Zhao,[1,2] Guocheng Ding,[4] and Wenshan Hu[3]

[1]*Nanjing NARI Group Corporation, State Grid Electric Power Research Institute, Nanjing, China*
[2]*Wuhan NARI Limited Liability Company, State Grid Electric Power Research Institute, Wuhan, China*
[3]*Department of Automation, Wuhan University, Wuhan, China*
[4]*State Grid Anhui Electric Power Co., Ltd., Electric Power Research Institute, Hefei, China*

Correspondence should be addressed to Wenshan Hu; wenshan.hu@whu.edu.cn

Received 28 February 2018; Accepted 10 May 2018; Published 11 June 2018

Academic Editor: Cui-Qin Ma

This paper introduces a networked closed-loop model for smart on-site maintenance of substation equipment using mobile networks, which is composed of a field-side Smart Operation and Maintenance (SOM) box with its related APP and a centre-side system platform for Operation and Maintenance (OM). As a bridge to connect the operation sites and data centre, the networked equipment maintenance model enables bidirectional communication among the management, maintenance teams, and diversely located equipment. This model not only realizes the formal data uploading in real-time, but also can provide the workers on site with guidance from the data centre.

1. Introduction

To improve the performance of equipment and provide security assurances of power generation, power grid equipment maintenance has been paid more attention to the power industry. With the development of the modern industry, the power system becomes huge and complex. There are thousands of nodes that need to be controlled [1, 2]. What is more, the power grid equipment is normally diversely located, which makes great difficulties for their daily servicing and maintenance.

According to the responsibilities, the daily work of the substation is generally divided into Operation and Maintenance (OM) to ensure the safety of the power grid. However, this division of labor may also lead to lower production efficiency and insufficient human resources. The increasingly complex background of the grid makes the requirements for safety and reliability higher and higher [3, 4]. To realize the task of "major overhaul" system construction proposed by the State Grid of China, the research on enhancing the assets safety life management is urgently necessary, mainly by integrating operation, management, and maintenance [5–7]. However, for the conventional on-site maintenance procedures, there is a gap between the management and the on-site maintenance teams due to the lack of real-time communication. If bridges between the management centre and the maintenance site could be built using the network such as WIFI and 4G, the work efficiency and reliability will be greatly improved.

In order to break the limits on the physical location of space and simplify the system connection, based on the development of network and control technologies, Networked Control Systems (NCS) have been broadly applied in modern industry to address these problems [8–11].

NCS is designed to achieve the control loop in the serial network; that is, the signals are exchanged among the controllers, sensors, actuators, and other components through the serial network. The system uses the network to transmit feedback signals to form a closed loop. The control loops are closed through communication networks which connect the cyberspace to physical space, which enables several tasks to be executed from a long distance [12, 13]. A

mobile network is a communication network where the last link is wireless. The mobile network has been widely used in daily and industrial applications in recent years together with the fast advancement of wireless communication technologies [14]. Using the mobile network and networked control technologies, distributed devices can be connected wirelessly and form complex systems.

Along with the advantages, new control strategies and data communication protocols and some other relative topics are studied in depth. A control system strategy designed for multivariable plants has been proposed by Goodwin et al. [15] from University of Newcastle. Through a digital, data-rate limited, communications channel, the controllers, sensors, and actuators of the control system are all connected. In Yang's survey on NCSs [16], a simple framework for the research on NCSs is presented, in which the impact of NCS on control methodologies of conventional large-scale system with a related application is also reviewed. Sala et al. [17] in Universidad Politécnica de Valencia presents a strategy for control on the basis of the retuning of the PID controller according to the variable delays in an NCS to avoid the decrease of control performance in her paper.

In the previous work in [18], a Smart Operation and Maintenance (SOM) system has been presented focusing on the online management of the substation maintenance work, covering the hardware/software design, online system design, and also the online maintenance routines. In consideration of the development of NCS and the issues of power grid equipment maintenance such as the communication between management centre and the maintenance site, this paper proposes a networked model for on-site maintenance of substation equipment. The new scheme is based on the mobile networks and wireless communication for substation OM [19, 20]. By developing an on-site SOM system, the management in the centre side and the equipment together with the maintenance teams on the field side are effectively connected through the mobile network. A closed-loop smart maintenance scheme is introduced to enable bidirectional communication among the management, maintenance teams, and diversely located equipment. Using a hand-held smart box, the real-time data on field side can be uploaded and checked in real-time. The workers can also call for help from experts on the centre side any time when they meet some difficulty during their work. Using the newly proposed system, both the efficiency and effectiveness of the on-site maintenance work can be significantly improved.

2. Architecture of Smart On-Site Maintenance Based on Mobile Network

2.1. The Architecture of Smart Maintenance System. The SOM system's whole structure is illustrated in Figure 1. It can be partitioned to the centre side and field side. The field-side system consists of a SOM box, working as the bridge between the two sides. There is also on-site SOM equipment that can be tested by many kinds of technologies. Through the mobile communication network, related guidance and support can be provided to field workers by an integrated OM platform in the centre of the power grid.

The OM work includes live detection, intelligent inspection, preventive test, major defect state monitoring, alarm for state assessment, and maintenance decision optimization. The work is completed with these devices such as ultrasonic testing, partial discharge detection, infrared temperature measurement, and spectral analysis. The SOM box is composed of data acquisition module, video conference module, 4G mobile communication module, power management module, etc. The OM platform includes data acquisition communication, decision support, data storage, centre side advanced application, and standardization advanced application framework. In the centre side of power grid company, the platform can communicate with the OM site through 4G mobile communication.

2.2. Networked Closed-Loop Smart Maintenance Model. Figure 2 shows the networked model for the substation equipment maintenance. In the centre side, the project managers assign the maintenance tasks online. When the new tasks are confirmed by the system, it would be pushed to the mobile device held by the corresponding maintenance teams using apps. After the maintenance teams receive the tasks, they carry the proper equipment to the specified substations. They can use a specially designed Smart Maintenance Box to carry out the routine work. Using the box, they can collect the data from all the sensors automatically. After the maintenance work is finished, the smart box can also generate the maintenance report and upload it to the data server on the centre side through the mobile networks. If the teams encounter any problems they cannot solve during the work process, they can call the centre side any time. The smart box is equipped with four high definition cameras. Video conference over the 4G mobile network can be established any time between the on-site personnel and the experts on the centre side.

After the maintenance work is finished, the smart box generates and uploads the report to the data server located on the centre side automatically. The management teams check the reports on the data server. If the reports are satisfactory, they can be proved online. Otherwise, feedback will be sent back to the maintenance team and guide them to redo part of the work.

Using the networked equipment maintenance model, the centre side and the field side are integrated by the mobile networks. The information can be shared and exchanged by both sides in real-time. From the task assignment, execution to the assessment, a closed-loop model through the network is established. With the help of the mobile network, the daily maintenance work can be carried out in an effective and efficient way, even though the power equipment is diversely located.

3. Design and Implementation of the SOM Box

Based on NCS technology, a networked closed-loop model has been applied to the SOM system. The kernel part of the SOM system is a SOM box which is connected to the on-site power detection equipment through a wireless network. The SOM box communicates with the on-site power detection

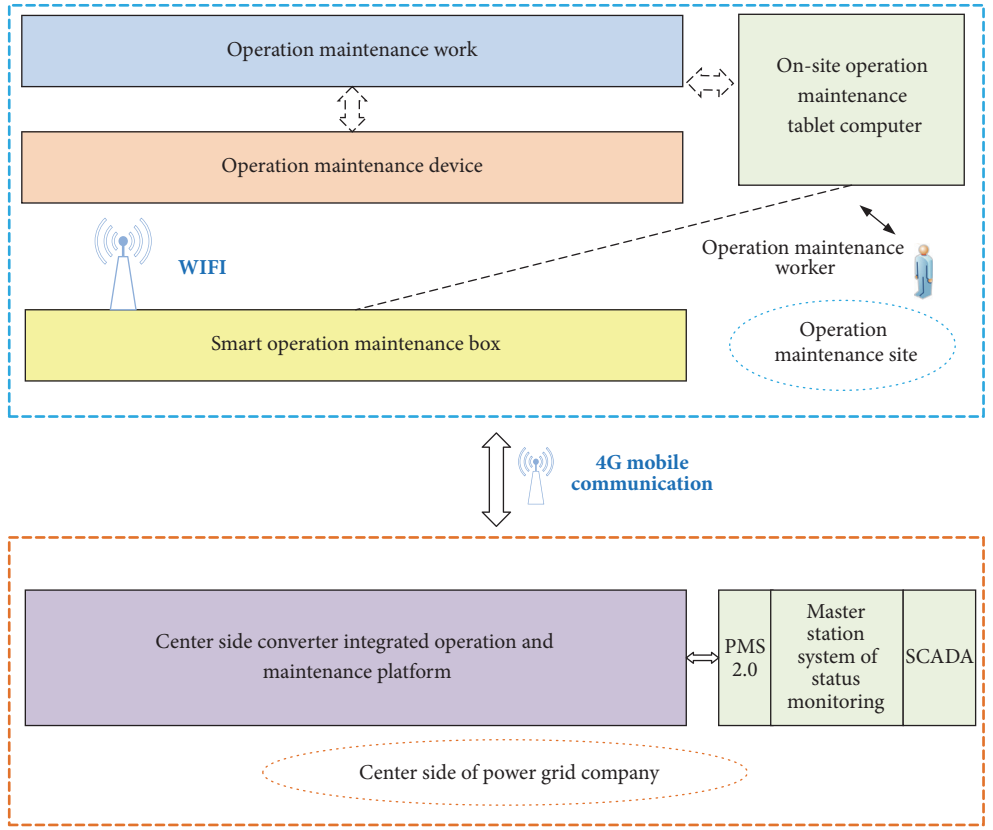

Figure 1: Architecture of the proposed system.

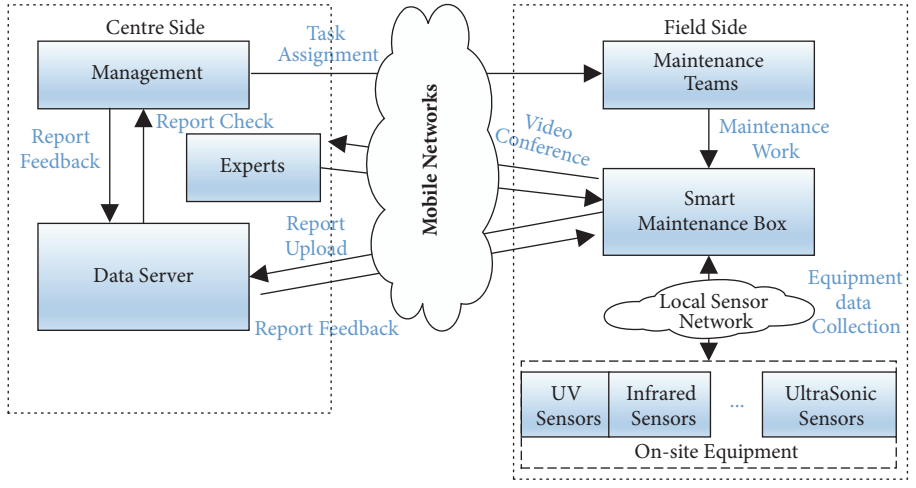

Figure 2: Structure of networked closed-loop smart maintenance model.

equipment using a unified protocol. The standardized box information can be used for intelligent assessment and detection, as long as it has been uploaded to and stored in the Power Grid Corp data centre.

The interactions between the centre-side source including big data analysis and calculation and the on-site maintenance work are achieved through the SOM box. For example, the senior application centre can analyse the data uploaded locally and match and analyse it through the built-in case library. In the event of abnormal data or emergency equipment failure, the maintenance team can be notified directly to intervene. When OM personnel face technical difficulties, professional on-site guidance can be obtained through the video conference call centre.

Figure 3: Hardware interface of the SOM box.

3.1. Hardware Design and Implementation. Considering the energy consumption and also the performance, the TI (Texas Instruments) OMAP5432 platform is adopted for the design of the SOM box, and Samsung's Exynos 5250 System-on-Chip (SoC) processor based on a dual-core ARM CorTex-A15 framework is also considered.

As shown in Figure 3, to support the data monitoring in real-time in this project, a TI 2D BitBLT graphics accelerator is adopted in the hardware interface. It can support four displays and three cameras simultaneously, enabling direct video conferencing. Embedded with an adaptive network communication module of Bluetooth, 4G, WIFI, and 10M/100M, the box is able to communicate with various on-site testing equipment and also the data centre.

3.2. Software Design and Implementation. Regarding the software, the Android 4.2.2 is used in the proposed system whose kernel is on the basis of Linux and the gcc 4.4.1 is used for cross-compilation. As for the file system, the combination of Ramdisk and Ext4 is adopted.

Figure 4 shows the multitier-structure software design of the SOM box. It can be seen that a variety of communication-driven management modules are integrated into the architecture, which can support various communication devices and protocol. Device drivers, for example, USB storage devices, cameras, and monitors, can also be deployed. The Android system provides the resource of kernel layer. In order to form a own special system, an open source operating system is applied and tailored to build up functionalities of the system.

The independently developed modules, including data processing, video conferencing clients, and data management, form the application tier module. Main functionalities, for example, data acquisition storage and uploading as well as interactions with the centre side can be realized by these modules supported by corresponding algorithms.

4. Communication Protocols for Data Collection

4.1. AMQP Based Communication Protocol. There are various maintenance devices which create all kinds of data such as charts, images, and data streams. Therefore, it is utterly important to unify the forms of the communication data between the smart box and maintenance devices. The communication protocol is based on an open standard application layer protocol, that is, Advanced Message Queuing Protocol (AMQP) that can be used for message-oriented middleware. There are many open source frameworks available in the market, such as Apache Qpid, Apache ActiveMQ, and RabbitMQ. Among them, RabbitMQ is a kind of light-weight AMQP supporting library which is suitable for embedded devices.

For the future maintenance devices, the new communication protocol can be embedded when they are designed and manufactured. However, there are many existing maintenance devices which were deployed before the networked smart maintenance project and may not support the newly proposed communication protocol. Therefore, they must be modified.

As most of the mainstream devices are equipped with the communication ports, the most convenient way is to add a plug-in module over the old communication ports. The module is a bridge between the old and new communication protocols. It is able to translate the data from old format into the new format, as shown in Figure 5.

4.2. Data Storage. During OM work, various forms of data are generated by the equipment. Some of the data are structured like numerical data and texts. Some of the data are unstructured like spectrum, videos, and images. The two different kinds of data should be stored in different ways.

4.2.1. Structured Data Storage. The structured data are stored in the XML format. Extensible Markup Language (XML) is used to define the rules for encoding documents in a format which is readable not only for human but also for the machine. Comparing with the conventional data storage model, it has an object-oriented structure which is much easier to transplant, with good scalability, compatibility, and portability. Algorithm 1 is a sample of the test data which is collected from a substation in Wuhan.

4.2.2. Unstructured Data Storage. The plain unstructured data like images and spectrum are hardly searchable in database. Their characteristics need to be extracted before they can be effectively stored in database. Figure 6 shows the normalization for the images of the power equipment. It is based on sparse coding and visual dictionary technologies.

For the unstructured data which can be normalized, they are converted and stored inside the XML structure directly. For the data which cannot be normalized such as images and videos, the original data are stored inside the database and their characteristics are extracted and marked inside the XML.

5. Work Procedure with SOM Box

By applying the proposed closed-loop model, the OM efficiency, as well as the data reliability, can be greatly raised. The work procedure of OM using intelligent transportation box is as shown in Figure 7. Two kinds of users are involved in this whole system according to the division of labor.

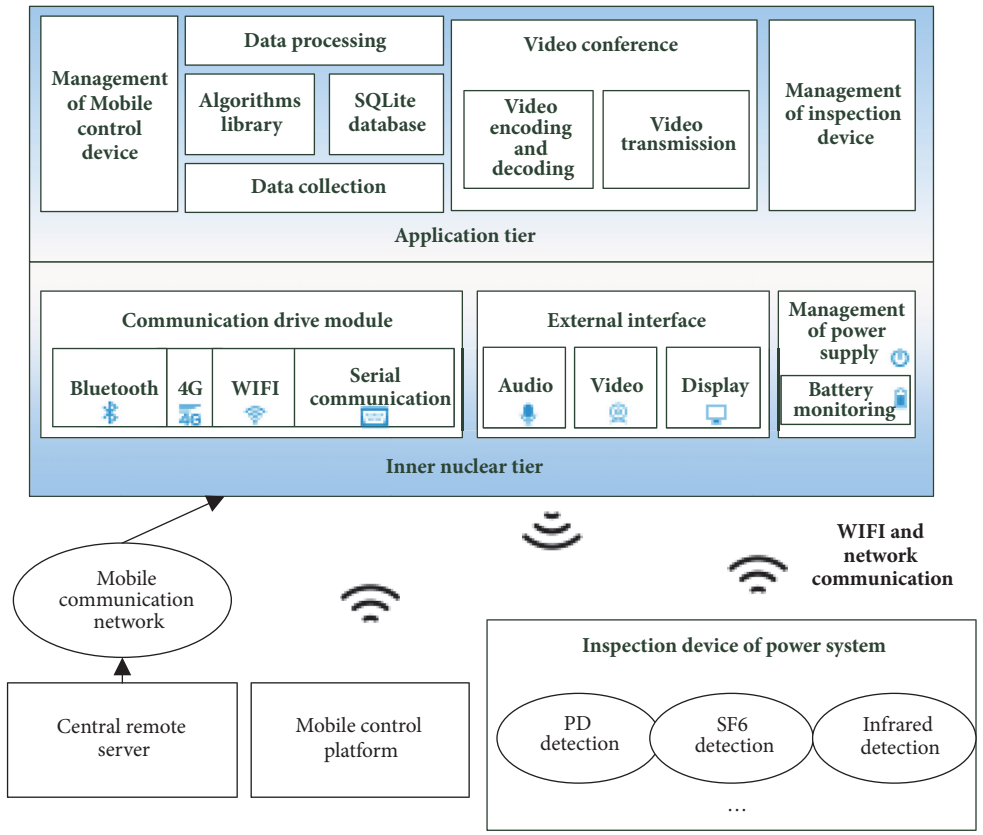

Figure 4: Software design of SOM box.

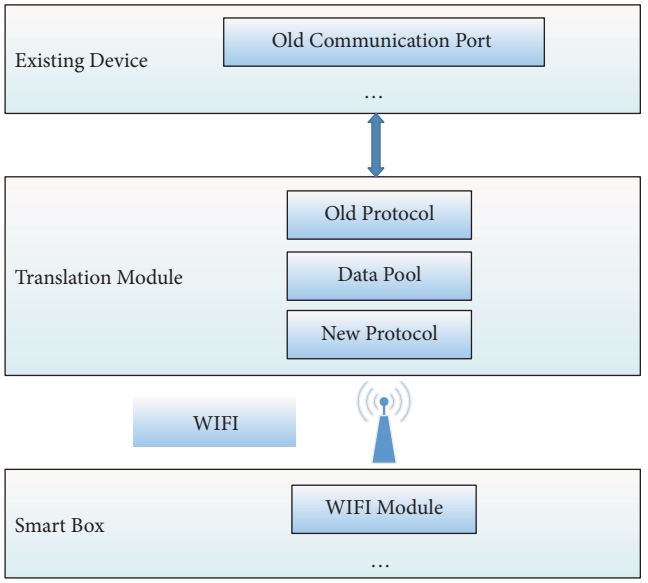

Figure 5: Modification of existing devices.

The project manager can comprehensively manage the substation inspection project. Firstly they assign and issue tasks for on-site OM personnel. Secondly, the data collected on site will be checked and they can supervise the completion of OM tasks. When the OM team encounters technical difficulties, they will respond to their call requests at any time and according to their needs arrange corresponding technical experts to conduct video conferences to solve their difficulties.

For the on-site OM team, under the supervision of the project manager, they can perform tasks through this APP, such as task downloading and data uploading on the live detection test to realize data interaction between the on-site and client-side. After that, live detection information will be displayed. With the networked closed-loop model, the team is also able to give the feedback of detection information to clients.

Seen from the work-flow, it can be concluded that the network closed-loop model greatly relieves the workload of the staff. The project manager is just responsible for management of the OM tasks through the web platform. In the on-site SOM, all devices are connected to the smart inspection box through the network, with unified management and unified data uploading. OM personnel do not need to manually record test data and can obtain real-time guidance through the network, which makes the entire OM work more efficient and reliable.

6. Conclusions

An on-site SOM system for substation equipment with a networked closed-loop model is proposed in this paper.

```
<TEST version="1.3">
        <DeviceInfo desc="Primary Device Information">
                <StationName>Wuhan Optical Valley East Substation</StationName>
         <Level desc="Voltage Level">500 kV</Level>
                .....
                <DeviceCode desc="Code">#12FF</DeviceCode>
        </DeviceInfo>
    <IED channelNum="2" desc="Partial Discharge Detection Device" vendor="Wuhan Nari" model="JFD-2000">
    ......
        </IED>
    <TestValue>
                <Channel chNo="1" sensorType="HFCT">
                        <Do name="AppDsch" desc="Apparent Discharge">
                                <Val>12</Val>
                                <t>2015-09-23 16:165:00.123</t>
                        </Do>
                </Channel>
                ......
    </TestValue>
    ...
    </TEST>
```

Algorithm 1

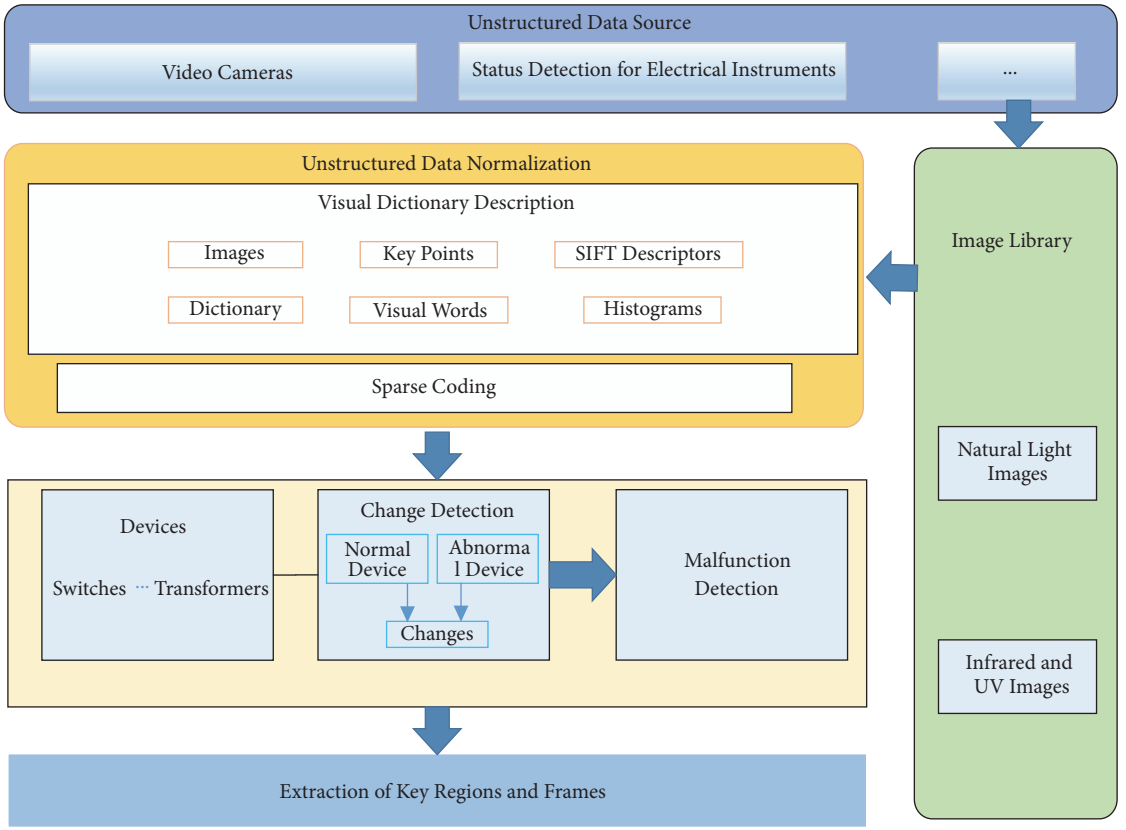

Figure 6: Transformation from nonstructural data to structural data.

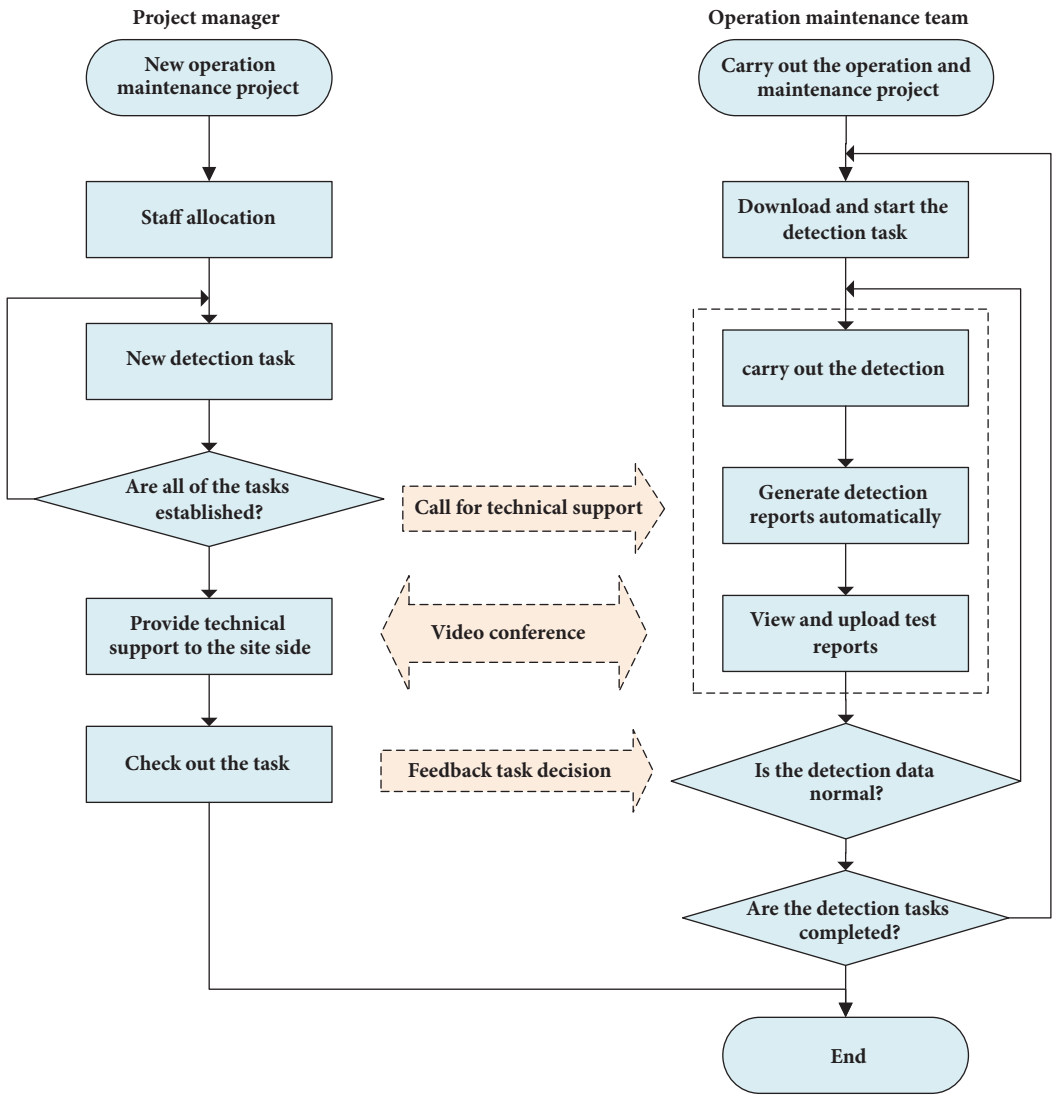

Figure 7: Workflow of OM work.

As a bridge to connect the communication with data, the networked closed-loop model based on an NCS integrates the control theory, communication technology, and computer technology together. It can be applied to a hugely complex system or remote control system because of its high information integration. In the proposed on-site SOM system, the networked closed-loop model takes intelligent field equipment as its material base and communicates high-speed Ethernet, to achieve the high efficiency and flexible operation, which in turn reduces the pressure on workers.

Data Availability

No data were used to support this study.

Conflicts of Interest

The authors declare that they have no conflicts of interest.

Acknowledgments

This work was supported by State Grid Corporation of China Science and Technology Project (524625160017).

References

[1] W. Zhang, M. S. Branicky, and S. M. Phillips, "Stability of networked control systems," *IEEE Control Systems Magazine*, vol. 21, no. 1, pp. 84–99, 2001.

[2] Y. Zhao, G. Liu, Y. Kang, and L. Yu, "A Brief Tutorial of Networked Control Systems," in *Packet-Based Control for Networked Control Systems*, pp. 1–11, Springer, Singapore, 2018.

[3] B. S. Reddy and S. Ulgiati, *Adoption of Smart-Grid Technologies by Electrical Utilities in India: An Exploratory Study of Issues and Challenges*, Springer, New Delhi, India, 2016.

[4] C. E. Gilbert, K. W. David, and K. J. Gregory, "Final Report on the Operation and Maintenance Improvement Program for Concentrating Solar Power Plants," Office of Scientific & Technical Information Technical Reports, 1999.

[5] Y. Hayashi, H. Fujimura, M. Furukawa, K. Shimizu, and Y. Hayasaka, "Operation and maintenance planning aiding system for power generation installation," US, US 20030004659 A1, 2003.

[6] R. S. Atlason and R. Unnthorsson, "Operation and Maintenance in Icelandic Geothermal Power Plants: Structure and Hierarchy," in *Proceedings of the ASME 2013 Power Conference*, Boston, Mass, USA, article V001T05A007, 2013.

[7] R. Bayindir, E. Hossain, and S. Vadi, "The path of the smart grid -the new and improved power grid," in *Proceedings of the 2016 International Smart Grid Workshop and Certificate Program (ISGWCP)*, pp. 1–8, Istanbul, Turkey, March 2016.

[8] L. Wang, Q. Chen, H. Gao, Z. Ma, Y. Zhang, and D. He, "Framework of Fault Trace for Smart Substation Based on Big Data Mining Technology," *Automation of Electric Power Systems*, vol. 42, no. 3, pp. 84–91, 2018.

[9] N. Ivancevic, "Information technology communications cabinet for electrical substation communications," US, US20060269207, 2006.

[10] H. Zamanian, J. Ghaisari, and F. Sheikholeslam, "Robust networked control of load frequency in multi-area interconnected power system," in *Proceedings of the 25th Iranian Conference on Electrical Engineering, ICEE 2017*, pp. 1126–1131, May 2017.

[11] K. Nimma and S. Faraj, "Modeling Intelligent Control Switch IEC 61850 Based Substation Automation Communication," *Applied System Innovation*, vol. 1, no. 1, p. 7, 2018.

[12] Y. B. Zhao, G. P. Liu, Y. Kang, and L. Yu, "Stochastic Stabilization of Packet-Based Networked Control Systems," in *Packet-Based Control for Networked Control Systems*, pp. 77–85, Springer, Singapore, 2018.

[13] Y. Wang and S. Yu, "An improved dynamic quantization scheme for uncertain linear networked control systems," *Automatica*, vol. 92, pp. 244–248, 2018.

[14] L. Litz, T. Gabriel, M. Groß, and O. Gabel, "Networked Control Systems (NCS) – Stand und Ausblick (Networked Control Systems (NCS) – State of the Art and Future)," *at - Automatisierungstechnik*, vol. 56, no. 1, pp. 4–19, 2008.

[15] G. C. Goodwin, H. Haimovich, D. E. Quevedo, and J. S. Welsh, "A moving horizon approach to networked control system design," *IEEE Transactions on Automatic Control*, vol. 49, no. 9, pp. 1427–1445, 2004.

[16] T. C. Yang, "Networked control system: a brief survey," *IEE Proceedings Control Theory and Applications*, vol. 153, no. 4, pp. 403–412, 2006.

[17] A. Sala, Á. Cuenca, and J. Salt, "A retunable PID multirate controller for a networked control system," *Information Sciences*, vol. 179, no. 14, pp. 2390–2402, 2009.

[18] L. Cheng, W. Hu, Z. Liu, and W. Cai, "On-site Smart Operation and Maintenance System for Substation Equipment Based on Mobile Network," *International Journal of Online Engineering (iJOE)*, vol. 14, no. 3, pp. 66–80, 2018.

[19] S. P. Dulman, "Maintenance operations console for an advanced intelligent network," in *US 5802146 A*, 1998.

[20] B. Qian, Z. Liu, L. Zhang, and J. Chen, "Study on the supplementary VR visual platform for intelligent substation operation and maintenance," *Electrical Automation*, vol. 40, no. 1, pp. 30–32, 2018.

Hindawi
Journal of Control Science and Engineering
Volume 2018, Article ID 2316957, 8 pages
https://doi.org/10.1155/2018/2316957

Research Article

Neural Network Predictive Control for Autonomous Underwater Vehicle with Input Delay

Jiemei Zhao

School of Mathematics and Computer Science, Wuhan Polytechnic University, Wuhan 430023, China

Correspondence should be addressed to Jiemei Zhao; jiemeizhao@163.com

Received 6 January 2018; Accepted 24 April 2018; Published 29 May 2018

Academic Editor: Jongrae Kim

A path tracking controller is designed for an autonomous underwater vehicle (AUV) with input delay based on neural network (NN) predictive control algorithm. To compensate for the time-delay in control system and realize the purpose of path tracking, a predictive control algorithm is proposed. An NN is used to estimate the nonlinear uncertainty of AUV induced by hydrodynamic coefficients and the coupling of the surge, sway, and yaw angular velocity. By Lyapunov theorem, stability analysis is also given. Simulation results show the effectiveness of the proposed control strategy.

1. Introduction

With the rapid development of demands for the resources, countries around the world have attached importance to the exploration and application of the marine resources. Autonomous underwater vehicle (AUV) is a mobile carrier which is small in size and convenient in controllability as the special equipment for resource exploration, environmental monitoring, and ocean investigation. It has the ability for long-time navigating and great-weight carrying and satisfies the different demands of the fields of military science and economics (see [1–3] and references therein).

In recent years, control problems of AUV such as setpoint stabilization, trajectory tracking control, and path tracking control have been actively considered by many researchers. Based on nonlinear control theory, several control methods have been proposed, such as sliding mode control [4–6], adaptive control [7–11], and predictive control [12–15]. However, a common problem of the above literatures is that the time-delays are not taken into account. In practical systems, time-delays are unavoidable in information acquisition and transmission. Time-delay phenomenon is often a source of instability and poor performance [16–18]. From this point of view, considerable amount of attention has been paid to the problem of stabilization and control of time-delay systems. Predictive control is a good method with the ability to handle constraints and time-delays [19–23]. Now, it has become one of the most popular control methodologies no matter in theory or the reality (see [24–27]). The NN predictive control for nonlinear dynamic systems with input delay was studied in [24], but the considered predictive model is required for linear ones and this condition is removed in this paper. The predictor-based control algorithm for an uncertain input delay Euler-Lagrange system was studied in [26], but the controller is an iteration form. To overcome the problem of input delay in Euler-Lagrange dynamical systems directly, a predictor with uncertain system dynamics was proposed in [27]. Recently, predictive control has been applied in many kinds of practical systems [28–31]. Up to now, only a few papers have considered this problem because of its complexity. Paper [32] addressed the control problem with input delay and synthesized a robust controller for underwater vehicles which requires only knowledge of mass matrix. The region tracking problem for AUV with input delay based on predictive control was studied in [33], but it assumes that all the states are known in advance. Therefore, it is a very challenging and significant work to investigate the path tracking control of AUV with input delay.

In this paper, a novel controller is investigated for path tracking control of AUV with input delay. Because of the hydrodynamic coefficients and the surge, sway, and yaw angular velocity coupling, an NN is used to identify the

nonlinear part of AUV at first. Then predictive control algorithm is employed to compensate for the delay produced in input channel. The proposed predictive model is a nonlinear model. Stability of the closed-loop system is guaranteed based on Lyapunov stability theory. Finally, a simulation example is presented to show the effectiveness of the proposed control strategy.

The remainder of this paper is organized as follows. The problem of path tracking for AUV is formulated in Section 2. Section 3 is devoted to identification of AUV system by NN. Stability analysis for the boundness of error state and NN weight estimation error are also performed. The predictor and the corresponding control are derived in Section 4. The problems of dealing with the time-delay and stability analysis are illustrated in Section 5. Section 6 validates the feasibility and performance of the proposed control law by simulation experiment. Some conclusions are given in Section 7.

2. Problem Formulation

In the horizontal plane, a 3-DOF AUV with input delay can be modeled as

$$\begin{aligned} \dot{\eta} &= J(\eta)\nu, \\ M\dot{\nu} + C(\nu)\nu + D(\nu)\nu + g(\eta) &= \overline{\tau}(t-d), \\ h &= \eta, \end{aligned} \tag{1}$$

where $\eta = [x \;\; y \;\; \psi]^T$ denotes the vehicle location and orientation in the earth-fixed frame. The vector $\nu = [u \;\; v \;\; r]^T$ is the velocities expressed in the body-fixed frame. $M = M_{RB} + M_A$ is the inertia matrix of rigid body M_{RB} with added mass M_A. The matrix $C(\nu)$ is skew symmetrical and it denoted the Coriolis and centripetal forces. Linear and quadratic damping forces are considered in the total hydrodynamic damping matrix $D(\nu)$. The vector $g(\eta)$ is the combined gravitational and buoyancy forces in the body-fixed frame. $\overline{\tau}$ is the input of the system and the vector of the forces and moments on AUV induced by the input and fins. d is a known constant time-delay. h is the output of the system. The kinematic transformation matrix transformation from the body-fixed frame to earth-fixed frame is denoted by $J(\eta)$, and

$$J(\eta) = R(\psi) = \begin{bmatrix} \cos\psi & -\sin\psi & 0 \\ \sin\psi & \cos\psi & 0 \\ 0 & 0 & 1 \end{bmatrix}. \tag{2}$$

Let

$$\begin{aligned} \xi_1 &= \eta, \\ \xi_2 &= J(\eta)\nu. \end{aligned} \tag{3}$$

Then system (1) changed to

$$\begin{aligned} \dot{\xi}_1 &= \xi_2, \\ \dot{\xi}_2 &= f(\xi_1, \xi_2) + J(\xi_1) M^{-1} \overline{\tau}(t-d), \\ y &= \xi_1, \end{aligned} \tag{4}$$

where nonlinear uncertain function

$$\begin{aligned} f(\xi_1, \xi_2) &= \dot{J}(\xi_1) J^{-1}(\xi_1)\xi_2 + J(\xi_1) \\ &\cdot M^{-1}\left[-C\left(J^{-1}(\xi_1)\xi_2\right)\right. \\ &\left. - D\left(J^{-1}(\xi_1)\xi_2\right) J^{-1}(\xi_1)\xi_2 - g(\xi_1)\right]. \end{aligned} \tag{5}$$

The objective of this paper is that the output y of system (4) tracks a desired trajectory η_d, with all internal signals and control commands remaining bounded. For this purpose, we make the following assumption.

Assumption 1. The desired trajectory vector $\zeta_d = [\eta_d \;\; \dot{\eta}_d \;\; \ddot{\eta}_d]^T$ is available for measurement, and η_d and $\dot{\eta}_d$ are bounded.

3. Identification of AUV System

There are two steps to design the output feedback controller for AUV with input delay. First, an NN is designed to identify system (4). Then we will use predictive control algorithm to compensate for the delay that presents in communication channel of AUV.

Let

$$\begin{aligned} A &= \begin{bmatrix} 0 & I_3 \\ A_1 & A_2 \end{bmatrix}, \\ B &= \begin{bmatrix} 0 \\ I_3 \end{bmatrix}, \\ C &= [I_3 \;\; 0]^T, \end{aligned} \tag{6}$$

where I_3 denotes the identity matrix; matrices A_1 and A_2 are parameters that can be chosen such that matrix A is stable. Then there exist symmetric positive definite matrices P and Q such that Lyapunov matrix equations $A^T P + PA = -Q$ hold.

Hence, system (4) can be expressed as

$$\begin{aligned} \dot{\xi} &= A\xi + B\left[f_0(\xi) + \tau(t-d)\right], \\ y &= C^T\xi, \end{aligned} \tag{7}$$

where $\xi = \left[\xi_1^T \;\; \xi_2^T\right]^T$, $\tau(t-d) = J(\xi_1)M^{-1}\overline{\tau}(t-d)$, and $f_0(\xi) = f(\xi) - A_1\xi_1 - A_2\xi_2$.

According to the approximation of NN, there exists a bounded reconstruction error $\varepsilon(\|\varepsilon\| \le \overline{\varepsilon})$ and an ideal weight W such that system (4) is described by

$$\begin{aligned} \dot{\xi} &= A\xi + B\left[W^T\Phi(\xi) + \tau(t-d) + \varepsilon\right], \\ y &= C^T\xi, \end{aligned} \tag{8}$$

where W is the ideal NN weight and $\|W\| \le \overline{W}$ ($\overline{W}$ is a positive constant). The sigmoid function $\Phi(Z) = [\Phi_1(Z), \Phi_2(Z), \cdots, \Phi_n(Z)]^T \in R^n$ is differentiable with respect to x and $\|\Phi(\cdot)\| \le \overline{\Phi}$ holds with a positive constant $\overline{\Phi}$.

Then the NN of system (8) can be written as

$$\begin{aligned}\dot{\widehat{\xi}} &= A\widehat{\xi} + B\left[\widehat{W}^T\Phi\left(\widehat{\xi}\right) + \tau\left(t-d\right)\right],\\ \widehat{y} &= C^T\widehat{\xi},\end{aligned} \tag{9}$$

where $\widehat{\xi}$ is a state vector of NN and $\widehat{W}$ is a synaptic weight matrix. The sigmoid function $\Phi(x) = a/(1+e^{-bx}) + c, \forall a, b \in R^+, c \in R$, where a, b, and the real number c are the bound, the slope, and the bias of sigmoidal curvature, respectively.

Let estimation error $\widetilde{\xi} = \xi - \widehat{\xi}$, output error $\widetilde{y} = y - \widehat{y}$, and NN weight error $\widetilde{W} = W - \widehat{W}$. Using (8) and (9), we have

$$\begin{aligned}\dot{\widetilde{\xi}} &= A\widetilde{\xi} + B\left[W^T\Phi\left(\xi\right) - \widehat{W}^T\Phi\left(\widehat{\xi}\right) + \varepsilon\right],\\ \widetilde{y} &= C^T\widetilde{\xi}.\end{aligned} \tag{10}$$

Next, a main result will be given. In the following, $\lambda_{\mathrm{m}}(P)$ and $\lambda_{\mathrm{M}}(P)$ denote the minimum and maximum eigenvalue of corresponding matrix P.

Theorem 2. *Consider system (1) with the identification model (9) and conditions (19). Let the NN weight update law be provided by*

$$\dot{\widehat{W}} = \Gamma\left(\widehat{y}^T\Phi\left(\widehat{\xi}\right) - \mu\widehat{W}\right), \tag{11}$$

in which $\Gamma = \Gamma^T > 0$ is the learning parameter and μ is a constant. Then the estimation error $\widetilde{\xi}$ and neural network weight error $\widetilde{W}$ are uniformly ultimately bounded (UUB).

Proof. Consider a Lyapunov function defined by

$$V = \frac{1}{2}\widetilde{\xi}^T P\widetilde{\xi} + \frac{1}{2}\operatorname{tr}\left(\widetilde{W}^T\Gamma^{-1}\widetilde{W}\right). \tag{12}$$

Calculate the derivative (12) along (10) and (11); we have

$$\begin{aligned}\dot{V} = &-\frac{1}{2}\widetilde{\xi}^T Q\widetilde{\xi} + \widetilde{\xi}^T PB\left[W^T\Phi\left(\xi\right) - \widehat{W}^T\Phi\left(\widehat{\xi}\right) + \varepsilon\right]\\ &+ \operatorname{tr}\left(\widetilde{W}^T\Gamma^{-1}\dot{\widetilde{W}}\right).\end{aligned} \tag{13}$$

From (11), it follows that

$$\begin{aligned}\dot{V} = &-\frac{1}{2}\widetilde{\xi}^T Q\widetilde{\xi} + \widetilde{\xi}^T PB\left[W^T\Phi\left(\xi\right) - \widehat{W}^T\Phi\left(\widehat{\xi}\right) + \varepsilon\right]\\ &- \widetilde{y}\widetilde{W}^T\Phi\left(\widehat{\xi}\right) + \mu\operatorname{tr}\left(\widetilde{W}^T\widehat{W}\right).\end{aligned} \tag{14}$$

From the definition of $\widetilde{W}$, we obtain the following equation:

$$\operatorname{tr}\left(\widetilde{W}^T\widehat{W}\right) = \operatorname{tr}\left(\widetilde{W}^T\left(W - \widetilde{W}\right)\right) = W^T\left\|\widetilde{W}\right\| - \left\|\widetilde{W}\right\|^2. \tag{15}$$

Moreover, there exist three positive constants α_1, α_2, and α_3 such that

$$\left\|W^T\Phi\left(\xi\right) - \widehat{W}^T\Phi\left(\widehat{\xi}\right) + \varepsilon\right\| \le \alpha_1\left\|\widetilde{\xi}\right\| + \alpha_2\left\|\widetilde{W}\right\| + \alpha_3. \tag{16}$$

So

$$\begin{aligned}\dot{V} \le &-\left(\frac{1}{2}\lambda_{\mathrm{m}}\left(Q\right) - \alpha_1\left\|PB\right\|\right)\left\|\widetilde{\xi}\right\|^2\\ &+ \left(\alpha_2\left\|PB\right\| + \overline{\Phi}\right)\left\|\widetilde{W}\right\|\left\|\widetilde{\xi}\right\| + \alpha_3\left\|PB\right\|\left\|\widetilde{\xi}\right\|\\ &+ \mu\overline{W}\left\|\widetilde{W}\right\| - \mu\left\|\widetilde{W}\right\|^2.\end{aligned} \tag{17}$$

According to Young's inequality $ab \le (a^2 + \kappa^2 b^2)/2\kappa$ with $\kappa > 0$; then there are $\kappa_0 > 0$, $\kappa_1 > 0$ and $\kappa_2 > 0$ such that

$$\begin{aligned}\left\|\widetilde{W}\right\|\left\|\widetilde{\xi}\right\| &\le \frac{\left\|\widetilde{\xi}\right\|}{2\kappa_0} + \frac{\kappa_0}{2}\left\|\widetilde{W}\right\|^2,\\ \alpha_3\left\|PB\right\|\left\|\widetilde{\xi}\right\| &\le \frac{\left(\alpha_3\left\|PB\right\|\right)^2}{2\kappa_1} + \frac{\kappa_1}{2}\left\|\widetilde{\xi}\right\|^2,\\ \left\|W\right\|\left\|\widetilde{W}\right\| &\le \frac{\left\|W\right\|^2}{2\kappa_2} + \frac{\kappa_2}{2}\left\|\widetilde{W}\right\|^2.\end{aligned} \tag{18}$$

Assume that

$$\begin{aligned}R_1 &= \frac{1}{2}\lambda_{\mathrm{m}}\left(Q\right) - \alpha_1\left\|PB\right\| - \frac{1}{2\kappa_0} - \frac{1}{2}\kappa_1 > 0,\\ R_2 &= \mu - \frac{1}{2}\mu\kappa_2 - \frac{1}{2}\kappa_0 > 0.\end{aligned} \tag{19}$$

Then

$$\dot{V} \le -R_1\left\|\widetilde{\xi}\right\|^2 - R_2\left\|\widetilde{W}\right\|^2 + R_3 \le -\eta V + R_3, \tag{20}$$

where

$$\begin{aligned}\eta &= \min\left\{\frac{R_1}{\lambda_{\mathrm{M}}\left(P\right)}, R_2\right\},\\ R_3 &= \frac{\alpha_3^2\left\|PB\right\|^2}{2\kappa_1} + \frac{\left\|W\right\|^2}{2\kappa_2}.\end{aligned} \tag{21}$$

Thus, estimator error $\widetilde{\xi}$ and NN weight error $\widetilde{W}$ are UUB. □

4. Predictive Control

Input delay (measurement delay and computational delay can be represented by input delay) is a source of instability, which is frequently encountered in the practical systems. For achieving tracking performance, a predictive controller is proposed to compensate for the time-delay present in AUV. Figure 1 is the control structure diagram of AUV system (1).

In fact, the NN weight $\widehat{W}$ stores the dynamical system information. Based on the structure of NN in (9), an online predictor is proposed. For improving the accuracy of path tracking effectively, the nonlinear prediction model is employed here. Now, let the predictor of system (8) be

$$\begin{aligned}\dot{\xi}_p\left(t+d \mid t\right) &= A\xi_p\left(t+d \mid t\right)\\ &\quad + B\left[\widehat{W}^T\Phi\left(\xi_p\left(t+d \mid t\right)\right) + \tau\left(t\right)\right],\\ y_p\left(t+d \mid t\right) &= C^T\xi_p\left(t+d \mid t\right),\end{aligned} \tag{22}$$

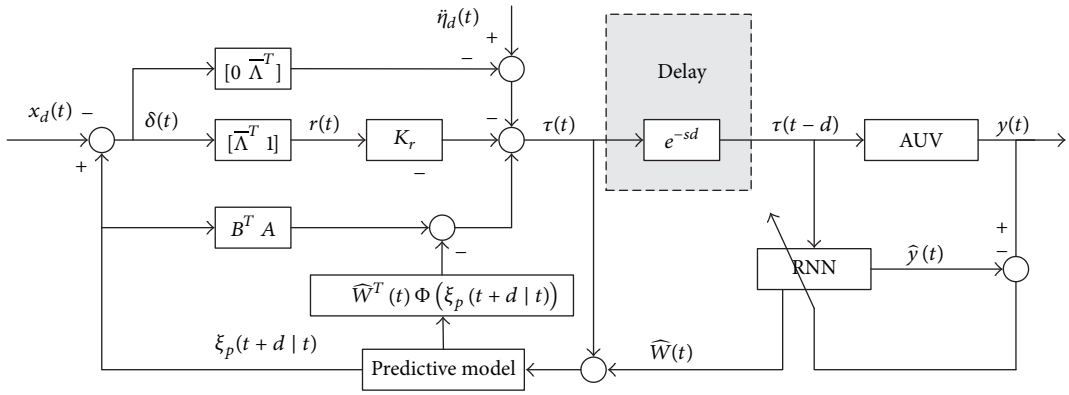

Figure 1: Control structure of AUV system (1).

where $\xi_p(t+d \mid t)$ and $y_p(t+d \mid t)$ are the prediction state and output of system (8) with the initial condition $\xi_p(d \mid 0) = \xi(0)$.

If prediction model (22) is precise, then $\xi_p(t+d \mid t) = \xi(t+d)$. This mean that ξ ahead of time d can be predicted via $\xi_p(t+d \mid t)$ in prediction model. Therefore, the difficulty in controlling time-delay plant can be overcome. However, due to the modeling errors, in prediction model (22) errors exist inevitably. Now, define a predictor error as $e(t) = \xi(t+d) - \xi_p(t+d \mid t)$. It follows from (8) and (22) that

$$\begin{aligned}\dot{e}(t) &= Ae(t) + B\left[W^T\Phi(\xi(t+d)) - \widehat{W}^T(t)\Phi\left(\xi_p(t+d \mid t)\right) + \varepsilon(t+d)\right],\\ y_e(t) &= C^T e(t).\end{aligned} \tag{23}$$

Next, we will prove that the predictor error (23) is bounded. Define an error vector as

$$\delta(t) = \xi_p(t+d \mid t) - \eta_d(t). \tag{24}$$

Define a filtered error as

$$r(t) = \Lambda^T\delta(t) = \left[\overline{\Lambda}^T\ \ 1\right]\delta(t), \tag{25}$$

where $\overline{\Lambda} = [\lambda_1\ \ \lambda_2]^T$ is an appropriately chosen coefficient vector such that $\delta(t) \to 0$ exponentially as $r(t) \to 0$. Then, using (22), the filtered error can be written as

$$\begin{aligned}\dot{r}(t) &= \Lambda^T\dot{\delta}(t) = \Lambda^T\left[A\xi_p(t+d \mid t) + B\left(\widehat{W}^T\Phi\left(\xi_p(t+d \mid t)\right) + \tau(t)\right)\right]\\ &= \left[0\ \ \overline{\Lambda}^T\right]\delta(t) - \ddot{\eta}_d + B^T A\xi_p(t+d \mid t) + \widehat{W}^T\Phi\left(\xi_p(t+d \mid t)\right) + \tau(t).\end{aligned} \tag{26}$$

Now choose $K_r > 0$ and let

$$\begin{aligned}\tau(t) &= -\left[0\ \ \overline{\Lambda}^T\right]\delta(t) + \ddot{\eta}_d - B^T A\xi_p(t+d \mid t) - \widehat{W}^T\Phi\left(\xi_p(t+d \mid t)\right) - K_r r(t)\\ &= -\left[0\ \ \overline{\Lambda}^T\right]\delta(t) + \ddot{\eta}_d - B^T A\delta(t) - B^T A\eta_d(t) - \widehat{W}^T\Phi\left(\xi_p(t+d \mid t)\right) - K_r r(t).\end{aligned} \tag{27}$$

That is, a control input of AUV is

$$\begin{aligned}\overline{\tau}(t) &= MJ^{-1}(\xi_1)\Big(-\left[0\ \ \overline{\Lambda}^T\right]\delta(t) + \ddot{\eta}_d - B^T A\xi_p(t+d \mid t) - \widehat{W}^T\Phi\left(\xi_p(t+d \mid t)\right) - K_r r(t)\Big)\\ &= MJ^{-1}(\xi_1)\Big(-\left[0\ \ \overline{\Lambda}^T\right]\delta(t) + \ddot{\eta}_d - B^T A\delta(t) - B^T Ax_d(t) - \widehat{W}^T\Phi\left(\xi_p(t+d \mid t)\right) - K_r r(t)\Big).\end{aligned} \tag{28}$$

Note that the predictor state $\xi_p(t+d \mid t)$ and the associated error $r(t)$ are used in AUV controller (28); the NN approximation term $\widehat{W}^T(t)\Phi(\xi_p(t+d \mid t))$ from (22) is employed to accommodate the unknown nonlinearity. Therefore, the stability of the closed-loop system can be guaranteed.

From (28), (26) becomes

$$\dot{r}(t) = -K_r r(t). \tag{29}$$

5. Stability Analysis

Assume that the parameters are chosen such that

$$\begin{aligned}R_4 &= R_2 + \frac{1}{2}\kappa_3 > 0,\\ R_5 &= \frac{1}{2}\lambda_{\mathrm{m}}(Q)\frac{1}{2\kappa_3} - \frac{1}{2}\kappa_4 - \beta_2 > 0,\\ R_6 &= -K_r > 0,\end{aligned} \tag{30}$$

where R_2 is defined as in Theorem 2 and κ_3, κ_4 are positive constants that can be chosen.

Theorem 3 (let Assumption 1 hold). *Consider the input delay AUV system (1) under condition (30), the NN weight update law (11), and controller (28). Then*

(1) *all the closed-loop signals are UUB;*

(2) *the path tracking error $\omega(t) = y(t+d) - \eta_d(t)$ converges to a neighborhood of the origin, whose size can be adjusted by control parameters.*

Proof. Consider a Lyapunov function defined by

$$\begin{aligned}\overline{V} &= \frac{1}{2}\widetilde{\xi}^T P\widetilde{\xi} + \frac{1}{2}\widetilde{W}^T\Gamma^{-1}\widetilde{W} + \frac{1}{2}e^T Pe + \frac{1}{2}r^2 \\ &\coloneqq V_1 + V_2 + V_3 + V_4.\end{aligned} \tag{31}$$

The derivative of V_1 and V_2 can be deduced following the proof of Theorem 2. Thus we have

$$\begin{aligned}\dot{V}_3 = {} & \frac{1}{2}e^T\left(A^T P + PA\right)e + e^T PB\left[W^T\Phi\left(\xi\left(t+d\right)\right)\right. \\ & \left. - \widehat{W}^T\Phi\left(\xi_p\left(t+d \mid t\right)\right) + \varepsilon\left(t+d\right)\right].\end{aligned} \tag{32}$$

In fact, via Taylor series expansion, there exist positive constants β_1, β_2, and β_3 such that

$$\begin{aligned}&\left\|W^T\Phi\left(\xi\left(t+d\right)\right) - \widehat{W}^T\Phi\left(\xi_p\left(t+d \mid t\right)\right)\right\| \\ &\quad = \left\|\widetilde{W}\Phi\left(\xi_p\left(t+d \mid t\right)\right)\right. \\ &\quad \left. + W^T\left[\Phi\left(\xi\left(t+d\right)\right) - \Phi\left(\xi_p\left(t+d \mid t\right)\right)\right]\right\| \\ &\quad \le \beta_1\left\|\widetilde{W}\right\| + \beta_2\|e\| + \beta_3.\end{aligned} \tag{33}$$

So

$$\dot{V}_3 \le -\frac{1}{2}Q_{\mathrm{m}}\|e\|^2 + \|e\|\left(\beta_1\left\|\widetilde{W}\right\| + \beta_2\|e\| + \beta_3 + \overline{\varepsilon}\right). \tag{34}$$

By using Young's inequality, there exist positive numbers κ_3 and κ_4 such that

$$\begin{aligned}\|e\|\left\|\widetilde{W}\right\| &\le \frac{\|e\|^2}{2\kappa_3} + \frac{\kappa_3}{2}\left\|\widetilde{W}\right\|^2, \\ \left(\beta_3 + \overline{\varepsilon}\right)\|e\| &\le \frac{\left(\beta_3 + \overline{\varepsilon}\right)^2}{2\kappa_4} + \frac{\kappa_4}{2}\|e\|^2,\end{aligned} \tag{35}$$

$$\begin{aligned}\dot{V}_3 \le {} & -\left(\frac{1}{2}Q_{\mathrm{m}} - \frac{1}{2\kappa_3} - \frac{1}{2}\kappa_4 - \beta_2\right)\|e\|^2 \\ & + \frac{1}{2}\kappa_3\left\|\widetilde{W}\right\| + \frac{\left(\beta_4 + \overline{d} + \overline{\varepsilon}\right)^2}{2\kappa_4},\end{aligned} \tag{36}$$

$$\dot{V}_4 = r\dot{r} = -K_r\|r\|^2. \tag{37}$$

Therefore,

$$\begin{aligned}\dot{\overline{V}} &\le -R_1\left\|\widetilde{\xi}\right\|^2 - R_4\left\|\widetilde{W}\right\|^2 - R_5\|e\|^2 - R_6\|r\|^2 + R_7 \\ &\le -\overline{\eta}\overline{V} + R_7,\end{aligned} \tag{38}$$

where R_1 is defined as in (19), and $\overline{\eta}$ is positive constant defined by

$$\begin{aligned}\overline{\eta} &= \min\left\{\frac{R_1}{\lambda_{\max}(P)}, R_4, \frac{R_5}{\lambda_{\max}(P)}, R_6\right\}, \\ R_7 &= R_3 + \frac{\left(\beta_4 + \overline{d} + \overline{\varepsilon}\right)^2}{2\kappa_4}.\end{aligned} \tag{39}$$

Then according to Lyapunov theorem, error $\widetilde{\xi}$, NN weight error $\widetilde{W}$, predictor error e, and filtered error r are all UUB. The control error δ is thus bounded based on (24) and Assumption 1. Therefore, the NN weights $\widehat{W}$ and $\xi_p(t+d \mid t)$ are bounded.

Finally, the boundedness of path tracking error $\omega(t)$ will be proved. Since

$$\begin{aligned}\omega\left(t\right) &= y\left(t+d\right) - \eta_d\left(t\right) \\ &= \xi_1\left(t+d\right) - \xi_{p1}\left(t+d \mid t\right) + \xi_{p1}\left(t+d \mid t\right) \\ &\quad - y_d = e_1\left(t\right) + \delta_1\left(t\right),\end{aligned} \tag{40}$$

then

$$\begin{aligned}\lim_{t\to\infty}\|\omega\left(t\right)\| &= \lim_{t\to\infty}\left\|e_1\left(t\right)\right\| + \lim_{t\to\infty}\left\|\delta_1\left(t\right)\right\| \\ &\le \lim_{t\to\infty}\|e\left(t\right)\| + \lim_{t\to\infty}\|\delta\left(t\right)\|.\end{aligned} \tag{41}$$

Therefore, the tracking error $\omega(t)$ is bounded because $e(t)$, $\delta(t)$, and $\xi(t)$ are bounded. □

Remark 4. Compared with [20–33], there are three advantages. Firstly, output feedback is considered in this paper. Secondly, the nonlinear prediction model is employed to improve the accuracy of predictive control. Finally, time-delay is considered in path tracking control of AUV which has more real significance.

6. Simulation Analysis

Example 5. The simplified dynamics model of INFANTE AUV [2] in the horizontal plane with input delay is adopted as follows in this paper:

$$\begin{aligned}\dot{x} &= u\cos\left(\psi\right) - v\sin\left(\psi\right), \\ \dot{y} &= u\sin\left(\psi\right) + v\cos\left(\psi\right), \\ \dot{\psi} &= r, \\ 0 &= m_v\dot{v} + m_{ur}ur + d_v, \\ \Gamma &= m_r\dot{r} + d_r,\end{aligned} \tag{42}$$

where x, y, and ψ are the surge position, sway position, and yaw angle in the body-fixed frame, and u, v, and r denote surge, sway, and yaw velocities, respectively. Γ is the yaw moment. The symbol I_z denotes the moment of inertia of the AUV, $N_{\{\cdot\}}$ is nonlinear hydrodynamic damping, and

$$
\begin{aligned}
m_v &= m - Y_{\dot{v}},\\
m_{ur} &= m - Y_r,\\
d_v &= -Y_v uv - Y_{v|v|} v|v|,\\
m_r &= I_z - N_{\dot{r}},\\
d_r &= -N_v uv - N_{v|v|} v|v| - N_r ur.
\end{aligned} \tag{43}
$$

Since the considered model (42) is in the horizontal plane and has no disturbance, we can assume that $u = 1m/s$ in principle. In the following, the desired path is $x_d(t) = 20\sin 2\pi t/200$, $y_d(t) = 20 - 20\cos 2\pi t/200$, and $\psi_d(t) = 2\pi t/200$.

The model parameters of INFANTE AUV are as follows:

$$
\begin{aligned}
m &= 2234.5kg,\\
I_z &= 2000Nm^2,\\
X_{\dot{u}} &= -142kg,\\
N_{\dot{r}} &= -1350Nm^2,\\
Y_{\dot{v}} &= -1715kg,\\
Y_v &= -346kg/m,\\
Y_r &= 435kg,\\
N_v &= -686kg,\\
N_r &= -1427kgm,\\
Y_{v|v|} &= -667kg/m,\\
N_{v|v|} &= 443kg.
\end{aligned} \tag{44}
$$

NN parameters are selected as follows: $\Phi(x) = 1/(1 + e^{-ax})$, where $a = 0.5$, $\mu = 0.3, \Gamma = 6$.

The delay constant $d = 2$. Other parameters in controller are $A_1 = -3I_3$, $A_2 = -2I_3$, $\lambda_1 = 2$, $\lambda_2 = 2$, and $K_r = 8$.

The initial position and the surge speed of the AUV are $(0, 20)$ and $0m/s$, respectively. The simulation results are shown in Figures 2–4. The path tracking errors in x, y, and ψ are given in Figure 2. The control forces in x and y and the control torque of yaw ψ are given in Figure 3. From these simulation figures, we can see that the tracking performance is unsatisfying at the beginning of simulation; this is because the controller performs mainly depending on the adaptive control. The good tracking of position is obtained by the proposed adaptive NN predictive controller by and by. Figure 4 is the path tracking in horizontal plane. From Figure 4 we can see that AUV can realize tracking control smoothly and converge to the desired trajectory.

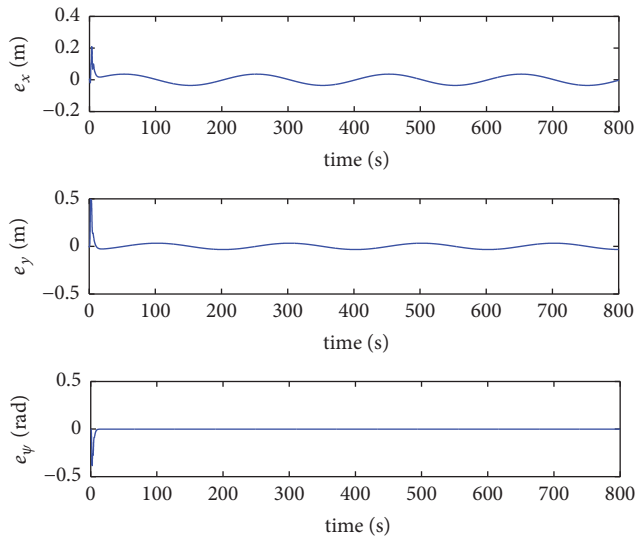

Figure 2: Path tracking errors.

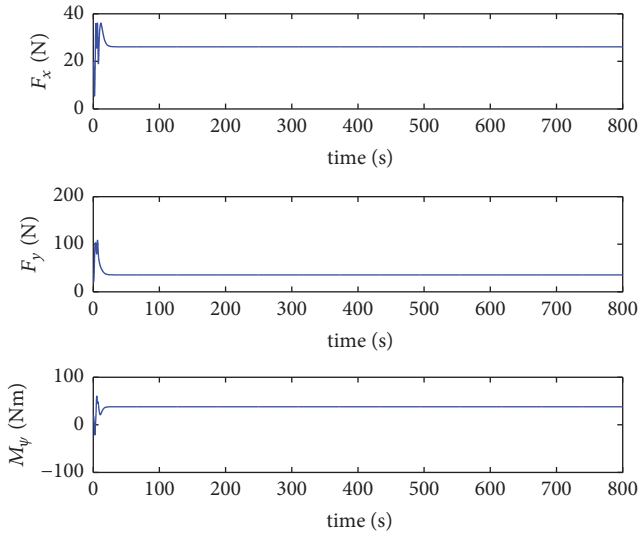

Figure 3: Control forces in x and y and control torque of yaw.

7. Conclusion

This paper investigates the path tracking problem for an AUV with input delay. Based on predictive and adaptive NN control theory, a predictive controller is given. The output feedback control algorithm is employed here. The NN is used to estimate the dynamic uncertain nonlinear function induced by hydrodynamic coefficients and coupling of the surge, sway, and yaw angular velocity. The predictive control is introduced to compensate the input delay present in AUV. The stability of the controller was analyzed by Lyapunov theorem. Simulation results showed that the proposed controller performs well with stability.

Data Availability

We are sorry that we cannot share the data in our article now because future works are based on its results. The methods in this paper are effective methods for investigation of path following for autonomous underwater vehicles with input

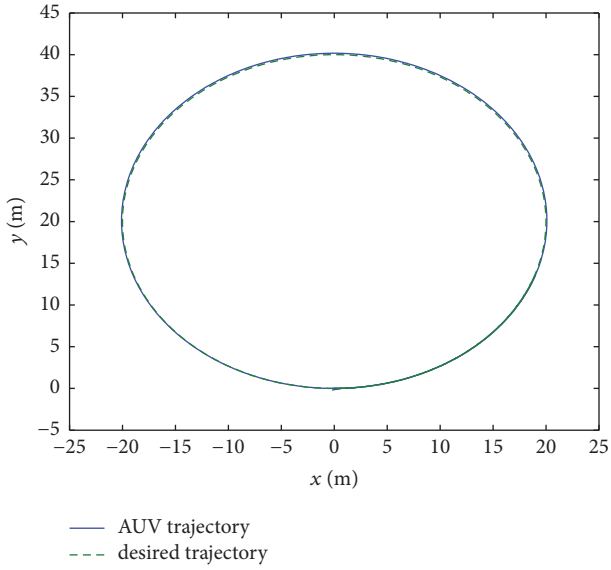

Figure 4: Path tracking response in xy plane.

delay. We will apply a patent on the relevant studies. So, we cannot share the data.

Conflicts of Interest

The authors declare that they have no conflicts of interest.

Acknowledgments

This work is supported by the Hubei Provincial Natural Science Foundation of China (2016CFB273) and the Research and Innovation Initiatives of WHPU (2018Y20).

References

[1] P. Jantapremjit and P. A. Wilson, "Guidance-control based path following for homing and docking using an autonomous underwater vehicle," in *Proceedings of the OCEANS'08 MTS/IEEE Kobe-Techno-Ocean'08 - Voyage toward the Future, OTO'08*, jpn, April 2008.

[2] L. Lapierre and D. Soetanto, "Nonlinear path-following control of an AUV," *Ocean Engineering*, vol. 34, no. 11-12, pp. 1734–1744, 2007.

[3] A. Adhami-Mirhosseini, M. J. Yazdanpanah, and A. P. Aguiar, "Automatic bottom-following for underwater robotic vehicles," *Automatica*, vol. 50, no. 8, pp. 2155–2162, 2014.

[4] M. Kim, H. Joe, J. Kim, and S.-c. Yu, "Integral sliding mode controller for precise manoeuvring of autonomous underwater vehicle in the presence of unknown environmental disturbances," *International Journal of Control*, vol. 88, no. 10, pp. 2055–2065, 2015.

[5] R. Cui, X. Zhang, and D. Cui, "Adaptive sliding-mode attitude control for autonomous underwater vehicles with input nonlinearities," *Ocean Engineering*, vol. 123, pp. 45–54, 2016.

[6] Y. Wang, L. Gu, M. Gao, and K. Zhu, "Multivariable output feedback adaptive terminal sliding mode control for underwater vehicles," *Asian Journal of Control*, vol. 18, no. 1, pp. 247–265, 2016.

[7] X. Qi, "Adaptive coordinated tracking control of multiple autonomous underwater vehicles," *Ocean Engineering*, vol. 91, pp. 84–90, 2014.

[8] R. Cui, C. Yang, Y. Li, and S. Sharma, "Adaptive Neural Network Control of AUVs With Control Input Nonlinearities Using Reinforcement Learning," *IEEE Transactions on Systems, Man, and Cybernetics: Systems*, vol. 47, no. 6, pp. 1019–1029, 2017.

[9] B. B. Miao, T. S. Li, and W. L. Luo, "A DSC and MLP based robust adaptive NN tracking control for underwater vehicle," *Neurocomputing*, vol. 111, pp. 184–189, 2013.

[10] Y.-C. Liu, S.-Y. Liu, and N. Wang, "Fully-tuned fuzzy neural network based robust adaptive tracking control of unmanned underwater vehicle with thruster dynamics," *Neurocomputing*, vol. 196, pp. 1–13, 2016.

[11] J. Ghommam and M. Saad, "Backstepping-based cooperative and adaptive tracking control design for a group of underactuated AUVs in horizontal plan," *International Journal of Control*, vol. 87, no. 5, pp. 1076–1093, 2014.

[12] C. Shen, B. Buckham, and Y. Shi, "Modified C/GMRES Algorithm for Fast Nonlinear Model Predictive Tracking Control of AUVs," *IEEE Transactions on Control Systems Technology*, vol. 25, no. 5, pp. 1896–1904, 2017.

[13] J. Gao, A. A. Proctor, Y. Shi, and C. Bradley, "Hierarchical Model Predictive Image-Based Visual Servoing of Underwater Vehicles with Adaptive Neural Network Dynamic Control," *IEEE Transactions on Cybernetics*, vol. 46, no. 10, pp. 2323–2334, 2016.

[14] J. Sun and J. Chen, "Networked predictive control for systems with unknown or partially known delay," *IET Control Theory & Applications*, vol. 8, no. 18, pp. 2282–2288, 2014.

[15] S. Li and G.-P. Liu, "Networked predictive control for nonlinear systems with stochastic disturbances in the presence of data losses," *Neurocomputing*, vol. 194, pp. 56–64, 2016.

[16] J. Zhao, L. Zhang, and X. Qi, "A necessary and sufficient condition for stabilization of switched descriptor time-delay systems under arbitrary switching," *Asian Journal of Control*, vol. 18, no. 1, pp. 266–272, 2016.

[17] S. Sirouspour and A. Shahdi, "Model predictive control for transparent teleoperation under communication time delay," *IEEE Transactions on Robotics*, vol. 22, no. 6, pp. 1131–1145, 2006.

[18] Y. Sheng, Y. Shen, and M. Zhu, "Delay-dependent global exponential stability for delayed recurrent neural networks," *IEEE Transactions on Neural Networks and Learning Systems*, 2016.

[19] O. M. Smith, "A controller to overcome deadtime," *ISA J*, vol. 6, p. 2833, 1959.

[20] C. F. Caruntu and C. Lazar, "Network delay predictive compensation based on time-delay modelling as disturbance," *International Journal of Control*, vol. 87, no. 10, pp. 2012–2026, 2014.

[21] M. Messadi, A. Mellit, K. Kemih, and M. Ghanes, "Predictive control of a chaotic permanent magnet synchronous generator in a wind turbine system," *Chinese Physics B*, vol. 24, no. 1, Article ID 010502, 2015.

[22] S. H. HosseinNia and M. Lundh, "A general robust MPC design for the state-space model: application to paper machine process," *Asian Journal of Control*, vol. 18, no. 5, pp. 1891–1907, 2016.

[23] Y. Ding, Z. Xu, J. Zhao, K. Wang, and Z. Shao, "Embedded MPC controller based on interior-point method with convergence depth control," *Asian Journal of Control*, vol. 18, no. 6, pp. 2064–2077, 2016.

[24] J.-Q. Huang and F. L. Lewis, "Neural-network predictive control for nonlinear dynamic systems with time-delay," *IEEE Transactions on Neural Networks and Learning Systems*, vol. 14, no. 2, pp. 377–389, 2003.

[25] B. An and G. Liu, "Model-based predictive controller design for a class of nonlinear networked systems with communication delays and data loss," *Chinese Physics B*, vol. 23, no. 8, p. 080202, 2014.

[26] N. Sharma, C. M. Gregory, and W. E. Dixon, "Predictor-based compensation for electromechanical delay during neuromuscular electrical stimulation," *IEEE Transactions on Neural Systems and Rehabilitation Engineering*, vol. 19, no. 6, pp. 601–611, 2011.

[27] N. Fischer, A. Dani, N. Sharma, and W. E. Dixon, "Saturated control of an uncertain nonlinear system with input delay," *Automatica*, vol. 49, no. 6, pp. 1741–1747, 2013.

[28] T. Wang, H. Gao, and J. Qiu, "A combined adaptive neural network and nonlinear model predictive control for multirate networked industrial process control," *IEEE Transactions on Neural Networks and Learning Systems*, vol. 27, no. 2, pp. 416–425, 2016.

[29] P. Dai, Z. Gong, and G. Guo, "Performance analysis of a modular multilevel converter drive system with model predictive control," *International Journal of Control and Automation*, vol. 9, no. 1, pp. 387–398, 2016.

[30] C. Wei, J. Luo, H. Dai, Z. Yin, W. Ma, and J. Yuan, "Globally robust explicit model predictive control of constrained systems exploiting SVM-based approximation," *International Journal of Robust and Nonlinear Control*, vol. 27, no. 16, pp. 3000–3027, 2017.

[31] M. Parvez Akter, S. Mekhilef, N. Mei Lin Tan, and H. Akagi, "Modified Model Predictive Control of a Bidirectional AC-DC Converter Based on Lyapunov Function for Energy Storage Systems," *IEEE Transactions on Industrial Electronics*, vol. 63, no. 2, pp. 704–715, 2016.

[32] R. Prasanth Kumar, A. Dasgupta, and C. S. Kumar, "Robust trajectory control of underwater vehicles using time delay control law," *Ocean Engineering*, vol. 34, no. 5-6, pp. 842–849, 2007.

[33] K. Mukherjee, I. N. Kar, and R. K. P. Bhatt, "Region tracking based control of an autonomous underwater vehicle with input delay," *Ocean Engineering*, vol. 99, pp. 107–114, 2015.